

Environmental Science and Engineering

Jamal Mabrouki
Azrour Mourade
Azeem Irshad
Shehzad Ashraf Chaudhry *Editors*

Advanced Technology for Smart Environment and Energy

 Springer

Environmental Science and Engineering

Series Editors

Ulrich Förstner, Buchholz, Germany

Wim H. Rulkens, Department of Environmental Technology, Wageningen,
The Netherlands

The ultimate goal of this series is to contribute to the protection of our environment, which calls for both profound research and the ongoing development of solutions and measurements by experts in the field. Accordingly, the series promotes not only a deeper understanding of environmental processes and the evaluation of management strategies, but also design and technology aimed at improving environmental quality. Books focusing on the former are published in the subseries Environmental Science, those focusing on the latter in the subseries Environmental Engineering.

Jamal Mabrouki · Azrour Mourade ·
Azeem Irshad · Shehzad Ashraf Chaudhry
Editors

Advanced Technology for Smart Environment and Energy

 Springer

Editors

Jamal Mabrouki
Faculty of Sciences
Mohammed V University
Rabat, Morocco

Azeem Irshad
Higher Education Department
Govt. Asghar Mall College Rawalpindi
Rawalpindi, Pakistan

Azroul Mourade
Department of Computer
Faculty of Sciences and Technologies
Moulay Ismail University of Meknès
Errachidia, Morocco

Shehzad Ashraf Chaudhry
Department of Computer Science
and Information Technology
College of Engineering, Abu Dhabi
University
Abu Dhabi, United Arab Emirates

ISSN 1863-5520

ISSN 1863-5539 (electronic)

Environmental Science and Engineering

ISBN 978-3-031-25661-5

ISBN 978-3-031-25662-2 (eBook)

<https://doi.org/10.1007/978-3-031-25662-2>

© The Editor(s) (if applicable) and The Author(s), under exclusive license to Springer Nature Switzerland AG 2023, corrected publication 2023

This work is subject to copyright. All rights are solely and exclusively licensed by the Publisher, whether the whole or part of the material is concerned, specifically the rights of translation, reprinting, reuse of illustrations, recitation, broadcasting, reproduction on microfilms or in any other physical way, and transmission or information storage and retrieval, electronic adaptation, computer software, or by similar or dissimilar methodology now known or hereafter developed.

The use of general descriptive names, registered names, trademarks, service marks, etc. in this publication does not imply, even in the absence of a specific statement, that such names are exempt from the relevant protective laws and regulations and therefore free for general use.

The publisher, the authors, and the editors are safe to assume that the advice and information in this book are believed to be true and accurate at the date of publication. Neither the publisher nor the authors or the editors give a warranty, expressed or implied, with respect to the material contained herein or for any errors or omissions that may have been made. The publisher remains neutral with regard to jurisdictional claims in published maps and institutional affiliations.

This Springer imprint is published by the registered company Springer Nature Switzerland AG
The registered company address is: Gewerbestrasse 11, 6330 Cham, Switzerland

Contents

1	Energy Optimization Analysis on Internet of Things	1
	Wasswa Shafik and Ali Tufail	
2	UAV-Enabled WSN and Communication Framework for Data Security, Acquisition and Monitoring on Large Farms: A Panacea for Real-Time Precision Agriculture	17
	Oladayo O. Olakanmi, Mbadiwe S. Benyeogor, Kosisochukwu P. Nnoli, and Kehinde O. Odeyemi	
3	Investigation of the Energy and Emission from the Combustion of Argain Cake in a CHP System	35
	Ayoub Najah EL Idrissi, Mohammed Benbrahim, and Nadia Rassai	
4	Identification, Simulation and Modeling of the Main Power Losses of a Photovoltaic Installation and Use of the Internet of Things to Minimize System Losses	49
	Mohammed Benchrifa, Mohamed Elouardi, Ghizlane Fattah, Jamal Mabrouki, and Rachid Tadili	
5	Mixed Thermal Boundary Condition Effects on Non-Darcian Model	61
	Hajar Lagziri and Hanae EL Fakiri	
6	Behavior and Electrocatalytic Degradation of Textile Azo Dye Under Acidic Conditions	73
	Sanaa El Aggadi, Amale Boutakiout, Mariem Ennouhi, Aicha Chadil, and Abderrahim El Hourch	
7	Modeling and Simulation of Phytoremediation Technology by Artificial Neural Network	83
	Saloua Elfanssi, Jamal Mabrouki, Kaoutar El Oumlouki, Ghizlane Fattah, and Laila Mandi	

8	Cryptocurrency Returns Clustering Using Japanese Candlesticks: Towards a Programmatic Trading System	93
	Ahmed El Youssefi, Abdelaaziz Hessane, Yousef Farhaoui, and Imad Zeroual	
9	Modelling and Simulating the Effect of Irradiation Variation on the Behavior of a Photovoltaic Cell and Its Influence on the Maximum Power Point	105
	Mohammed Benchrifa, Karima Azoulay, Imane Bencheikh, Jamal Mabrouki, Rachid Tadili, Ilham Ihoume, Nora Arbaoui, and Mohamed Daoudi	
10	Ecological Risks Related to the Influence of Different Environmental Parameters on the Microplastics Behavior	117
	Imane Bencheikh, Karima Azoulay, Meryem Ben Baaziz, and Jamal Mabrouki	
11	An Effective Ensemble Learning Model to Predict Smart Grid Stability Using Genetic Algorithms	129
	Mohamed Khalifa Boutahir, Abdelaaziz Hessane, Yousef Farhaoui, and Mourade Azrour	
12	Optimization of Performance the Waste in Treatment of Textile Wastewater Using Response Surface Methodology	139
	Abdelkader Anouzla, Amina Khalidi Idrissi, Oussam Hartal, Malika Kastali, Hayat Loukili, Khalid Digua, Salah Souabi, Bachar Redouane, Ali Moussadik, Mohamed Elouardi, Karima Azoulay, Imane Bencheikh, Mohamed Benchrifa, Younes Abrouki, Jamal Mabrouki, Adnane El Hamidi, Mohammed Dahhou, Hicham Harhar, Ghizlane Fattah, and Mohammed Salah	
13	An Overview of the Security Challenges in IoT Environment	151
	Souhayla Dargaoui, Mourade Azrour, Ahmed El Allaoui, Fatima Amounas, Azidine Guezzaz, Hanaa Attou, Chaimae Hazman, Said Benkirane, and Sara Haddou Bouazza	
14	Modeling of the Coagulation System for Treatment of Real Water Rejects	161
	Ghizlane Fattah, Mohamed Elouardi, Mohammed Benchrifa, Fouzia Ghrissi, and Jamal Mabrouki	
15	Effects of Heat Stress and Chemical Pollutants on Sheep Reproduction and Strategies to Mitigate Them	173
	Abdellatif Rahim and Bouchra El Amiri	

16 Dynamics of Tree Cover on the Adaptive Genetic Variation and Evolutionary Power of the Argan Forests from the Essaouira Region of Morocco Facing Climate Change 187
Mohammed Alami, Bouchra Belkadi, Chaimaa Yatrib, Leila Medraoui, Ouafae Pakhrou, Karim Rabeh, and Abdelkarim Filali-Maltouf

17 Deep-PDSC: A Deep Learning-Based Model for a Stage-Wise Classification of Parlatoria Date Scale Disease 207
Abdelaziz Hessane, Mohamed Khalifa Boutahir, Ahmed El Youssefi, Yousef Farhaoui, and Badraddine Aghoutane

18 Adsorption of Inorganic and Organic Pollutants in Urban Wastewater Treatment Using Pine Wood Activated Carbon 221
Karima Azoulay, Imane Bencheikh, Mohammed Benchrifa, Meryem Ben Baaziz, and Jamal Mabrouki

19 Control of COVID 19: Knowledge and Practices of Health Professionals in Hospitals Towards Patients and the Environment in Morocco (Meknes) 233
Karima El-Mouhdi, Smahane Mehanned, and Jawad Bouzid

20 The Evaluation of the Valorization of Cannabis Residues for the Production of Energy by Combustion 247
Mohamed Elouardi, Ghizlane Fattah, Mohammed Benchrifa, Jamal Mabrouki, Touriya Zair, and Mohammed Alaoui El Belghiti

21 Delineation of Groundwater Potential Zones in a Semi-arid Region Using Remote Sensing and GIS: A Case Study of Argana Corridor (Morocco) 257
Mohamed Ait Haddou, Youssef Bouchriti, Mustapha Ikirri, Abderrahmane Wanaim, Ali Aydda, Salih Amarir, Rachid Amiha, and Youssef El Boudribili

22 New Development in Renewable Energy Research 269
Tawaf Ali Shah, Li Zhihe, Li Zhiyu, and Andong Zhang

23 Building an Intelligent Anomaly Detection Model with Ensemble Learning for IoT-Based Smart Cities 287
Chaimae Hazman, Said Benkirane, Azidine Guezzaz, Mourade Azrour, and Mohamed Abdedaime

24 Embedded Web Server Implementation for Real-Time Water Monitoring 301
Mouaad Mohy-Eddine, Mourade Azrour, Jamal Mabrouki, Fatima Amounas, Azidine Guezzaz, and Said Benkirane

**25 Crystal Structure and Impedance Spectroscopy Studies
of New Orthophosphate $Ba_{2-x}Pb_xSr(PO_4)_2$; ($0 \leq x \leq 2$) 313**
M. Ben Baaziz, K. Azoulay, I. Bencheikh, R. Ghibate,
M. Azdouz, L. Bih, and M. Azrour

**Correction to: Investigation of the Energy and Emission
from the Combustion of Argain Cake in a CHP System C1**
Ayoub Najah EL Idrissi, Mohammed Benbrahim, and Nadia Rassai

Chapter 1

Energy Optimization Analysis on Internet of Things



Wasswa Shafik  and Ali Tufail 

Abstract Energy enhancement and renewable energy integration are crucial facilitators of renewable energy conversion and climate shift alleviations. The technological advancements supported by the current fifth generation (5G), like Internet of Things (IoT), Internet of Flying Things, and Internet of Drones have shown different merits within the energy market, including energy generation, storage, and delivery, as well as increased demand. It is predicted that the IoTs are to be utilized to enhance energy usage, increase sustainable energy use, and reduce the environmental effects of energy application. This study examines the latest studies on the IoT application in smart grids and overall energy networks. The study further details IoT's supporting technologies, like cloud storage and multiple data analysis tools. Moreover, a detailed identified problems for IoT deployment in the energy sector, like security and privacy and solutions, for instance, blockchain. The study offers energy regulators, managers, and analysts on the position of IoT in energy system optimization.

Keywords Internet of Things · Energy optimization · Smart energy system

1.1 Introduction

1.1.1 Concept

The future of smart networks. The wireless communications with 5G technology support regard massive connectivity as an important element of providing secure communication link and enormous IoT device quality of service and make many efforts to meet the requirements of large emerging services (Cui et al. 2020). Within the IoT, “Things” (refer to all devices that connect to the internet for resource sharing

W. Shafik · A. Tufail (✉)
School of Digital Science, Universiti Brunei Darussalam, Tungku Link, Gadong 1410, Brunei
e-mail: alitufail@ubd.edu.bn

W. Shafik
e-mail: 22h1701@ubd.edu.bn

purposes) and the connections are associated through radio frequency distinguishing proof hardware, sensors, and situated hardware taking a certain agreement to trade and communicate data, so that the acknowledgment, area, and supervision of the protest will be ended up more brilliantly.

Its most prominent include communication and discourse between things that can moreover interact and communicate with the environment (Zhang et al. 2019a). In the current 5G and beyond networks, smart devices in billions have hinted the technology market space. Such devices noticed in this technology era include autonomous drones (fully operational without human interaction), autonomous vehicles, e-healthcare, smart home devices, smartphones with advanced properties, and wearable devices which are rising tremendously. The connectivity of these “devices” to the internet results in IoT network development (Zhang et al. 2019b). We are therefore investigating the potential for implementing such an architecture through blockchain and software-defined networks (SDN) (Yazdinejad et al. 2020).

The SDN is a modern net architecture that eliminates from data plane to control planes using mainly the switch and controller components. These components have major duties to do as in regard to the SDNs, the switch is supposed to deal with packet forwarding as well as protocol management, the controller implements the rules, maintenance, and programmability of individual network switches (Yazdinejad et al. 2018a, 2018b, 2019).

To boost network performance, IoT and SDN capabilities can work together. Additionally, the SDN controller can govern and manage changes in the network configuration caused by the dynamic design of IoT devices (Obeis et al. 2022). The lack of a centralized controller in the IoT network is one of the main issues, which may be resolved by employing the SDN controller to give IoT devices access to a centralized controller (Ojo et al. 2016).

1.1.2 Motivation

In 2022, the worldwide energy need has increased to 4.3 percent over 2021 due to increased indoor activity caused by the Coronavirus disease 2019 pandemic world lockdown, the largest rise ever since 2010 (Energy and CO₂ Status Report 2019). Consequently, the energy related to carbon dioxide (CO₂) emissions touched a track record level in 2018. In comparison to preindustrial temperatures, the earth is warming by 1.5 °C, which will most likely happen in century.

In case these trends endure, the global warming is likely to exceed 2 °C targets, posing a serious threat to the earth and human life (Summary for Policymakers 2022). Although fortunately, or unfortunately, the Covid-19 and the resulting economic catastrophe affected practically each facet of energy production, distribution, and its consumption across the world. The Covid 19 pandemic fashioned the energy companies and emissions patterns as early as 2020 when the pandemic was declared, the main components of clean energy transformation were largely unaffected (Energy

and CO₂ Status Report [2019](#); Summary for Policymakers [2022](#); Home [2019](#); Al-Azez et al. [2019](#)).

The energy supply chain is divided into three sections: (a) energy supply, (b) energy conversion procedure, (c) energy demand, and the industrial sector (Bhattacharyya [2020](#)). These three elements, along with their related components. The roles of the IoT in all segments of the supply chain of energy are discussed in this study. The studies demonstrated how the IoT can help with energy efficiency and enhance the usage of renewable energy sources.

The supply chain of energy mainly has three categories (Consume, Transform, Supply). Within the supply category, several processes are done, energy extraction and treatment, followed by the primary energy supply that may include import or export stock exchange. The next step is transformation. To transform energy conversion technologies are used using T& D (transmission and distribution) systems (Bhattacharyya [2020](#)). For T& D systems, go to consume category, this category has three steps, i.e., final energy, and appliance and useful energy. Some minimal energy loss can be lost at end use appliance, during conversions, and T&D system operation.

Real-time data is sensed and relayed by sensors and communication technologies in the IoT, enabling quick computation and effective decision-making (Tamilselvan and Thangaraj [2020](#)). Furthermore, the IoT will assist the energy industry in transitioning from a consolidated to a smart, scattered, and interconnected energy infrastructure (Internet [2016](#)). Because a critical prerequisite for installing local dispersed renewable energy sources, for instance, wind and solar energy (Motlagh et al. [2018](#)), transforming a lot of small-scale energy consumers into prosumers while it is still advantageous for the grid to do so by pooling their production and maximizing their demand. To streamline, integrate, and keep an eye on operations, IoT systems employ sensors and communication technologies. Numerous people and devices' energy usage patterns can be monitored and managed over time with the aid of large data gathering and substantive data analysis (Ibarra-Esquer et al. [2017](#)) and (Thibaud et al. [2018](#)).

1.1.3 Methodology

The literature has extensively explored and analyzed the IoT application within various industries and sectors (Wang et al. [2020](#); Xing et al. [2019](#)). Furthermore, technological assessments of the difficulties and opportunities associated with the implementation of IoT tech-tecs, for instance, sensors (Daas et al. [2019](#)) or 5G networks (Risteska Stojkoska and Trivodaliev [2017](#)). Most survey studies in the energy sector have concentrated on one small section, like buildings where IoT technology is used, exceptionally minimal in the energy sector(s). In the same context, a brief overview of the IoT architecture and its supporting technologies to establish a foundation for examining their position in the sector.

To have this study completed, an efficient search was done to gather and analyze the most recent body of research on the application of IoT in the energy sector. During the systematic search, we first searched for two main terms “Internet of Things (IoT)” and “energy”, which are nonproprietary, within the titles and abstracts. Publication keywords accumulated in the IEEE, Google Scholar databases, Scopus and Hindawi with limiting our search to “management”, “engineering” and “economics.

Decisively, we then group the related literatures in subgroups of energy optimization in the IoT and energy generation, T&D systems, and the demand side. Then, we distributed the related studies into subgroups of energy optimization in the IoT, T&D systems, and demand-side as well. Instead of focusing on specific illustrations and their limitations, we converge on IoT applications that are generally applicable to most energy systems. For instance, we don’t go into detail about the type, number, and usage of home appliances, building typology, building materials, or occupant energy consumption patterns while discussing the function of IoT in smart buildings.

1.2 Internet of Things

The IoT is a novel technology that makes use of the Internet with the purpose of enabling communication between tangible objects, or “Things.” Appliances and manufacturing machinery are a few examples of physical devices (Hui et al. 2020; Petroşanu et al. 2019; Luo et al. 2019; Khatua et al. 2020; Gu et al. 2019; Haseeb et al. 2019; Zouinkhi et al. 2020; Motlagh et al. 2019; Ramamurthy and Jain 2017; Jia et al. 2019; Karunarathne et al. 2018; Li et al. 2018). These Things deliver effective data sharing and allow the public to receive services through employing appropriate sensors and communication network systems. For example, reducing energy costs accomplishes logically controlling building energy consumption (Internet of Things 2022). IoT may be applied not only in energy but also in transportation, construction, manufacturing (Group 2022).

The third part of the IoT network is communications protocols that allow separate devices to connect and share data together with controllers. The IoT platform(s) permit users to decide on the networking technology type might be the best depending on the demands. Examples of those systems include ZigBee (Haseeb et al. 2020), Bluetooth and the wi-fi. Examples of common own cellular networks in this perspective include Long-Term Evolution-4G, 5G, and 5G and beyond standards (Francia 2017).

1.3 Internet of Things in the Energy Sector

Now, the energy markets are heavily reliant on fuels (fossil-based), which account for almost 80% of global energy. Extreme manufacturing and burning fossil fuels, including air pollution and climate change have, for example, negative cultural,

health, and economic implications (Admin 2018). Energy efficiency or the use of less energy for the same reason are the two main choices for minimizing adverse fossil fuel use, as well as green energy sources. The first topic covered in this part is the use of IoT during the energy producing process. Then we go on to smart cities, which serves as a collective noun for IoT-based components, including smart grids, smart homes, smart factories, and intelligent transportation (Grubler et al. 2018). We will go over each of the above-mentioned components individually.

1.3.1 IoT and Energy Generation

Since the 1990s, industrial process automation, data acquisition as well as supervisory control systems in the energy sector (Tan et al. 2017; Ramamurthy and Jain 2017). The initial stages of IoT contribute to the energy sector by reducing the possibility of output failure or blackout by tracking and regulating equipment and processes. The key problems of old power plants are reliability, performance, environmental effects, and maintenance. The age of power plant equipment, as well as poor maintenance issues, can result in significant energy losses and unreliability. Assets are frequently over 516.353 months, enormously significant, and complicated in replacement.

Nations are pressuring RESs to use less fossil fuel and concentrate on domestic energy sources. The energy system is faced with contemporary issues known as the “intermittency challenge” because of the use of weather-dependent or intermittent renewable energy (VRE) sources including wind and solar energy (SIGFOX.COM. 2022). In an energy system with a sizable percentage of VRE, matching energy generation with demand can be challenging due to supply and demand volatility, which causes mismatches over a range of time scales. IoT solutions reduce the difficulties of adopting VRE, allowing for more flexibility in regulating generation and demand, leading to larger renewable energy integration shares and lower GHG emissions (the sum of emissions of various gases: carbon dioxide, methane, nitrous oxide, and smaller trace gases such as hydrofluorocarbons (HFCs) and sulfur hexafluoride (SF6)) (Al-Ali 2016; Karnouskos 2010; Lagerspetz et al. 2019). Additionally, by utilizing IoT, machine-learning algorithms that aid in selecting the ideal mix can be used to achieve more efficient energy utilization.

1.3.2 Smart Cities

This is a technology support city normal operation (smart urbanization), combined with overpopulation, has resulted in a slew of global issues, including pollution (Ejaz et al. 2017), power availability, and other ecological interests. The smart IoT application is supported by recent advancements in digital technologies backed by advanced high-tech features (Mohanty et al. 2016). In this era, it is possible to link smart factories, smart households, power plants, and farms to collect data on their

energy usage throughout the day. Energy allocated to other portions, like factories, that routinely reduced to stabilize the entire system at the lowest cost and risk of congestion or blackout if it is found that a segment, like residential regions, consumes the most energy in the afternoon.

1.3.3 Smart Grids

Smart grids are electric grids that consist of several operations and energy quantities. These grids that take advantage of the most reliable and reliable information and communications technology to optimize and monitor energy production, transmission and distribution grids, and end-user consumption. A smart grid generates a multiple directional information flow through linking several smart meters, which can be used for device optimization and energy distribution efficiency (Hossain et al. 2016) and (Bhardwaj 2015). Applications of smart grids can be illustrated in specific subgroups of the energy system, for example, energy storage, home, among others.

1.3.4 Smart Buildings

Cities' energy use can be categorized into three categories: Residential (home); commercial (services), including restaurants, offices, and schools; all the examples of domestic energy use of the housing sector are lighting, appliances, cooking, hothouse, water, ventilation, heating, cooling, and air-conditioning system (HVAC). The HVAC energy consumption constitutes half of the overall energy usage in most households (Avcı et al. 2012; Vakiloroyaya et al. 2014; Jagtap et al. 2022; Lee et al. 2017; Reinfurt et al. 2017). The control of the HVAC system is also important for reducing energy consumption.

1.3.5 Smart Industry Energy Use

In the industry, IoT can be employed to create an entirely associated and scalable system that reduces energy consumption while maximizing output. Conventional factories use lots of resources to manufacture and monitor the final product's quality. Furthermore, every phase must be monitored, which necessitates the involvement of human resources (Janssen et al. 2019). Utilizing a scalable and agile framework in smart industries, on the other hand, helps to detect faults at the same time rather than waiting until the end of the energy production.

1.3.6 Intelligent Transportation

One of the greatest contributors to air pollution and energy waste in big cities is the overuse of personal vehicles in place of public transportation. Instead of a practical transportation system where each component runs independently, using IoT technology, often known as “smart transportation,” offers a global management framework. Real-time data processing is also necessary for effective traffic management. It is possible to connect every element of the transportation system and the process its data at once (Su et al. 2022). Applications for smart transportation include online map-based smart parking and traffic control.

1.4 Identified Challenges of Applying Internet of Things

Apart from the numerous advantages of Internet of Things in terms of energy savings, implementing IoT in the energy segment also poses several problems that must be tackled. This segment discusses the obstacles to implement IoT-based energy systems as well as existing solutions.

1.4.1 Energy Consumption

IoT platforms are putting a lot of work into saving electricity in energy networks. To allow IoT communication in energy systems, many IoT Things transmit data. Operating the IoT system and transmitting the enormous volumes of data created by IoT devices both require a large amount of energy (Kaur and Sood 2017). IoT device energy consumption continues to be a significant issue. The power consumption of IoT devices has been reduced, although, using a variety of techniques. As an illustration, you could put the sensors in sleep mode and only use them when necessary. Other challenges include IoT integration with subsystems (Shaikh et al. 2017), user privacy (Anastasi et al. 2009; Energies 2022), security issues (Boroojeni et al. 2017), IoT standards acceptance (Wong et al. 2016; Porambage et al. 2016), and architecture design challenges (Chow 2017).

1.5 Future Trends

There are a lot of benefits in the previous sections to the application of existing IoT systems to provide energy-efficient solutions for the energy sector. However, new solutions and trends to boost IoT efficiency and resolve the challenges associated

with it are necessary to deploy IoT in the energy domain. In this segment, we present two approaches to the challenges of blockchain technology and green IoT (G-IoT).

1.5.1 Blockchain and IoT

Most today's IoT systems depend on centralized cloud systems (Jayaraman et al. 2017). In various IoT applications, thousands of IoT units and devices must be connected, which is challenging to synchronize. Because IoT is centralized and server-client in design, when one server is compromised, all linked objects are also readily affected, raising system security and user privacy issues. Fortunately, blockchain approach is suggested as a solution (Poyner and Sherratt 2018).

Verified transactions are always held in a block that is associated with the last block in a way that proofs are never lost. Besides, any person can document and view the history of all transactions at each node. Every member of the blockchain is therefore immediately aware of any modification of the block (Jayaraman et al. 2017; Poyner and Sherratt 2018). Furthermore, thousands of IoT Things can be easily organized by way of the distributed database of blockchain. A secure distributed database (Li et al. 2017) is made possible by using Blockchain consensus algorithms established on pair-to-peer nets. Blockchain (Song et al. 2017) would then provide a decentralized, private-by-design IoT to provide security.

More specifically, blockchain allows objects to store and exchange app updates. If an upgrade is applied to the blockchains as a legitimate block, it is hard to delete or alter it. There are innocuous testing nodes that accept the precision of updated information and guarantee security against any attacks. As a result, blockchain will offer alerts, availability, and innocuousness to IoT-based networks (Meddeb 2016; Chen et al. 2014; Al-Qaseemi et al. 2016; Kshetri 2017).

In the energy market, blockchains can improve energy stability and reliability by offering a shared network for storage systems. Real and high-quality data freely are shared between devices, and citizens can access energy information directly without the third-party intervention (Alladi et al. 2019). Neighbors can quickly share electricity. As a result, without the intervention of regulators, not only will people's confidence be strengthened, but also costs associated with connecting to centralized grids will be reduced. Another value is that through tracking an area's consumption data, Blockchain allows energy delivery to regulate energy transfer to that specific area centrally. Besides, blockchain-based IoT networks assist in the diagnosis and repair of smart grid equipment (Christidis and Devetsikiotis 2016; Hawlitschek et al. 2018; Huh et al. 2017; Conoscenti et al. 2016).

1.5.2 *Green Internet of Things*

As these systems are soon to be used on a large scale, the energy based IoT devices is a major obstacle. A great deal of energy is required to power billions of devices linked to the Internet. Low-carbon, high-efficiency linking networks are required to solve these problems. Fortunately, G-IoT (Boudguiga, et al. 2017; Green Internet of Things for Smart World 2015; Nguyen et al. 2022; Lee et al. 2014; Nesa and Banerjee 2019; Yang et al. 2021; Zhao et al. 2022; Shafik et al. 2019a, 2019b, 2020a, 2020b, 2020c, 2020d, 2020e, 2020f, 2020g, 2021, 2022a, 2022b; Meng et al. 2020; Shafik and Matinkhah 2018, 2019, 2020a, 2020b, 2021; Jun et al. 2021; Matinkhah et al. 2019; Thilakarathne et al. 2022; Lin et al. 2021; Shafik and Mostafavi 2019; Shafik and Matinkhah 2019; Matinkhah and Shafik 2019, 2019a; Matinkhah and Shafik 2019b; Mostafavi and Shafik 2019; Popli et al. 2022; Majumdar et al. 2022; Shafik 2021) was developed in these conditions. The energy-efficient characteristics of G-IoT, including architecture, production, implementation, and disposal are important during the life cycle (Shokoor et al. 2022) and (Shafik and Mostafavi 2020), radiofrequency identification scale is concentrated to reduce the volume of content in each radiofrequency identification tag, which is difficult to recycle (Shafik et al. 2019c; Shafik and Matinkhah 2020c; Ebrahimi et al. 2019; Azroul et al. 2021a, 2021b).

1.6 Conclusions

Energy services are about to enter a new age of transformation. Large-scale applications of variable renewable energy in clustered energy networks, the need for energy efficiency, necessitates system-wide, interconnected approaches to reduce energy and environmental effects. In this respect, new technologies similar to IoT will assist the power (energy) market is moving from a centralized to a smart decentralized and streamlined framework. We examined the IoT position in the energy sector in general, and smart grids in this study. We categorize multiple IoT usage cases in every segment of the energy supply from energy generation to energy grids to end-user(s) industries or factories. Furthermore, various IoT device components, for instance, facilitating connectivity and sensor technology, and how they can be used in the energy field. We talk about cloud storage and data system analytics, like data collection and simulation resolution that can be utilized in smart applications of energy, from small devices, buildings to smart home, smart villages to big smart cities. As prospective research paths, we emphasize Blockchain and green IoT as alternatives to these problems.

References

- Admin (2018) 8 types of sensors that coalesce perfectly with an IoT app—IT Firms, top IT Firms—result of in-depth research & analysis. <https://www.itfirms.co/8-types-of-sensors-that-coalesce-perfectly-with-an-iot-app/>. Accessed 04 Oct 2022
- Al-Ali AR (2016) Internet of things role in the renewable energy resources. *Energy Procedia* 100:34–38. <https://doi.org/10.1016/j.egypro.2016.10.144>
- Al-Azez ZT, Lawey AQ, El-Gorashi TEH, Elmirghani JMH (2019) Energy-efficient IoT virtualization framework with peer to peer networking and processing. *IEEE Access* 7:50697–50709. <https://doi.org/10.1109/ACCESS.2019.2911117>
- Alladi T, Chamola V, Rodrigues JJPC, Kozlov SA (2019) Blockchain in smart grids: a review on different use cases. *Sensors* 19(22). <https://doi.org/10.3390/s19224862>
- Al-Qaseemi SA, Almulhim HA, Almulhim MF, Chaudhry SR (2016) IoT architecture challenges and issues: aack of standardization. In: 2016 future technologies conference (FTC), pp 731–738. <https://doi.org/10.1109/FTC.2016.7821686>
- Anastasi G, Conti M, Di Francesco M, Passarella A (2009) Energy conservation in wireless sensor networks: a survey. *Ad Hoc Netw* 7(3):537–568. <https://doi.org/10.1016/j.adhoc.2008.06.003>
- Avci M, Erkoc M, Asfour SS (2012) Residential HVAC load control strategy in real-time electricity pricing environment. In: 2012 IEEE Energytech, pp 1–6. <https://doi.org/10.1109/EnergyTech.2012.6304636>
- Azrou M, Mabrouki J, Guezzaz A, Kanwal A (2021a) Internet of things security: challenges and key issues. *Secur Commun Netw* 1–11. <https://doi.org/10.1155/2021/5533843>
- Azrou M, Mabrouki J, Fattah G, Guezzaz A, Aziz F (2021b) Machine learning algorithms for efficient water quality prediction. *Model Earth Syst Environ* <https://doi.org/10.1007/s40808-021-01266-6>
- Bhardwaj A (2015) Leveraging the internet of things and analytics for smart energy management. TATA Consult Serv Mumbai India
- Bhattacharyya SC (2020) *Energy economics: concepts, issues, markets and governance*. Springer, London
- Borojoni K, Amini MH, Nejadpak A, Dragičević T, Iyengar SS, Blaabjerg F (2017) A novel cloud-based platform for implementation of oblivious power routing for clusters of microgrids. *IEEE Access* 5:607–619. <https://doi.org/10.1109/ACCESS.2016.2646418>
- Boudguiga A et al (2017) Towards better availability and accountability for IoT updates using a Blockchain. In: 2017 IEEE European symposium on security and privacy workshops (EuroSPW), pp 50–58. <https://doi.org/10.1109/EuroSPW.2017.50>
- Chen S, Xu H, Liu D, Hu B, Wang H (2014) A Vision of IoT: applications, challenges, and opportunities with China perspective. *IEEE Internet Things J* 1(4):349–359. <https://doi.org/10.1109/JIOT.2014.2337336>
- Chow R (2017) The last mile for IoT privacy. *IEEE Secur Priv* 15(6):73–76. <https://doi.org/10.1109/MSP.2017.4251118>
- Christidis K, Devetsikiotis M (2016) Blockchains and smart contracts for the internet of things. *IEEE Access* 4:2292–2303
- Conoscenti M, Vetrò A, Martin JCD (2016) Blockchain for the Internet of Things: a systematic literature review. In: 2016 IEEE/ACS 13th international conference of computer systems and applications (AICCSA), pp 1–6. <https://doi.org/10.1109/AICCSA.2016.7945805>
- Cui G, Li X, Xu L, Wang W (2020) Latency and energy optimization for MEC enhanced SAT-IoT networks. *IEEE Access* 8:55915–55926. <https://doi.org/10.1109/ACCESS.2020.2982356>
- Daas MJ, Jubran M, Hussein M (2019) Energy Management Framework for 5G Ultra-Dense Networks Using Graph Theory. *IEEE Access* 7:175313–175323. <https://doi.org/10.1109/ACCESS.2019.2957378>
- Di Francia G (2017) The development of sensor applications in the sectors of energy and environment in Italy 1976–2015. *Sensors* 17(4), Article no. 4. <https://doi.org/10.3390/s17040793>

- Ebrahimi MM, Shafik W, Matinkhah SM (2019) A networked 5G unmanned aerial vehicle communication pricing and challenges. In: International conference on networking, communication and computing technology
- Ejaz W, Naem M, Shahid A, Anpalagan A, Jo M (2017) Efficient energy management for the internet of things in smart cities. *IEEE Commun Mag* 55(1):84–91. <https://doi.org/10.1109/MCOM.2017.1600218CM>
- Energies | Free Full-Text | Internet of Things for modern energy systems: state-of-the-art, challenges, and open issues. <https://www.mdpi.com/1996-1073/11/5/1252>. Accessed 19 Mar 2022
- Global Energy & CO₂ Status Report 2019—Analysis. IEA. <https://www.iea.org/reports/global-energy-co2-status-report-2019>. Accessed 15 Mar 2021
- Group TM Smart sensor technology for the IoT. <https://www.techbriefs.com/component/content/article/tb/pub/features/articles/33212>. Accessed 12 Apr 2022
- Grubler A et al (2018) A low energy demand scenario for meeting the 1.5 °C target and sustainable development goals without negative emission technologies. *Nat Energy* 3(6). <https://doi.org/10.1038/s41560-018-0172-6>
- Gu S, Li J, Wang Y, Wang N, Zhang Q (2019) DR-MDS: an energy-efficient coding scheme in D2D distributed storage network for the internet of things. *IEEE Access* 7:24179–24191. <https://doi.org/10.1109/ACCESS.2019.2900537>
- Haseeb K, Almogren A, Islam N, Ud Din I, Jan Z (2019) An energy-efficient and secure routing protocol for intrusion avoidance in IoT-based WSN. *Energies* 12(21). <https://doi.org/10.3390/en12214174>
- Haseeb K, Almustafa KM, Jan Z, Saba T, Tariq U (2020) Secure and energy-aware heuristic routing protocol for wireless sensor network. *IEEE Access* 8:163962–163974. <https://doi.org/10.1109/ACCESS.2020.3022285>
- Hawlichek F, Notheisen B, Teubner T (2018) The limits of trust-free systems: a literature review on blockchain technology and trust in the sharing economy. *Electron Commer Res Appl* 29:50–63. <https://doi.org/10.1016/j.elerap.2018.03.005>
- Home (2019) SDG Summit. <https://sustainabledevelopment.un.org/sdgsummit>. Accessed 07 Mar 2022
- Hossain MS, Madloul NA, Rahim NA., Selvaraj J, Pandey AK, Khan AF (2016) Role of smart grid in renewable energy: an overview. *Renew Sustain Energy Rev* 60:1168–1184. <https://doi.org/10.1016/j.rser.2015.09.098>
- Huh S, Cho S, Kim S (2017) Managing IoT devices using blockchain platform. In: 2017 19th international conference on advanced communication technology (ICACT), pp 464–467. <https://doi.org/10.23919/ICACT.2017.7890132>
- Hui H, Ding Y, Shi Q, Li F, Song Y, Yan J (2020) 5G network-based Internet of Things for demand response in smart grid: a survey on application potential. *Appl Energy* 257:113972. <https://doi.org/10.1016/j.apenergy.2019.113972>
- Ibarra-Esquer JE, González-Navarro FF, Flores-Rios BL, Burtseva L, Astorga-Vargas MA (2017) Tracking the evolution of the internet of things concept across different application domains. *Sensors* 17(6). <https://doi.org/10.3390/s17061379>
- Internet of Things. <https://www.ibm.com/cloud/internet-of-things>. Accessed 24 July 2022
- Jagtap S, Rahimifard S, Duong LN (2022) Real-time data collection to improve energy efficiency: a case study of food manufacturer. *J Food Process Preserv* 46(8)
- Janssen M, Luthra S, Mangla S, Rana NP, Dwivedi YK (2019) Challenges for adopting and implementing IoT in smart cities: an integrated MICMAC-ISM approach. *Internet Res* 29(6):1589–1616. <https://doi.org/10.1108/INTR-06-2018-0252>
- Jayaraman PP, Yang X, Yavari A, Georgakopoulos D, Yi X (2017) Privacy-preserving Internet of Things: from privacy techniques to a blueprint architecture and efficient implementation. *Future Gener Comput Syst* 76:540–549. <https://doi.org/10.1016/j.future.2017.03.001>
- Jia M, Komeily A, Wang Y, Srinivasan RS (2019) Adopting Internet of Things for the development of smart buildings: a review of enabling technologies and applications. *Autom Constr* 101:111–126. <https://doi.org/10.1016/j.autcon.2019.01.023>

- Jun Y, Craig A, Shafik W, Sharif L (2021) Artificial intelligence application in cybersecurity and cyberdefense. *Wirel Commun Mob Comput*. <https://doi.org/10.1155/2021/3329581>
- Karnouskos S (2010) The cooperative internet of things enabled smart grid, pp 07–10
- Karunaratne G, GKWMSIR, Kulawansa KADT, Firdhous MFM (2018) Wireless communication technologies in the Internet of Things: a critical evaluation. In: 2018 international conference on intelligent and innovative computing applications (ICONIC), pp 1–5. <https://doi.org/10.1109/ICONIC.2018.8601226>
- Kaur N, Sood SK (2017) An energy-efficient architecture for the internet of things (IoT). *IEEE Syst J* 11(2):796–805. <https://doi.org/10.1109/JSYST.2015.2469676>
- Khatua PK, Ramachandaramurthy VK, Kasinathan P, Yong JY, Pasupuleti J, Rajagopalan A (2020) Application and assessment of internet of things toward the sustainability of energy systems: challenges and issues. *Sustain Cities Soc* 53:101957. <https://doi.org/10.1016/j.scs.2019.101957>
- Kshetri N (2017) Can blockchain strengthen the internet of things? *IT Prof* 19(4):68–72
- Lagerspetz E et al (2019) MegaSense: feasibility of low-cost sensors for pollution hot-spot detection. In: 2019 IEEE 17th international conference on industrial informatics (INDIN), pp 1083–1090. <https://doi.org/10.1109/INDIN41052.2019.8971963>
- Lee C, Kim D, Kim J (2014) An energy-efficient active RFID protocol to avoid overhearing problem. *IEEE Sens J* 14(1):15–24. <https://doi.org/10.1109/JSEN.2013.2279391>
- Lee CKM, Zhang SZ, Ng KKH (2017) Development of an industrial Internet of things suite for smart factory towards re-industrialization. *Adv Manuf* 5(4):335–343. <https://doi.org/10.1007/s40436-017-0197-2>
- Li Z, Shahidehpour M, Aminifar F (2017) Cybersecurity in distributed power systems. *Proc IEEE* 105(7):1367–1388. <https://doi.org/10.1109/JPROC.2017.2687865>
- Li S, Xu LD, Zhao S (2018) 5G Internet of Things: a survey. *J Ind Inf Integr* 10:1–9. <https://doi.org/10.1016/j.jii.2018.01.005>
- Lin Y, Ahmad Z, Shafik W, Khosa KS, Almaspoor Z, Alsuhabi H et al (2021) Impact of facebook and newspaper advertising on sales: a comparative study of online and print media. *Comput Intell Neurosci*. <https://doi.org/10.1155/2021/5995008>
- Luo X, Zhang H, Zhang Z, Yu Y, Li K (2019) A new framework of intelligent public transportation system based on the internet of things. *IEEE Access* 7:55290–55304. <https://doi.org/10.1109/ACCESS.2019.2913288>
- Majumdar P, Mitra S, Bhattacharya D (2022) Green IoT for smart agricultural monitoring: prediction intelligence with machine learning algorithms, analysis of prototype, and review of emerging technologies. In: *Handbook of intelligent computing and optimization for sustainable development*, pp 637–53
- Matinkhah SM, Shafik W (2019a) Smart grid empowered by 5G technology. In: 2019a smart grid conference (SGC), Tehran, Iran, pp 1–6. <https://doi.org/10.1109/SGC49328.2019.9056590>
- Matinkhah SM, Shafik W (2019b) A study on financial pricing and applications models on 5g. In: 4th international conference in financial mathematics, Yazd, Iran, pp 54–60
- Matinkhah SM, Shafik W (2019c) Broadcast communication analysis for 5g media radio access networks. In: 16th conference on broadcast and exhibition, Tehran, Iran.
- Matinkhah SM, Shafik W, Ghasemzadeh M (2019) Emerging artificial intelligence application: reinforcement learning issues on current internet of things. In: 2019 16th international conference in information knowledge and technology, Tehran, Iran. <https://civilica.com/doc/982297/>
- Meddeb A (2016) Internet of things standards: who stands out from the crowd? *IEEE Commun Mag* 54(7):40–47. <https://doi.org/10.1109/MCOM.2016.7514162>
- Meng H, Shafik W, Matinkhah SM, Ahmad Z (2020) A 5g beam selection machine learning algorithm for unmanned aerial vehicle applications. *Wirel Commun Mob Comput*. <https://doi.org/10.1155/2020/1428968>
- Mohanty SP, Choppali U, Kougiianos E (2016) Everything you wanted to know about smart cities: the Internet of things is the backbone. *IEEE Consum Electron Mag* 5(3):60–70. <https://doi.org/10.1109/MCE.2016.2556879>

- Mostafavi S, Shafik W (2019) Fog computing architectures, privacy and security solutions. *J Commun Technol, Electron Comput Sci* 24:1–14. <https://doi.org/10.22385/jctecs.v24i0.292>
- Motlagh NH, Khajavi SH, Jaribion A, Holmstrom J (2018) An IoT-based automation system for older homes: a use case for the lighting system. In: 2018 IEEE 11th conference on service-oriented computing and applications (SOCA), pp 1–6. <https://doi.org/10.1109/SOCA.2018.8645771>
- Motlagh NH, Bagaa M, Taleb T (2019) Energy and delay aware task assignment mechanism for UAV-based IoT platform. *IEEE Internet Things J* 6(4):6523–6536. <https://doi.org/10.1109/JIOT.2019.2907873>
- Nesa N, Banerjee I (2019) SensorRank: an energy-efficient sensor activation algorithm for sensor data fusion in wireless networks. *IEEE Internet Things J* 6(2):2532–2539. <https://doi.org/10.1109/JIOT.2018.2871469>
- Nguyen D, Dow C, Hwang S (2022) An efficient traffic congestion monitoring system on internet of vehicles. *Wirel Commun Mob Comput*. <https://www.hindawi.com/journals/wcmc/2018/9136813/>. Accessed 12 Sept 2022.
- Obeis NT, Lehmoud AA, Mutar AF (2022) Content delivery network for secure of software defined networking by using IPv4, OpenFlow, and ALTO. *Period Eng Nat Sci (PEN)* 10(2):231–240. <https://doi.org/10.4108/eetiot.v8i29.1108>
- Ojo M, Adami D, Giordano S (2016) An SDN-IoT architecture with NFV implementation. In: IEEE globecom workshops (GC Wkshps), pp 1–6. <https://doi.org/10.1109/GLOCOMW.2016.7848825>
- Petroșanu DM, Căruțașu G, Căruțașu NL, Pîrjan A (2019) A review of the recent developments in integrating machine learning models with sensor devices in the smart buildings sector to attain enhanced sensing, energy efficiency, and optimal building management. *Energies* 12(24). <https://doi.org/10.3390/en12244745>
- Popli S, Jha RK, Jain S (2022) Green IoT: a short survey on technical evolution & techniques. *Wirel Pers Commun* 123(1):525–53
- Porambage P, Ylianttila M, Schmitt C, Kumar P, Gurtov A, Vasilakos AV (2016) The quest for privacy in the internet of things. *IEEE Cloud Comput* 3(2):36–45. <https://doi.org/10.1109/MCC.2016.28>
- Poyner IK, Sherratt RS (2018) Privacy and security of consumer IoT devices for the pervasive monitoring of vulnerable people. <https://doi.org/10.1049/cp.2018.0043>
- Ramamurthy A, Jain P (2017a) The internet of things in the power sector opportunities in Asia and the pacific. <https://think-asia.org/handle/11540/7821>. Accessed 09 Apr 2022
- Ramamurthy A, Jain P (2017b) The internet of things in the power sector: opportunities in Asia and the pacific, vol 48. Asian Development Bank
- Reinfurt L, Falkenthal M, Breitenbücher U, Leymann F (2017) Applying IoT patterns to smart factory systems. *Adv Summer Sch Serv Oriented Comput Summer SOC*
- Risteska Stojkoska BL, Trivodaliev KV (2017) A review of Internet of Things for the smart home: challenges and solutions. *J Clean Prod* 140:1454–1464. <https://doi.org/10.1016/j.jclepro.2016.10.006>
- Shafik W, Matinkhah SM (2020a) A portable fuzzy sink scheme for wireless sensor network life expectancy enhancement. *IEEE Iran Jt Congr Fuzzy Intell Syst*. <https://doi.org/10.1109/CFIS49607.2020.9238684>
- Shafik W, Matinkhah SM (2021) Unmanned aerial vehicles analysis to social networks performance. *CSI J Comput Sci Eng* 18(2):24–31
- Shafik W, Mostafavi S (2020) Knowledge engineering on internet of things through reinforcement learning. *Int J Comput Appl (IJCA)* 177(44):1–7
- Shafik W, Matinkhah SM, Ghasemzadeh M (2019b) Fog-mobile edge performance evaluation and analysis on internet of things. *J Adv Res Mob Comput* 1(3):1–17. <https://doi.org/10.5281/zenodo.3591228>
- Shafik W, Matinkhah SM, Ghasemzadeh M (2020g) Theoretical understanding of deep learning in uav biomedical engineering technologies analysis. *SN Computer Science* 1(6):1–13. <https://doi.org/10.1007/s42979-020-00323-8>

- Shafik W (2021) A fast machine learning for beam selection in 5G unmanned aerial vehicle communications, MSc. dissertation, computer engineering department, Yazd University
- Shafik W, Matinkhah SM (2018) How to use Erlang B to determine the blocking probability of packet loss in a wireless communication. In: 13th symposium on advances in science & technology, Mashhad, Tehran
- Shafik W, Matinkhah SM (2019) Admitting new requests in fog networks according to erlang b distribution. In: 27th Iranian conference on electrical engineering, Yazd, Iran. <https://doi.org/10.1109/IranianCEE.2019.8786518>
- Shafik W, Matinkhah SM (2020b) Dimensional fast machine learning algorithm for mobile unmanned aerial vehicle base stations. *Int J Adv Appl Sci* 28–38. <https://doi.org/10.11591/ijaas.v10.i1>
- Shafik W, Matinkhah SM (2020c) A study of reinforcement learning on internet of things. In: International conference on science, engineering & technology, Singapore, Singapore
- Shafik W, Matinkhah SM (2019) Privacy issues in social web of things. In: 5th international conference on web research, Tehran, Islamic Republic of Iran, pp 208–214. <https://doi.org/10.1109/ICWR.2019.8765254>
- Shafik W, Mostafavi SA (2019) Knowledge engineering on internet of things through reinforcement learning. *Int J Comput Appl* 975. <https://doi.org/10.5120/ijca2020919952>
- Shafik W, Matinkhah SM, Ghasemzadeh M (2019a) A fast machine learning for 5g beam selection for unmanned aerial vehicle applications. *J Inf Syst Telecommun* 7(28):262–278. <https://doi.org/10.7508/jist.2019.04.003>
- Shafik W, Matinkhah SM, Ghasemzadeh M (2019c) Emerging artificial intelligence application reinforcement learning issues on current internet of things. In: 10th conference on information and knowledge technology (IKT), Tehran, Iran
- Shafik W, Matinkhah SM, Afolabi SS, Sanda MN (2020a) A 3-dimensional fast machine learning algorithm for mobile unmanned aerial vehicle base stations. *Int J Adv Appl Sci* <https://doi.org/10.11591/ijaas.v10.i1.pp28-38>
- Shafik W, Matinkhah SM, Ghasemzadeh M (2020b) A mobile fuzzy sink scheme for wireless sensor network period improvement. In: 8th Iranian joint congress on fuzzy and intelligent systems, Mashhad, Iran, pp 211–216. <https://doi.org/10.1109/CFIS49607.2020.9238684>
- Shafik W, Matinkhah SM, Asadi M, Ahmadi Z, Hadiyan Z (2020c) A study on internet of things performance evaluation. *J Commun Technol, Electron Comput Sci* 1–19. <https://doi.org/10.22385/jctecs.v28i0.303>
- Shafik W, Matinkhah SM, Ghasemzadeh M (2020d) Internet of things-based energy management, challenges, and solutions in smart cities. *J Commun Technol, Electron Comput Sci* 27:1–11. <https://doi.org/10.22385/jctecs.v27i0.302>
- Shafik W, Matinkhah SM, Sanda MN (2020e) Network resource management drives machine learning: a survey and future research direction. *J Commun Technol, Electron Comput Sci* 1–15. <https://doi.org/10.22385/jctecs.v30i0.312>
- Shafik W, Matinkhah SM, Etemadinejad P, Sanda MN (2020f) Reinforcement learning rebirth, techniques, challenges, and resolutions. *Int J Inform Vis* 4(3):127–135. <https://doi.org/10.30630/joiv.4.3.376>
- Shafik W, Matinkhah SM, Sanda MN, Shokoor F (2021) Internet of things-based energy efficiency optimization model in fog smart cities. *Int J Inform Vis* 5(2):105–112. <https://doi.org/10.4108/eetiot.v8i29.1108>
- Shafik W, Matinkhah SM, Shokoor F, Sharif L (2022a) A reawakening of machine learning application in unmanned aerial vehicle: future research motivation. *EAI Endorsed Trans Internet Things* 8(29). <https://doi.org/10.4108/eetiot.v8i29.987>
- Shafik W, Matinkhah SM, Shokoor F (2022b) Recommendation system comparative analysis: internet of things aided networks. *EAI Endorsed Trans IoT* 8(29). <https://doi.org/10.4108/eetiot.v8i29.1108>
- Shaikh FK, Zeadally S, Exposito E (2017) Enabling technologies for green internet of things. *IEEE Syst J* 11(2):983–994. <https://doi.org/10.1109/JSYST.2015.2415194>

- Shokoor F, Shafik W, Matinkhah SM (2022) Overview of 5G & beyond security. *EAI Endorsed Trans Internet Things* 8(30) SIGFOX.COM. <https://www.sigfox.com/en>. Accessed 12 Apr 2022
- Song T, Li R, Mei B, Yu J, Xing X, Cheng X (2017) A privacy-preserving communication protocol for IoT applications in smart homes. *IEEE Internet Things J* 4(6):1844–1852. <https://doi.org/10.1109/JIOT.2017.2707489>
- Su Z, Feng W, Tang J, Chen. Z, Fu Y, Zhao N, Wong KK (2022) Energy efficiency optimization for D2D communications underlying UAV-assisted industrial iot networks with SWIPT. *IEEE Internet Things J*
- Summary for Policymakers—Global Warming of 1.5 °C. <https://www.ipcc.ch/sr15/chapter/spm/>. Accessed 06 June 2022
- Tamilselvan K, Thangaraj P (2020) Pods—a novel intelligent energy-efficient and dynamic frequency scalings for multi-core embedded architectures in an IoT environment. *Micro process Microsyst* 72. <https://doi.org/10.1016/j.micpro.2019.102907>
- Tan YS, Ng YY, Low JS (2017) Internet-of-things enabled real-time monitoring of energy efficiency on manufacturing shop floors. *Procedia CIRP* 61:376–381. <https://doi.org/10.1016/j.procir.2016.11.242>
- Thibaud M, Chi H, Zhou W, Piramuthu S (2018) Internet of Things (IoT) in high-risk Environment, Health and Safety (EHS) industries: a comprehensive review. *Decis Support Syst* 108:79–95. <https://doi.org/10.1016/j.dss.2018.02.005>
- Thilakarathne NN, Kagita MK, Priyashan WD (2022) Green internet of things: the next generation energy efficient internet of things. *Appl Inf Process Syst* 391–402. Springer, Singapore. https://doi.org/10.1007/978-981-16-2008-9_38
- Vakiloroaya V, Samali B, Fakhar A, Pishghadam K (2014) A review of different strategies for HVAC energy saving. *Energy Convers Manag* 77:738–754. <https://doi.org/10.1016/j.enconman.2013.10.023>
- Wang J, Jiang C, Zhang K, Hou X, Ren Y, Qian Y (2020) Distributed Q-learning aided heterogeneous network association for energy-efficient IIoT. *IEEE Trans Ind Inform* 16(4):2756–2764. <https://doi.org/10.1109/TII.2019.2954334>
- Wong TY, Shum C, Lau WH, Chung SH, Tsang KF, Tse CF (2016) Modeling and co-simulation of IEC61850-based microgrid protection. In: 2016 IEEE international conference on smart grid communications (SmartGridComm), pp 582–587. <https://doi.org/10.1109/SmartGridComm.2016.7778824>
- Xing G et al (2019) Energy consumption in relay underwater acoustic sensor networks for NDN. *IEEE Access* 7:42694–42702. <https://doi.org/10.1109/ACCESS.2019.2907693>
- Yang Z, Jianjun L, Faqiri H, Shafik W, Talal Abdulrahman A et al (2021) Green internet of things and big data application in smart cities development. *Complexity*. <https://doi.org/10.1155/2021/4922697>
- Yazdinejad A, Parizi RM, Dehghantaha A, Zhang Q, Choo KKR (2020) An energy-efficient SDN controller architecture for IoT networks with blockchain-based security. *IEEE Trans Serv Comput* 13(4):625–638. <https://doi.org/10.1109/TSC.2020.2966970>
- Yazdinejad A, Bohlooli A, Jamshidi K (2018a) Efficient design and hardware implementation of the OpenFlow v1.3 Switch on the Virtex-6 FPGA ML605. *J Supercomput* 74(3):1299–1320. <https://doi.org/10.1007/s11227-017-2175-7>
- Yazdinejad A, Bohlooli A, Jamshidi K (2018b) P4 to SDNet: automatic generation of an efficient protocol-independent packet parser on reconfigurable hardware. In: 2018b 8th international conference on computer and knowledge engineering (ICCKE), pp 159–164. <https://doi.org/10.1109/ICCKE.2018.8566590>
- Yazdinejad A, Bohlooli A, Jamshidi K (2019) Performance improvement and hardware implementation of open flow switch using FPGA. In: 2019 5th conference on knowledge-based engineering and innovation (KBEI), pp 515–520. <https://doi.org/10.1109/KBEI.2019.8734914>

- Zhang X, Zhang X, Han L (2019a) An energy-efficient internet of things network using restart artificial bee colony and wireless power transfer. *IEEE Access* 7:12686–12695. <https://doi.org/10.1109/ACCESS.2019.2892798>
- Zhang G, Shen F, Liu Z, Yang Y, Wang K, Zhou M (2019b) FEMTO: fair and energy-minimized task offloading for fog-enabled IoT networks. *IEEE Internet Things J* 6(3):4388–4400. <https://doi.org/10.1109/JIOT.2018.2887229>
- Zhao L, Zhu D, Shafik W, Matinkhah SM, Ahmad Z et al (2022) Artificial intelligence analysis in cyber domain: a review. *Int J Distrib Sens Netw* 18(4). <https://doi.org/10.1177/15501329221084882>
- Zhou K, Yang S, Shao Z (2016) Energy internet: the business perspective. *Appl Energy* 178:212–222. <https://doi.org/10.1016/j.apenergy.2016.06.052>
- Zhu CM, Leung VC, Shu L, Nga EC (2015) Green internet of things for smart world. *IEEE Access* 3:2151–2162. <https://doi.org/10.1109/ACCESS.2015.2497312>
- Zouinkhi A, Ayadi H, Val T, Boussaid B, Abdelkrim MN (2020) Auto-management of energy in IoT networks. *Int J Commun Syst* 33(1). <https://doi.org/10.1002/dac.4168>

Chapter 2

UAV-Enabled WSN and Communication Framework for Data Security, Acquisition and Monitoring on Large Farms: A Panacea for Real-Time Precision Agriculture



Oladayo O. Olakanmi, Mbadiwe S. Benyeogor, Kosisochnikwu P. Nnoli, and Kehinde O. Odeyemi

Abstract Precision agriculture necessitates the use of sensors and wireless communications technologies for data security, gathering, and analysis. However, most farms are located outside telecommunications infrastructure coverage, thereby creating challenges to their usage for precision farming. Also, the vulnerability of sensitive agricultural data to unauthorized access can undermine food security, prompting the need for a cybersecurity framework to safeguard data communications between farm-wide wireless sensor networks (FWSNs) and cloud server/ground base stations. To collect data from FWSN and relay them to the cloud server/ground base station, we adopted an unmanned aerial vehicle (UAV) to carry a special data acquisition gadget that we developed. As an intermediary airborne system, this acts as a mobile base or repeater station that relays data between farm sensor nodes and the cloud server/ground base station. We also proposed a security scheme to secure the UAV-routed data transmission between the FWSN and the cloud server/ground base station. Results show that our system reduces data traffic, improves response time, and ensures the security of the FWSN.

Supported by the Nigerian Communications Commission (NCC).

O. O. Olakanmi · K. O. Odeyemi

Department of Electrical and Electronics Engineering, University of Ibadan, Ibadan, Nigeria

e-mail: olakanmi.oladayo@ui.edu.ng

K. O. Odeyemi

e-mail: ko.odeyemi@ui.edu.ng

M. S. Benyeogor (✉)

Department of Physics, University of Münster, Münster, Germany

e-mail: mbyenyog@uni-muenster.de

K. P. Nnoli

Department of Computer Science and Electrical Engineering, Jacobs University Bremen, 28759 Bremen, Germany

e-mail: k.nnoli@jacobs-university.de

© The Author(s), under exclusive license to Springer Nature Switzerland AG 2023
J. Mabrouki et al. (eds.), *Advanced Technology for Smart Environment and Energy*,
Environmental Science and Engineering,
https://doi.org/10.1007/978-3-031-25662-2_2

Keywords Data acquisition · Edge computing · Internet of things · Precision agriculture · Unmanned aerial vehicles · Radio communication · Wireless sensor network

2.1 Introduction

Precision farming involves the collection, transmission, processing, and archiving of farm-borne data and information for efficient farm management and decision making (Abd El-kader and Mohammad El-Basioni 2013). This is based on the effective integration of smart sensors and communication technologies, such as wireless sensor networks (WSNs). The WSNs make it possible to monitor and specifically target each farm activity at a low cost, regardless of the farm's geographical area and location. However, an obstacle to precision agriculture is the limitation of readily available WSN technology, as most farms are located in regions with little or no telecommunication network coverage. Although the adoption of fixed base stations (i.e. repeaters) may solve these problems, however, this would increase the overhead cost of the project. In general, WSNs produce large amounts of sensitive data at regular intervals, which are not only susceptible to cyber attacks but also require high-bandwidth channels.

To solve these problems, we adopted the latest variant of the unmanned aerial vehicle (UAV) model in Benyeogor et al. (2022), coupled with radio or Internet capability and a secure data aggregation scheme for effective data acquisition. The UAV acts as an airborne mobile base station with integrated cyberphysical and tele-metric capabilities that extends its data communication coverage at a minimal cost (Yaqot et al. 2021; Bacco et al. 2018; Radoglou-Grammatikis et al. 2020). Each farm-wide WSN (FWSN) comprises several sensor nodes that, in turn, consist of a radio-enabled microcontroller that aggregates data from heterogeneous sensors. These low-level sensors could be used to measure farm variables such as soil fertility, moisture, pH, temperature, humidity, egg counts, animal health status and/or location. The proposed system could enable farm managers to monitor and respond to different situations on the farm in real-time via a remote server or base station with analytical front-end applications for interpreting sensors' data and proffering appropriate decisions to actors (i.e., actuation mechanisms) such as an irrigation system or other farm mechanization for effective precision farming.

2.2 Related Work

The UAV is not only capable of providing ideal remote monitoring platforms, but is also capable of solving compatibility and reliability problems in precision farming. It provides small ground sampling distances, coverage on demand, and fast turnaround of information to farmers (Jr. and Daughtry 2018). This was demonstrated in Haque

et al. (2014), where an autonomous low-weight, and low-cost UAV was developed using an Android-based flight controller. This system also uses the Google Maps application for localization, trajectory planning, and navigation.

To improve UAV performance, Daniel et al. (2015) proposed two approaches for mathematical modeling of UAV dynamics and kinematics. Their dynamics model was based on Lagrangian mechanics and Denavit-Hartenberg formulas, while their kinematic mathematical model was derived from classical mechanics equations. They applied their model for the control of one axis motion of a UAV. In Yang and Wang (2013), Runfeng and Xi introduced a novel solution for the incline detection of UAVs, which involved coupling a special robot vision camera with an inclinometer to analyze and formulate intelligent behavior for UAVs. Their system-aided a prototype UAV that is controlled by an on-board microprocessor to achieve and maintain level attitude for sustained periods of time (a crucial feat for the deployment of UAVs as airborne mobile base stations). Most of these UAVs have low battery life, poor power-material balance or are too expensive for economic use, and are therefore not suitable for use as mobile base stations for widely separated FWSNs as required for large-scale precision farming. In a closely related work, Caruso et al. investigated how near a UAV must fly over the sensors of an on-the-ground WSN to properly collect data (Caruso et al. 2021). According to them, this might be used as a criterion for selecting the suitable UAV, installing sensors at the appropriate spacing on the field, and resolving trade-offs between field size and UAV autonomy and flight path. Also, Zeng et al. explored various applications of UAVs as aerial base stations (i.e., signal amplifiers or repeaters) in future wireless communications systems, citing the cost-effectiveness of the approach (Zeng et al. 2016). Similar to this, Singh and Sharma devised a UAV-based platform for collecting and managing agricultural crop information in real-time. Singh et al. (2022). According to them, their system is 96.3% efficient and has high potential in agricultural applications such as crop health monitoring, spraying fertilizers, and pesticides. This method was experimentally explored by Lottes et al. in (2022), where they employed a machine learning-based approach for analyzing the spatial distribution of crops and weeds on farms using aerial photographs captured by a UAV.

Secondly, FWSNs could produce large amounts of sensitive data, which are not only susceptible to cyber-attacks but also require high bandwidth channels. Many security and aggregation approaches have been proposed for different networks (Geneiatakis et al. 2017; Ren et al. 2017; Tanaka et al. 2016; Zhou et al. 2019; Sivaraman et al. 2015; Olakanmi 2017; Azrour et al. 2021; Guezzaz et al. 2022). However, these aggregation schemes would be too complex for resource-constrained FWSN gateways. Meanwhile, Bayerlein et al. in (2021) proposed a multi-UAV Path Planning scheme for wireless data harvesting with deep reinforcement learning that can be adapted to various parametric changes of a data harvesting mission, such as the number of deployed UAVs, number, geospatial factors, maximum flight time, etc., without the need to perform expensive recomputations or relearn control policies. In relation to this, several approaches were already proposed to improve the observability of precision farming by enhancing data communication in FWSN systems (Olakanmi and Adama 2020; Gong et al. 2015; Saikia et al. 2017; Kim et al. 2017;

Lu et al. 2008; Kim et al. 2008; Gupta et al. 2016; Mabrouki et al. 2021). However, these favor the adoption of multipath as the best approach to developing WSN protocols for reliable data communication in FWSNs. Inline with this, Olakanmi and Adama (2020) proposed a secure multipath routing protocol based on sectorization and best-neighboring node selection models. According to them, this could satisfy the performance requirements of FWSNs in precision agriculture. Overall, multipath solutions are capable of increasing the reliability of FWSN system even though they could incur high computational and communication costs. Therefore, they are stark choices for precision farming. In essence, this suggests a dual approach involving the improvement of both the design and model of the UAV and FWSN systems, respectively, for effective data harvesting and precision farming. To solve the latter, we adopted and improved on the UAV model of Benyeogor et al. in (2022), which has demonstrates high aerodynamic efficiency, and sufficient payload carrying capacity/flight time. Hence, based on these literature, especially the works of Caruso et al. (2021); Zeng et al. (2016); Singh et al. (2022); Olakanmi (2017), the present paper focuses on employing the UAV model in Benyeogor et al. (2022) for efficient and cost effective aerial data communication in the FWSN.

2.3 Data Aggregation Scheme for FWSN Gateway

Our FWSN is clusterized into different clusters, the core of which is the gateway that consists of a microcontroller and a transceiver. The wireless transceiver serves as an access point through which data enter or exit a cluster. Each gateway aggregates the readings of its sensors and sends them to the UAV once they reach the range (≈ 100 m) during data collection. The UAV is embedded with a wireless transceiver to collect data from a specific FWSN, which comprises several sensor nodes, as shown in Fig. 2.1. The UAV semi-autonomously flies to the vicinity of the base station that houses the Farm manager server (FMS) to relay the harvested data, by means of radio telemetry. Meanwhile, the same data are uploaded to the cloud server, using a WiFi connection, once the UAV is within the coverage of the mobile network.

Each multisensor node (or simply sensor node) can comprise sensors such as a temperature sensor to measure the temperature of a farmland soil, as shown in Fig. 2.2. The soil temperature would be a good indicator to inform a farmer on how much irrigation his farmland would require. A soil moisture sensor is also included to estimate the percentage of moisture contained in a farmland soil. This enables a farmer to determine when the soil is saturated with water and when to stop irrigation. A leaf moisture sensor can also be used to estimate the average volume of moisture on the surface of a leaf, which, together with soil temperature and moisture sensors, is a pointer to the level and timing of the required irrigation. The air temperature and relative humidity sensors are sensors that could help a farmer correctly estimate the weather and atmospheric conditions of the farm. This information would further help the farmer in determining what type of crops to plant per time and when to plant such crops. Obtaining environmental farmland data from a single geographical

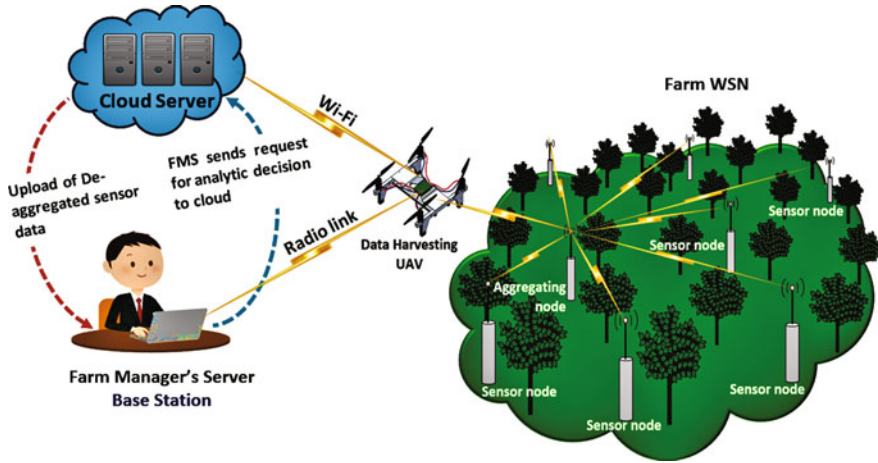


Fig. 2.1 Model of the farm wireless sensor network system

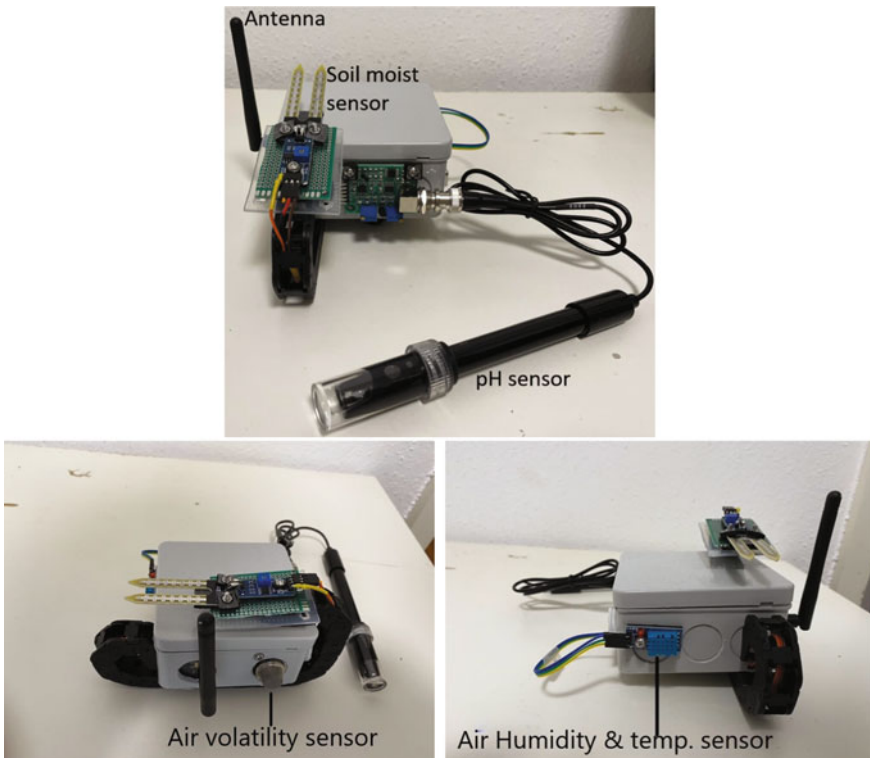


Fig. 2.2 Different views of the developed multisensor node consisting of soil pH sensor, soil moisture sensor, air volatility sensor and air humidity or temperature sensor

location is not a true picture of the overall measured phenomena. This is because the real-time values of such measured phenomena are not always uniform across a farmland. There are usually regions of peak value and regions of low values across a farmland. Therefore, it is more accurate to take measurements at multiple sites and evaluate the average values. This would provide a more accurate estimate of the environmental variables measured on farmland. An important aspect of this is how these information are securely transmitted from the FWSN gateway to the data acquisition system, before being relayed to the cloud serverbase station, at minimal computational communication cost. Therefore, we propose a data aggregation scheme that can be embedded in the cluster gateway to secure and reduce the number of transmission sessions between the gateway and the UAV. The following cryptography primitives are used in the proposed scheme.

1. **Hash Function:** A key based hash function $H(\cdot)$ is a mathematical operator that maps a message M of arbitrary length to strings of bits of fixed length (n bits) to give strings of bits of fixed length (l bits). That is, $H: \{0, 1\}^* \times \{0, 1\}^n \rightarrow \{0, 1\}^l$. It is used to generate a message digest to confirm that the content of the message has not changed. A hash function is easy to compute, has public functionality, pre-image and collision resistance.
2. **Elliptic Curve Cryptography:** Elliptic curve is a mathematical group that can be represented as: $E_q(a, b) : y^2 = x^3 + ax + b \pmod{p}$ over a prime finite field F_q , where $q > 3$, $a, b \in F_q$, and $4a^3 + 27b^2 \pmod{p} \neq 0$. It has the following properties; with a group member P and $\kappa \in Z_p^*$, the point $Q = \kappa * P$ where Q is a point on the elliptic curve, such that Q can be computed given κ_1 and P (scalar multiplication), while finding κ_1 given Q and P is infeasible. This infeasibility is known as the Elliptic Curve Discrete Logarithm Problem. Also, the addition of any points of $E_q(a, b)$ with $R \in Z_p^*$ gives a value that is not an element of $E_q(a, b)$ but an element of Z^* .

The formulated data aggregation scheme contains three algorithms; registration and key management, separable data aggregation, and de-aggregation algorithms.

2.3.1 Registration and Key Management

Registration and key management algorithm involves the generation of cryptographic key parameters for each cluster gateway (BS), Farm Manager Server (FMS) and sensors in the data harvesting system. The FMS registers each of the gateways and sensors in the FWSNs through the following steps:

- **Step 1:** The FMS randomly generates $b_k \in Z_p^*$ as master secret key for each BS k and randomly generates $a_{i,k} \in Z_p^*$ for each of the sensors i under the BS k to compute:

$$A_{i,k} = (b_k + a_{i,k})P; gp_k = b_k P,$$

where $A_{i,k}$ is the sensor's secret key and gp_k is the BS's public key.

- **Step 2:** FMS keeps a triple $\{A_{i,k}, b_k, gp_k, \kappa\}$ then publishes gp_k to the BS and securely sends a $A_{i,k}$ as $B_{i,k} = A_{i,k} \oplus \kappa$ and $Y_k = b_k \oplus \kappa$ to BS k , where session κ is the mutually generated session key between the FMS and BS generated as follows:
 - BS of each cluster randomly generates x_1 , computes, and publishes $w_1 = x_1 P$ and $q_1 = w_1 P$.
 - FMS randomly generates x_2 , computes, and publishes both $w_2 = x_2 P$ and $q_2 = w_2 P$.
 - Then, the BS computes its session key with the FMS as $\kappa = x_1 q_2$.
 - FMS also computes its session key with BS as $\kappa = x_2 q_1$.
- **Step 3:** BS decrypts $B_{i,k}$ and Y_k as: $A_{i,k} = B_{i,k} \oplus \kappa, b_k = Y_k \oplus \kappa$ and keeps a copy of $\{A_{i,k}, b_k, gp_k\}$.

2.3.2 Data Aggregation

A simple but efficient data aggregation approach is proposed for each BS to aggregate and secure their sensors data. To secure data and reduce traffic, at each synchronized interval, each sensor forwards its data $M_{i,k}$ as $m_{i,k} = M_{i,k} \oplus A_{i,k}$ to its BS, which generates the sensor aggregation parameters $D_k, \Delta_k, \tau_k, \varphi_k, \omega_k$ as follows:

- **Step 1:** BS k randomly selects $\gamma_k, \beta_k \in \mathbb{Z}_q^*$ and time stamp t_s and computes its aggregation parameters as:

$$\varphi_k = (b_k \oplus \gamma_k)$$

$$D_k = \gamma_k \oplus \beta_k$$

$$\Delta_k = H(gp_k \parallel D_k \parallel b_k)$$

$$\tau_k = D_k * \gamma_k - \beta_k$$

$$\omega_k = (b_k \oplus \beta_k \oplus t_s).$$
- **Step 2:** BS then publishes φ_k, D_k of each sensor to FMS, who will later use it for data deaggregation.
- **Step 3:** BS aggregates all sensor data $m_{i,k}$ in the synchronized interval as $\rho_k = \sum_{i=1}^n m_{i,k}$
- **Step 4:** Signs the aggregated data as $\sigma_k = (H_{b_k}(\varphi_k \parallel \omega_k \parallel \beta_k \parallel t_s \parallel \tau_k \parallel \rho_k) \parallel \Delta_k)$
- **Step 5:** For each sensor data $m_{i,k}$ BS computes the aggregation ratio $\hat{h}_{i,k}$ as $\hat{h}_{i,k} = \frac{m_{i,k}}{\min(m_{1,k}, \dots, m_{n,k})}$ and computes the signature ratio η as $\eta_{i,k} = \sigma_k * \hat{h}_{i,k}$
- **Step 6:** BS uploads $\rho_k \parallel \sigma_k \parallel (\eta_{1,k} \parallel \dots \parallel \eta_{n,k} \parallel \parallel \varphi_k \parallel D_k$ to the harvester as their aggregated data, who then transfers them to FMS.

2.3.3 Data De-Aggregation

The major problem with most existing aggregation schemes is how the receiver separates the individual data from the aggregated data received. To obtain individual sensor data from the aggregated data received, we developed the following separation procedure for the aggregation scheme as follows.

- **Step 1:** FMS recomputes $\tau'_k, \omega'_k, \Delta_k, t_s$ as:

$$\begin{aligned}
 - \gamma'_k &= \varphi_k \oplus b_k \\
 - \beta'_k &= D_k \oplus \gamma'_k \\
 - t'_s &= \omega_k \oplus t_s \oplus b_k \oplus \beta'_k \\
 - \tau'_k &= D_k * \gamma'_k - \beta'_k \\
 - \Delta'_k &= H(gp_k \parallel D_k \parallel b_k) \sigma'_k = (H_{b_k}(\varphi'_k \parallel \omega'_k \parallel \beta'_k \parallel t'_s \parallel \tau'_k \parallel \rho'_k) \parallel \Delta'_k)
 \end{aligned}$$

- **Step 2:** FMS checks if the computed $\sigma'_k = \sigma_k$, accepts the aggregated data ρ_k and proceeds to step 3, otherwise rejects ρ_k .
- **Step 3:** To deaggregate the aggregated data ρ_k , for each sensor, FMS extracts the signature ratio $\eta_{i,k}$ from the cluster data $\rho_k \parallel \sigma_{i,k} \parallel (\eta_{1,k} \parallel \dots \parallel \eta_{m,k})$ to calculate the aggregation ratio $\hat{h}_{i,k}$ as $\hat{h}_{i,k} = \frac{\eta_{i,k}}{\sigma'_{i,k}}$, and generates the sensor data $m_{i,k} = \frac{\eta'_{i,k} * \min(m_{1,k}, m_{2,k}, \dots, m_{n,k})}{\sigma_k}$.
- **Step 4:** Decrypts $m_{i,k}$ to obtain $M_{i,k} = m_{i,k} \oplus A_{i,k}$.

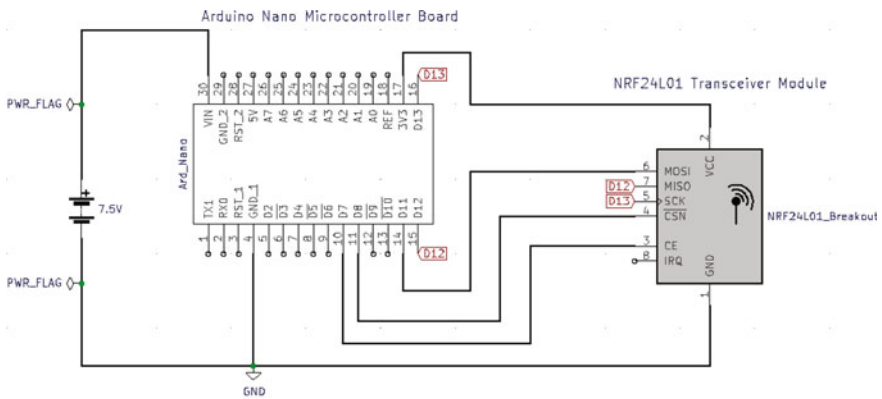
FMS repeats steps 1–4 for each of the sensors in each cluster to obtain their data. FMS securely sends the de-aggregated data to the cloud server for analytical requests from actors. Possible technological processes by which these data packages could be communicated between the various FWSN gateways and the data acquisition system, and between the latter and the cloud server or base station are explained in Sect. 2.4.

2.4 Farm Wireless Sensor Network System

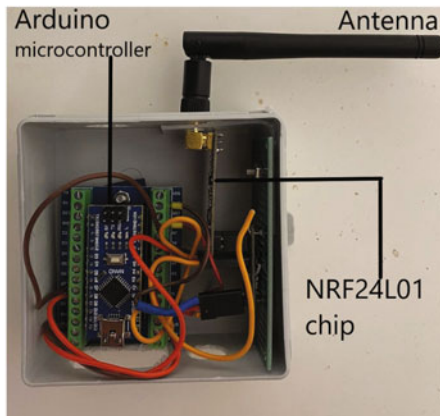
For the purpose at hand, the UAV serves to transport the data acquisition system (as its only payload) to FWSNs for proximity data harvesting. This involves the integration of ground-based and airborne instrumentation or telematic systems to form an intelligent FWSN system over the entire farmland to collect information about the state of farm animals or plantations in real-time. For efficient wireless transmission or acquisition of information in FWSN systems, the combination of radio, serial Bluetooth, and WiFi communication is used. The radio communication medium is operated within the industrial scientific medical (ISM) range of bands. Using this medium, it was possible to relay the pre-processed data from various FWSN to the cloud server and base station for further analysis. The various communication models, protocols, and circuitry designs of this system are technically described as follows.

2.4.1 Farm Wireless Sensor Network (FWSN)

The hardware implementation of this system comprises a central microcontroller that is digitally interfaced with an NRF24L01 transceiver module, as shown in Fig. 2.3. The operational parameters of this system are given in Table 2.1. This is a *RF* front-end device that can be programmed to function as a transmitter or receiver, or a combination of both. In addition, it enables the interconnection of several similar transceiver modules, which could be used to set up a WSN cybernetics and cyber-physical system. In the current work, it is configured to harvest sensors' data from a given FWSN and transmit them as a single data package to the data acquisition system on the UAV.



(a) Circuit diagram of microcontroller based NRF24L01 transceiver system



(b) Constructed NRF24L01 transceiver module

Fig. 2.3 The NRF24L01 transceiver module

Table 2.1 Parameters for radio transmission of data packages using the NRF24L01 transceiver module

S/N	Parameter	Value
1	Frequency range	2.4–2.5 GHz
2	Radiation power	8 dBm
3	Transmission rate	250 kbps–2 Mbps
4	Effective range	≈ 100 m
5	Available no. of channels	125
6	Possible addresses/channel	6

2.4.2 Data Acquisition System

This is the IoT-based or radio communication system that is onboard the UAV, which constitutes the augmentation of the NRF24L01 transceiver system in Fig. 2.3 with the WiFi ESP32 WiFi module. Its function is to receive data packages from the FWSN transmitter and then relay them to the base station and a cloud server via the RF communication channel and WiFi connectivity, respectively. The WiFi ESP32 WiFi module is adopted for the latter to effectively extend the capability of the RF communication medium and transmit the same data package to a remote server or beyond the LoS cloud server via the Internet. To implement the software components of the FWSN system, the security scheme in Sect. 2.3 is used and consists of the data aggregation and deaggregation algorithms (including intrinsic security features) that are core components of the software layer of the FWSN system. In pseudocode, these computational processes are simplified to Algorithms 1 and 2 for the transmitter (ground-based) and receiver (airborne) ends, respectively, of the FWSN system.

2.5 Performance Analysis

Our practical demonstration of this FWSN system is captured in Fig. 2.4, which entails real-time streaming and visualization of sensors data from a single multisensor node deployed in our experimental farm. This shows the applicability of the system for the collection, transmission, classification, visualization, and increase in response speed of farm data. This telemetric method was applied in the field evaluation of the complete FWSN system. Several sensor nodes were geospatially sampled at different locations of the FWSN. The results of these are discussed below.

Algorithm 1 Data aggregation and transmission

Require: *moist_sensor*, *temp_sensor*, *Channel_Address*,
Require: *pH_sensor*, *gas_sensor*
Ensure: *data_package*

- 1: **Activate** RADIO_PROTOCOL
- 2: **Assign** port (7,8) \leftarrow (*CE*, *CSN*)
- 3: **function** SETUP_FUNC ▷ Sets device as transmitter
- 4: **Open** RADIO_WRITE
- 5: **Stop** LISTENING_MODE
- 6: **end function**
- 7: **repeat** ▷ Transmission iteration
- 8: **function** AGGREGATION(*data_package*)
- 9: $\rho = \text{humi} + \text{temp} + \text{pH} + \text{conc}$
- 10: $\text{temp_ratio} = \frac{\text{temp}}{\min(\text{humi}, \text{temp}, \text{pH}, \text{conc})}$
- 11: $\text{humi_ratio} = \frac{\text{humi}}{\min(\text{humi}, \text{temp}, \text{pH}, \text{conc})}$
- 12: $\text{conc_ratio} = \frac{\text{conc}}{\min(\text{humi}, \text{temp}, \text{pH}, \text{conc})}$
- 13: $\text{pH_ratio} = \frac{\text{pH}}{\min(\text{humi}, \text{temp}, \text{pH}, \text{conc})}$
- 14: $\sigma_k = (H_{b_k}(\varphi_k \parallel \omega_k \parallel \beta_k \parallel t_s \parallel \tau_k \parallel \rho_k) \parallel \Delta_k)$
- 15: $\text{temp_sign_ratio} = \text{temp_ratio} * \sigma_k$
- 16: $\text{conc_sign_ratio} = \text{conc_ratio} * \sigma_k$
- 17: $\text{humi_sign_ratio} = \text{humi_ratio} * \sigma_k$
- 18: $\text{pH_sign_ratio} = \text{pH_ratio} * \sigma_k$
- 19: $\text{data_package} = \rho_k \parallel \sigma_k \parallel (\text{temp_sign_ratio} \parallel \text{temp_sign_ratio} \parallel$
 $\text{humi_sign_ratio} \parallel \text{conc_sign_ratio} \parallel \text{pH_sign_ratio} \parallel \varphi_k \parallel D_k)$
- 20: **end function**
- 21: **while using** *Channel_Address do* ▷ Transmits data package to receiver
- 22: **Bulk_Transmit** *data_package*
- 23: **end while**
- 24: **until** (*false*) ▷ Iteration logic

2.5.1 Quantity-Specific Geospatial Sensing

Having demonstrated the visualization of sensors' data at each node, we also demonstrated the practicality of large-scale data harvesting on large farms, based on the model in Fig. 2.1. To do this, data from a specific type of sensor in 10 different multisensor nodes installed at different geographical locations in a FWSN are collected and sampled. Here, we harvested data from the soil humidity sensor, temperature sensor, pH sensor, and air volatility sensor of each multisensor node in the FWSN. Coupled with the geographical positions of each these nodes as shown in Fig. 2.5a, the values of which were predetermined during their installation, the 3D bar charts in Fig. 2.5b–d visualizes the geospatial variation of soil humidity, soil temperature, soil pH, (at a depth of 20 cm), and air volatile organic compound (VOC) concentration (such as methane, carbon dioxide, smoke, etc.) across the farmland. For instance, Fig. 2.5d allows us to assess the atmospheric chemical profile and perform an air quality assessment of the geographical location of the farm. This method provides geospatial situational awareness of various environmental changes on the farm for effective and progressive planning.

Algorithm 2 De-aggregation and re-transmission

Require: *data_package, Channel_Address, IP_Address, Port_Address*
Ensure: *serial_data, data_package*

```

1: Activate RADIO_PROTOCOL
2: Activate WIFI_PROTOCOL
3: Activate SERIAL_COM ▷ For Bluetooth USB com.
4: Assign port (7,8) ← (CE, CSN)
5: function SETUP_FUNC ▷ Sets device as receiver
6:   Open RADIO_READ
7:   Open WIFI_GATEWAY
8:   Open SERIAL_PORT
9:   Start LISTENING_MODE
10: end function
11: repeat ▷ Acquisition iteration
12:   if Radio_Signal AVAILABLE then
13:     while using Channel_Address do
14:       Fetch data_package ▷ From transmitter
15:     end while
16:     while using Port_Address do ▷ To serially transmit data to FMS station
17:       Serial_Transmit (data_package)
18:       function DEAGGREGATION(data_package)
19:          $temp = \frac{temp\_sign\_ratio * \min(humi, temp, conc, pH)}{\sigma_k}$ 
20:          $conc = \frac{conc\_sign\_ratio * \min(humi, temp, conc, pH)}{\sigma_k}$ 
21:          $humi = \frac{humi\_sign\_ratio * \min(humi, temp, conc, pH)}{\sigma_k}$ 
22:          $pH\_ratio = \frac{pH\_sign\_ratio * \min(humi, temp, conc, pH)}{\sigma_k}$ 
23:          $deaggregate\_data\_package = temp, humi, conc, pH$ 
24:       end function
25:     end while
26:     while using IP_Address do ▷ Transmits data package to cloud
27:       Bulk_Transmit data_package
28:     end while
29:   end if
30: until (false)

```

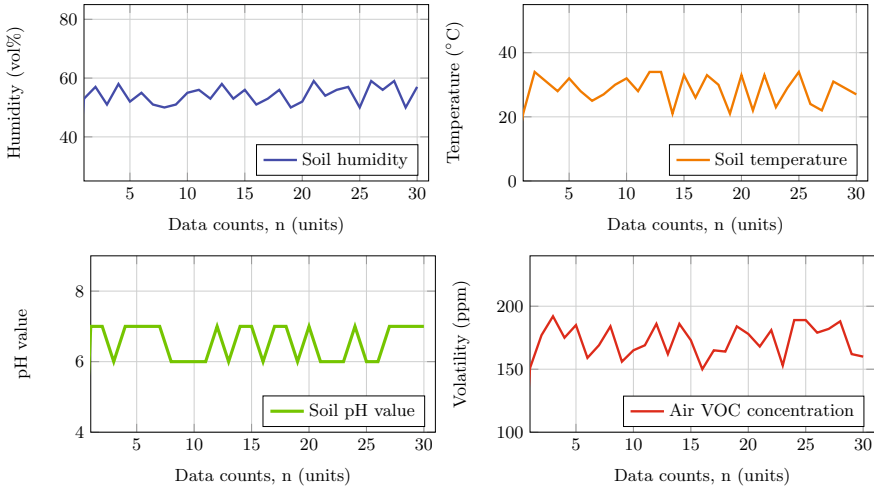
2.5.2 Evaluation of FWSN System

To test the performance of the FWSN system (incorporating the FWSN gateways, data acquisition system, and aggregation schemes), we used three 50 by 100m farmlands each with twenty different wireless sensors with a communication range between 75 and 100m. Also, to evaluate the effect of the data acquisition system and our schemes (i.e., Algorithms 1 and 2) on the turnaround of the sensors' data, we measured the average round trip time of the sensors to two cloud servers with and without the aggregation scheme. Figure 2.6 shows the average round-trip time for various numbers of sensors data of different 32-byte size harvested, aggregated and uploaded to Google (note that t_1 denotes the time latency for data transmission with the data harvester aggregation scheme while t_2 denotes data without two entities). These analyzes reveal that the data aggregation scheme reduces the average round-

```

File Edit Setup Control Window Help
n, soil_humidity, soil_temperature, soil_ph, voc_concentration
0, 0.00, 0.00, 0.00, 0.00
1, 52.00, 24.00, 7.00, 151.00
2, 52.00, 34.00, 7.00, 172.00
3, 51.00, 31.00, 6.00, 192.00
4, 52.00, 28.00, 7.00, 175.00
5, 52.00, 32.00, 7.00, 185.00
6, 55.00, 28.00, 7.00, 159.00
7, 51.00, 25.00, 7.00, 169.00
8, 50.00, 27.00, 6.00, 184.00
9, 51.00, 30.00, 6.00, 156.00
10, 55.00, 32.00, 6.00, 165.00
11, 56.00, 28.00, 6.00, 169.00
12, 53.00, 34.00, 7.00, 186.00
13, 58.00, 34.00, 6.00, 162.00
14, 52.00, 21.00, 7.00, 186.00
15, 56.00, 32.00, 7.00, 173.00
16, 51.00, 26.00, 6.00, 150.00
17, 52.00, 33.00, 7.00, 165.00
18, 56.00, 30.00, 7.00, 164.00
19, 50.00, 21.00, 6.00, 184.00
20, 52.00, 33.00, 7.00, 178.00
21, 59.00, 22.00, 6.00, 168.00
22, 54.00, 33.00, 6.00, 181.00
23, 56.00, 23.00, 6.00, 153.00
24, 57.00, 29.00, 7.00, 189.00
25, 50.00, 34.00, 6.00, 182.00
26, 59.00, 22.00, 6.00, 179.00
27, 56.00, 22.00, 7.00, 182.00
28, 59.00, 31.00, 7.00, 188.00
29, 50.00, 29.00, 7.00, 162.00
30, 57.00, 27.00, 7.00, 160.00
    
```

(a) Real-time streaming of farm data using the FWSN



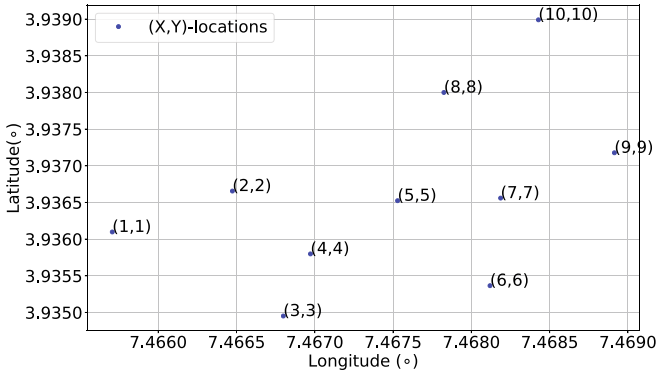
(b) Visualization of sensors data from a single node in the FWSN

Fig. 2.4 Practical demonstration of farm data acquisition with the FWSN system

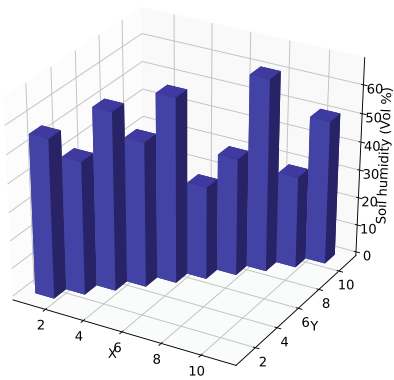
trip time, regardless of the number of sensors on the farm compared to when the data aggregation scheme is not engaged. This indicates that the use of the developed data aggregation scheme improves the data harvester in terms of latency and traffic.

2.5.3 Latency of RF-Based Data Transmission

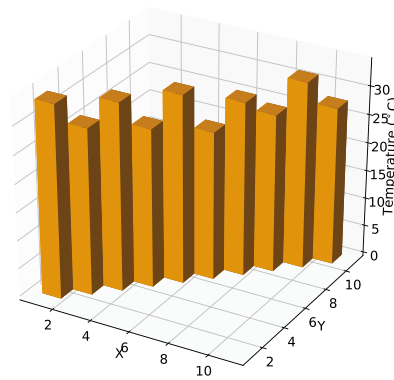
To determine the rate at which multisensor data packages are transmitted, communication latency analysis is performed as a function of the number of sensors in a node.



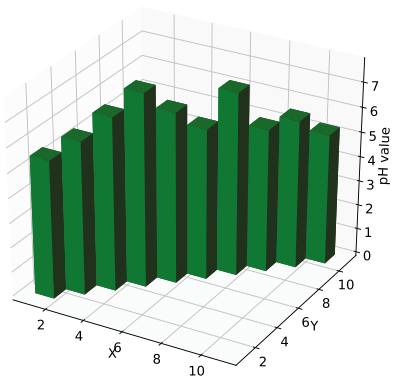
(a) Real-time locations of different FWSN nodes



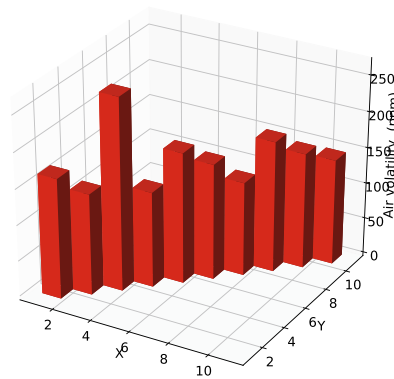
(b) Soil humidity



(c) Soil temperature



(d) Soil pH value



(e) VOC concentration

Fig. 2.5 Visualization of geospatial variations of environmental changes on the farm

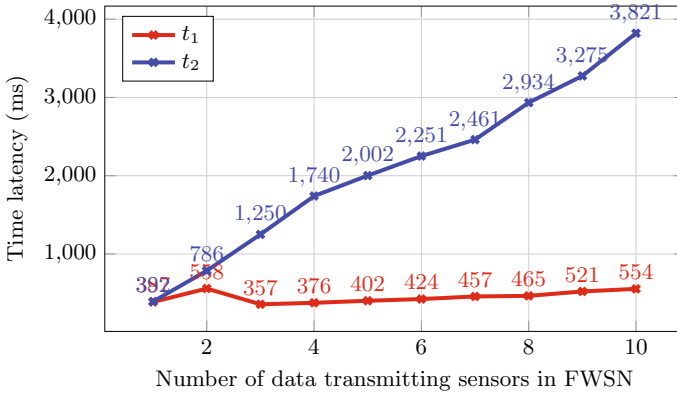


Fig. 2.6 Comparison in the average round trip time (i.e., time latency) between FWSN and Google cloud with and without data harvester and aggregation for different sensors

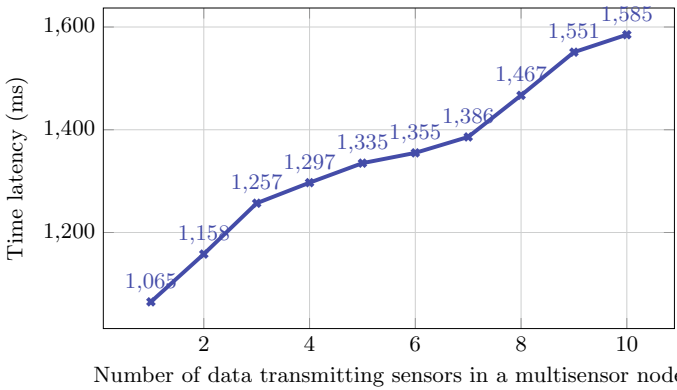


Fig. 2.7 Latency of RF-based data transmission (From node, through gateway, to base-station)

Figure 2.7 shows a latency of 1.1 s for 1 sensor and 1.3 s for 4 sensors is real-time and applicable to precision agriculture, based on the scope and technical requirements of our experimental farm.

2.6 Conclusion

This paper presents low-cost technological capabilities that could be used to monitor and improve agricultural productivity. These include the development of modular multisensor data acquisition systems, reliable mid-range and long-range communication technologies, and software-oriented security schemes (for secure transmission and processing of information), coupled with the adoption of UAVs as mobile base

stations. Experiments were performed to ascertain the applicability of the system to modern agriculture. The preliminary results show that the developed system is robust and effective for real-time precision agriculture. In addition, deployment tests show that the adopted UAV has effective hovering capability over a particular location for the onboard data acquisition system to relay farm sensors' data. Meanwhile, the aggregated scheme, the associated edge computing and communication systems have high reliability to secure the telemetry of farm data while reducing communication traffic between the farm multisensor nodes and the cloud server or base station. Therefore, we hope that the present work incites interest in the developed system and the general applications of electronics and computing to agriculture. In view of this, we envisage that this work would also improve scientific collaborations between scientists, engineers, and farmers to fully exploit the capabilities of the developed FWSN system.

References

- Abd El-kader SM, Mohammad El-Basioni BM (2013) Precision farming solution in Egypt using the wireless sensor network technology. *Egypt Inform J* 14(3):221–233
- Azrou M, Mabrouk J, Guezaz A, Kanwal A (2021) Internet of things security: challenges and key issues. *Secur Commun Netw* 2021:1–11
- Bacco M, Berton A, Gotta A, Caviglione L (2018) IEEE 802.15.4 air-ground UAV communications in smart farming scenarios. *IEEE Commun Lett* 22(9):1910–1913
- Bayerlein H, Theile M, Caccamo M, Gesbert D (2021) Multi-UAV path planning for wireless data harvesting with deep reinforcement learning. *IEEE Open J Commun Soc* 2:1171–1187
- Benyeogor MS, Olakanmi OO, Nnoli KP, Odeyemi KO, Gratton EJ (2022) Supplementary material: optimization of low-weight cargo UAV with real-time controller by CAD design, FEM simulation and dynamic modeling. <https://dx.doi.org/10.21227/7gkv-3h45>. *IEEE Dataport*
- Caruso A, Chessa S, Escolar S, Barba J, López JC (2021) Collection of data with drones in precision agriculture: analytical model and LoRa case study. *IEEE Internet Things J* 8(22):16692–16704
- Geneiatakis D, Kounelis I, Neisse R, Nai-Fovino I, Steri G, Baldini G (2017) Security and privacy issues for an IoT based smart home. In: 2017 40th international convention on information and communication technology, electronics and microelectronics (MIPRO), pp 1292–1297
- Gheorghita D, Vintu I, Mirea L, Braescu C (2015) Quadcopter control system. In: 2015 19th international conference on system theory, control and computing (ICSTCC), pp 421–426
- Gong W, Zhang M, Yang X, Li J, Zhang N, Long K (2015) Waras: an adaptive WSN multipath selection model inspired by metabolism behaviors of *Escherichia coli*. In: 2015 IEEE/CIC international conference on communications in China (ICCC), pp 1–6
- Guezaz A, Benkirane S, Azrou M (2022) A novel anomaly network intrusion detection system for internet of things security. In: *IoT and smart devices for sustainable environment*. Springer, Berlin
- Gupta SK, Kuila P, Jana PK (2016) Energy efficient multipath routing for wireless sensor networks: A genetic algorithm approach. In: 2016 International conference on advances in computing, communications and informatics (ICACCI), pp 1735–1740
- Haque MR, Muhammad M, Swarnaker D, Arifuzzaman M (2014) Autonomous quadcopter for product home delivery. In: 2014 international conference on electrical engineering and information & communication technology, pp 1–5
- Hunt Jr ER, Daughtry CST (2018) What good are unmanned aircraft systems for agricultural remote sensing and precision agriculture? *Int J Remote Sens* 39(15–16):5345–5376

- Kim S, Cho H, Yang T, Kim C, Kim S (2017) Low-cost multipath routing protocol by adapting opportunistic routing in wireless sensor networks. In: 2017 IEEE wireless communications and networking conference, WCNC 2017, San Francisco, CA, USA, March 19–22, 2017. IEEE, pp 1–6
- Kim M, Jeong E, Bang Y-C, Hwang S, Kim B (2008) Multipath energy-aware routing protocol in wireless sensor networks. In: 2008 5th international conference on networked sensing systems, pp 127–130
- Lottes P, Chebrolu N, Liebisch F, Stachniss C (2022) UAV-based field monitoring for precision farming. In: 25th workshop on computer image analysis in agriculture. <https://www.ipb.uni-bonn.de/wp-content/papercite-data/pdf/lottes2019cbaws.pdf>. Accessed 9 Oct 2022
- Lu Y, Wang G, Jia W, Peng S (2008) Multipath-based segment-by-segment routing protocol in manets. In: 2008 The 9th international conference for young computer scientists, pp 527–532
- Mabrouki J, Azrou M, Hajjaji SE (2021) Use of internet of things for monitoring and evaluation water's quality: comparative study. *Int J Cloud Comput* 10:633–644
- Olakanmi OO, Adama P (2020) An efficient multipath routing protocol for decentralized wireless sensor networks for mission and safety-critical systems. *Int J SensS, Wirel Commun Control* 2020 10. <https://doi.org/10.2174/2210327909666190531113558>
- Olakanmi O (2017) Secure and privacy-oriented obfuscation scheme for smart metering in smart grid via dynamic aggregation and lightweight perturbation. *Int J Inf Priv, Secur Integr* 3(1):38–57
- Radoglou-Grammatikis P, Sarigiannidis P, Lagkas T, Moscholios I (2020) A compilation of UAV applications for precision agriculture. *Comput Netw* 172:107148
- Ren Z, Liu X, Ye R, Zhang T (2017) Security and privacy on internet of things. In: 2017 7th IEEE international conference on electronics information and emergency communication (ICEIEC), pp 140–144
- Saikia M, Das UK, Hussain M (2017) Secure energy aware multi-path routing with key management in wireless sensor network. In: 2017 4th international conference on signal processing and integrated networks (SPIN), pp 310–315
- Singh PK, Sharma A (2022) An intelligent WSN-UAV-based IoT framework for precision agriculture application. *Comput Electr Eng* 100:107912
- Sivaraman V, Gharakheili HH, Vishwanath A, Boreli R, Mehani O (2015) Network-level security and privacy control for smart-home IoT devices. In: 2015 IEEE 11th international conference on wireless and mobile computing, networking and communications (WiMob), pp 163–167
- Tanaka S, Fujishima K, Mimura N, Ohashi T, Tanaka M (2016) IoT system security issues and solution approaches. *Hitachi Rev* 65(8)
- Yang R, Wang X (2013) Vision control system for quadcopter. In: 2013 IEEE third international conference on information science and technology (ICIST), pp 261–264
- Yaqot M, Menezes BC (2021) Unmanned aerial vehicle (UAV) in precision agriculture: Business information technology towards farming as a service. In: 2021 1st international conference on emerging smart technologies and applications (eSmarTA), pp 1–7
- Zeng Y, Zhang R, Lim TJ (2016) Wireless communications with unmanned aerial vehicles: opportunities and challenges. *IEEE Commun Mag* 54(5):36–42
- Zhou W, Jia Y, Peng A, Zhang Y, Liu P (2019) The effect of IoT new features on security and privacy: new threats, existing solutions, and challenges yet to be solved. *IEEE Internet Things J* 6:1606–1616

Chapter 3

Investigation of the Energy and Emission from the Combustion of Argain Cake in a CHP System



Ayoub Najah EL Idrissi, Mohammed Benbrahim, and Nadia Rassai

Abstract This study aims to recycle Moroccan argain waste in a small-scale furnace in order to generate electricity using a Stirling engine. To that end, the physico-chemical properties of argain waste were determined and the results were compared with other studies of argain nut and olive cake and computational fluid dynamics (CFD) modeling of argain cake combustion was presented, the temperature and CO₂ emissions, were illustrated and discussed.

Keywords Biomass · Combustion · Stirling engine

3.1 Introduction

Nowadays, in the field of energy All communities share the goal of producing sustainable energy at the lowest feasible cost and having the minimum possible impact on the environment. From 2005 to 2050, the world plans to reduce CO₂ emissions in half, hence many studies and research are aimed at reducing greenhouse CO₂ emissions by introducing revolutionary technology. Certainly, fossil fuels have a higher energy density, but their effects on the environment humans and animals force us to stop using them immediately and look for other combustibles. Agricultural residue is an alternative solution might be used to generate energy from a natural resource with low emission Using the thermochemical conversion process.

The use of a CFD tool to model the combustion is an alternative method for investigating the behavior of gas inside the combustion chamber of the furnace, such as velocity, temperature, pressure flow gas, and concentration species, and can

The original version of this chapter has been revised: The name of corresponding author of chapter 3 has been corrected from Ayoub Najah ELIdrissi to Ayoub Najah EL Idrissi. The correction to this chapter is available at https://doi.org/10.1007/978-3-031-25662-2_26

A. N. EL Idrissi (✉) · M. Benbrahim · N. Rassai
Advanced Systems—Engineering Laboratory—National School of Applied Science, Ibn Tofail University, University Campus, Po Box 242, Kenitra, Morocco
e-mail: ayoub.najahelidrissi@uit.ac.ma

© The Author(s), under exclusive license to Springer Nature Switzerland AG 2023, 35
corrected publication 2023

J. Mabrouki et al. (eds.), *Advanced Technology for Smart Environment and Energy*,
Environmental Science and Engineering,
https://doi.org/10.1007/978-3-031-25662-2_3

simulate their interaction (Silva et al. 2017). The results show that the CFD calculation is an efficient tool for as it reasonably predicts the emissions of carbon monoxide and CO₂ inside the furnace.

As well as CHP systems that produce heat and power is an innovative and efficient new technology that is compatible with the use of agricultural waste as combustible (Ding et al. 2021). Combining a biomass furnace and a Stirling engine is one option for building this kind of system (Marra et al. 2020). The Stirling Engine is a closed-cycle heat and external combustion engine that converts thermal energy to mechanical work. A Stirling engine is, often used to generate electricity or mechanical work.

The recent tests confirmed that this combination produces good results. For example in 2021, KRAMENS studied the energy yielded from 1 kg of wood, and as a result, this quantity was able to create 2.23 kwh of thermal energy and 7.84 Wh of electricity, and the electrical power generated at 600 °C was 590 Wh, the temperature of the combustion chamber was measured using a thermal camera, and it was discovered that there was a direct relationship between the temperature and the electrical power generated (Kramens et al. 2021) also, in Rassai et al. (2018) evaluated the influence of olive size and air excess at the combustion process, using a small-scale CHP system with a Stirling engine and a furnace, and the simulation was done in Ansys fluent. As a result, the temperature was greater with the short size olive and high air excess rate (Rassai et al. 2018).

3.2 General Framework

This study aim:

- To estimate the energy produced from the Argan residue at Essaouira region measuring the HHV for different moisture.
- To compare between argain waste argain nut and olive cake.
- To study the suitability for using Argan cake as substituted for olive cake and argain nut by discussing the composition, Temperature and emissions.
- To use the Stirling engine to convert the thermal energy present in the argain cake to electrical energy.
- To compare between an olive cake, argain nut and Argan residu and define the most suitable for a CHP system.
- To optimise the Argan cake combustion.
- To simulate the energy and emissions of argain and compare the results with other studies.

This study will be treated as illustrated in Fig. 3.1.

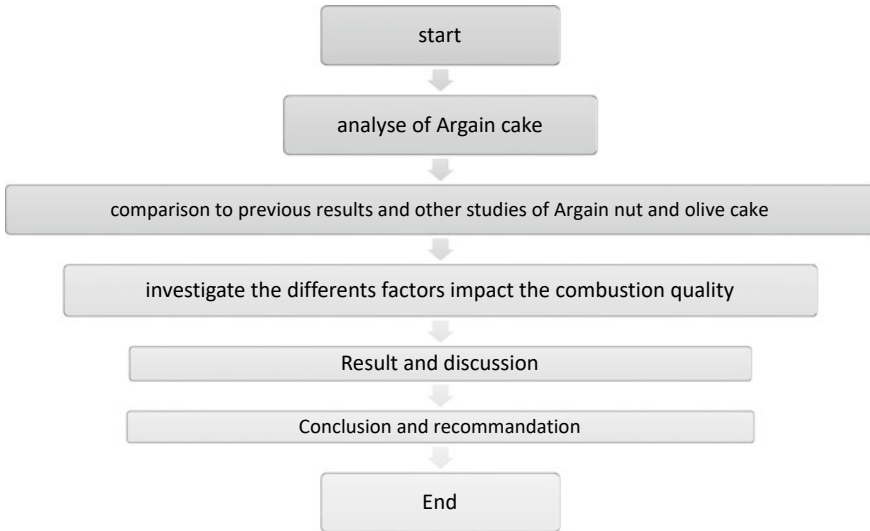


Fig. 3.1 Diagram of the sequence study

3.3 Materiel and Method

3.3.1 *Materials, Sample Preparation Analysis and Measurement*

Argain cake is a by-product of the Argain kernels pressing process (Zouhair et al. 2020); it is regarded as an agricultural resource capable of being used as a biofuel; 1 kg Argain nut yields 70 g of cake, accounting for 70% of the total mass. The sample was collected from a local association in Essaouira City in May 2022. The sample were dried at 101 °C, grinded, pulverized and passed through a sieve of 0.15 mm, then collected for analysis and measurement. Argain cake storage is simple and requires no special equipment; it can be kept at room temperature.

Measure moisture:

In the absence of a moisture meter, we use a traditional method to determine the moisture content of our argain cake using the following formula:

$$\%(moistute) = \frac{m(water)}{m(sample)} \times 100.$$

using the analytical balance (KERN ALS 220-4 N) We dried 10 g measured of sample for 4 h in a lab furnace and set his temperature to 100 °C, then measured the final mass, which was 9.5 g, then the moisture content of the sample was 5 g (Figs. 3.2, 3.3).

Measure HHV

The HHV of the argain cake was measured using a Parra 6200 calorimeter, which will automatically generate its energy equivalent value from a series of calculations, with the operator determining the initial condition as the sample's mass and temperature.

The calorimeter also calculates the sulfur value; no sulfur was detected in Argain cake. No corrosive element was existed.

Fig. 3.2 6200 calorimeter



Fig. 3.3 Argain nut and cake



Table 3.1 Proximate analysis (wt.%)

Volatile matter (%)	Fixed carbon (%)	Moisture (%)	Ash (%)
60	26.5	5.5	8

Table 3.2 Ultimate analysis (wt.%)

Carbon (%)	Nitrogen (%)	Oxygen (%)	Hydrogen (%)	Suffer
49	0.5	45	5.5	0

Accurate results from proximate and ultimate Argain Cake analysis are crucial for characterizing the biomass. Ultimate analysis tests produce more comprehensive results than the proximate analyses. The carbon/hydrogen/suffer/Nitrogen percentage of Argain Cake was determined using the *Elementrac* analyzer for the organic sample and the ash, volatile matter, and fixed carbon of the Argain cake received sample were measured using a thermogravimetric analyzer TGA thermostep (Tables 3.1, 3.2 and Fig. 3.4).

Result

Three measurements were taken, and the results were approximate with a margin of error of 5%. The moisture of the sample as received was 10% and the HHV obtained was 16.8 MJ/kg. But after drying the sample of argain cake until it reached a moisture content of 5.5% the HHV improved until 22.68 MJ/kg (Table 3.3).

Effect of moisture on HHV

The HHV values vary in direct proportion to the moisture content of the biomass. The change is not linear. For greater precision, the final HHV value was the average

Fig. 3.4 HHV result after calorimeter measurement

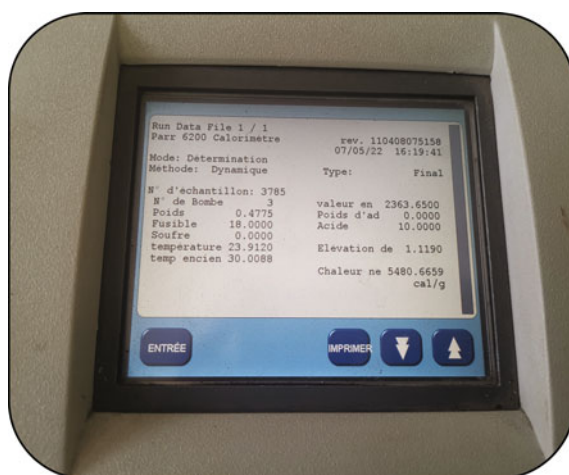
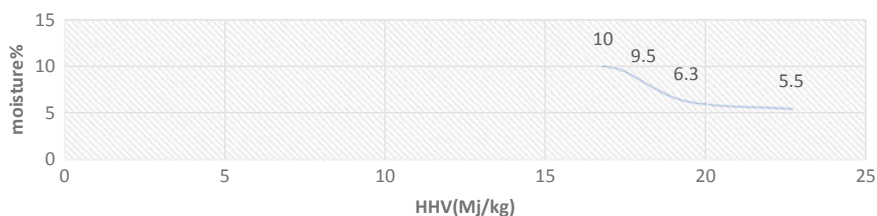
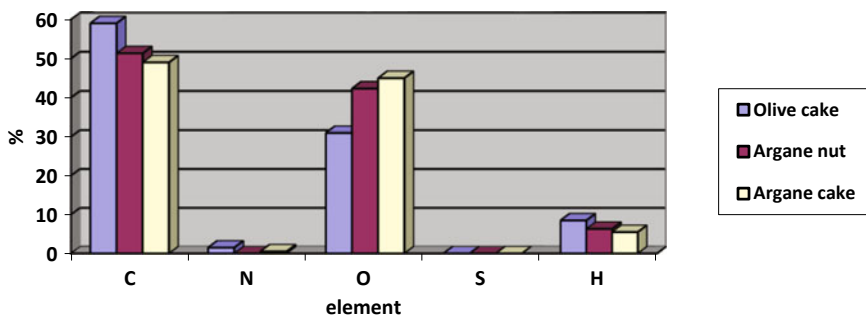


Table 3.3 Moisture impact on HHV for different values

Moisture (%)	HHV (Mj/Kg)
10 (as received basis)	16.8
9.5	17.4
6.3	19.4
5.5	22.68

**Fig. 3.5** The impact of moisture on biomass HHV

of the three measurements. It is noted that there is a 5% margin of error (Figs. 3.5, 3.6 and Table 3.4).

**Fig. 3.6** Comparison of proximate analysis of the three biomasses**Table. 3.4** Proximate analysis of the three biomasses

Elements	C	N	O	S	H
Olive cake	59	1.5	31	0	8.5
Argain nut	51.33	0.005	42.34	0	6.32
Argain cake	49	0.5	45	0	5.5

3.3.2 *Physic Chemical Properties Comparison (Rahib et al. 2019; Elorf et al. 2022)*

- Argan cake yields 52.2% less CO₂ than argan nut.
- Argan nut yields 70% more CO than olive cake.
- And the same way using to H₂, H₂O N₂ concentration (Table 3.5 and Fig. 3.7).

Comparison Ash emission between the Argan cake and olive cake.

- Argan cake shell is not preferable to olive cake for reducing slag formation after combustion because it contains more ash. However, because they contain a higher amount of volatile matter, it is not recommended to avoid the formation of ash fly.
- As received basis, the argain nut shell contains more moisture than the olive cake, which can have a negative impact on combustion and burn more fuel to dewater the H₂O particles.
- The lower fixed carbon values indicate their easiness of combustion and ignition.

The cause of the variation between result

The HHV is the main parameter indicating a combustible's thermal energy, and it is reduced by high moisture or vice versa because it slows the burning rate. The HHV values of the three biomasses are close, but with different moisture percentages.

Volatile matter: Volatile matter is a major health and safety concern because samples high in volatiles are more likely to spontaneously combust.

Fixed carbon: The sample's fixed carbon content is calculated by deducting the percentages of moisture, volatile matter, and ash from the original mass of the Argain cake sample. A lower value indicates that ignition and combustion are easier.

Table 3.5. Ultimate analysis of the three biomasses

Elements	Moisture (%)	Volatile matter (%)	Fixed carbon (%)	Ash (%)
Olive cake	6.3	64	23.2	6.5
Argain nut	9.5	67.5	21.5	1.5
Argain cake	5.5	60	26.5	8

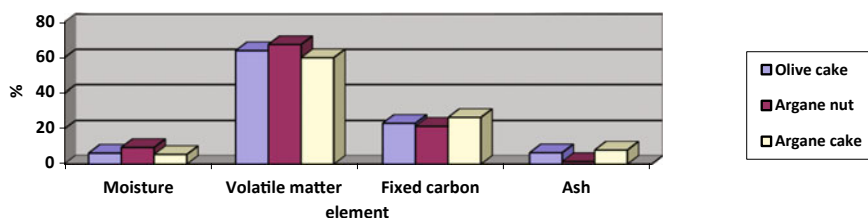


Fig. 3.7 Comparison of ultimate analysis of the three biomasses

Fig. 3.8 Model of the adaptable Stirling engine (alpha)

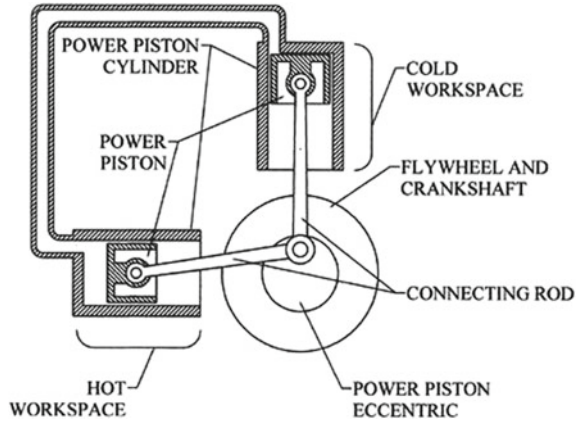


Table 3.6 Properties of the used α -type Stirling engine

Heat input (j/cycle)	Power output (W)	Power output (j/cycle)	Thermal efficiency (%)
273	4125	98.5	39.5

Ash content: responsible for the formation of slag inside the furnace during combustion. The biomass contains the most value of ash and volatile matter is the most pollutant of combustion.

The presence of a high percentage of carbon and hydrogen raises the combustible’s HHV, while oxygen lowers it.

3.3.3 Stirling Engine to Built CHP System

The Stirling engine as thermal engine is suggested to build a CHP system in order to generate heat and mechanical energy (work). A Stirling engine is based on a thermodynamic cycle that converts heat into mechanical work by exploiting a temperature difference (Fig. 3.8 and Table 3.6).

3.4 Result and Discussion

3.4.1 Comparison of the Electricity Generated as a Function of the Flow Rate Injection of Three Biomasses

The electricity generation is proportional to the flue injection for the three biomasses. Because his HHV is higher, the flue of injection fuel of olive cake is less than that

Table. 3.7 The electricity generated for the three biomasse injection

Power Stirling energy (wh)	MFR(g/s)		
	Argain nut	Olive cake	Argain cake
5	0.02	0.01	0.03
7	0.038	0.018	0.05
10	0.05	0.022	0.09
12	0.07	0.03	0.14
15	0.1	0.05	0.17

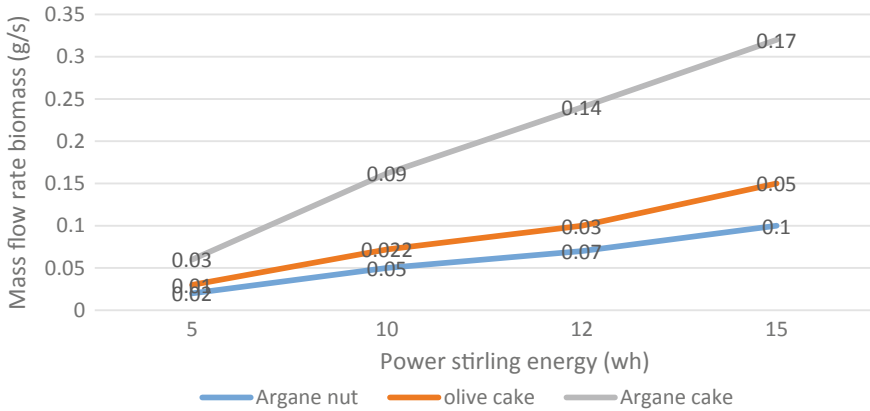
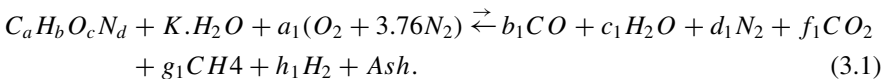


Fig. 3.9 Electricity generated and mass flow rate combustible injected

of argain cake and argain nut for same value of electricity generated (Table 3.7 and Fig. 3.9).

3.4.2 Methodology and Math Modeling

The chemical reaction of the biomass for a stoichiometric combustion.



where a, b, c, d : biomass components, K moisture content and $a_1, b_1, c_1, d_1, f_1, g_1, h_1$: molar coefficients that can be calculated using mass balance for C, H, N, O.

The following chemical reaction describes the unburnt particles caused by a lack of oxygen



Combustion product energy equation

$$\nabla u \cdot (\rho \cdot E) \nabla u (\rho \cdot E_f + P) = \nabla \left[C_{ef} \nabla T - \sum h_s \cdot D_s + (\tau_{ef} \times u) \right] + S_c \quad (3.4)$$

C_{ef} is the effective conductivity, D_s : diffusion flux of species s .

The other term represents the sum of energy transfer due to conduction, species diffusion, and viscous dissipation. The heat of chemical reaction is included in S_c .

Stirling Engine

The power output of Stirling engine can be calculated as

$$W_{SE} = \eta_{pc} (Q_{High} - Q_{rej}) \quad (3.5)$$

where η_{pc} polytropic efficient, Q_{high} is heat gas absorbed by the Stirling Engine and Q_{rej} is rejected heat.

When the gas expands in the cylinder from volume v_1 to volume v_2 , the pressure of the gas changes as the relation $PV = nRT$ and this variation results in a mechanic work as illustrated in the following formula

$$W = \int_{v_1}^{v_2} P \cdot dV \quad (3.6)$$

The Carnot efficiency is the ideal efficiency of the Stirling engine, and it is expressed as

$$\eta_{car} = 1 - \frac{T_2}{T_1} \quad (3.7)$$

where T_1 and T_2 are the temperature successively in the heater and the cooler.

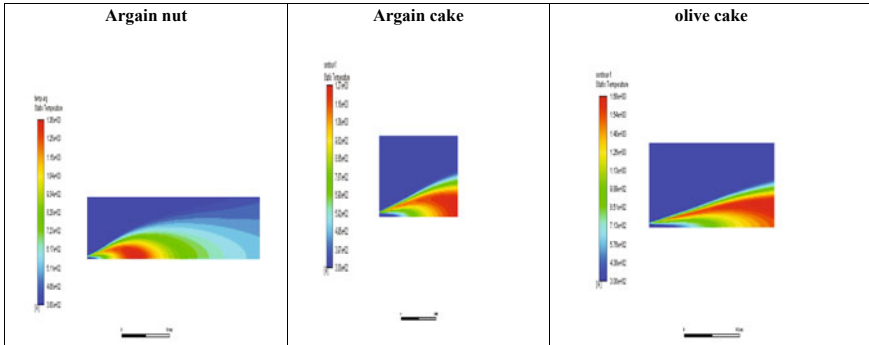


Fig. 3.10 Temperature contour

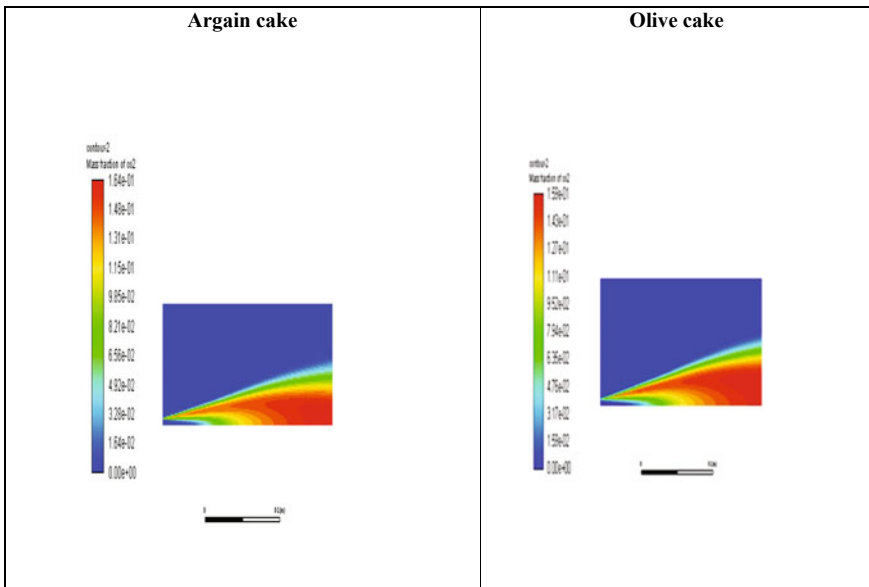


Fig. 3.11 CO₂ emissions contour

3.4.3 Comparison of Temperature and CO₂ Emissions of Argain Cake, Argain Nut and Olive Cake Using Ansys Fluent

Contour of temperature and CO₂ of the three biomasses

The simulation was carried out under the same combustion conditions, the maximum temperature of the argain cake was 1270 K, while the temperature of the argain nut

was 1380 K and the temperature of the argain cake was 1680 K. The variation in these results can be explained by the fact that olive cake has a higher HHV than argan nut and argan cake, which means it is more energetic and yields a higher temperature value (Figs. 3.10 and 3.11).

On the other hand, the argain nut is the most emettor of CO₂ gas, followed by the argain cake, then olive cake and their mass fraction values are 0.169, 0.164, and 0.59, respectively.

The flame shape and the contour of the combustion gas flow are not symmetrical at the level of the furnace. Because it is proposed to inject combustion air into a single channel rather than two symmetrical channels in relation to the fuel input.

3.5 Conclusion

In this study, the thermo-physical properties of agricultural wastes from argain cake, argain nut and olive cake during combustion were investigated. The characterization of waste argain nut and olive cake and the suitability for use in applications was also determined. A comparison of the emission properties CO₂ gases and temperature during the combustion suggested that olive cake was more suitably used as a biomass for thermochemical conversion, also:

- The difference between Argan cake and olive cake HHV depend on the physio chemical properties.
- Argan cake produce 60% more of H₂ and 20% more CO than olive cake.
- Argan cake is not suitable to replace the olive cake as combustible.
- The three biomasses have the same physicochemical properties; the difference is in the proportion of their elements; thus, their combustion results in the same ignition, energy, and emission. A possible alternative for creating a new biomassic combustible is to mix them.
- This project can contribute to reduce 0.18 g of CO₂ emitted to produce 1 Kwh.

References

- Ding H, Li J, Heydarian D (2021) Energy, exergy, exergoeconomic, and environmental analysis of a new biomass-driven cogeneration system. *Sustain Energy Technol Assess* 45:101044. <https://doi.org/10.1016/j.seta.2021.101044>
- Elorf A, Bakhatar I, Asbik M, Sarh B, Gillon P (2022) Fixed-bed biomass combustor: air mass flow rate and particles size effects on ignition front propagation of solid olive waste. *Combust Sci Technol* 194(2):365–377. <https://doi.org/10.1080/00102202.2019.1680070>
- Kramens et al (2021) Research of a biomass boiler with Stirling engine .pdf
- Marra FS, Miccio F, Solimene R, Chirone R, Urciuolo M, Miccio M (2020) Coupling a Stirling engine with a fluidized bed combustor for biomass. *Int J Energy Res* 44(15):12572–12582. <https://doi.org/10.1002/er.5662>

- Rahib Y, Boushaki T, Sarh B et al (2019) Combustion analysis of fixed beds of Argan Nut Shell (ANS) biomass in a batch type reactor. In: 2019 7th international renewable and sustainable energy conference (IRSEC). IEEE, pp 1–7. <https://doi.org/10.1109/IRSEC48032.2019.9078217>
- Rassai N, Boutammachte N, Laazaar K (2018) Valorization of moroccan olive cake in small scale bumer through Stirling engine: case study. In: 2018 6th international renewable and sustainable energy conference (IRSEC). IEEE, pp 1–5. <https://doi.org/10.1109/IRSEC.2018.8703029>
- Silva J, Teixeira J, Teixeira S, Preziati S, Cassiano J (2017) CFD modeling of combustion in biomass furnace. Energy Procedia 120:665–672. <https://doi.org/10.1016/j.egypro.2017.07.179>
- Zouhair FZ, Benali A, Kabbour MR et al (2020) Typical characterization of argane pulp of various Moroccan areas: a new biomass for the second generation bioethanol production. J Saudi Soc Agric Sci 19(3):192–198. <https://doi.org/10.1016/j.jssas.2018.09.004>

Chapter 4

Identification, Simulation and Modeling of the Main Power Losses of a Photovoltaic Installation and Use of the Internet of Things to Minimize System Losses



Mohammed Benchrifra, Mohamed Elouardi, Ghizlane Fattah, Jamal Mabrouki, and Rachid Tadili

Abstract Photovoltaic panels are made from photovoltaic cells, generally based on silicon, their semiconductor properties allow the panels to capture solar radiation and transform it into electrical voltage by the photovoltaic effect. The design of an efficient photovoltaic system requires the consideration of several power losses that have a direct influence on the overall efficiency of the system. The aim of this chapter is to identify the main factors causing power losses in a photovoltaic installation including temperature rise, the effect of shading, the effect of series resistance, and the effect of shunt resistance as well as losses in the electrical cables and to simulate these losses for each installation components. The results of this study showed that about 40% of the output of a photovoltaic installation is lost, with losses ranging from 3 to 14% for each element. These results can be used by manufacturers to optimize the choice of materials for photovoltaic cells as well as the components constituting the photovoltaic installation in order to reduce these power losses. Therefore, an intelligent cooling system guided by an Arduino board was proposed to reduce the losses caused by the temperature increase.

Keywords Photovoltaics · Losses · Power · Modelling · Optimization · Internet of Things

M. Benchrifra (✉) · R. Tadili

Solar Energy and Environment Team, Faculty of Science, Mohammed V University in Rabat, Rabat, Morocco

e-mail: simobenchrifra@gmail.com

M. Elouardi · J. Mabrouki

Laboratory of Spectroscopy, Molecular Modeling, Materials, Nanomaterials, Water and Environment, Faculty of Science, CERNE2D, Mohammed V University in Rabat, Rabat, Morocco

G. Fattah

Water Treatment and Reuse Structure, Civil Hydraulic and Environmental Engineering Laboratory, Mohammadia School of Engineers, Mohammed V University in Rabat, Avenue Ibn Sina B.P 765 Agdal Rabat, 10090 Rabat, Morocco

4.1 Introduction

An alternate energy source that humanity can employ is solar photovoltaic (PV) energy, which is a renewable resource (Shahzad 2012; Prieto et al. 2013; Franzitta et al. 2016). Because of its numerous benefits, including zero pollution, ease of installation, and quick building times, this energy is being used more and more in a variety of industries, from residential and commercial installations to space systems. Photovoltaic panels are currently the most important evolution in the renewable energy field. A few years ago, fossil fuels were the main source of energy (Mekhilef et al. 2011; Kamalapur and Udaykumar 2011). Today, the situation is gradually changing and the production of electrical energy through the use of solar radiation by photovoltaic panels is a major new trend, especially because it is renewable and inexhaustible.

It is well known that a photovoltaic module's output of electrical power might be significantly lower than under ideal production conditions (maximum power point). In fact, many factors, such as shading, temperature, illumination, series and shunt resistances, the choice of inverter and cables can significantly affect the electrical output of a photovoltaic panel. In this work, we are generally interested in the above factors (Reich et al. 2012; Triki-Lahiani et al. 2018). There are other factors that influence the energy output of a PV system, such as the ageing of the photovoltaic panels. Despite these acceptable efficiencies, there is still a significant technological challenge to be overcome before we can expect industrial production for nomadic applications. In fact, during the use of the solar panels a rapid loss of optoelectronic properties is observed depending on the conditions of use: in particular, it has been shown that the presence of oxygen causes a rapid decrease in photovoltaic efficiency. The components must therefore be protected from the atmosphere by a suitable encapsulation device called a passive layer.

The aim of this chapter is to identify the different power losses in a photovoltaic installation, to determine their causes, to simulate the impact of these factors on the optimal PMPP power and to simulate the different power losses for a real photovoltaic installation connected to the grid and determining their percentages. Finally, an intelligent system was proposed to minimize the losses caused by the temperature rise of the PV panels.

Thus this chapter is divided into 5 sections, the first section is an introduction, the second is a background, the third is an explanation of the principle of photovoltaic production, the fourth section is on the materials and methods used for the study and simulation and in the fifth section the results of the simulation of the effect of temperature increase on PV cells, the Simulation of the series resistance effect the Simulation of the shunt resistance effect and the Simulation of all losses in a real photovoltaic installation are shown and finally an Intelligent solar panel cooling system to reduce the losses was proposed.

4.2 Photovoltaic Production

The photovoltaic cell is composed of a semiconductor whose basic material is generally silicon (more than 80% of the cases) which is found in abundant quantities on our planet in the form of silicon dioxide (SiO_2), the main constituent of sand (Grätzel 2011; Bagher et al. 2015). The photovoltaic effect consists of using the energy of sunlight photons in a semiconductor to excite electrons and make them move from the valence band to the conduction band (Butler et al. 2015), which in turn creates charge gaps in the valence band called holes. Once released, these charges move through the material forming a continuous electric current (DC).

In order to control the displacement of the e^- , to prevent the recombination of the electron—hole and to be able to recover them towards the electrodes, it is necessary to create a junction by bringing together two differently doped semiconductors: for example, tetravalent silicon (4 valence e^-) doped with pentavalent phosphorus (5 valence e^-) provides an N-doped material in which the e^- remains free (Degiorgio and Cristiani 2016). The same silicon doped with trivalent boron (3 valence e^-) will give a P-type material characterized by a lack of electrons. The contact between these two types of silicon provides a junction with an electric field that selectively orients the positive carriers (holes) and negative carriers (e^-). consequently, an electric current is generated.

In the industry there are several types of photovoltaic cells:

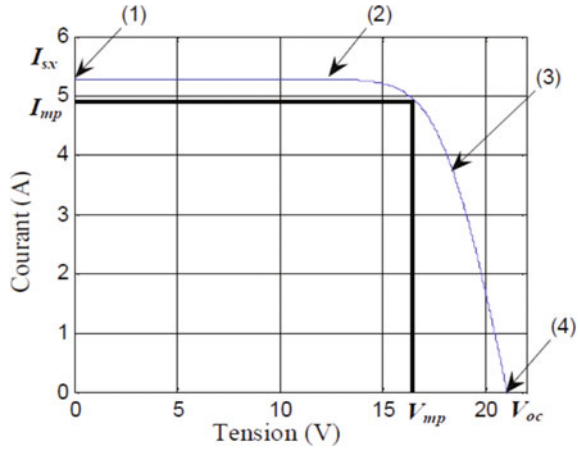
Monocrystalline cells: A silicon block condensed into a single crystal to create a monocrystalline cell. Monocrystalline panels offer an efficiency of 14–18%. The production method is complex and expensive (a lot of energy is needed to obtain pure silicon crystal), so these panels are expensive (Munzer et al. 1999; Bergmann et al. 2002; Chen et al. 2022).

Poly-crystalline cells: A block of silicon that has been crystallized into many crystals is used to make poly-crystalline cells. They look to be rectangular. The efficiency of polycrystalline solar panels is between 11 and 15% lower than that of monocrystalline solar panels. Because of their lower production cost, they offer the best price/performance ratio.

Amorphous cells: Using a vacuum vaporization method, a “silicon gas” is sprayed on the surface of glass, flexible plastic, or metal to create amorphous photovoltaic cells. The usage of extremely thin silicon layers is made possible by this method. Although amorphous photovoltaic cells produce power at a lower cost than their predecessors, they are only 7–9% efficient. Amorphous silicon has a disordered, non-crystalline, glassy atomic structure, but it has a light absorption coefficient about 1000 times greater than crystalline silicon. A thin layer of 0.3 mm is therefore enough to absorb most of the visible spectrum. These cells are used in small electronic applications such as calculators and watches (Rech and Wagner 1999; Takahashi and Konagai 1986; Sreejith et al. 2022). A photovoltaic cell is defined by its electrical characteristic curve (current–voltage). It shows the variation of the produced current as a function of the voltage across the cell from short circuit to open circuit (Fig. 4.1).

With:

Fig. 4.1 The different operating areas of a PV module



V_{oc} : The open circuit voltage

I_{sc} : The short-circuit current

I_{mp} , V_{mp} : the optimum operating point.

And the different operating zones are as follows:

- **Zone 1–2**: voltage generator operation.
- **Zone 2–3**: preferred zone for the operation of the module, the optimal operating point defined by the current I_{mp} and the voltage V_{mp} .
- **Zone 3–4**: operation as a constant current generator proportional to the illuminance.

4.3 Materials and Methods

4.3.1 The Effect of Temperature on Photovoltaic Panels

Temperature has a considerable influence on the cells behavior and consequently on their efficiency. This influence is mainly reflected by a decrease in the generated voltage (a very slight increase in the current). Depending on the model, this behavior leads to a loss of 0.5% of the efficiency per degree compared to the maximum efficiency of the cell.

It should be noted that the increase in current caused by a rise in temperature can be neglected at the point of maximum power, and the overall behaviour of the cell is a loss of 0.4–0.5/°c.

4.3.2 Electrical Cables Requirements in a Photovoltaic Field

After producing photovoltaic energy, in order to exploit it, it must be transferred, and to ensure the transport of the energy from the modules to the charge controller, not just any electrical cable can be used. Solar cables are designed to withstand the special conditions associated with their use. They are the only ones that can ensure a long life (over 30 years) while minimizing energy losses. Ordinary cables, even if they are designed for outdoor use, are not able to resist to the temperature variations (from – 20 to 80 °C near the modules), as well as to the ultraviolet rays exposition. The solar cables are in most cases double insulated and do not contain any flammable or toxic substances, which increases their safety. The DC current part of the installation has the highest currents, so this is where the problem of joule losses and voltage drops in the cables arises (Carmichael and Noel 1985; Parise et al. 2013).

The resistance of an electric cable does not depend on the voltage or current flowing through it, but on the resistivity (ρ) of the material used (copper, silver, iron, ...), the length of the cable, its cross-section, and the temperature. Copper is by far the most commonly used conductor, and its resistivity varies between 16×10^{-9} at 0 °C and 17×10^{-9} at 25 °C. The equation to determine the resistance is as follows:

$$R = \rho \times L/s \quad (4.1)$$

with:

- The resistance R in ohm (Ω)
- The resistivity ρ in ohm meter ($\Omega.m$)
- The length of the cable L in metres (m)
- The section of the cable s in metre-square (m^2)

A very important remark is that when the section decreases the resistance increases. Because of the cable's resistance, a part of the transported electricity is transformed into heat. This is called the "Joule effect" (Orellana et al. 2021). The resistance of the cable is also added to the resistances of other devices in the installation. In addition to a voltage drop, there will be a reduction in current. On the other hand, the cable cross-section, s, can be calculated by the following formula:

$$S = \frac{\rho \times L \times I}{\epsilon \times V_A} \quad (4.2)$$

where ρ : is material resistivity.

L: is the length of the cable in m.

ϵ : is the voltage drop in V.

V_A : is the voltage at the start of the cable in V.

For off-grid photovoltaic systems, the maximum acceptable voltage drop is 3%.

The choice of quality cabling is important, not only to reduce electrical losses, but also to avoid damage and failure of the whole installation (Zhang et al. 2019).

For example, the cables must also be correctly sized to handle the maximum voltage and current characteristics they will carry. They must also have strong UV-resistant insulation.

It should be noted that the losses in the cable depend directly on the amount of current flowing in the cable [A], the length of the cable [m], the cross-sectional area of the cable [mm²], as well as the specific electrical conductivity of the selected cable material [m/Ωmm²]. Copper has a higher conductivity (lower resistivity) compared to aluminum. Therefore, copper cables will have lower losses (and are also much more expensive). Also, a higher current on the line leads to higher losses, as can be seen in the equation:

$$P_{\text{pertes}} = I^2 \times R \quad (4.3)$$

Therefore, a higher voltage on the line will lead to a relatively low loss, because voltage is inversely proportional to current, as can be seen in the basic equation

$$p = V * I \quad (4.4)$$

and therefore

$$I = P/V \quad (4.5)$$

4.3.3 *Introducing the Simulation Program*

PVSYST is a program for sizing solar panels that makes it possible to get a variety of data, including energy production, installation costs, the needed surface, and annual energy production. A more advanced mode enables the collection of significantly more data for an extensive research. The software operates primarily in two modes. The first is a pre-sizing application that is easy to learn and accessible to the novice. The second mode gives a more detailed study and considers many parameters because it is based on concrete material for its calculations, contrary to the first mode which makes its calculations for a very general case (Kumar et al. 2021; https://www.pvsys.com/help/carbon_balance_tool.htm).

4.4 Results and Discussion

4.4.1 Simulation of the Effect of Temperature Increase on PV Cells

The influence of temperature is not negligible on the current/voltage characteristic and on the power/voltage characteristic. Therefore, to visualize the effect of temperature increase, we simulated the behavior of a PV cell at different temperatures while keeping the same irradiation. The results of this simulation are presented in Fig. 4.2.

From the Fig. 4.2 it can be seen that the open circuit voltage decreases with increasing temperature, but the current varies very little with temperature. Therefore, the maximum power delivered by the cell decreases. The influence of temperature is therefore very significant, which requires careful consideration when starting up photovoltaic systems.

4.4.2 Simulation of the Series Resistance Effect

The series resistance depends on the resistivity of the material, the contact resistances of the electrodes and the resistance of the collector grid. To visualise its effect on photovoltaic cells we varied the resistance value in a range between $0 \Omega < R_s <$ and 20Ω .

The result of this simulation is given in Fig. 4.3.

From Fig. 4.3 it can be seen that the series resistor directly influences the slope of the characteristic in the area where the photodiode behaves as a voltage generator. On the other hand, when this resistance is high, it decreases the short-circuit current value.

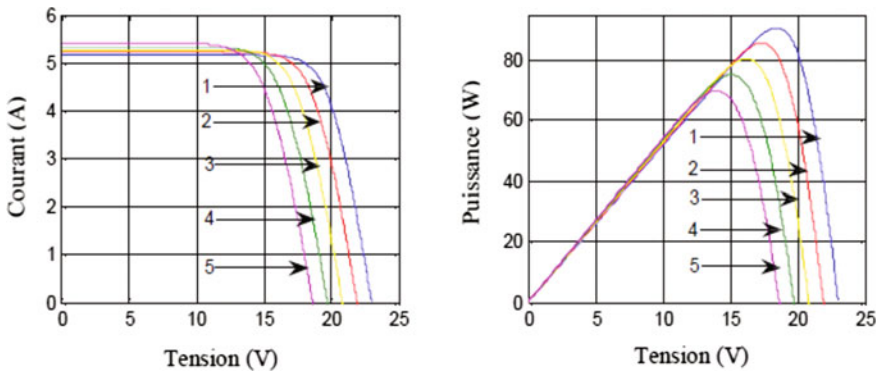
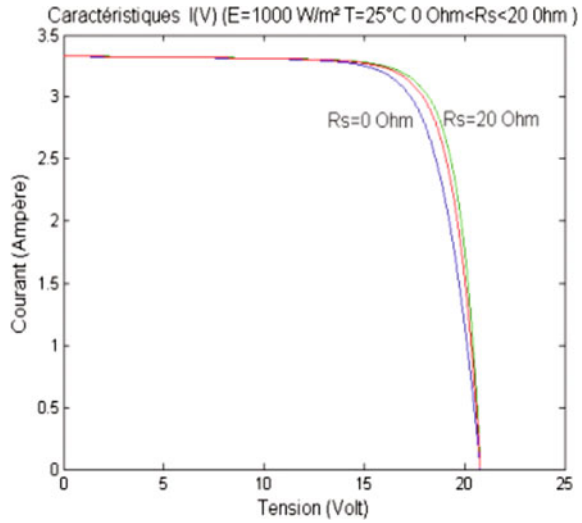


Fig. 4.2 Influence of temperature on the I(V) and P(V) characteristic at $E = 1000 \text{ W/m}^2$ and $T(^{\circ}\text{C}) = (1): 0^{\circ}\text{C}; (2): 15^{\circ}\text{C}; (3): 30^{\circ}\text{C}; (4): 45^{\circ}\text{C}; (5): 60^{\circ}\text{C}$

Fig. 4.3 Series resistance effect



4.4.3 Simulation of the Shunt Resistance Effect

The shunt resistance can be caused by defects in the material, such as: dislocations in the depletion zone or along the solar cell. To visualize its effect on photovoltaic cells we have varied the value of this resistance (Fig. 4.4).

From figure, it is clear that the shunt resistor changes the slope of the characteristic curve in the region of the short-circuit current. In fact, a too low shunt resistance will

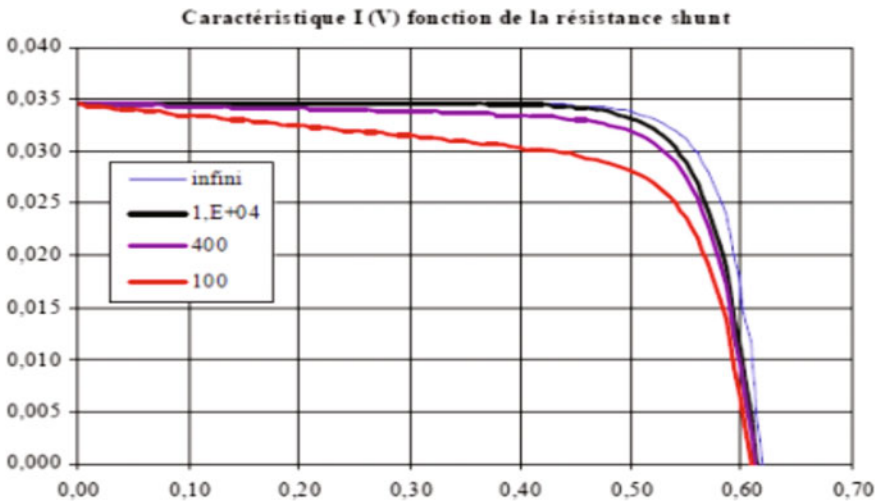


Fig. 4.4 Shunt resistance effect

Table 4.1 PV field sizing

Year used energy (MWh)	Maximum power (kWp)	Per-unit power of PV module	Inverter power per unit	PV panels number	Inverter number	Installation required area (m ²)
57	30	320 Wc	22 W	95	3	184

have an impact on the open circuit voltage of the solar cell; because of this a solar cell with a too low shunt resistance will not give any voltage under low illumination.

4.4.4 Simulation of all Losses in a Real Photovoltaic Installation

To assess the power losses in an actual solar installation, we first sized the photovoltaic field that could offset the electricity usage of the annex I of Rabat's Faculty of Science. Then, we simulated the various power losses at the level of the various elements. Therefore, the annual electricity consumption is 57 MWh, giving a peak output of 30 kWp. We determined the size of the PV field based on the solar panels and inverters that are offered on the Moroccan market. Table 4.1 displays the study's findings.

On the other hand, the results of the power loss simulation are presented in the following figure.

We were able to calculate the power losses and their percentage from Fig. 4.5. As a result, the increase in panel temperature, which decreased electricity generation by -9.2% , is what led to the greatest loss. The losses resulting from the inverter's operational loss (3.1%), the reflection loss based on the angle of incidence corrected by the (IAM) factor, which is equal to -2.7% , the ohmic losses (-1.2%), the mismatch losses resulting from the fact that the panels don't have the same characteristics (-1%) and the losses resulting from the quality of the modules (-1.5%) are the next losses to be considered. 18.4% of the power generated was lost in the production, which dropped by 8.8 MWh from 65.9 to 56.8 MWh as a result of the losses..

4.4.5 Intelligent Solar Panel Cooling System

The simulation and modelling study showed that the photovoltaic (PV) panel absorbed only about 16.53% of the incident solar energy and the efficiency of the PV cells decreases when the temperature increases. This increase in temperature led to a power loss of -9.2% . Knowing, for example, that silicon solar cells can maintain nominal efficiency by keeping the cell temperature at $25\text{ }^{\circ}\text{C}$ and that the cells will also undergo long term degradation if the temperature exceeds a certain limit. This problem can be avoided by maintaining a uniform temperature throughout the panel.

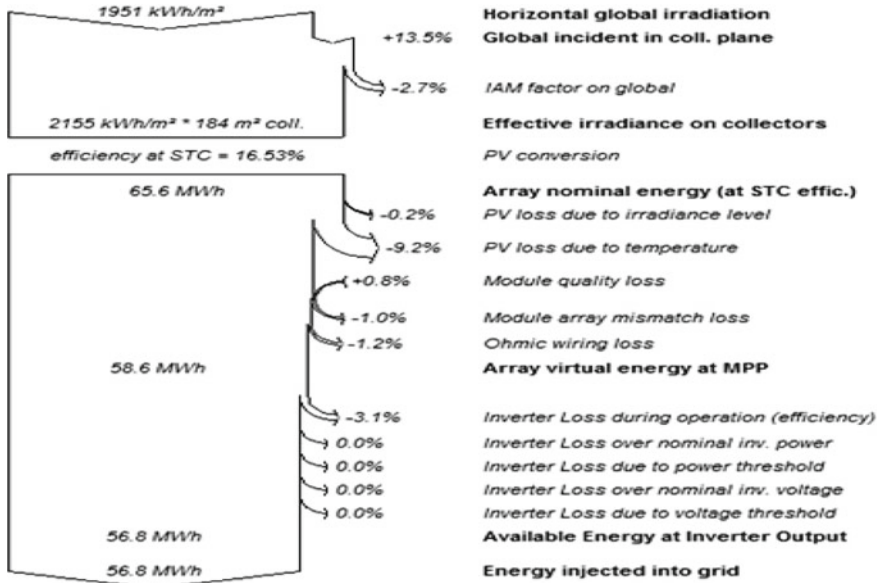


Fig. 4.5 Total power losses at various PV system components throughout the course of a single year of operation

Natural or forced air circulation is a simple and inexpensive way to remove heat from the PV modules, but it is less effective if the ambient air temperature exceeds 20 °C. Another, more efficient way is to use a liquid as a panel coolant, to absorb more heat and cool the panel more efficiently.

In our case, in order to reduce the power losses caused by the increase of the panel temperature, a photovoltaic device with a cooling system has been designed. This system ensures an optimal increase in the yield of the solar panel.

The proposed system is based on the Internet of Things and consists of an Arduino UNO Board, a DS18B20 temperature sensor to measure the panel temperature, a water pump and a 5 V trigger relay module.

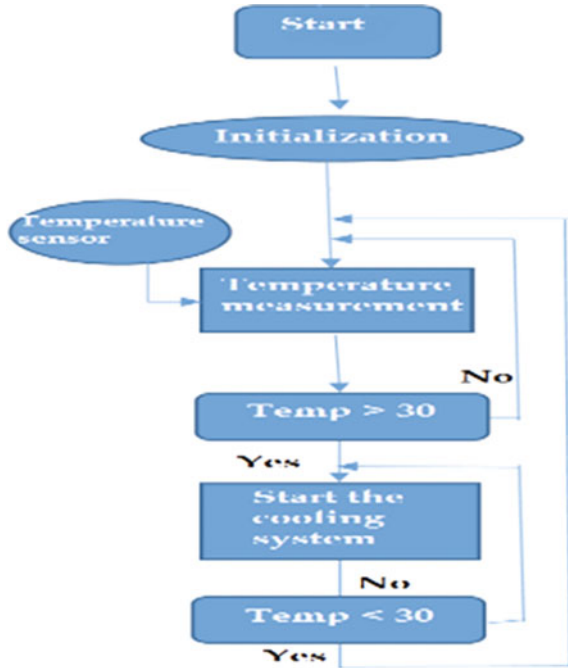
When the solar panel heats up and reaches 30 °C the system automatically starts the pump to send water stored in a tank through pipes, dropping it on the panel to reduce their temperature and when the temperature returns to normal the cooling system automatically stops. The following flow chart summarizes the operating principle (Fig. 4.6).

By using the proposed cooling system on the simulated PV system, we can gain about 9% of the production, which is equivalent to 6 MWh.

Conclusion

Photovoltaic panels are made from photovoltaic cells, which are generally based on silicon. Their semiconductor properties enable the panels to capture solar radiation and transform it into electrical voltage by the photovoltaic effect. This electricity

Fig. 4.6 Flowchart of the operating principle of the cooling system



produced is called “green” because it does not emit greenhouse gases and is notably non-polluting. The voltage created is a direct current. In order to transform this direct current into alternating current, suitable for consumption by residential equipment, an inverter is required, which is placed near the electrical panel. The panels are powered by sunlight, not heat. This energy is inexhaustible, as its source is the sun, which makes it particularly suitable for future energy needs. Solar energy is the energy of the future. The design of an efficient photovoltaic installation requires the consideration of several losses that have a direct influence on the efficiency of the system.

Shading losses: The environment of a solar module can include trees, mountains, walls, buildings, etc. It can cause shading of the module. It can cause shading of the module which directly affects the energy collected.

Finally with the help of the proposed cooling system we can gain more than 9% of the generated power and consequently increase the efficiency of the photovoltaic system. On the other hand, the future work will focus on the improvement and development of intelligent systems to minimize the various power losses caused by other factors such as shading, dust deposits and panel orientation.

References

- Bagher AM, Vahid MMA, Mohsen M (2015) Types of solar cells and application. *Am J Opt Photonics* 3(5):94–113
- Bergmann RB, Berge C, Rinke TJ et al (2002) Advances in monocrystalline Si thin film solar cells by layer transfer. *Sol Energy Mater Sol Cells* 74(1–4):213–218
- Butler KT, Frost JM, Walsh A (2015) Ferroelectric materials for solar energy conversion: photoferroics revisited. *Energy Environ Sci* 8(3):838–848
- Carmichael DC, Noel GT (1985) Development of low-cost modular designs for photovoltaic array fields. *IEEE Trans Power Appar Syst* 5:1005–1011
- Chen K, Bothwell A, Guthrey H et al (2022) Measurement of poly-Si film thickness on textured surfaces by X-ray diffraction in poly-Si/SiO_x passivating contacts for monocrystalline Si solar cells. *Sol Energy Mater Sol Cells* 236:111510
- Degiorgio V, Cristiani I (2016) Semiconductor devices. In: *Photonics*. Springer, Cham, pp 145–169
- Franzitta V, Curto D, Rao D et al (2016) Hydrogen production from sea wave for alternative energy vehicles for public transport in Trapani (Italy). *Energies* 9(10):850
https://www.pvsyst.com/help/carbon_balance_tool.htm
- Grätzel M (2011) Photoelectrochemical cells. In: *Materials for sustainable energy: a collection of peer-reviewed research and review articles from nature publishing group*, pp 26–32
- Kamalapur GD, Udaykumar RY (2011) Rural electrification in India and feasibility of photovoltaic solar home systems. *Int J Electr Power Energy Syst* 33(3):594–599
- Kumar R, Rajoria CS, Sharma A et al (2021) Design and simulation of standalone solar PV system using PVsyst software: a case study. *Mater Today: Proc* 46:5322–5328
- Mekhilef S, Saidur R, Safari A (2011) A review on solar energy use in industries. *Renew Sustain Energy Rev* 15(4):1777–1790
- Munzer KA, Holdermann KT, Schlosser RE et al (1999) Thin monocrystalline silicon solar cells. *IEEE Trans Electron Devices* 46(10):2055–2061
- Nakaya H, Nishida M, Takeda Y et al (1994) Polycrystalline silicon solar cells with V-grooved surface. *Sol Energy Mater Sol Cells* 34(1–4):219–225
- Orellana J, Moreno-Villoslada I, Bose RK et al (2021) Self-healing polymer nanocomposite materials by Joule effect. *Polymers* 13(4):649
- Prieto PA, Hall CAS, Melgar R (2013) *Spain's photovoltaic revolution: the energy return on investment*. Springer, New York
- Parise G, Martirano L, Parise L (2013) Life monitoring tool of insulated cables in photovoltaic installations. *IEEE Trans Ind Appl* 50(3):2156–2163
- Reich NH, Mueller B, Armbruster A et al (2012) Performance ratio revisited: is PR > 90% realistic. *Prog Photovoltaics Res Appl* 20(6):717–726
- Rech B, Wagner H (1999) Potential of amorphous silicon for solar cells. *Appl Phys A* 69(2):155–167
- Sreejith S, Ajayan J, Kollem S et al (2022) A comprehensive review on thin film amorphous silicon solar cells. *Silicon* 1–17
- Shahzad U (2012) The need for renewable energy sources. *Energy* 2:16–18
- Takahashi K, Konagai M (1986) *Amorphous silicon solar cells*. New York
- Triki-Lahiani A, Abdelghani ABB, Slama-Belkhdja I (2018) Fault detection and monitoring systems for photovoltaic installations: a review. *Renew Sustain Energy Rev* 82:2680–2692
- Vairavasundaram I, Varadarajan V, Pavankumar PJ et al (2021) A review on small power rating PV inverter topologies and smart PV inverters. *Electronics* 10(11):1296
- Wöhrlé D, Meissner D (1991) Organic solar cells. *Adv Mater* 3(3):129–138
- Zhang Y, Chen H, Du Y (2019) Lightning protection design of solar photovoltaic systems: methodology and guidelines. *Electr Power Syst Res* 174:105877

Chapter 5

Mixed Thermal Boundary Condition Effects on Non-Darcian Model



Hajar Lagziri and Hanae EL Fakiri

Abstract The chapter tackles the influence of inertia and thermal boundary effects on thermoconvective instability in the configuration of non Darcian model by using a root-finding algorithm of the shooting method. The set-up assumed here is a homogeneous horizontal isotropic saturated porous layer sandwiched between two rigid impermeable walls where the upper layer is maintained at the isothermal condition and the lower one at the Robin-type thermal boundary condition whose expression is modelled as Newton's cooling law equation. The thermal non-equilibrium regime (LTNE) is applicable by imposing different temperatures between Newtonian fluid and the solid medium. The LTNE existence creates two independent Biot numbers besides other non-dimensionless parameters. Normal modes technique is adopted here by applying small disturbances to the dimensionless governing equations. Overall, the finding results will discuss at which instability takes place with respect to different physical numbers.

Keywords Brinkman model · Biot number · Thermal non-equilibrium · Linear stability analysis

5.1 Introduction

In the industrial sector, materials with higher porosity such as metal foams are often used to enhance heat exchange between two bodies or structures. Furthermore, their large surface area and lightweight make them good candidates for recycling energy efficiently. In this case, the usual Darcy's law becomes no longer suitable for describing fluid motion and, it is necessary to adopt the Brinkman-Darcy model instead (Nield 2017; Dubey and Murthy 2019; Bouachir et al. 20121; Caprone and Rionero 2016).

H. Lagziri (✉) · H. EL Fakiri
Department of Physics, Abdelmalek Essaadi University, Quartier M'haneche II,
avenue Palestine, 93000 Tetouan, Morocco
e-mail: lagziri-hajar7@hotmail.fr

© The Author(s), under exclusive license to Springer Nature Switzerland AG 2023
J. Mabrouki et al. (eds.), *Advanced Technology for Smart Environment and Energy*,
Environmental Science and Engineering,
https://doi.org/10.1007/978-3-031-25662-2_5

Moreover, many man-made materials like porous media have anisotropic mechanical and thermal properties. Because of that, thermal instability can be managed by the permeability and thermal conductivity of the medium (Storesletten and Rees 1997; Tyvand and Storesletten 2015; Govender and Vadasz 2007; Mahjoob and Vafai 2008). Rotation also plays a vital role in thermoconvective instability, for example rotating machinery and centrifugal filtration processes. A reference to a rotating frame must be established to investigate the situations in which the solid matrix rotates (Vadasz 2016, 2019; Govender and Vadasz 2007). Otherwise, thermal instability or convection in the subjects of rotating solid matrix, free and forced convection layer with cavities, a non-Darcian model with open boundaries or saturating Oldroyd-B fluid are ones of the several papers that deal with the convection phenomenon (Malashetty et al. 2006; Shivakumara et al. 2006; Rees 2002; Baytas 2004; Saeid 2004). Most papers in the last decade are predicated on the idea that the Newtonian fluid phase and the solid medium are everywhere under the same temperature, which is known as the thermal equilibrium regime (LTE). However, this assumption becomes inadequate for many real-world applications, especially when high-speed flows or significant temperature gradients between both phases are present (Fathi-Kelestani et al. 2020; Gandomkar and Gray 2018; Lagziri and Bezzazi 2019; Barletta 2019). In such cases, it is necessary to consider a two-field energy equation model to represent each phase separately, and this emerges as a virtue of no thermal equilibrium behaviour (LTNE). In addition, it is anticipated that the model of LTNE will have an important role in future technology consisting of porous media such as computer chips, tube refrigerators, heat exchangers and others (Mahjoob and Vafai 2008; Pulvirenti et al. 2020).

The chapter studies the emergence of thermal instability cells in a non-Darcian flow using mixed thermal boundary conditions and a thermal non-equilibrium regime. The influence of these two features on instability behaviour is investigated in detail.

5.2 Mathematical Modeling

A homogeneous fluid-saturated porous layer sandwiched between two rigid impermeable walls is shown in Fig. 5.1. An external heat source is imposed at the lower boundary with two different external heat transfer coefficients h_f and h_s . In other words, Robin's thermal boundary conditions are considered. On the other hand, uniform perfect conducting temperature T_1 is applied at the upper layer. The local thermal nonequilibrium model and linear Oberbeck Boussinesq approximation are both pertinent here. The Brinkman-Darcy equation describes the saturating non-Darcian flow in a solid matrix. Following these descriptions the Mathematical equations of the problem are

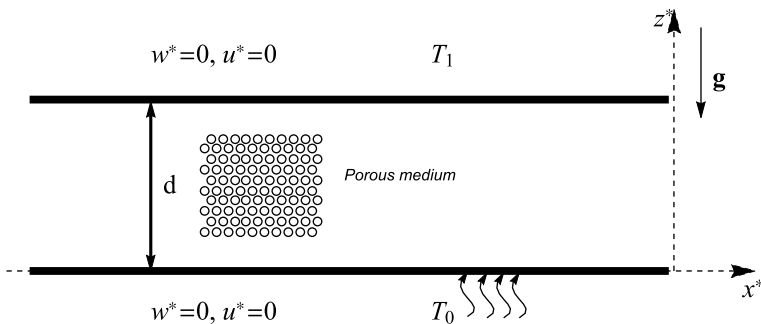


Fig. 5.1 Sketch of Brinkman model with mixed thermal boundary conditions

$$\nabla^* \cdot \vec{u}^* = 0, \quad (5.1a)$$

$$\rho \left[\frac{1}{\phi} \frac{\partial \vec{u}^*}{\partial t^*} + \frac{1}{\phi^2} (\vec{u}^* \cdot \nabla^*) \vec{u}^* \right] + \frac{\mu}{K} \vec{u}^* = -\nabla^* P^* + \mu' \nabla^{*2} \vec{u}^* + \rho_f \beta g (T_f^* - T_0) \vec{e}_z, \quad (5.1b)$$

$$(1 - \phi)(\rho C)_s \frac{\partial T_s^*}{\partial t^*} = (1 - \phi) \alpha_s \nabla^{*2} T_s^* + h(T_f^* - T_s^*), \quad (5.1c)$$

$$\phi(\rho C)_f \frac{\partial T_f^*}{\partial t^*} + (\rho C)_f (\vec{u}^* \cdot \nabla^*) T_f^* = \phi \alpha_f \nabla^{*2} T_f^* - h(T_f^* - T_s^*). \quad (5.1d)$$

The temperature and velocity conditions suggested at the boundary are

$$z^* = d : \quad w^* = 0, u^* = 0, \quad T_s^* = T_f^* = T_1. \quad (5.2a)$$

$$z^* = 0 : \quad w^* = 0, u^* = 0, \quad k_s \frac{\partial T_s^*}{\partial z^*} = h_s (T_s^* - T_0), \quad k_f \frac{\partial T_f^*}{\partial z^*} = h_f (T_f^* - T_0) \quad (5.2b)$$

The superscript of the star notation refers to dimensional variables. The vector \vec{u} means the velocity field. Otherwise, we have also other physical properties such as the thermal diffusivity α with $[m^2/s]$, the effective viscosity μ' with $[N.s/m^2]$, the dynamic viscosity of the fluid μ with $[N.s/m^2]$, the coefficient of thermal expansion β the pressure P , the temperature at the lower wall T_0 , the reference density ρ with $[Kg/m^3]$, the inter-phase volumetric heat transfer coefficient h with $[W/(m^3 K)]$, the heat capacity per unit of mass C with $[J/(KgK)]$, the porosity ϕ , the time t with $[s]$, the thickness of the layer d with $[m]$, the thermal conductivity k with $[W/(mK)]$, the superficial heat transfer coefficient between both phases $h_{s,f}$ with $[W/(m^2 K)]$ and the permeability K with $[m^2]$.

The dimensionless expression of the governing equations is,

$$\begin{aligned}\nabla \times (D^{-1}\vec{u} - \nabla^2\vec{u}) &= RD^{-1}[\nabla \times T_f]\vec{e}_z, \\ \lambda \frac{\partial T_s}{\partial t} &= \nabla^2 T_s + \gamma H(T_f - T_s), \\ \frac{\partial T_f}{\partial t} + \vec{u} \cdot \nabla T_f &= \nabla^2 T_f + H(T_s - T_f),\end{aligned}\quad (5.3)$$

We get the resulting boundary conditions as

$$\begin{aligned}z = 1 : \quad w &= 0, \quad u = 0, \quad T_s = T_f = 0, \\ z = 0 : \quad w &= 0, \quad u = 0, \quad \frac{\partial T_s}{\partial z} = B_s(T_s - 1), \quad \frac{\partial T_f}{\partial z} = B_f(T_f - 1).\end{aligned}\quad (5.4)$$

The notations ‘‘s’’ and ‘‘f’’ signify the saturating Newtonian fluid phase and solid structure. The dimensionless forms of R and H mean the modified thermal Rayleigh number and the inter-heat transfer coefficient while B_s and B_f describe the Biot number of the solid matrix and fluid phase. Besides, we have γ and D whose physical meanings are the thermal conductivity ratio and the Darcy number respectively.

The dimensionless parameters that emerge in (5.3) and (5.4) are:

$$\begin{aligned}\lambda &= \frac{\alpha_f}{\alpha_s}, \quad k_m = (1 - \phi)k_s + \phi k_f, \quad \gamma = \frac{\phi k_f}{(1 - \phi)k_s}, \\ H &= \frac{hd^2}{\phi k_f}, \quad B_{s,f} = \frac{h_{s,f}d}{k_{s,f}}, \quad \alpha_f = \frac{k_f}{(\rho C)_f}, \quad \alpha_m = \frac{k_m}{(\rho C)_f}, \\ D &= \frac{\mu' K}{\mu d^2}, \quad R = \frac{\rho_f \beta \Delta T g K d}{\nu k_f \phi}, \quad \Delta T = \frac{\phi(T_1 - T_0)d}{k_m}.\end{aligned}\quad (5.5)$$

where the rescaling variables applicable in the set of governing equations are,

$$\nabla^* \rightarrow \nabla \frac{1}{d}, \quad t^* \rightarrow \frac{d^2}{\alpha_f}, \quad \vec{u}^* \rightarrow \vec{u} \frac{\phi \alpha_f}{d}, \quad T_{s,f}^* \rightarrow T_0 + T_{s,f} \Delta T. \quad (5.6)$$

5.3 Basic Profile

We consider a motionless flow whose basic state is

$$\vec{u}_b = 0, \quad T_{f,b} = T_{fb}(z), \quad T_{s,b} = T_{sb}(z). \quad (5.7)$$

We have used ‘‘b’’ as a symbol of the basic flow.

5.3.1 Linear Stability Analysis

Let us disturb the basic flow by writing that

$$\begin{aligned}\vec{u} &= \vec{u}_b + \epsilon \vec{U}, \\ T_{fs} &= T_{sfb}(z) + \epsilon \theta_{s,f}.\end{aligned}\quad (5.8)$$

We are concerned only with the first-order terms of disturbances, therefore, the linearized form of the equations is

$$\nabla \times (D^{-1} \vec{U} - \nabla^2 \vec{U}) = RD^{-1} [\nabla \times \theta_f] \vec{e}_z = 0, \quad (5.9a)$$

$$\theta_s'' - a^2 \theta_s + \gamma H(\theta_f - \theta_s) = 0, \quad (5.9b)$$

$$\theta_f'' - a^2 \theta_f + H(\theta_s - \theta_f) - a T'_{fb} \vec{U} = 0, \quad (5.9c)$$

$$z = 1 : W = 0, \quad U = 0, \quad \theta_s = \theta_f = 0. \quad (5.9d)$$

$$z = 0 : W = 0, \quad U = 0, \quad \theta_s' - \theta_s B_s = 0, \quad \theta_f' - \theta_f B_f = 0, \quad (5.9e)$$

Now we apply the normal modes method by defining the functions as

$$\begin{aligned}\vec{U}(x, z, t) &= \Re\{i \hat{U}(z) e^{i(ax - \omega t)}\}, \\ \theta_f(x, z, t) &= \Re\{\theta(z) e^{i(ax - \omega t)}\}, \\ \theta_s(x, z, t) &= \Re\{\varphi(z) e^{i(ax - \omega t)}\}\end{aligned}\quad (5.10)$$

Hence the symbols of \hat{U} , θ and φ are used to describe the perturbed functions with respect to z . The wave number is defined by the symbol a while the growth rate and the angular frequency are noted with ω_r and ω_i respectively. The complex parameter ω is defined as the sum of the imaginary and real parts.

In the meantime, the velocity components can be expressed in the stream functions as,

$$\hat{U} = \frac{\partial \psi}{\partial z}, \quad \hat{W} = -\frac{\partial \psi}{\partial x}. \quad (5.11)$$

Otherwise, the definition of T'_{fb} is

$$T'_{fb} = \frac{-B_f B_s (\gamma + 1) \sinh(\Omega) + (-\Omega)(B_f \gamma + B_s) \cosh(\Omega) + (B_s - B_f) \Omega \cosh(\Omega z)}{(B_f (B_s \gamma + B_s + 1) + B_s \gamma) \sinh(\Omega) + \Omega (B_f \gamma + B_s + \gamma + 1) \cosh(\Omega)}. \quad (5.12)$$

With $\Omega = \sqrt{(1 + \gamma)H}$.

By substituting (5.10) and (5.11) into (5.13) the set of equations become,

$$-\psi'''' + (2a^2 + D^{-1})\psi'' - a^2(a^2 + D^{-1})\psi + aD^{-1}R\theta = 0, \quad (5.13a)$$

$$\varphi'' - a^2\varphi + \gamma H(\theta - \varphi) = 0, \quad (5.13b)$$

$$\theta'' - a^2\theta + H(\varphi - \theta) - aT'_{f,b}\psi = 0, \quad (5.13c)$$

$$z = 1 : W = 0, \quad U = 0, \quad \varphi = \theta = 0. \quad (5.13d)$$

$$z = 0 : W = 0, \quad U = 0, \quad \varphi' - \varphi B_s = 0, \quad \theta' - \theta B_f = 0, \quad (5.13e)$$

As our motivation is to seek the marginal curves, the imaginary part of ω has to be neglected. Meanwhile, the principle of exchange of instabilities is achieved numerically thus we can eliminate both parts of ω and write (5.13).

5.4 Numerical Solutions

The numerical method adopted for dealing with (5.13) is the shooting method and Range-Kutta solver. In general, this latter required the definition of extra boundary conditions as a first step to manage (5.13) in the form of an initial value problem. Thus, we can add

$$\psi''(0) = \zeta_1, \quad \psi'''(0) = \zeta_2, \quad \varphi(0) = \zeta_3, \quad \theta(0) = 1. \quad (5.14)$$

The condition noted by $\theta(0) = 1$ is included as a virtue of the homogeneity in the governing equations. The parameters of ζ_1 , ζ_2 and ζ_3 are considered as unknowns with real values. The next step here is to define these unknown constants together with R for any given value of H , γ , a , D , B_s and B_f through the use of the shooting method and boundary conditions of the upper wall. The shooting method consists in employing the root-finding algorithm in Mathematica 10 to determine the value pair of (R_c, a_c) .

5.5 Discussion and Results

Table 5.1 exhibits the critical values of the modified Rayleigh number and wave number for different values of B_s , B_f and H in the cases where $D = 0.01$ and $D = 0.1$. Overall, we note that the Darcy number consists in having the viscous diffusion at the region nearer to the boundary layers. In other words, as much as the viscous effects decrease the fluid can flow and move more rapidly and easily without resistance, thereby the onset of convection can be yielded at a small critical Rayleigh number. Besides, we mention the values of $H = 10$ and $H = 0.1$ as the two approaches of the thermal equilibrium and non-equilibrium one. A small value

Table 5.1 Critical values of R_c and a_c for fixed $\gamma = 1$ and variable values of H , B_s , B_f and D

$B_s = 10, D = 0.01$ and $H = 0.1$			$B_s = 10, D = 0.01$ and $H = 10$		
B_f	a_c	R_c	B_f	a_c	R_c
10^{-2}	2.511038	1079.598493	10^{-2}	3.104816	112.986416
10^{-1}	2.558604	390.796352	10^{-1}	3.115111	111.056979
10^0	2.771452	97.466144	10^0	3.192665	99.369782
10^1	3.123249	62.807080	10^1	3.380695	83.971631
10^2	3.224927	60.824797	10^2	3.468684	80.081593
$B_f = 10, D = 0.01$ and $H = 0.1$			$B_f = 10, D = 0.01$ and $H = 10$		
B_s	a_c	R_c	B_s	a_c	R_c
10^{-2}	3.123464	63.182457	10^{-2}	3.324845	93.982412
10^{-1}	3.123442	63.149355	10^{-1}	3.326237	93.474899
10^0	3.123335	62.980012	10^0	3.338512	90.032296
10^2	3.123237	62.772448	10^2	3.402791	82.268740
$B_s = B_f, D = 0.01$ and $H = 0.1$			$B_s = B_f, D = 0.01$ and $H = 10$		
10^{-2}	2.536034	4623.735494	10^{-2}	2.912826	6722.170507
10^{-1}	2.567577	508.663163	10^{-1}	2.936807	736.272960
10^0	2.772213	99.083327	10^0	3.095060	139.361525
10^2	3.224927	60.824797	10^2	3.468684	80.081593
$B_s = 10, D = 0.1$ and $H = 0.1$			$B_s = 10, D = 0.1$ and $H = 10$		
B_f	a_c	R_c	B_f	a_c	R_c
10^{-2}	2.547663	3916.656653	10^{-2}	3.049394	406.099765
10^{-1}	2.590804	1409.760163	10^{-1}	3.057606	399.046135
10^0	2.771510	349.394966	10^0	3.118962	356.437503
10^1	3.062273	223.926148	10^1	3.265212	300.650240
10^2	3.144334	216.690171	10^2	3.321342	289.612267
$B_f = 10, D = 0.1$ and $H = 0.1$			$B_f = 10, D = 0.1$ and $H = 10$		
B_s	a_c	R_c	B_s	a_c	R_c
10^{-2}	3.062456	225.261482	10^{-2}	3.217395	336.521693
10^{-1}	3.062437	225.143664	10^{-1}	3.218693	334.689564
10^0	3.062348	224.541123	10^0	3.229690	322.297643
10^2	3.062263	223.803036	10^2	3.283231	294.616629
$B_s = B_f, D = 0.1$ and $H = 0.1$			$B_s = B_f, D = 0.1$ and $H = 10$		
B_s	a_c	R_c	B_s	a_c	R_c
10^{-2}	2.572029	16660.158434	10^{-2}	2.893640	24122.803423
10^{-1}	2.598972	1831.364896	10^{-1}	2.912764	2641.510203
10^0	2.772161	355.135619	10^0	3.039128	499.382360
10^2	3.144336	216.633727	10^2	3.333511	286.691853

Table 5.2 Comparison of R_c and a_c with others results for the case of $D = 0$ and $\gamma = 1$

Postelnicu results (Postelnicu 2008)			Shivakumara results (Shivakumara et al. 2010)		Present results	
H	R_c	a_c	R_c	a_c	R_c	a_c
10^{-2}	40.020810	3.163	40.2467	3.171	40.1084	3.166
10^{-1}	40.192163	3.169	40.4271	3.178	40.1523	3.171
10^0	41.897	3.232	42.1288	3.241	41.3623	3.211
10^1	52.991	3.460	53.2635	3.470	52.3608	3.436
10^2	73.258	3.293	73.6547	3.303	72.3404	3.270

Table 5.3 Comparison of R_c and a_c with others results for the case of $D = 1$ and $\gamma = 1$

Postelnicu results (Postelnicu 2008)			Shivakumara results (Shivakumara et al. 2010)		Present results	
H	R_c	a_c	R_c	a_c	R_c	a_c
10^{-2}	1753.1005	3.121	1753.1005	3.121	1753.1005	3.1208
10^{-1}	1761.0641	3.126	1761.0641	3.126	1761.0641	3.1256
10^0	1836.336	3.168	1836.3356	3.168	1836.3356	3.1680
10^1	2330.852	3.311	2330.2069	3.311	2330.2069	3.3108
10^2	3210.852	3.206	3210.8516	3.206	3210.85149	3.2055

of H leads the heat to be poorly exchanged between the two phases whereas for a higher one the ability to heat transfer becomes extremely large. Otherwise, the range assumed for B_s and B_f extends from 10^{-2} to 10^2 to recover the both thermal conditions of uniform heat flux and perfect conducting temperature. The finding results of Table 5.1 show that the thermal stability increases in the cases where the combined effect of LTNE and fluid inertia is present. In addition, we can notice that even both Biot numbers can have the tendency to emerge stable behaviour.

The results computed by our numerical method in Tables 5.2, 5.3 for the case of $D = 0$ (Darcian flow) and $D = 1$ display a good congruence with those of Postelnicu (2008) and Shivakumara (2010). These two tables confirm that the fluid inertia can retard the fluid motion which decreases later the buoyancy effects in the medium.

The neutral curves evaluated numerically for various values of γ and fixed $D = 0.01$ are drawn in Fig. 5.2. We remind that stability takes place in the regions situated below the concave curves. In fact, all these curves follow the same standard shape of the well-known Benard problem. Therefore, if we look at the behaviour of these curves in the function of γ and both Biot numbers we can notice that stability effects increase with the reduction of these two parameters. The small value of γ manages the heat to be transported only through the solid structure, this in turn slows the onset of convection especially when both phases at the upper layer have no ability to enter

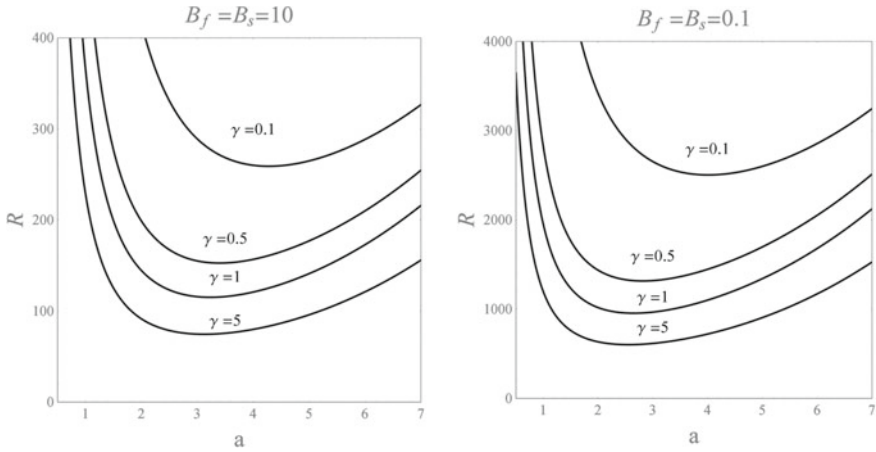


Fig. 5.2 Neutral curves for $H = 100$ and $D = 0.01$

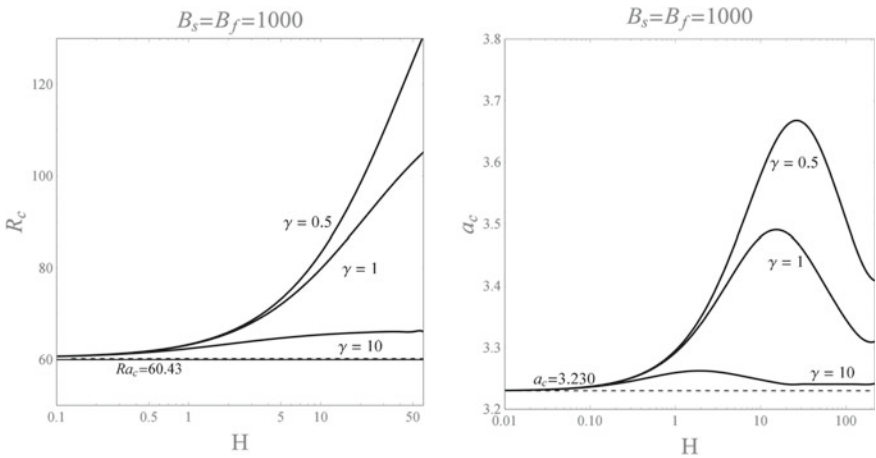


Fig. 5.3 Plots for R_c and a_c versus H with $B_f = B_s = 1000$ and $D = 0.01$

or outer the heat with the external environment. Otherwise, Figs. 5.3, 5.4 display the variation of R_c and a_c with respect to H for $D = 0.01$. The broken lines in both figures describe the critical values at thermal equilibrium. The results extracted from both figures confirm that the stability effects prevail more in the case of uniform heat flux as $R_c = 11427.15$ and $a_c = 2.5$ for $\gamma = 10$.

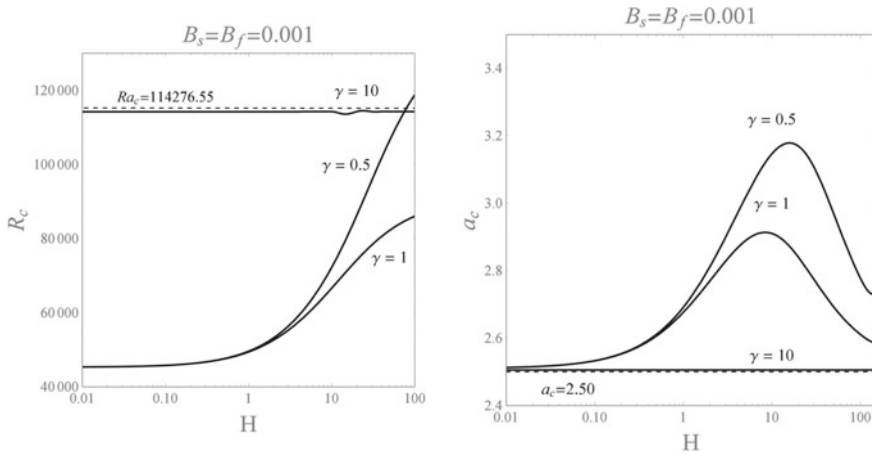


Fig. 5.4 Plots for R_c and a_c versus H with $B_f = B_s = 0.001$ and $D = 0.01$

5.6 Conclusion

The combined effect of non Darcian model and LTNE regime in a porous layer with mixed thermal boundary conditions is investigated in this chapter. The root-finding algorithm of the shooting method and Runge-Kutta solver are considered to solve numerically the eigenvalue problem tackled by linear stability analysis. Briefly, the finding results may be summed up as

- The thermal non-equilibrium (LTNE) regime with weak heat exchange at the upper layer by fluid phase creates more stability than the solid one.
- The growth of Darcy’s number hastens the stability as a result of the fluid inertia. In other words, the buoyancy effects become less dominant in front of inertia effects.
- The reduction in both Biot numbers brings about stabilizing effects in the medium either in LTE or LTNE model.

Acknowledgements This research was not funded by any grant.

References

AL-Sumaily Gazy F, Al Ezzi A, Dhahad Hayder A, Thompson Mark C, Yusaf T (2021) Legitimacy of the local thermal equilibrium hypothesis in porous media: a comprehensive review. *J Eng* (14):2–47

Barletta A, Rees DAS on the onset of convection in a highly permeable vertical porous layer with open boundaries. *AIP Phys Fluids* 31:112 (2019)

Baytas AC (2004) Thermal non-equilibrium free convection in a cavity using the non-Darcy porous medium. In: Ingham DB (2004)

- Bouachir A, Mamon M, Rebhi R, Benissaadi S (2021) Linear and nonlinear stability analyses of double-diffusive convection in a vertical brinkman porous enclosure under Soret and Dufour effects. *Fluids* 6:292
- Caprone F, Rionero S (2016) Brinkman viscosity action in porous MHD convection. *Int J Non-Linear Mech* 85:109–117
- Dubey R, Murthy PVS (2019) The onset of double-diffusive convection in a Brinkman porous layer with convective thermal boundary conditions. *AIP Adv* 9:045322
- Fathi-Kelestani A, Nazari M, Mahmoudi Y (2020) Pulsating flow in a channel filled with a porous medium under local thermal non-equilibrium condition: an exact solution. *J Therm Anal Calori* 145:2753–2775
- Gandomkar A, Gray KE (2018) Local thermal non-equilibrium in porous medium with heat conduction. *Int J Heat Mass Trans* 124:1212–1216
- Govender S, Vadasz P (2007) The effect of mechanical and thermal anisotropy on the stability of gravity-driven convection in rotating porous media in the presence of thermal non-equilibrium. *Transp Porous Media* 69:55–66
- Lagziri H, Bezzazi M (2019) Robin boundary effects in the Darcy-Rayleigh problem with local thermal non-equilibrium model. *Trans Porous Media* 129:701–720
- Mahjoob S, Vafai K (2008) A synthesis of fluid and thermal transport model for metal foam heat exchangers. *Int J Heat Mass Trans* 51:3701–3711
- Malashetty MS, Shivakumara IS, Kulkarni S (2005) The onset of convection in an anisotropic porous layer using a thermal non-equilibrium model. *Transp Porous Media* 60:199–215
- Malashetty MS, Shivakumara IS, Kulkarni S, Swamy M (2006) Convective instability of Oldroyd-B fluid saturated porous layer heated from below using a thermal non-equilibrium model. *Transp Porous Media* 64:123–139
- Nield AD, Bejan A (2017) *Convection in porous media*, 5th edn. Springer, New York
- Postelnicu A (2008) The onset of Darcy-Brinkman convection using a thermal non-equilibrium model—Part II. *Int J Thermal Sci* 47:1587–1594
- Pulvirenti B, Celli M, Barletta A (2020) Flow and convection in metal foams: a survey and new CFD results. *Fluids* 5:155–225
- Rees DAS, Pop I (2002) Vertical free convective boundary layer flow in a porous medium using a thermal non-equilibrium model: elliptic effects. *J Appl Math Phys* 53:1–12
- Saeid NH (2004) Analysis of mixed convection in a vertical porous layer using the non-equilibrium model. *Int J Heat Mass Trans* 47:5619–5627
- Shivakumara IS, Malashetty MS, Chavaraddi KB (2006) Onset of convection in a viscoelastic fluid saturated sparsely packed in a porous layer using a thermal non-equilibrium model. *Can J Phys* 84:973–990
- Shivakumara IS, Mamatha AL, Ravisha M (2010) Boundary and thermal non-equilibrium effects on the onset of Darcy-Brinkman convection in a porous layer. *J Eng Math* 47:317–328
- Storesletten L, Rees DAS (1997) An analytical study of free convective boundary layer flow in porous media: the effect of anisotropic diffusivity. *Transp Porous Media* 27:289–304
- Tyvand PA, Storesletten L (2015) Onset of convection in an anisotropic porous layer with vertical principal axes. *Transp Porous Media* (10)8:581–593 (2015)
- Vadasz P (2019) Instability and convection in rotating porous media. *Rev Fluids* 4:147 (2019)
- Vadasz P (2016) *Fluid flow and heat transfer in rotating porous media*. Springer, New York

Chapter 6

Behavior and Electrocatalytic Degradation of Textile Azo Dye Under Acidic Conditions



Sanaa El Aggadi , Amale Boutakiout, Mariem Ennouhi, Aicha Chadil, and Abderrahim El Hourch

Abstract The decomposition of textile azo dye Violet 5R in H_2SO_4 (1 M) solution was investigated by electrochemical method. Electrochemical behavior of dye was realized with cyclic voltammetry (CV). A conventional three-electrode cell was employed to study a dye concentration and potential scan rate effect, with the platinum (Pt) electrode employed as the working electrode. The potential chosen for the azo dye was between -0.24 V/SCE to 1.5 V/SCE. A linear relationship was found between the square root of the potential scan rate ($v^{1/2}$) and the current density. Such behavior appears characteristic of a diffusion-controlled process. Charge transfer coefficient (α) and the diffusion coefficient (D) were calculated and were found to be 0.49 and $1.84 \times 10^{-5} \text{ cm}^2 \cdot \text{s}^{-1}$, respectively. The electrochemical treatment of the Violet 5R dye in H_2SO_4 solution was performed using the chronoamperometry method by imposing a potential of 1.5 V/SCE for 2 h. The voltammograms before and after electrolysis show a decrease of the current density of anodic peaks after electrolysis. The efficiency of dye removal in the acidic electrolyte achieved 65% after 2 h of electrolysis using the chronoamperometric technique.

Keywords Violet 5R · Cyclic voltammetry · Electrooxidation · Diffusion coefficient · Chronoamperometry · Azo dyes

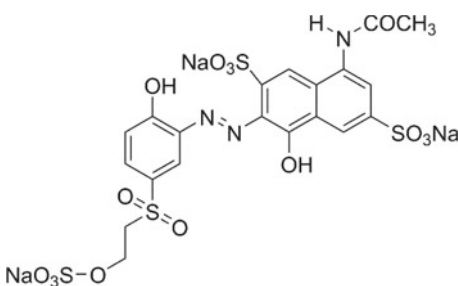
6.1 Introduction

Large quantities of wastewater with various types of reactive dyes are released from the textile industry. Such substances cause not only wastewater pollution, but also lead to an increase in the concentration of chemical oxygen demand (COD) over the limits allowed by the current regulations (Khellouf et al. 2020; Swati and Faruqui 2018). Azo dyes are the most commonly used dyes in the textile industry, they represent between 60 and 70% of all kinds of used dyes (Carliell et al. 1998). Azo dyes in

S. El Aggadi (✉) · A. Boutakiout · M. Ennouhi · A. Chadil · A. El Hourch
Department of Chemistry, Faculty of Sciences, Mohammed V University in Rabat, 4 Avenue Ibn Battouta, BP:1014, Rabat, Morocco
e-mail: sanaa_elaggadi@um5.ac.ma

general are synthetic dyes which contain aromatic groups, so that they are connected to one or several azo groups. ($R_1-N=N-R_2$) (Yu et al. 2018; Unnisa et al. 2020; Liu et al. 2020; El-Khawaga et al. 2021). Various substitutions on the aromatic ring provide a varied as well as polyvalent structural group of compounds due to their recalcitrance and toxicity (Zhang et al. 2021; Albahnasawi et al. 2020). The removal of dyestuffs as a component of textile wastewater can be accomplished by several methods, including adsorption (El-Defrawy et al. 2019; Fawal et al. 2019; Aggadi and Hourch 2021), coagulation (Luo et al. 2019; Sonal and Mishra 2021), reverse osmosis (Jing et al. 2021), or biological degradation (Mishra et al. 2020; Thangaraj et al. 2021). But they don't always allow the complete elimination of dyes and organic matter in wastewater. In this context, scientists are experimenting several alternative processes, like electrooxidation technology (Nabizadeh Chianeh and Avestan 2020; Pirkarami and Fereidooni 2019), ozonation, photocatalytic method (Aminuzzaman et al. 2020; Kaur et al. 2020; Titus and Samuel 2019) for the decomposition of the organics. Among such advanced oxidation processes, electrochemical treatment has received increased focus in recent years because of its unique characteristics, such as, energy efficiency, versatility, cost-effectiveness (Wang et al. 2020; Rafaqat et al. 2022; Aggadi et al. 2021a, 2021b), and promising results (Escalona-Durán et al. 2019; Clematis and Panizza 2021). The aims of this work was to investigate the Violet 5R azo dye removal by electrochemical oxidation with platinum electrode, this pollutant was chosen because it's highly applied in the textile industry. The chemical structure of Violet 5R is listed in Table 6.1 (Ayed et al. 2017).

Table 6.1 The chemical structure and characteristics of Violet 5R dye

Dye name	C.I. Reactive Violet 5
Chemical class	Azo dye
Molecular formula	$C_{20}H_{16}N_3O_{15}S_4Na_3$
Molecular weight	735.58 g/mol
λ_{max}	546 nm
Molecular structure	

6.2 Experimental

Displayed equations are centered and set on a separate line. A three-electrode cell with a Pt electrode (0.2 cm^2) serving as the working electrode (WE), glassy carbon acting as the counter electrode (CE), and a saturated calomel electrode (SCE) as the reference electrode (RE) were used for electrochemical oxidation. Measurements of cyclic voltammetry and chronoamperometry were conducted by means of a PGZ 301 potentiostat/galvanostat that is controlled by the VoltMaster 4 software. Violet 5R was obtained from OH YOUNG INDUSTRIAL CO. LTD. Sulfuric acid (96%, Sigma-Aldrich) was employed for electrolyte ($1 \text{ M H}_2\text{SO}_4$) preparation. All solutions are made using ultrapure water. Prior to all scans, and to provide a reproducible surface, the electrode was prepared by polishing, the electrode was prepared to provide a reproducible surface by polishing, rinsing with distilled water, and then cleaned electrochemically by CV in a $1 \text{ M H}_2\text{SO}_4$ solution until obtaining a reproducible voltammogram. All electrochemical investigations were carried out at room temperature ($25 \text{ }^\circ\text{C}$).

6.3 Results and Discussion

6.3.1 Influence of Violet 5R Dye Concentration

The cyclic voltammograms recorded for various concentrations between 0.5 and 10 mM of Violet 5R dye during cycling in the potential area from -0.24 to 1.5 V/SCE in H_2SO_4 (1 M) solution at a scan rate of 50 mV/s are shown in Fig. 6.1. The voltammetric curve of the dye shows, for all concentrations, the presence of anodic peaks at 0.42 V/SCE , 0.75 V/SCE and 1.33 V/SCE in forward sweep and cathodic peaks at 1.14 V/SCE , 0.46 V/SCE and -0.08 V/SCE in reverse scan. An oxidation and reduction peak were observed just for the 5 mM and 10 mM concentrations. According to this figure, it can be easily observed that when the concentration of Violet 5R dye increases, the current density of the anodic peaks increases and their position moves to the highest potential levels.

The obtained voltammograms demonstrate that it is possible to detect even millimolar concentrations of dye. Figure 6.2a displays the oxidation peaks current density plotted against Violet 5R concentration. The peak current density increases when the concentration of Violet 5R increases, with a linear variation ($R^2 = 0.98$). Figure 6.2b shows the evolution of the peak potential versus the logarithm of Violet 5R concentration. The anodic peak potential is linearly varied with respect to the logarithm of Violet 5R concentration ($R^2 = 0.98$).

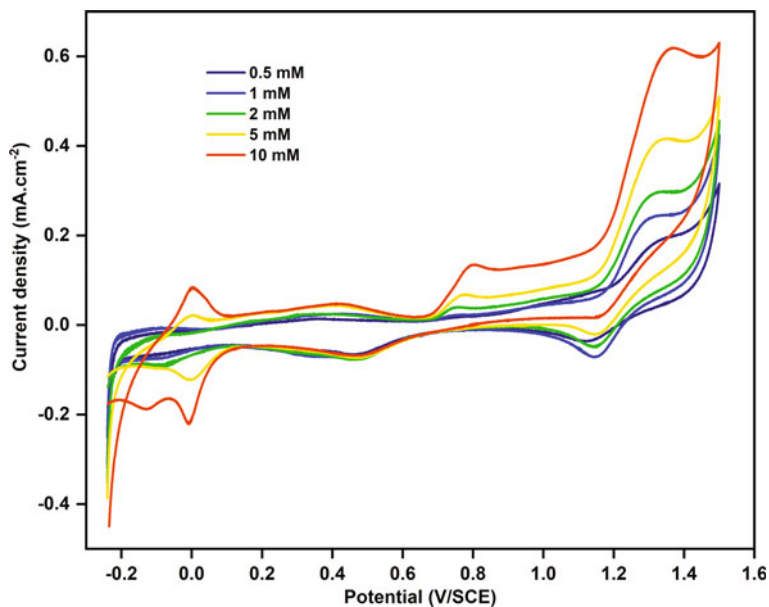


Fig. 6.1 Cyclic voltammograms plotted with the Pt electrode at a potential scan rate of 50 mV/s for various concentrations of Violet 5R dye in 1 M H₂SO₄

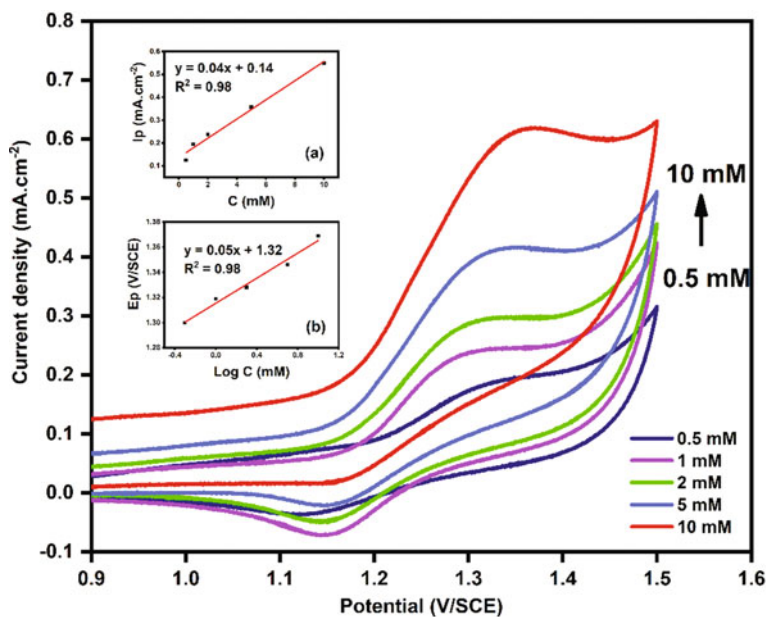


Fig. 6.2 Cyclic voltammograms for the oxidation of Violet 5R at various concentrations, **a** Dependence of the oxidation peak current density versus concentration, **b** Evolution of the oxidation peak potential as function of $\log(C)$

6.3.2 Influence of Potential Scan Rate

From the relation between scan rate (v) and peak current, constructive information is obtained about the electro-chemical process. The electrochemical behavior of Violet 5R at various scan rates was explored through the use of cyclic voltammetry method from 20 to 500 mV/s recorded at Pt working electrode for 1 M H_2SO_4 and 10 mM of Violet 5R (See Fig. 6.3). An increase in the scan rates led to an increase in the anodic peak currents (I_{pa}) and the peak potential (E_p) moves to the highest potential levels. A possible explanation for this behavior is that species are depleted near the Platinum surface when sufficient potential is imposed on the Pt- surface leading to species oxidation in the solution (Sayyah et al. 2014).

The peak currents for the anodic oxidation of Violet 5R dye were proportional to the square root of the scan rate ($v^{1/2}$) over the range 20–500 mV/s as shown in Fig. 6.3a (inset). This result demonstrates that up to the scan rate = 500 mV/s, the reaction is controlled by the diffusion of Violet 5R (Gowda and Nandibewoor 2014), and the formula can be written as follows:

$$I_p \text{ (mA)} = 1.80v^{1/2} \text{ (V/s)}^{1/2} + 0.16, \quad (R^2 = 0.99) \quad (6.1)$$

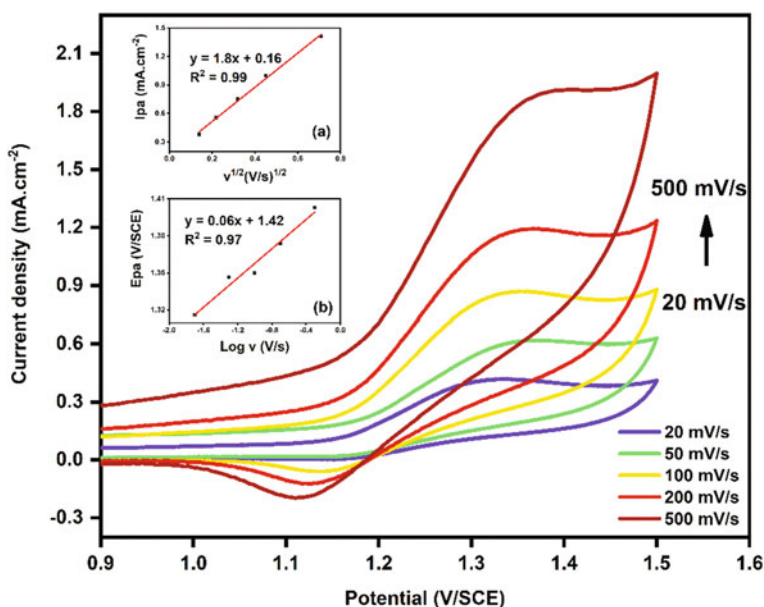


Fig. 6.3 Cyclic voltammograms recorded at different potential scan rate (v) (20–500 mV/s) of violet 5R dye (10 mM) in 1 M H_2SO_4 , **a** Evolution of the oxidation peak current density as function of $v^{1/2}$, **b** Evolution of the oxidation peak potential as function of $\log v$

The E_p of the oxidation peak was also a function of the scan rate. By increasing the scan rate, the peak potential moved to more positive values, indicating the irreversibility of the oxidation mechanism, and the following equation can be used to express a linear relationship between the peak potential and the logarithm of the scan rate (See Fig. 6.3b):

$$E_p (V) = 0.06 \log v (V/s) + 1.42, (R^2 = 0.97) \quad (6.2)$$

Furthermore, a straight line of the Tafel plot between the E_p and the logarithm of the scan rates is shown in the lower inset of Fig. 6.3. The linear formula is given as follows: $E_p = 0.06 \log v + 1.42, R^2 = 0.97$.

In order to determine the diffusion coefficient, we use the peak current density I_p of cyclic voltammetry curve for an irreversible process, expressed as (Wei et al. 2022):

$$I_p = 0.4958 \times nF(\alpha nF/RT)^{1/2} \times A \times C \times D^{1/2} \times v^{1/2} \quad (6.3)$$

where:

- D: Diffusion coefficient;
- n: Number of electrons transferred;
- T: Temperature;
- C: Initial concentration of Violet 5R;
- α : Charge transfer coefficient;
- A: Active surface area of the WE;
- R: Ideal gas constant;
- F: Faraday's constant;
- V: Potential scan rate.

α can be found from the following equation:

$$E_p = 0.5b \log v + K \quad (6.4)$$

With:

- B: Tafel slope;
- K: Potential intercept.

Based on Eq. (6.3), the slope of $E_p = f(\text{Log } v)$ is:

$$dE_p/d\log v = b/2 \quad (6.5)$$

With:

$$b = 2.3RT/\alpha nF \quad (6.6)$$

Form the slope of the linear evolution of E_p with $\text{Log } v$ from data exhibited in Fig. 6.3b, the α value can be found utilizing Eq. (6.6). With the α values, the diffusion coefficient D of Violet 5R is determined by the slope of the right lines depicted in

Fig. 6.3a through the use of Eq. (6.3). The deduced values of α and D of Violet 5R are 0.49 and $1.84 \times 10^{-5} \text{ cm}^2 \cdot \text{s}^{-1}$.

6.3.3 Electrolysis of Violet 5R Dye by Chronoamperometry

Chronoamperometry experiment was carried out at a constant potential of 1.5 V/SCE during 2 h of electrolysis in a solution containing 10 mM of Violet 5R in 1 M H_2SO_4 (See Fig. 6.4). The plots depict a typical current drop within the first seconds related to the oxidation of Violet 5R on the Pt electrode by applying 1.5 V/SCE, succeeded by a smaller change with respect to time, attributed to the oxidation of Violet 5R at equilibrium conditions. In Fig. 6.4 (Insert), we found a linear dependence between $t^{-1/2}$ and I the current density. This means that the transient current must be controlled by a diffusion process (Li et al. 2020). According to the graph, the current stabilizes after a nucleation phase. The curve therefore reflects the degradation of Violet 5R dye in H_2SO_4 . Indeed, the color of the solution is becoming more and more pastel.

We plotted voltammograms of Violet 5R in H_2SO_4 before and after electrolysis. We can observe that the cyclic voltammogram taken after 2 h of electrolysis showed a pronounced diminution of the oxidation peak of Violet 5R dye as well as the color

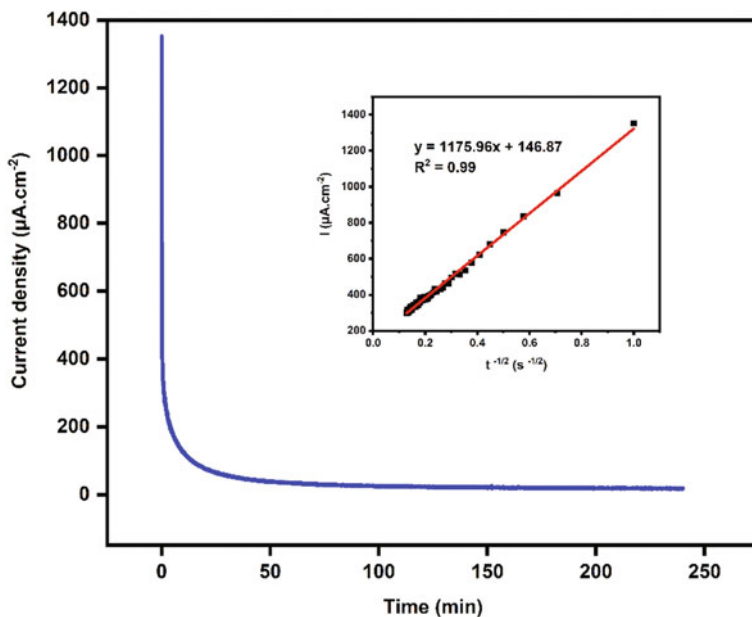


Fig. 6.4 Chronoamperometry plot of Violet 5R dye (10 mM) dissolved in H_2SO_4 (1 M) solution for 2 h at 1.5 V/SCE. *Insert:* I versus $t^{-1/2}$

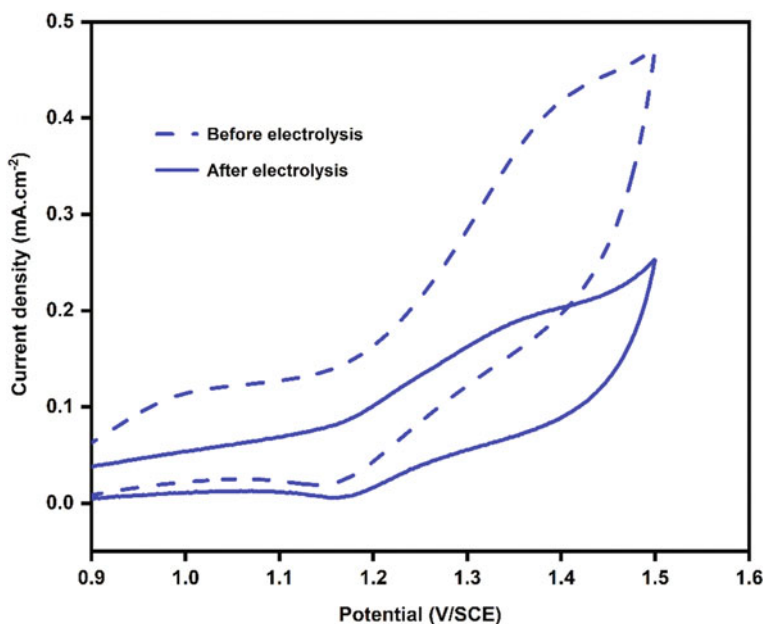


Fig. 6.5 Cyclic voltammograms registered prior and after the electrolysis process of Violet 5R dye (10 mM) using 50 mV/s

of the solution becomes paler (See Fig. 6.5). It can be said that the concentration of Violet 5R dye in H₂SO₄ has decreased, which shows that there is a degradation of the dye after electrolysis.

The % of dye elimination was calculated using the formula (Anantha et al. 2020):

$$R(\%) = \frac{C_0 - C}{C_0} * 100\% \quad (6.7)$$

where:

C₀: Concentrations of the dye before electrolysis (mol.L⁻¹);

C: Concentrations of the dye after electrolysis (mol.L⁻¹).

The dye removal efficiency is 65% after 2 h of electrolysis in H₂SO₄ medium at room temperature.

6.4 Conclusion

At room temperature, the decolorization of textile azo dye Violet 5R in H₂SO₄ was realized by the electro-chemical degradation, the process was performed in a three-electrode cell at constant potential with a Pt wire used as WE. A strong relationship

between the peak current density (I) and Violet 5R dye concentration, as the dye concentration increases with a linear variation ($R^2 = 0.98$), the peak current density increases, it means that Violet 5R easily oxidizes on the Pt electrode surface. The electrocatalytic oxidation of dye is affected significantly by faster potential scan rates. The charge transfer coefficient (α) and the diffusion coefficient (D) were calculated and found to be 0.49 and $1.84 \times 10^{-5} \text{ cm}^2 \cdot \text{s}^{-1}$ respectively. The percent of color removal in acid environment is 65% after 2 h of electrolysis. The global experimental results show that the electrochemical process is able to be employed as a pretreatment step before conventional treatment.

References

- Anantha MS, Olivera S, Hu C, Jayanna BK, Reddy N, Venkatesh K, Muralidhara HB, Naidu R (2020) Comparison of the photocatalytic, adsorption and electrochemical methods for the removal of cationic dyes from aqueous solutions. *Environ Technol Innov* 17:100612
- Aminuzzaman M, Chong CY, Goh WS, Phang YK, Lai-Hock T, Chee SY, Akhtaruzzaman M, Ogawa S, Watanabe A (2020) Biosynthesis of NiO nanoparticles using soursop (*Annona muricata* L.) fruit peel green waste and their photocatalytic performance on crystal violet dye. *J Clust Sci* 1–10
- Albahnasawi A, Yüksel E, Gürbulak E, Duyum F (2020) Fate of aromatic amines through decolorization of real textile wastewater under anoxic-aerobic membrane bioreactor. *J Environ Chem Eng* 8:104226
- Ayed L, Bekir K, Achour S, Cheref A, Bakhrouf A (2017) Exploring bioaugmentation strategies for azo dye CI Reactive Violet 5 decolorization using bacterial mixture: dye response surface methodology. *Water Environ J* 31:80–89
- Carliell CM, Barclay SJ, Shaw C, Wheatley AD, Buckley CA (1998) The effect of salts used in textile dyeing on microbial decolourisation of a reactive azo dye. *Environ Technol (United Kingdom)* 19:1133–1137
- Clematis D, Panizza M (2021) Application of boron-doped diamond electrodes for electrochemical oxidation of real wastewaters. *Curr Opin Electrochem* 30:100844
- El Aggadi S, El Abbassi Z, El Hourch A (2021a) Color removal from dye-containing aqueous solutions by electrooxidation. *Desalin Water Treat* 215:232–236
- El Aggadi S, Kaichouh G, El Abbassi Z, Fekhaoui M, El Hourch A (2021b) Electrode material in electrochemical decolorization of dyestuffs wastewater: a review. In: *E3S web of conferences*
- El Aggadi S, El Hourch A (2021) Removal of reactive blue 21 (RB21) phthalocyanine dye from aqueous solution by adsorption process: a review. *Polish J Environ Stud* 30:3425–3432
- Escalona-Durán F, Villegas-Guzman P, dos Santos EV, da Silva DR, Martínez-Huitile CA (2019) Intensification of petroleum elimination in the presence of a surfactant using anodic electrochemical treatment with BDD anode. *J Electroanal Chem* 832:453–458
- El-Defrawy MM, Kenawy IMM, ZAKI E, El-tabey RM (2019) Adsorption of the anionic dye (Diamond Fast Brown KE) from textile wastewater onto chitosan/montmorillonite nanocomposites. *Egypt J Chem* 62:13–14
- El Fawal G, Ibrahim A, Akl M (2019) Methylene blue and crystal violet dyes removal (as a binary system) from aqueous solution using local soil clay: kinetics study and equilibrium isotherms. *Egypt J Chem* 62:541–554
- El-Khawaga AM, Farrag AA, Elsayed MA, El-Sayyad GS, El-Batal AI (2021) Promising antimicrobial and azo dye removal activities of citric acid-functionalized magnesium ferrite nanoparticles. *J Clust Sci* 1–17
- Gowda JI, Nandibewoor ST (2014) Electrochemical behavior of paclitaxel and its determination at glassy carbon electrode. *Asian J Pharm Sci* 9:42–49

- Jing X, Yuan J, Cai D, Li B, Hu D, Li J (2021) Concentrating and recycling of high-concentration printing and dyeing wastewater by a disc tube reverse osmosis-Fenton oxidation/low temperature crystallization process. *Sep Purif Technol* 266:118583
- Kaur H, Kaur S, Kumar S, Singh J, Rawat M (2020) Eco-friendly approach: synthesis of novel green TiO₂ nanoparticles for degradation of reactive green 19 dye and replacement of chemical synthesized TiO₂. *J Clust Sci* 1–14
- Khellouf M, Chemini R, Salem Z, Khodja M, Zeriri D, Jada A (2020) A new activated carbon prepared from cypress cones and its application in the COD reduction and colour removal from industrial textile effluent. *Environ Dev Sustain* 1–16
- Liu Y, Huang L, Mahmud S, Liu H (2020) Gold nanoparticles biosynthesized using ginkgo biloba leaf aqueous extract for the decolorization of azo-dyes and fluorescent detection of Cr(VI). *J Clust Sci* 31:549–560
- Li C, Li S, Che Y, Li J, Shu Y, He J, Song J (2020) Electrochemical behavior of niobium ions in molten KCl-NaCl. *J Mater Res Technol* 9:9341–9347
- Luo X, Liang C, Hu Y (2019) Comparison of different enhanced coagulation methods for azo dye removal from wastewater. *Sustainability* 11:4760
- Mishra S, Nayak JK, Maiti A (2020) Bacteria-mediated bio-degradation of reactive azo dyes coupled with bio-energy generation from model wastewater. *Clean Technol Environ Policy* 22(22):651–667
- Nabizadeh Chianeh F, Avestan MS (2020) Application of central composite design for electrochemical oxidation of reactive dye on Ti/MWCNT electrode. *J Iran Chem Soc* 17:1073–1085
- Pirkarami A, Fereidooni L (2019) Titanium electrode modified by nano-PMDAH as a highly efficient polymer for removal of reactive red 13 using solar cells for energy-harvesting applications. *J Iran Chem Soc* 16:851–864
- Rafaqat S, Ali N, Torres C, Rittmann B (2022) Recent progress in treatment of dyes wastewater using microbial-electro-Fenton technology. *RSC Adv* 12:17104–17137
- Sayyah SM, Abd-Elrehim SS, Azooz RE, Mohamed F (2014) Electrochemical study of the copolymer formation between o-chlorophenol and o-hydroxyphenol. *J Korean Chem Soc* 58:289–296
- Sonal S, Mishra BK (2021) Role of coagulation/flocculation technology for the treatment of dye wastewater: trend and future aspects. *Water Pollut Manag Pract* 303–331
- Swati SS, Faruqui AN (2018) Investigation on ecological parameters and COD minimization of textile effluent generated after dyeing with mono and bi-functional reactive dyes. *Environ Technol Innov* 11:165–173
- Thangaraj S, Bankole PO, Sadasivam SK (2021) Microbial degradation of azo dyes by textile effluent adapted, enterobacter hormaechei under microaerophilic condition. *Microbiol Res* 250:126805
- Titus D, Samuel EJJ (2019) Photocatalytic degradation of azo dye using biogenic SnO₂ nanoparticles with antifungal property: RSM optimization and kinetic study. *J Clust Sci* 30:1335–1345
- Unnisa A, Abouzied AS, Baratam A, Lakshmi KNVC, Hussain T, Kunduru RD, Banu H, Fatima SB, Hussian A, Selvarajan KK (2020) Design, synthesis, characterization, computational study and in-vitro antioxidant and anti-inflammatory activities of few novel 6-aryl substituted pyrimidine azo dyes. *Arab J Chem* 13:8638–8649
- Wang AJ, Wang HC, Cheng HY, Liang B, Liu WZ, Han JL, Zhang B, Wang S (2020) Sen: Electrochemistry-stimulated environmental bioremediation: development of applicable modular electrode and system scale-up. *Environ Sci Ecotechnology* 3:100050
- Wei X, Wang G, Li F, Zhang J, Chen J, Wang R (2022) High performance positive electrolyte with potassium diformate (KDF) additive for vanadium redox flow batteries. *Int J Electrochem Sci* 17:2
- Yu X, Liu H, Diao J, Sun Y, Wang Y (2018) Magnetic molecularly imprinted polymer nanoparticles for separating aromatic amines from azo dyes—synthesis, characterization and application. *Sep Purif Technol* 204:213–219
- Zhang C, Chen H, Xue G, Liu Y, Chen S, Jia C (2021) A critical review of the aniline transformation fate in azo dye wastewater treatment. *J Clean Prod* 321:128971

Chapter 7

Modeling and Simulation of Phytoremediation Technology by Artificial Neural Network



**Saloua Elfanssi, Jamal Mabrouki, Kaoutar El Oumlouki, Ghizlane Fattah,
and Laila Mandi**

Abstract Nowadays, Constructed wetland (CW) technologies present an advantageous alternative system for wastewater treatment. However, there is not an effective model admitted to providing an implement for forecasting their performances. In this study, the neural network model was applied to predict the effluent physicochemical parameters and total coliforms and fecal streptococci in a hybrid constructed wetland plant (HCW) processing domestic wastewater. The Tidili treatment plant was made up of three parallel vertical flow beds (VF), followed by two horizontal flow beds (HF) working in parallel, with *Phragmites australis* as the vegetation. The Tidili treatment plant was controlled every 15 days for 2 years. Sampling was taken at the tank inlet, and at both the VF and HF outlets. The Sigmoidal activation functions with a Feed-Forward Back-Propagation were used to foretell the removal rates of pollutants from domestic wastewater. The main removal percentages of physicochemical parameters were 94% of TSS, 92% of BOD₅, 90% of COD, 66% of TN and 63% of TP. HCWs showed a high capacity to eliminate coliforms (4.44 Log units total coliforms, 4.30 Log units fecal coliforms) and fecal streptococci (4.08

S. Elfanssi (✉) · L. Mandi

National Center for Research and Studies On Water and Energy (CNEREE), Cadi Ayyad University, P.O.Box 511, 40000 Marrakech, Morocco
e-mail: elfanssi90@gmail.com

Laboratory of Hydrobiology, Ecotoxicology and Sanitation (LHEA, URAC 33), Faculty of Sciences Semlalia, Marrakech, Morocco

J. Mabrouki

Laboratory of Spectroscopy Molecular Modelling, Materials, Nanomaterial, Water and Environment, CERNE2,D Faculty of Science, Mohammed V, University in Rabat, Avenue IbnBattouta, BP1014 Rabat, Agdal, Morocco

K. E. Oumlouki

Faculty of Sciences, Advanced Materials and Process Engineering Laboratory, Ibn Tofail University, Kenitra, Morocco

Ghizlane Fattah

Water Treatment and Reuse Structure, Civil Hydraulic and Environmental Engineering Laboratory, Mohammadia School of Engineers, Mohammed V University in Rabat, Avenue IbnSina B.P 765, 10090 Agdal Rabat, Morocco

Log units). Artificial neural networks (ANNs) was calibrated and validated based on the physicochemical parameters (TSS, BOD₅, COD) and microbiological parameters (TC, FS). The model indicated that the simulated values of physicochemical parameters and microbiological parameters were in close coordination with their target values. Thus, ANN model was found to be a useful implement to forecast the examined performances using HCWs.

Keywords Constructed · Wetland · Domestic wastewater · Removal efficiency · Model · Artificial neural networks · Systems · Performances · Parameters · Treatment · Quality · Modeling

7.1 Introduction

Waste management, in general, and liquid waste in particular, is today a very serious environmental issue in developing countries. If this observation is general, the situation is particularly serious in rural areas because of the nature of dispersed populations and mountainous terrain. This has been accentuated with the notable evolution of potable water access, by the Rural Water Supply Projects, which raises the rate to over 91% (4) without worrying about the future of wastewater. In fact, apart from a few rural centers those have sanitation and wastewater collection network, the rural habitat does not have adequate infrastructure for collective or individual sanitation. Wastewater from most of these centers is released into the natural environment without prior treatment which has a negative impact on the health of the population, water resources and the environment in general (Senzia et al. 2003).

The ecological systems such as CW have characteristics that make them particularly suitable for small communities from technical and socio-economic point of view (Vymazal 2011). Indeed, these extensive purification devices are a cheaper alternative for operation and construction than intensive systems. The CW succeeds to protect environment from many contaminants from domestic wastewater for instance: organic substances, solids suspended, bacteria, and nutrients (Ranieri et al. 2013) and (Elfanssi et al. 2018) and (Rizzo et al. 2020). Furthermore, they are effective to eliminate the physicochemical parameters as well as removing emerging organic pollutants (Matamoros and Bayona 2008).

Modeling for HCW is key in order to provide an implement for simulating its operation and to form a basis for monitoring the biological and physical process. Artificial neural networks (ANN) are composed of layers of interconnected neurons or neural nodes. They are determined by the network architecture, the topology, the characteristics neuron, and learning rules (Lippmann 1987). The neural networks most commonly used in engineering are multi-layered, pro-active, backward propagation with node architecture. The number of calculation units in the input and output layers represents the desirable shape of inputs and outputs, however the optimal figure of neural nodes in the hidden layer (s) is usually determined by trial and error. The neural network with a hidden layer is generally adopted in process engineering

although very complex correlations between the inlet and outlet data need more than one hidden layer with a large number of neural nodes. So many hidden neural nodes could cause over-learning or undesirable consequences like learning process noise. The neural nodes can be attached to all other neural nodes in the next layer via weighed connections. Weights are true numbers, usually in the range of $[0, 1]$. In the process of learning, the weights of the connections are adjusted iteratively, usually beginning with small values given randomly and ending with weights producing an outgoing network that corresponds to the desired output within a certain margin of error.

In a pro-active neural network, the input neural nodes are only used to store and propagate normalized following data to the network. Hidden nodes and output nodes perform two calculations. First, a weighed sum of all inputs from nodes connected in the previous layer or outside the network is formed. Then the output of the neural nodes is obtained through the sum weighed by a nonlinear transfer function. The most commonly used transfer function is the sigmoid function.

Upon learning, the model compares the estimated and target output values during the repeated introduction of example output and input data peer trends, and it modifies the weights associated with the connections between the neural nodes by back propagation. In rear propagation, the weights are changed through the propagation of an error signal coming from the output to the input.

The aim of this experiment is to develop an artificial neural networks model to perform the task of predicting the physicochemical and biological parameters.

7.2 Materials and Methods

7.2.1 Description of the Phytoremediation System

The established ANN model was tested to the Tidili wastewater plant, which is studied for the first time in Morocco, The Tidili WWTP is it is oriented in the direction of $31^{\circ} 29'47.39''$ “north latitude, $7^{\circ} 34'4.03''$ ” of longitude and 876 m NGM altitude and primarily constructed to manipulate the following loads: population served = 200,000; hydraulic loading rates of $66 \text{ m}^3/\text{day}$ (Fig. 7.1).

The flow process line consists of a lifting station, at the entrance to the plant to raise domestic wastewater to a retention basin; the latter allows the evacuation of raw wastewater to five beds planted with *Phragmites australis*. The characteristics of the two beds are presented in Table 7.1. The first stage is consist of 3 vertical flow constructed wetlands (VF) that has a surface area of 130 m^2 (length = 13 m, width = 10 m, depth = 90), and the second of 2 horizontal subsurface flow constructed wetlands (HF) in parallel as well; with (length = 11 m, width = 8 m) each at a depth of 60 cm. Each basin has a slope of 1% and feeds for 2 days and then incurs a pause to permit the control of the plant biomass and to maintain aerobic conditions inside the bed (Avellan et al. 2017).

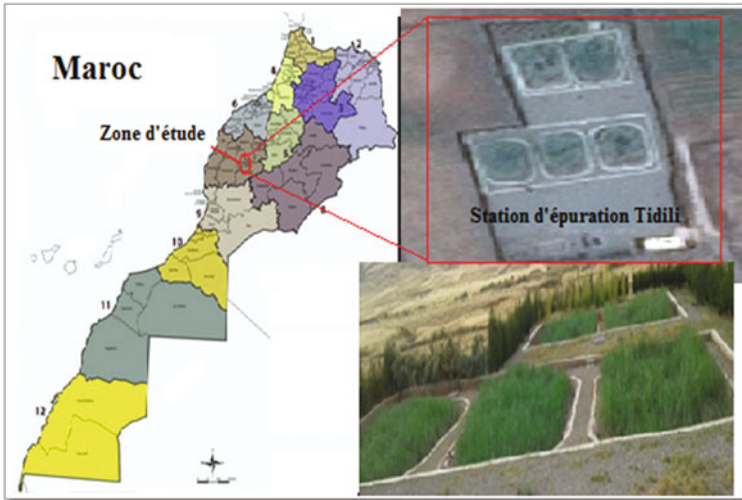


Fig. 7.1 Location wastewater treatment plant of Tidili

Table 7.1 Characteristics of Tidili wastewater treatment plant

Parameter	Unit	Value	
		VF	HF
Surface area	m ²	130	88
HRT (theoretical)	days	2	3
Gravel depth	m	90	60
OLR	g BOD/m ² /d	194 ± 14.66	28 ± 11.36

Notes: ±. standard deviations; Abbreviations: VF. Vertical flow constructed wetlands; HF. Horizontal subsurface flow constructed wetlands; OLR. Organic loading rate

7.2.2 Data Collection

The hybrid constructed wetlands plant was controlled each 15 days during 2 years. This duration was adequate as it covers all expected seasonal fluctuations in the experiment variables. Water samples were collected manually in 500 ml sterile bottles from the storage tank inlet, and at both the VF and HF outlets. The samples were stored in ice tanks, sent to laboratory and analyzed for BOD₅, COD, TSS, TC, and FS. The influent and effluent pollutants concentrations were evaluated according to APHA (2005) and (Standards 2006).

The ANN was designed in the geographic aggregation Tool R, with reverse feed-forward propagation to predict the results of the hybrid constructed wetlands plant. The input and output contaminants for the models are physicochemical and biological parameters. To evaluate the predicted results of different neural models, the root mean square error (RMSE), mean absolute error, the correlation coefficient (R) for the training set and the Nash were used between all observed and measured parameters and described as follows:

$$R = \frac{\sum(\alpha_{obs} - \bar{\alpha}_{obs}) \times (\alpha_{cal} - \bar{\alpha}_{cal})}{\sqrt{\sum(\alpha_{obs} - \alpha_{obs})^2 \times \sum(\alpha_{cal} - \alpha_{cal})^2}} \quad (7.1)$$

$$RMSE = \sqrt{\frac{\sum(\alpha_{obs} - \alpha_{cal})^2}{n}} \quad (7.2)$$

$$Nash = 1 - \frac{\sum(\alpha_{obs} - \alpha_{cal})^2}{\sum(\alpha_{obs} - \alpha_{obs})^2} \quad (7.3)$$

where: α_{obs} : observed value; α_{cal} : calculated value; n : number of observations; and $\bar{\alpha}$: average of observed and calculated values.

7.3 Results and Discussion

A neural network modeling was used to analyze the effectiveness level of the Tidili wastewater treatment plant. The effectiveness of the treatment plant was evaluated for 2 years applying this advanced developed. The multi-layer neural network modeling was developed in “R” software, which provides a program for the simulation. The inlet pollutants applied in this survey are organic matter, suspended matter and coliforms. The system of the model created in this survey was consists of (5) input and output layer of neuron and (3) hidden layers and (Fig. 7.2).

The performance for organic matter, suspended matter and coliforms are showed in Fig. 7.3 by following the observed and simulated out-put contaminants. The noted values of the physicochemical and biological parameters were in related accordance with their corresponding simulated values. It should be indicated that, findings of calibration method are encouraging since they precisely reflect the predicted values.

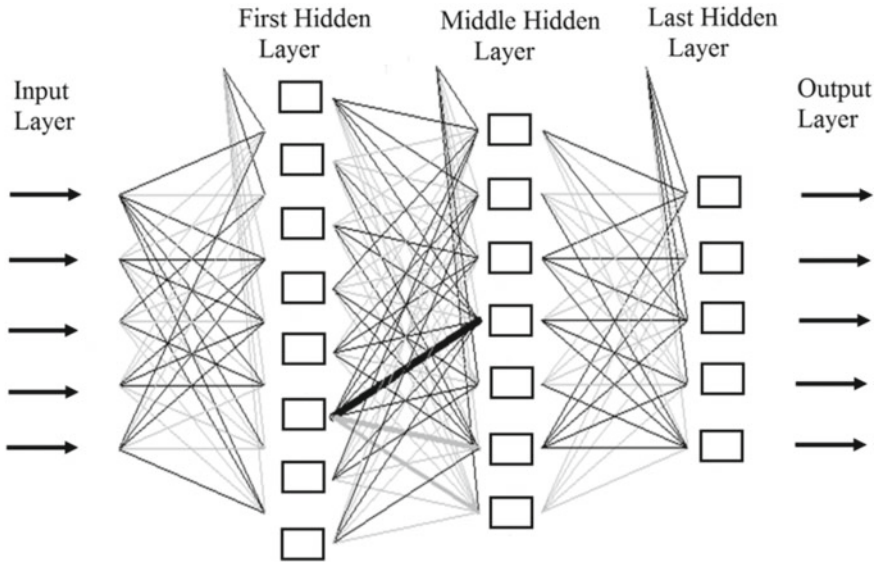


Fig. 7.2 Structure of ANN model

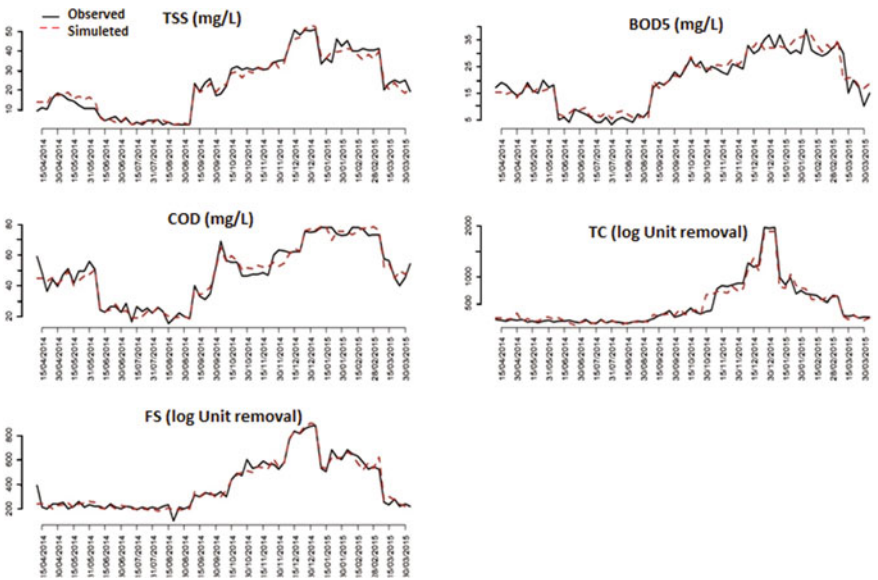


Fig. 7.3 Calibration of effluent organic matter, suspended matter and coliforms using artificial neural networks

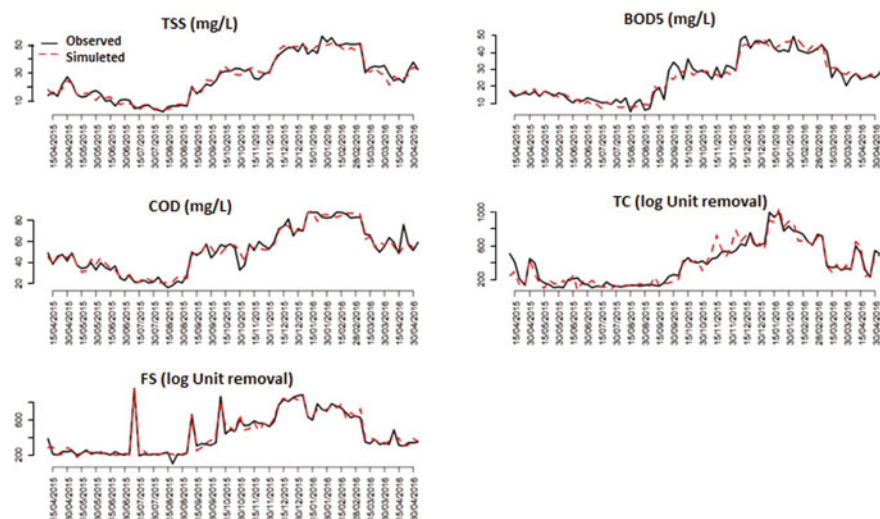


Fig. 7.4 Validation of effluent organic matter, suspended matter and coliforms using artificial neural network

Figure 7.4 shows the performance validation results for the second 50% of the inlet values. The model outcomes were particularly suitable. The experimental output concentrations for organic matter, suspended matter and coliforms are quite similar to the ANN model outcome concentrations. The findings pronounced the highest correlation coefficient (R-value) between the observed and simulated outcome variables, excess up to 0.9. These metrics are in agreement with the results of Vijayan and Mohan (2016); Zidan et al. 2015), who applied ANN systems to predict the effectiveness of Tidili WWTP.

Table 7.2 presents the RMSE values and Nash criterion gotten for the calibration and validation period for physicochemical and biological parameters. In calibration, the RMSE rate fluctuated between 2.70 for the TSS and 88.19. In addition, the values of the validation criteria seem good and oscillate between 0.91 and 0.97. The RMSE values ranging between 3.11 and 76.65. The Nash rates fluctuate from 0.91 and 0.97 for calibration with the multi-layer network modeling (Table 7.2).

7.4 Conclusion

This work described an assessment of hybrid constructed wetlands in a small community in a mountainous region of Morocco. The Tidili of hybrid constructed wetlands plant has operated remarkably well. The mean removal efficiencies of BOD5, COD, TSS, TN and TP exceeding 94, 92, 90, 66 and 63%, respectively. As well, the removal of TC, FC and FS were 4.44, 4.30 and 4.08 Log units respectively. Despite the simplicity and thrifty of this methods of treatment, they are well recommended in

Table 7.2 RMSE values and Nash criterion gotten for the modeling process

	RMSE	Nash
	Formule	
Paramètres	$RMSE = \sqrt{\frac{\sum (Q_{obs} - Q_{calc})^2}{n}}$	$Nash = 1 - \frac{\sum (Q_{obs} - Q_{calc})^2}{\sum (Q_{obs} - Q_m)^2}$
MES	2.70* 3.11**	0.97* 0.95**
DBO5	2.86* 3.29	0.92* 0.93**
DCO	4.21* 4.86**	0.95* 0.94**
CT	88.19* 76.65**	0.95* 0.91**
SF	38.02* 42.08**	0.96* 0.96**

RMSE, root mean square error; *calibration; **validation

rural regions of Morocco, because this method depends low cost, low energy but high technology process which imply subtle hydrological and biological phenomena. Thus, it may be inferred that Tidili wastewater treatment plant showed to be a reliable system to treated and reuse domestic wastewater in the montagne rural areas of Morocco.

Acknowledgements This work was supported by the National Centre for Studies and Research on Water and Energy (CNEREE), University of Cadi Ayyad.

References

- APHA (2005) Standard methods for the examination of water and wastewater, 20th edn. American Public Health Association, American Water Works Association, and Water Environment Federation, Washington, DC
- Avellan CT, Ardakanian R, Gremillion P (2017) The role of constructed wetlands for biomass production within the water-soil-waste nexus. *Water Sci Technol* 75(10):2237–2245
- Elfanssi S, Ouazzani N, Latrach L, Hejjaj A, Mandi L (2018) Phytoremediation of domestic wastewater using a hybrid constructed wetlands in mountainous rural area. *Inter J Phyto* 20(1):75–87
- Lippmann RP (1987) An introduction to computing with neural nets. *IEEE ASSP Mag* 4(2):4–22
- Matamoros V, Bayona JM (2008) Behavior of emerging pollutants in constructed wetlands. In: Barceló D, Petrovic M (eds) Emerging contaminants from industrial and municipal waste. The handbook of environmental chemistry, vol 5/5S/5S/2. Springer, Berlin, Heidelberg
- Moroccan Standards (2006) Moroccan standard approved by order of the minister of industry, trade and economy last level. Moroccan Industrial Standardization Service

- Ranieri E, Gikas P, Tchobanoglous G (2013) BTEX removal in pilot-scale horizontal subsurface flow constructed wetlands. *Desalin Water Treat* 51:3032–3039
- Rizzo A, Tondera K, Pálffy TG, Dittmer U, Meyer D, Schreiber C, Zacharias N, Ruppelt JP, Esser D, Molle P, Troesch S, Masia F (2020) Constructed wetlands for combined sewer overflow treatment: a state-of-the-art review. *Sci Total Environ* 727
- Senzia M, Mashauri DA, Mayo AW (2003) Suitability of constructed wetlands and waste stabilisation ponds in wastewater treatment: nitrogen transformation and removal. *Phys Chem Earth, Parts a/b/c* 28:1117–1124
- Vijayan A, Mohan GS (2016) Prediction of effluent treatment plant performance in a dairy industry using artificial neural network technique. *J Civil Environ Eng* 6:6. <https://doi.org/10.4172/2165-784X.1000254>
- Vymazal J (2011) Constructed wetlands for wastewater treatment: five decades of experience. *J Environ Sci Technol* 45(1):61–69
- Zidan AA, Rashed AA, Hatata AY, Abd El-Hady MA (2015) Artificial neural networks to predict wastewater treatment in different media hssf constructed wetlands. In: J eighteenth international water technology conference (IWTC18)

Chapter 8

Cryptocurrency Returns Clustering Using Japanese Candlesticks: Towards a Programmatic Trading System



Ahmed El Youssefi, Abdelaaziz Hessane, Yousef Farhaoui, and Imad Zeroual

Abstract Cryptocurrency trading drove the attention of individual traders during and after the lockdown period caused by COVID-19 restrictions. Trading systems use Japanese candlesticks-derived technical indicators to decide on behalf of traders. They offer insights into the market trend and help traders to decide how to manage their cryptocurrency portfolio. Japanese candlesticks help visualize the movement of cryptocurrencies' prices over a given period. This transformation is widely used to forecast the future trend, volatility, and prices of a cryptocurrency. Most of the research on forecasting returns suggests using three classes, uptrend, downtrend, and insignificant changes. Within this paper, we applied KMeans clustering to the Japanese candlesticks over a daily period of five of the highest capitalized non-stable coins (Bitcoin, Ethereum, BNB coin, Cardano, and Solana). Results indicate that the optimal number of clusters is ranging from 5 to 6 clusters using the elbow method for all the considered cryptocurrencies. The range of obtained results suggests that we should opt for a per cryptocurrency number of classes when dealing with cryptocurrencies classification tasks rather than using the three classes mentioned above.

Keywords Cryptocurrency · Trading · Clustering · KMeans · Elbow method

8.1 Introduction

8.1.1 Cryptocurrency Trading

Following the mass adoption of cryptocurrencies, trading platforms were developed to make their trading more accessible for ordinary people. A trading platform is a system where users can sell and buy enlisted cryptocurrency pairs. A tradable

A. El Youssefi (✉) · A. Hessane · Y. Farhaoui · I. Zeroual
STI Laboratory, T-IDMS, Faculty of Sciences and Techniques, Moulay Ismail University of
Meknes, Errachidia, Morocco
e-mail: ah.elyoussefi@edu.umi.ac.ma

cryptocurrency pair is a set of two cryptocurrencies or assets that could be traded one for the other.

Cryptocurrency prices surged on many occasions mainly in 2017 and 2021 amid the covid lockdown which drove the attention of individual cryptocurrency traders fueled by the dream of making huge profits, and those who use it as a pastime (Guzmán et al. 2021). These traders use feedback from fundamental and technical analysis approaches to understand the market dynamics and hence make the decision about buying, selling, or holding (Hodling in the cryptocurrency world (Trimborn and Li 2021)) a tradable cryptocurrency within a trading platform. Fundamental analysis relies mainly on the information gathered about the blockchain project tied to the cryptocurrency or token, its development, and partnerships disclosed on the main website and social media. On the other hand, technical analysis uses regularly released and easily retrievable information such as historical trends of prices and volumes (Haq et al. 2021) alongside many other derived indicators to understand the market trend.

Trading systems, are a set of pre-programmed procedures that allow automatic trading between different pairs within a trading platform (Fang et al. 2022). Traders make use of signals emitted by trading systems to help them forecast the trend of the market and hence to decide their next move, or they delegate the trading decision-making process completely to the system. One of the most used indicators within trading systems in the visualization and analytics of asset markets is the Japanese Candlesticks (JC) which is an aggregation transformation applied to the cryptocurrency price time series in a fixed period. JCs can be calculated for any period (1, 3, 5, 15, 30 min, hourly, ..., daily, weekly, monthly, or yearly). Each JC is based on the OHLC (open, high, low, close) data of that period and has three components:

The body: Represents the price range between the open and close prices, it can be calculated using formula (8.1)

$$body = \max(open, close) - \min(open, close) \quad (8.1)$$

The upper shadow: Correspond to the movement of the price above the body. Formula (8.2) presents how to calculate this value.

$$upperShadow = high - \max(open, close) \quad (8.2)$$

The bottom shadow: Stands for the movement of the price below the body, the formula of this value is presented below in (8.3) (Fig. 8.1)

$$lowerShadow = low - \min(open, close) \quad (8.3)$$

A JC is called bullish if its close price is higher than its open price and is described as bearish if the close price is lower than the open price.

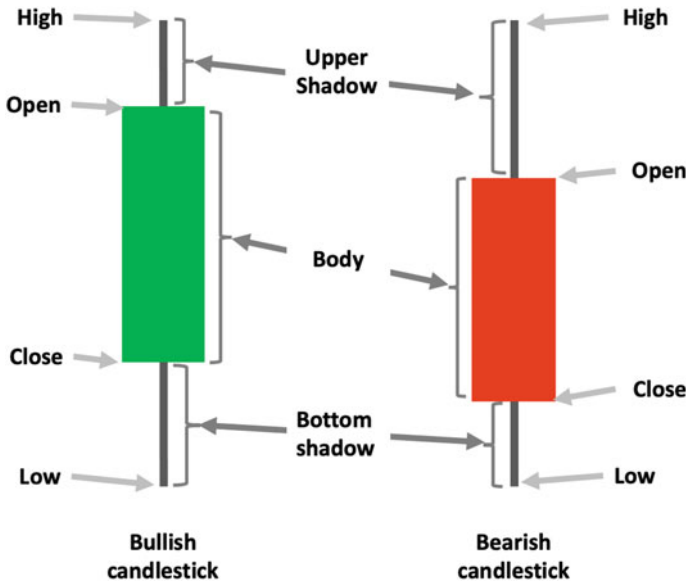


Fig. 8.1 Bullish and bearish Japanese candlestick components

8.1.2 Clustering

Clustering is an unsupervised method in machine learning. It helps in hidden pattern discovery within an unlabeled dataset by finding a cluster structure characterized by: (1) the highest possible similarity within the same cluster. (2) the highest possible dissimilarity between different clusters (Xu and Tian 2015). Partitioning clustering is a straightforward clustering method which arranges dataset items into different exclusive clusters. KMeans clustering is one of the most widely used partitioning clustering algorithms in different research fields. It requires however to specify the number of clusters k which affect the performance of the KMeans method. To define the optimal number of clusters (k) elbow method could be used. Elbow method decide the number of clusters k after which adding another cluster doesn't add sufficient information (Madhulatha 2012).

8.1.3 Returns

In assets and stock data, the use of logarithmic returns instead of simple returns is popular. For the sake of simplicity, we will refer to it as log-return in the rest of this work. due to its statistical properties, especially symmetry and time additivity, which makes it the go-to feature when dealing with returns in research such as in Sung et al. (2022), Yazdani et al. (2022), Kim et al. (2022). The log-return formula

for a cryptocurrency i on period p is:

$$r_i(p) = \ln(\text{ClosePrice}_i(p)) - \ln(\text{ClosePrice}_i(p - 1)) \quad (8.4)$$

Clustering JCs and log-returns will help traders in the decision-making process (Buy, sell, or hold). The Most trivial way of defining clusters for a classification task is by using predefined returns intervals to forecast the returns, we can consider a certain positive value $\alpha \in \mathbb{R}^+$. For any return r , such as $r \in [-\alpha, +\alpha]$ it is considered insignificant, and if $r \in]-\infty, -\alpha[$, r is considered negative, and r is positive for any $r \in]+\alpha, +\infty[$.

Within this work we applied KMeans clustering algorithm to a selected set of cryptocurrency’s JC features to decide the better number of classes to be used for cryptocurrency log-returns classification.

8.2 Data and Methods

8.2.1 Data Retrieval

Binance is a centralized exchange for trading multiple cryptocurrency pairs branding itself to be the biggest exchange in the world considering the daily cryptocurrency traded volume. We used Binance api to retrieve historical spot trading data from Binance’s historical data download center (Binance Data Collection 2022). Binance api, offer access to several historical data, of different cryptocurrencies’ markets. We retrieved daily K-line spot trading data of 5 cryptocurrencies in the USDT market. This data contain: OHLC, volume, and the number of trades. Although, the considered cryptocurrencies are on the highest capitalized cryptocurrencies list, the final list was defined empirically. Table 8.1 gives more information about selected trading pairs.

Table 8.1 Information about selected trading pairs for this study

Cryptocurrency	Trading symbol	Start date	End date
Bitcoin	BTC/USDT	August 2017	May 2022
Ethereum	ETH/USDT	August 2017	May 2022
Binance coin	BNB/USDT	November 2017	May 2022
Solana	SOL/USDT	August 2020	May 2022
Cardano	ADA/USDT	November 2019	May 2022

8.2.2 Data Preprocessing

After data retrieval and for each row, the JC indicator according to Eqs. (8.1)–(8.3), and the log returns were calculated and appended to the data set as features. Standard normalization was applied to all the data columns. We shifted the log-return column by minus one, to be considered as the future one-step log-return for each JC. In addition to the aforementioned features, we used the volume and number of trades downloaded from binance historical data.

8.2.3 Kmeans and Elbow Method

We decided to choose empirically, a range from 2 to 10 for the value of k to be tested with the KMeans algorithms. We used yellowbrick (Bengfort and Bilbro 2019) machine learning visualization library to plot the different inertia result for each value of k , and to calculate and plot the optimal number of cluster.

8.3 Results and Discussion

We applied KMeans clustering with k ranging from 2 to 10, to the preprocessed dataset and we used the elbow method to identify the best number of clusters. The obtained results suggest that the optimal number of clusters varies from 5 to 6 for the five selected cryptocurrencies. The following figures show the detailed elbow plot for each cryptocurrency.

The obtained clustering results suggest that the use of 2 or 3 classes or using the same number even if it's greater than the number of clusters, for different cryptocurrencies isn't a good choice either. Hence, we suggest that research related to forecasting returns must consider clustering JCs to help label the JCs before any classification task (Figs. 8.2, 8.3, 8.4, 8.5 and 8.6).

Figures from 8.7, 8.8, 8.9, 8.10 to 8.11 display the shifted log-returns column (one-step target log-returns) for each cluster. There is an overlapping of the KMeans suggested clusters on the target returns columns. Multiple clusters have both negative and positive log-returns which might be challenging if we are to use the results of clustering in a forecasting system since such a system will need to be able to differentiate between a positive and a negative return. For instance, cluster 2 in the ADA/USDT pair, has both negative and positive targets which will confuse a decision-making helper system about which signal to issue, is it time to buy, sell, or hodl?

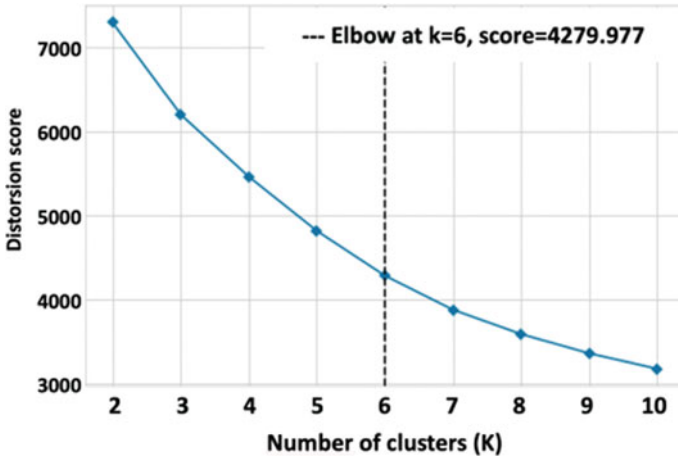


Fig. 8.2 Elbow method results for KMeans algorithm applied to the BTC/USDT pair

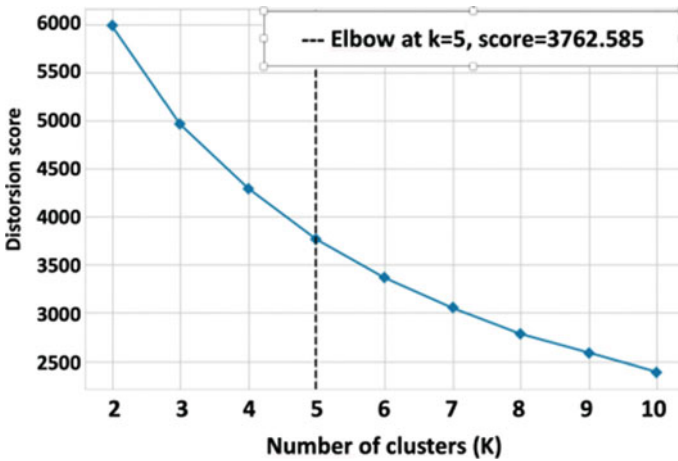


Fig. 8.3 Elbow method results for KMeans algorithm applied to the ETH/USDT pair

8.4 Conclusion and Perspectives

Within this work, we conducted a clustering of the JCs aggregated data from Binance’s historical data center of five non-stable cryptocurrencies. Our results show that we need to consider five to six classes when we aim for forecasting the one-step log-returns of one of the considered cryptocurrencies. The results suggest that we should consider working on each cryptocurrency to decide the optimal number of clusters. While the results are useful, we need to conduct more research in the future to tackle some of the current research limitations.

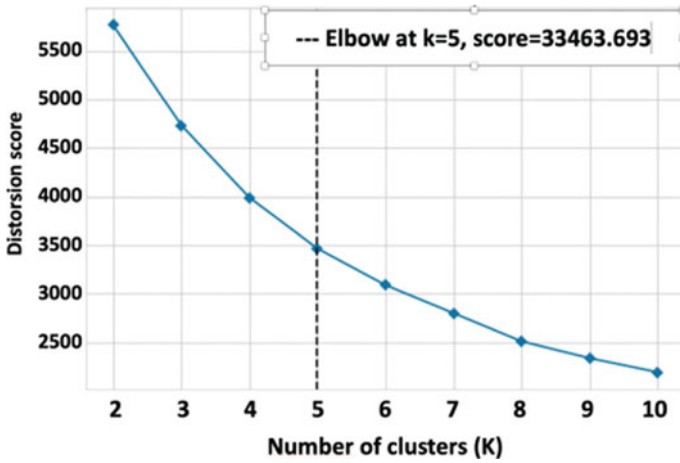


Fig. 8.4 Elbow method results for KMeans algorithm applied to the BNB/USDT pair

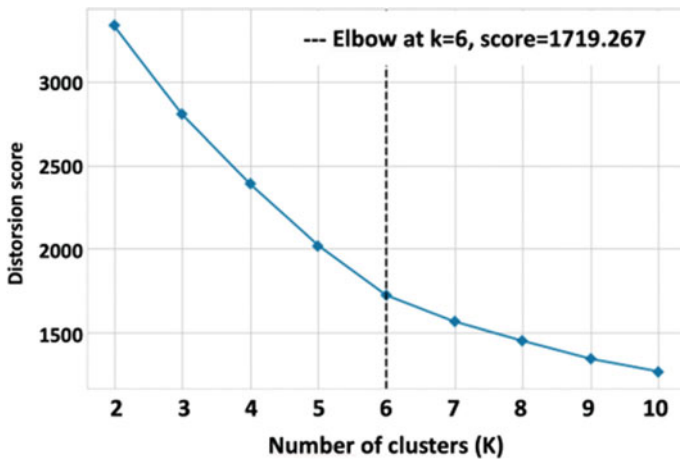


Fig. 8.5 Elbow method results for KMeans algorithm applied to the SOL/USDT pair

For instance, a comparative study involving more clustering algorithms from different clustering approaches need to be applied to more cryptocurrencies data to evaluate the consistency of the obtained results. We should also make use of other evaluation metrics such as the silhouette score alongside the elbow method, to decide on the optimal number of clusters for the KMeans algorithm.

To overcome the overlapping issue, co-clustering of the JCs and the log-returns can be explored. Such a method could be very useful for a trading system. Clustering similar JCs while keeping the values of each cluster as distinct as possible, will be helpful for traders during decision making process.

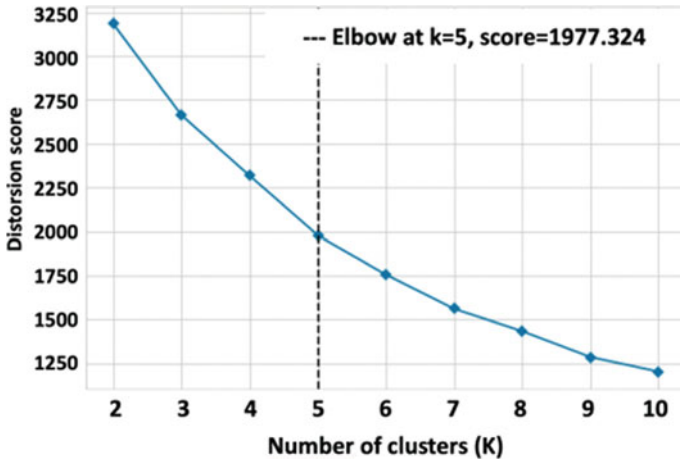


Fig. 8.6 Elbow method results for KMeans algorithm applied to the ADA/USDT pair

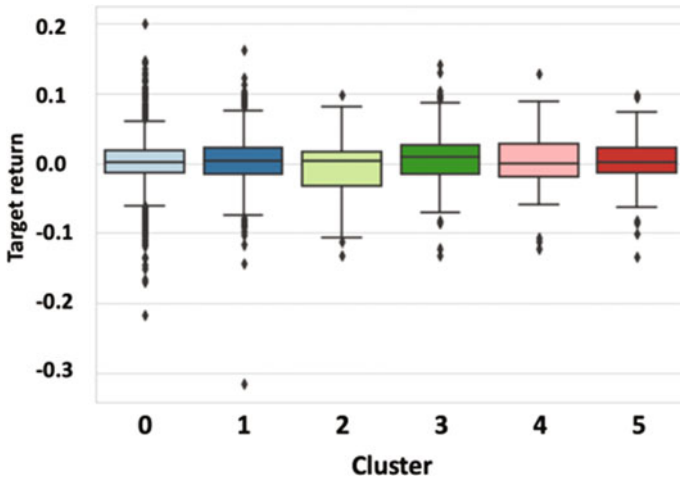


Fig. 8.7 BoxPlot of the target column of the BTC/USDT pair

The obtained clusters within our work is limited to one JC, it doesn't consider the succession of JCs, hence it is necessary for future work to be able to cluster a sequence of JCs, to capture the sequential nature of JCs.

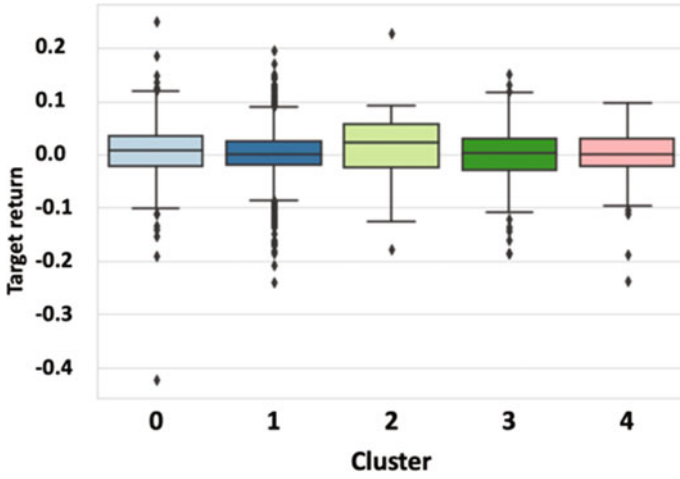


Fig. 8.8 BoxPlot of the target column of the ETH/USDT pair

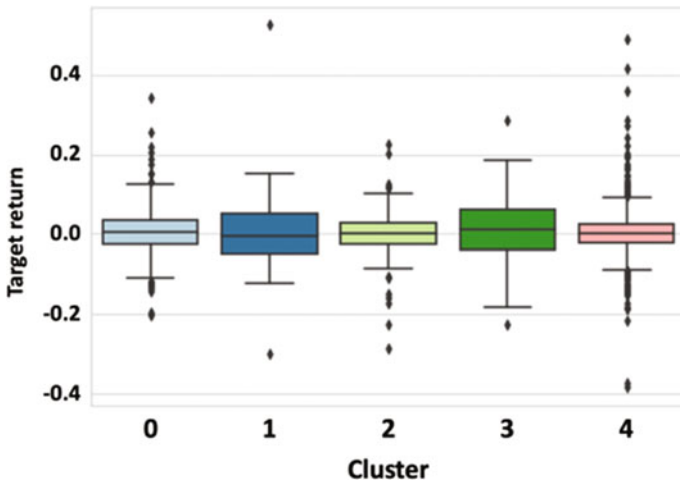


Fig. 8.9 BoxPlot of the target column of the BNB/USDT pair

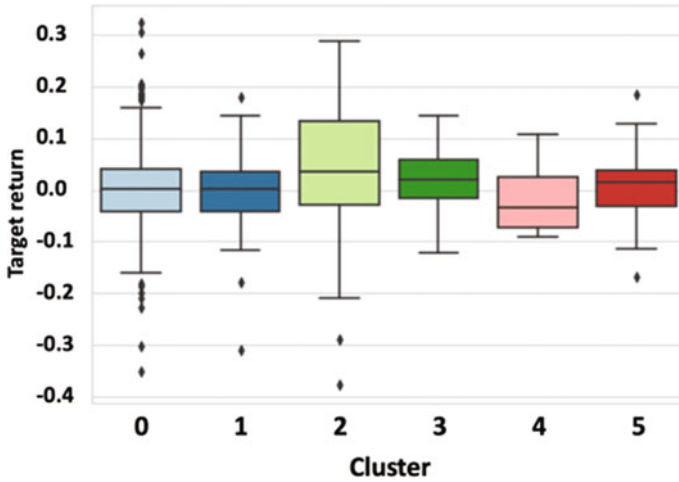


Fig. 8.10 BoxPlot of the target column of the SOL/USDT pair

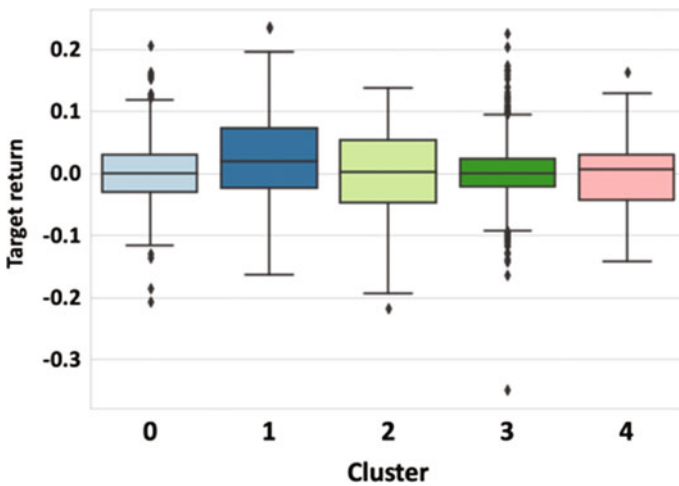


Fig. 8.11 BoxPlot of the target column of the ADA/USDT pair

References

Bengfort B, Bilbro R (2019) Yellowbrick: visualizing the scikit-learn model selection process. JOSS 4:1075. <https://doi.org/10.21105/joss.01075>

Binance Data Collection (2022) <https://data.binance.vision/?prefix=data/spot/daily/klines/>. Accessed 4 Oct 2022

Fang F, Ventre C, Basios M, Kanthan L, Martinez-Rego D, Wu F, Li L (2022) Cryptocurrency trading: a comprehensive survey. Financ Innov 8:13. <https://doi.org/10.1186/s40854-021-00321-6>

- Guzmán A, Pinto-Gutiérrez C, Trujillo M-A (2021) Trading cryptocurrencies as a pandemic pastime: COVID-19 pockdowns and Bitcoin volume. *Mathematics* 9:1771. <https://doi.org/10.3390/math9151771>
- Haq AU, Zeb A, Lei Z, Zhang D (2021) Forecasting daily stock trend using multi-filter feature selection and deep learning. *Expert Syst Appl* 168:114444. <https://doi.org/10.1016/j.eswa.2020.114444>
- Kim J-M, Cho C, Jun C (2022) Forecasting the price of the cryptocurrency using linear and nonlinear error correction model. *JRFM* 15:74. <https://doi.org/10.3390/jrfm15020074>
- Madhulatha TS (2012) An overview on clustering methods. <https://doi.org/10.48550/ARXIV.1205.1117>
- Sung S-H, Kim J-M, Park B-K, Kim S (2022) A study on cryptocurrency log-return price prediction using multivariate time-series model. *Axioms* 11:448. <https://doi.org/10.3390/axioms11090448>
- Trimborn S, Li Y (2021) Informative effects of expert sentiment on the return predictability of cryptocurrency. *SSRN J*. <https://doi.org/10.2139/ssrn.3834279>
- Xu D, Tian Y (2015) A comprehensive survey of clustering algorithms. *Ann Data Sci* 2:165–193. <https://doi.org/10.1007/s40745-015-0040-1>
- Yazdani S, Hadizadeh M, Fakoor V (2022) Computational analysis of the behavior of stochastic volatility models with financial applications. *J Comput Appl Math* 411:114258. <https://doi.org/10.1016/j.cam.2022.114258>

Chapter 9

Modelling and Simulating the Effect of Irradiation Variation on the Behavior of a Photovoltaic Cell and Its Influence on the Maximum Power Point



Mohammed Benchrifa, Karima Azoulay, Imane Bencheikh, Jamal Mabrouki, Rachid Tadili, Ilham Ihoume, Nora Arbaoui, and Mohamed Daoudi

Abstract The study of a photovoltaic module means, in particular, the determination of the main parameters that influence its electrical characteristics. Once these parameters are known, they can easily be used to determine the performance of the photovoltaic module (maximum power, efficiency, form factor). It is important to note that these determined performances will only be meaningful if they are presented in the form defined by the standard test conditions. However, the main factor influencing the operation of a PV module is solar radiation. In fact, the aim of this paper is to study and simulate the influence of irradiance on the $I(V)$ and $P(V)$ characteristics of a PV cell, as well as to study the variation of the maximum power point PMPP with irradiance. Therefore, the simulations showed that the maximum power point varies proportionally with the irradiation since it is equal to 50.8 W for an irradiation of 1000 W/m^2 , 40.7 W for an irradiation of 800 W/m^2 , 35.5 W for an irradiation of 700 W/m^2 and it continues to decrease until arriving at 4.7 W for an irradiation of 100 W/m^2 . On the other hand the power generated by the PV module at the PMPP increases with increasing irradiation as well as a slight increase of the generated voltage.

Keywords Modelling · Simulating · Solar irradiation · Photovoltaic cell · Solar energy

M. Benchrifa (✉) · R. Tadili · I. Ihoume · N. Arbaoui · M. Daoudi
Solar Energy and Environment Team, Faculty of Science, Mohammed V University in Rabat,
Rabat, Morocco
e-mail: simobenchrifa@gmail.com

K. Azoulay · I. Bencheikh
Mohammed V University in Rabat, Rabat, Morocco

J. Mabrouki
Laboratory of Spectroscopy, Molecular Modeling, Materials, Nanomaterials, Water and
Environment, CERNE2D, Faculty of Science, Mohammed V University in Rabat, Rabat, Morocco

9.1 Introduction

The most useful type of energy is electricity. It is used for lighting, refrigeration, hygiene, controlling the internal climate in homes, etc. Thus, access to electricity is closely correlated with the standard of living. The United Nations has established a human development index calculated for more than 90% of the world's population on the basis of life expectancy and progress in education in relation to the GDP per capita (Pasternak 2001). The analyses of the values of this index have shown that the improvement of lifestyle in several countries requires an increase in electricity consumption by a factor of 10 or more. The world's energy consumption is rising due to population expansion, urbanization, and economic development, especially in industrialized nations, while developing nations will require an increasing amount of energy to carry out their development (Trabold-Nübler 1991). Fossil fuels make up a significant portion of the energy produced in the world today, and using them results in the emission of greenhouse gases (Demirbas 2009; Ritchie et al. 2020). Additionally, the overuse of natural resources depletes the supply of this kind of energy in a way that is risky for future generations. And as a result of the numerous economic and energy crises, scientific attention has turned to renewable resources, which are a critical industry and enjoy special status in the sectors of research and development.

Renewable energy comes from a variety of sources, including hydroelectricity, geothermal energy, biomass energy, wind energy, and photovoltaic energy (Odeh et al. 2022; Rahman et al. 2022). The primary benefit of these renewable energy sources is that they do not harm the environment by emitting greenhouse gases like carbon dioxide and nitrous oxide, which are to blame for global warming (Mohtasham 2015).

Since the 1970s, photovoltaic conversion has shown that people may produce a sizable amount of their own electrical energy without using nuclear fission processes or burning fossil fuels (coal, oil, or natural gas). In addition to many other advantages, photovoltaic technology aids in avoiding the dangers and risks related to conventional power generation methods. It has demonstrated its ability to produce electricity for a variety of applications. Isolated sites far from the conventional electricity grid can be supplied with electricity through photovoltaic installations, thus benefiting from the conveniences necessary for comfort (television, radio, household appliances, ...). The advantages of photovoltaics are not just applicable to this kind of use. Indeed, the advantages of photovoltaics have also benefitted the communication industry. Without the need to construct highways to transport fuel to them, photovoltaic arrays can provide electricity to remote transmitter stations (in the highlands, for example). They can also be connected to the traditional electrical grid, acting as a backup to handle the busiest times during the sweltering summers when air conditioners must run continuously (Mahmoud and Lehtonen 2021; Yang and Zou 2016). Additionally, photovoltaic conversion offers families and businesses a higher level of guaranteed energy security and availability. Even in the field of space exploration, photovoltaics has been the source of power for satellites orbiting the earth for over 30 years.

However, the use of photovoltaic conversion on a large scale is dependent on certain technical and economic factors (Winter et al. 2012; Khan and Arsalan 2016). In this case, the PV array is the main element in a system. Firstly, it is the most expensive element in a photovoltaic chain, and secondly, the performance of any photovoltaic system depends directly on the efficiency of the generator (photovoltaic module). Indeed, in any photovoltaic system, the module plays a major role in the energy balance. Therefore, it must be considered more closely in the analysis of the operation of a photovoltaic system.

9.2 Materials and Methods

9.2.1 Solar Radiation

The photons that make up solar radiation have wavelengths that range from the ultraviolet (0.2 m) to the far infrared (2.5 m) (Fig. 9.1). This solar radiation’s energy is divided into its component parts by roughly (Benchrifra et al. 2019, 2021, 2022b):

- 9% in the ultraviolet band (<0.4 μm).
- 47% in the visible band (0.4 to 0.8 μm).
- 44% in the infrared band (>0.8 μm).

The solar constant has been estimated at 1367 W/m² by Claus Fröhlich and Christoph Wehrli of the World Radiometric Centre in Davos, Switzerland. Solar energy collectors must therefore be compatible with these wavelengths in order to

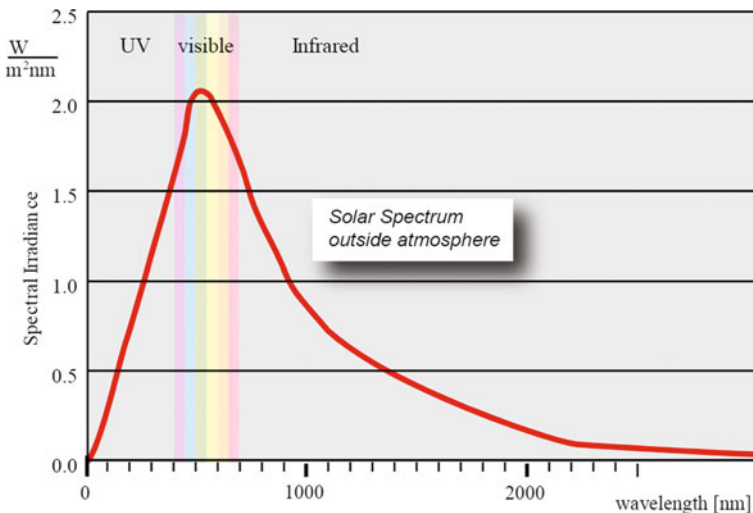


Fig. 9.1 Solar spectrum outside atmosphere

be able to trap the photons and release them in the form of heat or electrons. In order for solar radiation to produce an electric current in a given material, which then acts as a sensor, the photons must first be absorbed by one or more materials sensitive to the wavelength of the photons, which are then collected to form an overall electric current.

9.2.2 Basic Properties of Semiconductors

Understanding some fundamental solid state physics principles is important in order to comprehend how semiconductor-based solar cells operate. Numerous materials can be used to create solar cells, but monocrystalline, polycrystalline, and amorphous silicon (Si) are the most used ones (Goetzberger et al. 2002). Additionally, there are cells made of materials like GaAs, GaInP, Cu(InGa)Se₂, and CdTe (Yamaguchi et al. 2017). Materials for solar cells are primarily selected based on their solar spectrum absorption properties and their manufacturing costs. Due to its reasonable absorption that is well suited to the sun spectrum and the fact that silicon dominates the semiconductor devices sector, its technology has long been a solid choice.

9.2.3 Photovoltaic Cells

9.2.3.1 Ideal Photovoltaic Cell

A photovoltaic cell can be defined as an ideal current source that, in parallel with a diode (Fig. 9.2) that corresponds to the p-n transition area of the PV cell, provides a current I_{ph} proportional to the incident light power (Gray 2003; Goel et al. 2022; Kaswan et al. 2022; Setsoafia et al. 2022; Wenham and Green 1996; Hu et al. 2020; Sharma et al. 2015; Spirkel and Ries 1995; Kumari and Babu 2012).

Fig. 9.2 Ideal PV cell model

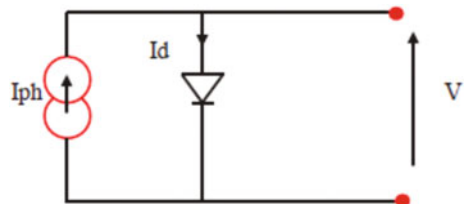
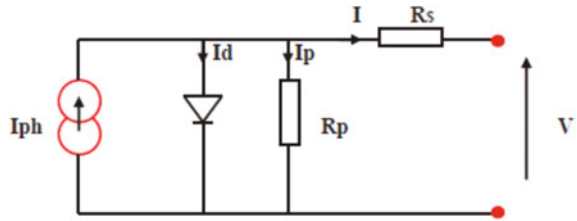


Fig. 9.3 The real photovoltaic cell model



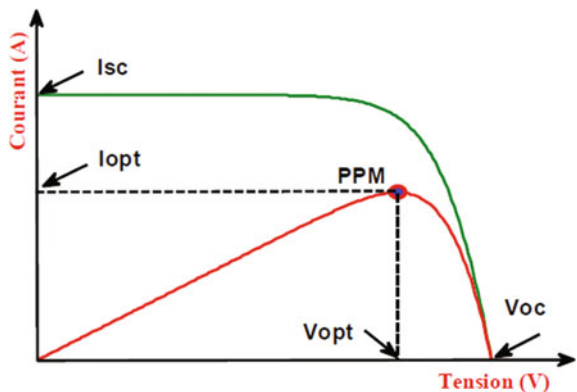
9.2.3.2 Real Photovoltaic Cell

All the processes that occurred during the conversion of light energy were not taken into consideration by the prior photovoltaic model. In fact, we notice leakage currents and a voltage loss at the output in the real instance. A parallel resistor R_p and a series resistor R_s are used to mimic the leakage currents and voltage loss, respectively (Azzouzi and Stork 2014; Maammeur et al. 2013) (Fig. 9.3).

9.2.3.3 Electrical Characteristics of a Photovoltaic Module

To produce more power, several cells are assembled as a module. The individual cells are usually connected in a series string (typically 36 or 72) to achieve the desired output voltage. The peak power obtained under maximum illumination will be proportional to the surface area of the module. The rigidity of the front panel (glass) and the vacuum seal provided by the vacuum welded back panel give the assembly its durability (Peter and Saha 2019). The curve in Fig. 9.5 shows the non-linear characteristics of the solar panel, which is particularly dependent on sunlight and temperature conditions (Huang et al. 2022; Gao et al. 2018, 2020; Benchrifra et al. 2022b). However, the electrical quantities describing the operation of the photovoltaic module are (Fig. 9.4):

Fig. 9.4 Characteristic curves of the solar panel



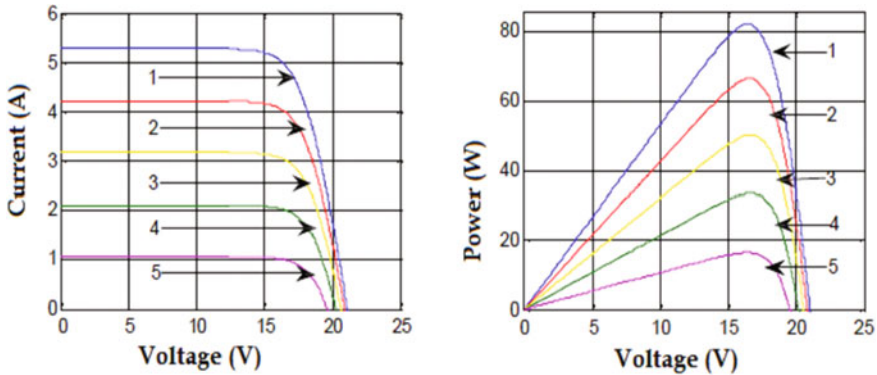


Fig. 9.5 Influence of illuminance on the I(V) and P(V) characteristic at $T = 25\text{ }^{\circ}\text{C}$ (1): 1000 W/m^2 ; (2): 800 W/m^2 ; (3): 600 W/m^2 ; (4): 400 W/m^2 ; (5): 200 W/m^2

- The maximum current (I_{sc}). It occurs when the terminals of the module are short-circuited. It is called short-circuit current (I_{sc}) and is highly dependent on the illumination level.
- The open-circuit voltage (V_{oc}) for zero current. This voltage is called the open circuit voltage.
- The optimal operating point PPM (the maximum power of the module) (Elgohary et al. 2018).

9.2.3.4 The MATLAB/SIMULINK Environment

MATLAB/Simulink is a product of MathWorks Inc. and is used in hundreds of countries around the world for the development of computational techniques and model-based design. MATLAB/Simulink is the fourth most widely used electronics design environment (after Cadence Design Systems, Synopsys, and Mentor Graphics) and has a 65% user satisfaction rating. With the set of products associated with and complementary to MATLAB/Simulink, there are several possibilities and services to design and to accelerate innovation in system design and testing. MATLAB is primarily intended for mathematical calculations, visualization and analysis of results, and editing of new user programs. Simulink is the graphical extension of MATLAB and is used for modelling and simulating dynamic systems. This graphical environment is a multi-domain simulation platform based on signal streams. It contains a set of libraries that can be adapted and/or enhanced to the designer's needs.

9.3 Results

9.3.1 *Influence of Illuminance on the I(V) AND P(V) Characteristic*

The efficiency of solar energy conversion using photovoltaics is crucial. For a very long period, research has been done to create techniques for efficiency prediction. Photovoltaic cells have a significant impact on the efficiency of solar cells. The value of a solar cell's efficiency is constrained by a number of factors. In reality, there is still some light energy left behind after turning it into electrical energy. A cell's effectiveness is impacted by a variety of losses. These are typically caused by the nature of the material and the technology being used. The maximum efficiency of a silicon photovoltaic cell is approximately 80% when these energy losses are taken into account, optical losses are nil, and each photon with energy greater than E_g produces an electron/hole pair. Silicon has a metallic appearance and is highly reflective. The reflection coefficient of an air-silicon interface is about 30%, which is the major cause of photon losses. On the other hand, there is a proportion of photons which, although having the necessary energy, pass through the thickness of the cell without being absorbed. This term becomes important when the cell is very thin ($<100 \mu\text{m}$) leading to transmission losses. This can be minimised by using a reflective layer on the back of the cell.

In fact, the illuminance is a very important parameter because it has a special effect on the electrical efficiency. Therefore, in order to visualise this effect, the influence of illumination on the I(V) AND P(V) characteristic was simulated (Fig. 9.5).

When the illuminance varies during the day, the characteristic of a photovoltaic cell changes. There is a proportionality between the photo-current and the luminous flux incident on the cell (Benchrifra and Mabrouki 2022). Figure 9.6 shows the characteristics of a solar cell under different irradiation intensities. It can be seen that the electric current is directly proportional to the illumination level of the solar radiation. However, the voltage is slightly degraded in relation to the current as the light intensity decreases. The short-circuit current in turn increases proportionally with the level of incident illumination, while the open circuit voltage increases logarithmically. Consequently, there is a strong influence of the irradiance on the current delivered by the solar cell. This influence results in an increase in the total power output and the maximum power of the cell.

9.3.2 *The Variation of the Maximum Power Point PMPP as a Function of the Irradiance*

In order to know the influence of the variation of the illuminance on a photovoltaic production, we will choose a model of 36 polycrystalline silicon cells of 60 W peak

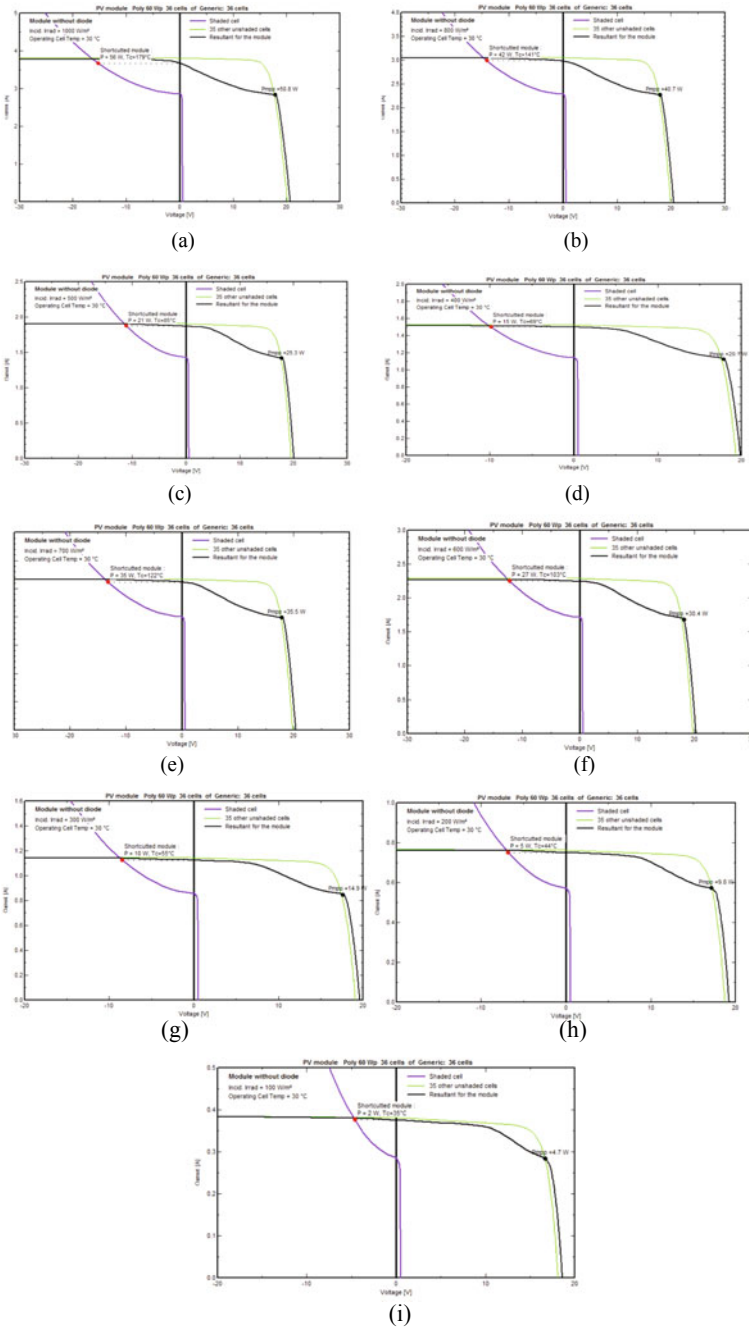


Fig. 9.6 The variation of the maximum power point PMPP as a function of illumination: **a** Illuminance 1000 (W/m²) **b** Illuminance 800 (W/m²) **c** Illuminance 700 (W/m²) **d** Illuminance 600 (W/m²) **e** Illuminance 500 (W/m²) **f** Illuminance 400 (W/m²) **g** Illuminance 300 (W/m²) **h** Illuminance 200 (W/m²) **i** Illuminance 100 (W/m²)

power, we fix the cell temperature at 30 °C. We vary the illuminance and assume that only one cell is shaded by 25%. NB: All calculations and curves are relayed by the PV system software.

From Fig. 9.6 it can be seen that the maximum power point varies proportionally with the irradiation since it is equal to 50.8 W for an irradiation of 1000 W/m², 40.7 W for an irradiation of 800 W/m², 35.5 W for an irradiation of 700 W/m² and it continues to decrease until arriving at 4.7 W for an irradiation of 100 W/m². On the other hand the current generated by the PV module at the PMPP increases with increasing irradiation from 0.3A(100 W/m²) to 3A(1000 W/m²) as well as a slight increase of the generated voltage. This result will push researchers to increase the intensity of the solar radiation incident on the PV panels either by using concentrators or trackers to increase the power generated.

To better understand the relationship between solar irradiation and the power generated by the PV panel, the maximum power found after simulation (Fig. 9.6) was plotted as a function of the irradiation. The curve obtained is as follows

From Fig. 9.7 we can deduce that the maximum power PMPP varies linearly with irradiation. When the irradiance varies during the day, the characteristic of a photovoltaic cell changes. There is therefore a proportionality between the photo-current and the luminous flux incident on the cell. On the other hand, the variation of the photo-current has a direct influence on the power generated by the PV modules, which is presented in detail in Fig. 9.8.

From Fig. 9.8 we can see that the power generated by the PV module increases with increasing irradiance and that there is a slight increase in the voltage generated, while the points of maximum power are approximately at the same voltage.

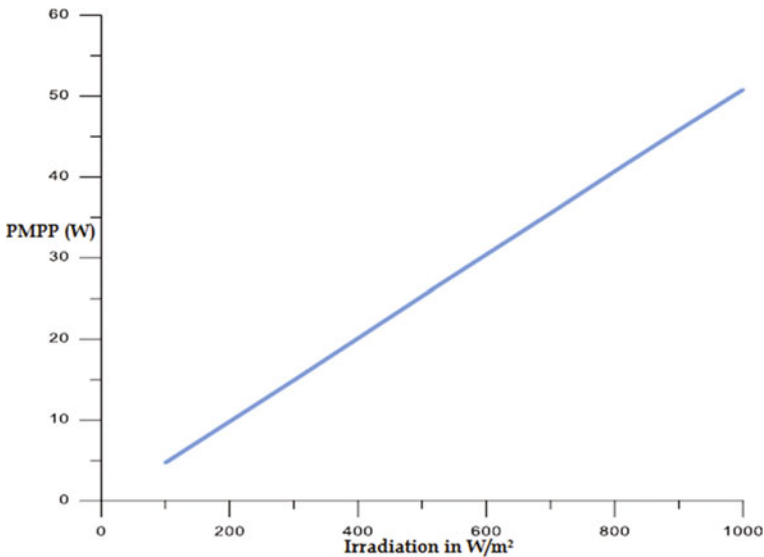


Fig. 9.7 The variation of PMPP as a function of irradiation

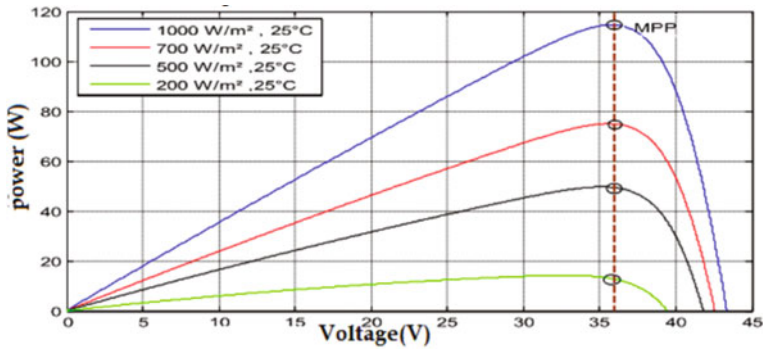


Fig. 9.8 The variation of the generated power with voltage

The variation in irradiance affects the short-circuit current, which decreases with decreasing irradiance. The open circuit voltage is not very sensitive to this variation, which implies that the optimum power of the cell is proportional to the illuminance.

9.4 Conclusion

Today, photovoltaic energy has progressively developed into a major source of energy. It is being used more and more to create electrical energy. First off, solar photovoltaic energy is unpolluted, silent, readily available, and cost-free. But there is also an ever-increasing need for electrical energy, particularly for the demands of remote and rural areas and water pumping. But there are still a lot of barriers in the way of its growth. This sort of power production's "weak" element is the high initial investment, which makes it an expensive and unreliable energy source.

The problem with the design of a solar photovoltaic system is the high cost per kWh. Therefore, it is necessary to optimize the performance of the photovoltaic system to produce electricity at an affordable cost. To do this, it is necessary to accurately determine the different factors that influence the performance of a PV system.

Since solar irradiation is the main parameter influencing the operation of a PV module, the focus was on its effect on the I(V) and P(V) characteristic of a PV cell, on the variation of the maximum power point PMPP and on the power generated by the PV module.

Therefore, the study and the simulations carried out showed that the maximum power point varies in a linear way with the irradiation since it is equal to 50.8 W for an irradiation of 1000 W/m², 40.7 W for an irradiation of 800 W/m², 35.5 W for an irradiation of 700 W/m² and it continues to decrease until arriving 4.7 W for an irradiation of 100 W/m². On the other hand the power generated by the PV module

increases with increasing irradiation as well as a slight increase of the generated voltage while the points of maximum power are approximately at the same voltage.

References

- Azzouzi MESSAOUDA, Stork MILAN (2014) Modelling and simulation of a photovoltaic cell considering single-diode model. *Recent Adv Environ Sci Biomed* 175–182
- Benchrif M, Essalhi H, Tadili R, Bargach MN, Mechaqrane A (2019) Development of a daily databank of solar radiation components for Moroccan territory. *Int J Photoenergy*
- Benchrif M, Tadili R, Idrissi A, Essalhi H, Mechaqrane A (2021) Development of new models for the estimation of hourly components of solar radiation: tests, comparisons, and application for the generation of a solar database in Morocco. *Int J Photoenergy*
- Benchrif M, Mabrouki J (2022) Simulation, sizing, economic evaluation and environmental impact assessment of a photovoltaic power plant for the electrification of an establishment. *Adv Build Energy Res* 1–18
- Benchrif M, Essalhi H, Tadili R, Nfaoui H (2022a) Estimation of daily direct solar radiation for Rabat. In: *Sustainable energy development and innovation*. Springer, Cham, pp 629–634
- Benchrif M, Mabrouki J, Elouardi M, Azrour M, Tadili R (2022b) Detailed study of dimensioning and simulating a grid-connected PV power station and analysis of its environmental and economic effect, case study. *Model Earth Syst Environ* 1–9
- Demirbas A (2009) Global renewable energy projections. *Energy Sources, Part B* 4(2):212–224
- Elgohary R, Elela AA, Elkholy A (2018) Electrical characteristics modeling for photovoltaic modules based on single and two diode models. In: *2018 twentieth international middle east power systems conference (MEPCON)*. IEEE, pp 685–688
- Gao Y, Wang Z, Zhang J, Zhang H, Lu K, Guo F, Zhang Y (2018) Two-dimensional benzo [1, 2-b: 4, 5-b'] difuran-based wide bandgap conjugated polymers for efficient fullerene-free polymer solar cells. *J Mater Chem A* 6(9):4023–4031
- Gao Y, Shen Z, Tan F, Yue G, Liu R, Wang Z, Zhang W (2020) Novel benzo [1, 2-b: 4, 5-b'] difuran-based copolymer enables efficient polymer solar cells with small energy loss and high VOC. *Nano Energy* 76:104964
- Goel M, Verma VS, Tripathi NG (2022) Solar light energy: a photovoltaic cell. In: *Solar energy*. Springer, Singapore, pp 51–63
- Goetzberger A, Luther J, Willeke G (2002) Solar cells: past, present, future. *Sol Energy Mater Sol Cells* 74(1–4):1–11
- Gray JL (2003) The physics of the solar cell. *Handb Photovolt Sci Eng* 2:82–128
- Hu Z, Wang J, Ma X, Gao J, Xu C, Yang K, Zhang F (2020) A critical review on semitransparent organic solar cells. *Nano Energy* 78:105376
- Huang J, He S, Zhang W, Saparbaev A, Wang Y, Gao Y, Tu Y (2022) Efficient and stable all-inorganic CsPbIBr₂ perovskite solar cells enabled by dynamic vacuum-assisted low-temperature engineering. *Solar RRL* 6(4):2100839
- Kaswan OP, Sonel A, Yadav SK (2022) Conversion of solar radiation into electrical energy by using solar cell. *Cent Asian J Theor Appl Sci* 3(7):104–107
- Khan J, Arsalan MH (2016) Solar power technologies for sustainable electricity generation—a review. *Renew Sustain Energy Rev* 55:414–425
- Kumari J, Babu CS (2012) Mathematical modeling and simulation of photovoltaic cell using matlab-simulink environment. *Int J Electr Comput Eng* 2(1):26
- Maammeur H, Hamidat A, Loukarfi L (2013) A numerical resolution of the current-voltage equation for a real photovoltaic cell. *Energy Procedia* 36:1212–1221

- Mahmoud K, Lehtonen M (2021) Comprehensive analytical expressions for assessing and maximizing technical benefits of photovoltaics to distribution systems. *IEEE Trans Smart Grid* 12(6):4938–4949
- Mohtasham J (2015) Renewable energies. *Energy Procedia* 74:1289–1297
- Odeh AA, Al Taie WA, Al-Douri Y (2022) Renewable energy analysis and resources. *Renewable energy: analysis, resources, applications, management, and policy*. AIP Publishing LLC, Melville, New York, pp 1–1
- Pasternak AD (2001) Global energy futures and human development: a framework for analysis
- Peter AG, Saha AK (2019) Electrical characteristics improvement of photovoltaic modules using two-diode model and its application under mismatch conditions. In: 2019 Southern African universities power engineering conference/robotics and mechatronics/pattern recognition association of South Africa (SAUPEC/RobMech/PRASA). IEEE, pp 328–333
- Rahman A, Farrok O, Haque MM (2022) Environmental impact of renewable energy source based electrical power plants: solar, wind, hydroelectric, biomass, geothermal, tidal, ocean, and osmotic. *Renew Sustain Energy Rev* 161:112279
- Ritchie H, Roser M, Rosado P (2020) CO₂ and greenhouse gas emissions. *Our world in data*
- Setsoafia DDY, Ram KS, Rad HM, Ompong D, Elumalai NK, Singh J (2022) Optimizing device structure of PTB7-Th: PNDI-T10 bulk heterojunction polymer solar cells by enhancing optical absorption. *Energies* 15(3):711
- Sharma S, Jain KK, Sharma A (2015) Solar cells: in research and applications—a review. *Mater Sci Appl* 6(12):1145
- Spirkl W, Ries H (1995) Luminescence and efficiency of an ideal photovoltaic cell with charge carrier multiplication. *Phys Rev B* 52(15):11319
- Trabold-Nübler H (1991) The human development index—a new development indicator? *Inter-economics* 26(5):236–243
- Wenham SR, Green MA (1996) Silicon solar cells. *Prog Photovoltaics Res Appl* 4(1):3–33
- Winter CJ, Sizmann RL, Vant-Hull LL (eds) (2012) *Solar power plants: fundamentals, technology, systems, economics*. Springer Science & Business Media
- Yamaguchi M, Yamada H, Katsumata Y, Lee KH, Araki K, Kojima N (2017) Efficiency potential and recent activities of high-efficiency solar cells. *J Mater Res* 32(18):3445–3457
- Yang RJ, Zou PX (2016) Building integrated photovoltaics (BIPV): costs, benefits, risks, barriers and improvement strategy. *Int J Constr Manag* 16(1):39–53

Chapter 10

Ecological Risks Related to the Influence of Different Environmental Parameters on the Microplastics Behavior



Imane Bencheikh, Karima Azoulay, Meryem Ben Baaziz, and Jamal Mabrouki

Abstract Microplastics found in continental surface waters have various sources, from cosmetics to agriculture. In addition, it is difficult to estimate the quantity of microplastics that reach the oceans each year, mainly transported by rivers but also by air. Therefore there is unquantifiable toxicity. In terms of occurrence, numerous studies have confirmed the ubiquitous and abundant nature of contamination caused by microplastics in continental water surfaces, sediment and biota. Regarding the ecotoxicological impact, it seems that the shape of the microplastics plays a role. Indeed, microfibers seem to have more harmful effects than microbeads. Besides the form, the chemical contaminants initially present or adsorbed on the particles, and the organisms that colonize their surface also represent a potential danger associated with the presence of microplastics in water.

Keywords Microplastics · Ecological risks · Environmental factors

10.1 Introduction

Microplastics are emerging pollutants considered as secondary debris from plastic waste in the marine environment. Plastic waste goes through biotic and abiotic processes inducing its aging and then a loss of its integrity (i.e. a decrease in molecular weight, color change, modification of surface properties) leading to erosion and fragmentation processes until at micro- and nanoscale sizes according to experimental data (Andrady 2011; Ekvall et al. 2019; Gewert et al. 2015; Mabrouki et al. 2018; Mabrouki et al. 2020). The particles resulting from this degradation and fragmentation therefore constitute the secondary MNPs (Andrady 2011). This secondary

I. Bencheikh (✉) · K. Azoulay · J. Mabrouki
Mohammed V University in, Rabat, Morocco
e-mail: imaneben98@gmail.com

M. Ben Baaziz
Laboratory of Materials Engineering for the Environment and Natural Resources, Department of Chemistry, Faculty of Science and Technology, Moulay Ismail University, 52000 Errachidia, Morocco

waste would represent between 97 and 99.9% of ocean contamination (Sebille et al. 2015). At the scale of the open ocean, an important quantity of plastic debris float on the surface (Eriksen et al. 2014). Particles smaller than 5 mm represent the vast majority of debris (> 90% of the number of items) (Gewert et al. 2015). The extensive environmental data on MPs contamination of surface waters and sediments is compiled in the open-access database “Litterbase” (<http://litterbase.awi.de/litter> 107 particles.m⁻³ for debris ×). A non-exhaustive summary of different environmental MPs concentrations is available in Table 1. To date, Arctic sea ice is the environment in which the highest MPs concentration has been recorded with 1.2 > 10 μm (Peeken et al. 2018). According to recent predictions, the amount of MPs in the water column could exceed 1000 mg.m⁻³ in certain oceanic regions (Southeast Asia, North Pacific) (Mabrouki et al. 2021). The danger of microplastics is not limited to their presence but also depends on several parameters either present or characteristic of the environment or other natural parameters such as uv and time (aging) which can aggravate and amplify their effects on the ecosystem. The polymers that make up microplastics have variable densities that will influence their original position in the ocean, at least for micrometric particles and macro-waste (Cole et al. 2011; Kooi et al. 2017). MPs larger than 1 μm will have a behavior mainly governed by flotation and sedimentation processes (Mabrouki et al. 2021, 2022a ; Kooi et al. 2017). For MPs equivalent in size, the density of the polymer is the first parameter influencing its movement in the water column (Kooi et al. 2017). Thus, EPS (0.01–0.04 g/cm³) tends to float while PVC (1.16–1.58 g/cm³) quickly leaves the surface to sediment towards the benthic domain. Apart from the influence of the intrinsic characteristics of the particles (e.g. size, polymer, surface properties), once in the environment, MNPs undergo aging, a term used to encompass all changes in the properties of polymers over a period of time. given time (Mabrouki et al. 2021). These changes include surface modification (Mabrouki et al. 2019), colonization by microorganisms (Fattah et al. 2021), adsorption of pollutants (Zettler et al. 2013; Abrouki et al. 2021) and metals (Kooi et al. 2017; Rochman et al. 2013), release of additives and fragmentation of waste (Mabrouki et al. 2019). The effect of these interaction have more negative impacts than positive for example the combining organic pollutants with MPs may decrease the concentration of these organic pollutants in aquatic systems (Rahmani et al. 2021) but it amplifies the danger by giving a combination of which combines the toxicity of both of them (Gewert et al. 2015). So this review we will discuss the influence of different environmental parameters as well as the physico-chemical properties of microplastics on the marine ecosystem.

10.2 Materials and Methods

This review was carried out based on various reports and scientific articles on the following databases and search engines; Science direct, google scholar.

10.3 Results and Discussion

10.3.1 Microplastics in the Marine Environment

Influence of particle properties. Polymers have varying densities that will influence their original position in the ocean, at least for micrometric particles and macro-debris (Rehse et al. 2016). MPs larger than 1 μm will have a behavior mainly governed by flotation and sedimentation processes (Rehse et al. 2016; Mai et al. 2013). For MPs equivalent in size, the density of the polymer is the first parameter influencing its movement in the water column (Kooi et al. 2017). Thus, EPS (0.01–0.04 g/cm^3) tends to float while PVC (1.16–1.58 g/cm^3) quickly leaves the surface to sediment towards the benthic domain. Nanometric particles exhibit a naturally different behavior, of a colloidal nature. This would explain the presence of chemical signals associated with nanometric PVC in the surface waters of the North Atlantic Subtropical Gyre (Gigault et al. 2018; Halle et al. 2017). Brownian motion, i.e. interactions with water molecules, thus makes the behavior of NPs dynamic and random. Particle surface properties (e.g. charge, associated chemical moieties) also influence behavior based on experimental data obtained through the use of commercially available polystyrene nano- and microspheres (Alimi et al. 2018; Mabrouki et al. 2022b). For example, in a controlled seawater environment, NP-COOH (50 nm, charge–) instantly form micrometric homoaggregates ($> 1 \mu\text{m}$) which will sediment while NP-NH₂ (50 nm, charge +) remain at a nanometric size (Alimi et al. 2018; Paul-Pont et al. 2018). Although the analysis of PM collected on 47 different beaches revealed the presence of a carboxylated surface in connection with the oxidation processes that the waste undergoes in the environment (Mgalaa et al. 2022), new studies are necessary. To assess the evolution of surface properties of primary MNPs from environmental deposition.

Implications of aging in the marine environment. In the following paragraphs we will discuss the impact of aging on different types of molecules.

Macromolecular interactions. The first stage of aging is the set of macromolecular interactions between MNPs and compounds present in the surrounding environment (e.g. organic matter, persistent organic pollutants [POPs], metals, polysaccharides) (Mgalaa et al. 2022; Wegner et al. 2012). These interactions modify the coating of the particle, creating an envelope called “eco-corona”. This new coating is formed of two distinct layers, the “tough” corona composed of macromolecules with high affinity with the particle and the “soft” corona composed of macromolecules with low affinity which are easily exchanged with the surrounding medium (Fotopoulou and Karapanagioti 2012). Apart from the importance of the medium considered, the nature of the corona is highly dependent on the surface properties of the particle (e.g. size, surface groupings) (Mgalaa et al. 2022). The high surface-to-volume ratio of NPs improves their reactivity compared to MPs (Galloway et al. 2017; Lundqvist et al. 2008). Thus, the theoretical influence of the corona should increase going down in the debris size (Wegner et al. 2012; Ghizlane et al. 2022). It should be noted

that NPs can thus accumulate a greater quantity of POPs than PMs for the same mass (Lundqvist et al. 2008). During subsequent aging processes, the composition of the corona could influence the interactions of the particle with the surrounding environment, including microbial communities (Ghizlane et al. 2022).

Formation of a biofilm and hetero-aggregation. Recent studies have demonstrated the presence of specific assemblages of microorganisms associated with PM (e.g. bacteria, microalgae, protozoa, fungi), distinct from those present in the surrounding environment (Fotopoulou and Karapanagioti 2012; Galloway et al. 2017; Lowry et al. 2012). These specific communities form the “plastisphere” (Fotopoulou and Karapanagioti 2012). The biofilm present on the PM has physico-chemical consequences (i.e. increased density) and influences the fate and bioavailability of the debris (Mabrouki et al. 2021). Thus PE or PP particles can leave the surface of the oceans following the installation of a biofilm (Mabrouki et al. 2021). The rate of biofilm formation is dependent on the size of the particles, i.e. large particles (10 μm) have higher collision frequencies with microalgae than small particles (1 μm), which increases the density of the microalgae more rapidly. Particle (Velzeboer et al. 2014). The theoretical model developed by Kooi et al. (2017), taking into account the formation of a biofilm, shows a slowdown in sedimentation speeds when the size of the particles decreases (from 10 mm to 1 μm). According to this model, a PVC or PS particle (1 μm) would take 278 and 4317 years respectively to descend 4000 m, while a 100 μm particle would need 10 (PVC) and 159 (PS) days. However, the exo-polysaccharide matrices from the biofilm would allow the MNPs to reach the ocean floor more quickly because they would promote the integration of the MNPs inside marine aggregates composed of microalgae, organic matter or even detritus such as this has been demonstrated in the laboratory for MP (Tender et al. 2022) and NP (Fotopoulou and Karapanagioti 2012). In situ, 70% of marine aggregates were contaminated with MPs ($1290 \pm 1510 \text{ MP}\cdot\text{m}^{-3}$; 90% < 1000 μm) during sampling at Avery Point (Connecticut, United States) (Mgalaa et al. 2022). This hetero-aggregation would cause vertical movements of the MNPs towards deep zones with sedimentation on the benthic bottoms as suggested by the positive correlation between chlorophyll a concentration and quantity of MPs at the benthic station HAUSGARTEN located in the Arctic (Tender et al. 2017). In addition, the incorporation of particles inside the faecal pellets of copepods or salps is also a vertical transport vector (Lundqvist et al. 2008; Lowry et al. 2012; Tender et al. 2017). Thus, benthic habitats can be areas of debris accumulation. In the sediments of a hadal zone in the Mariana Trench, between 200 and 2000 items. L1 (MP > 20 μm) were observed (Frère et al. 2018). However, during vertical transfer, communities of microorganisms can theoretically degrade the biofilm to remineralize organic matter. This would thus stimulate the rise of MPs by recovering their original density while the NPs would be less affected by this degradation of the biofilm due to their colloidal behavior (Tender et al. 2017). Turbulence in the water column (e.g. currents, geological processes, actions of marine organisms) could also resuspend the particles that have sedimented (Lundqvist et al. 2008).

Fragmentation and release of additives. The longest stage (several decades/centuries) of aging is the process of fragmentation. It should be noted that

the presence of a biofilm can slow down the degradation processes (Cole et al. 2011). Simultaneously during the degradation of the compound, the additives—potentially toxic—added during manufacturing can be released into the environment (Frère et al. 2018; McCormick et al. 2014). For example, the aging of PE bags and PVC cables in natural seawater for 90 days in the laboratory revealed the release of phthalates, one of the main groups of additives, up to at 120 ± 18 and 69 ± 10 ng. g⁻¹ of plastic respectively (Tender et al. 2017).

10.3.2 Toxicological Impact Resulting from the Behavior of Microplastics with Different Environmental Factors

In these paragraph we will discuss the different toxicological impacts of microplastic relative to their interaction with macromolecules (e.g. adsorption of polysaccharides, organic matter, proteins) leading to the development of bio- (in organism) or eco-coronas (in environment).

Interaction with organic pollutants. It is very difficult to determine the effects of substances such as residual monomers, non-deliberately added substances (impurities, polymerization by-products, degradation products), catalysts, solvents and additives that leach plastic materials. The leaching of these mixtures depends on the chemical, biological or physical conditions of the receiving environment (Frère et al. 2018). Plastic materials do not represent a danger for the environment in themselves, since they are initially biochemically inert. A new name has emerged following a classification that takes into consideration the addition of submicronic additives in commercial plastics, and which bears the name of “plasticides”, these additives are of molecular size. The effects of the addition of these additives go back to their lipophilic nature, which makes them more able to infiltrate cell membranes and participate in biochemical reactions, resulting in a serious behavioral change, alterations in reproduction. The first stage of aging is the set of macromolecular interactions between MNPs and compounds present in the surrounding environment (e.g. organic matter, persistent organic pollutants [POPs], metals, polysaccharides) (Tender et al. 2022; Frère et al. 2018; Michels et al. 2018). These interactions modify the coating of the particle, creating an envelope called “eco-corona”. This new coating is formed of two distinct layers, the “tough” corona composed of macromolecules with high affinity with the particle and the “soft” corona composed of macromolecules with low affinity which are easily exchanged with the surrounding medium (Tender et al. 2017). Apart from the importance of the medium considered, the nature of the corona is highly dependent on the surface properties of the particle (e.g. size, surface groupings) (Michels et al. 2018). The high surface-to-volume ratio of NPs improves their reactivity compared to MPs (Michels et al. 2018; Loukili et al. 2022). Thus, the theoretical influence of the corona should increase going down in the debris size (Ghizlane

et al. 2022; Frère et al. 2018). It should be noted that NPs can thus accumulate a greater quantity of POPs than PMs for the same (Lowry et al. 2012).

POPS and PCB. POPs, PCBs and suspended matter are among the molecules that can combine with MPs in the aquatic environment. POPs and PCBs are molecules that break down very little in the environment and accumulate in different environments, including the aquatic environment (sea, river, etc.). They can attach themselves to suspended solids and sediments in canals and waterways. The mass of microplastics is low compared to other solid phases with which contaminants are potentially associated; and the contaminant fluxes associated with microplastics are therefore lower. The presence of organic matter and microorganisms on microplastics can also influence the sorption processes of chemical contaminants on them, although these processes remain little studied (Loukili et al. 2022). Indeed, characteristics such as porosity, specific surface, particle polarity, temperature, biofouling influence the adsorption of the same POP. This, combined with the variety of substances present in the medium competing for adsorption, results in a myriad of cases leading to enormous inter-microplastic, spatial and temporal variability of the vectorization of POPs by microplastics (Tender et al. 2022; Samghouli et al. 2022; Hu et al. 2019) which can only be approached by prioritizing all the factors. The bioavailability of POPs adsorbed on microplastic remains is lower than those adsorbed on sediments, for worms present in the sediment. For Hu et al. (2019), this observation should be tempered according to the type of POP: “historic” POPs (PAHs, PCBs) have solubilities, or partition coefficients, which do not favor their desorption. This combination of POPS and PCBs impacts different components of the ecosystem, including humans and human health. It has been proven that some POPS, PCBs and pesticides can mimic natural hormones, leading to reproductive disorders. The absorption rate of these POPS in the plastic material depends essentially on the nature of the polymer and the pollutant together, as well as the type, density, molecular weight and hydrophobicity (Hydrophobicity characterizes surfaces which seem to repel ‘water’). When hydrophobic contaminants are ingested, they are able to enter the food webs and be involved in phenomena such as bioaccumulation or biomagnification which are not without consequences for animal and human health. This explains that the particles can pass through certain organs of the body such as the liver, the testicles and the blood to reach the brain, which can have serious consequences on the self-regulation of the vital signs of the species.

Pharmaceutical residues. The global consumption of drugs for both human and veterinary use has been estimated at several hundred thousand tons per year (Hu et al. 2019). The various therapeutic and diagnostic uses of drugs lead to the discharge of residues which eventually reach the marine environment, a sensitive receiving environment subject to global changes (anthropogenic pressures, acidification and temperature change). The origin of the contamination of the marine environment by drug residues, which we will call pharmaceutical products (PP), is mainly continental, carried by rivers but also by wastewater from coastal cities, treated or not, discharged directly at sea through outfalls. Added to this contamination are activities practiced in situ, such as aquaculture (Rochman et al. 2013; Brennecke et al. 2016), which occasionally pollute the coastal areas where livestock farms are located. These

pressures on coastal areas continue to grow. Estimates place between 50 and 60% the percentage of the world's population living in the large coastal zone, which represents 2% of the earth's surface. About 3.8–4.0 billion people reside within 150 km of the shore. Eight of the ten largest cities on the planet are located on the coast (Mabrouki et al. 2022a). In this context of growing pressure on coastal and marine ecosystems, which in the presence of other pollutants such as microplastics represent an additional stress to be taken into consideration. In this context, we cite that certain pharmaceutical residues have been transferred to microalgae (Prunier et al. 2019; Samghouli et al. 2022) or to bivalves (Brennecke et al. 2016), opening up the possibility of an accumulation along the trophic chain. Rocheman et al. (2013) demonstrated liver toxicity after exposure to microplastics with adsorbed contaminants, and also reported impaired endocrine system when fish were exposed in the laboratory to environmentally relevant concentrations of microplastics. However, when it comes to wild fish, the contribution of microplastics to the body burden of contaminants remains to be demonstrated, as fish are also exposed to the complex mix of contaminants found in water. Bakir et al. (2016) do not consider microplastics as major contributors to the exposure flux of marine biota to POPs: the mass of microplastics is low compared to other solid phases with which contaminants are potentially associated, and the contaminant fluxes associated with microplastics are therefore lower.

Interaction with inorganic pollutants. The vectorization of mineral elements is inherent to plastic materials, through the fillers, pigments and residues of catalysts they carry Barboza et al. (2018). Highlighted the potentiation of mercury (Hg) bioaccumulation in the muscle and brain of young bass (*Dicentrarchus labrax*) in the presence of microplastics. Although a marine species, similar effects on freshwater species cannot be ruled out. Other non-essential elements, such as cadmium (Cd) or lead (Pb), may represent a risk in the event of high doses or chronic exposure at low doses (Wu et al. 2016). Their bioavailability will depend on their type of bond with the polymer (adsorption or formulation), as well as the specific surface and the type of polymer (Paul-Pont et al. 2018; Benchrifa and Mabrouki 2022).

Interaction between PM and marine organisms. Microplastics possess the same toxic characteristics as larger plastics, but due to their small sizes, the pathways and levels of exposures are different and affect a greater number of species (Long et al. 2015; Benchrifa et al. 2022). As with macroplastics, the danger comes from ingesting microplastics and associated pollutants. The intrinsic properties of plastics (buoyancy, persistence) as well as their ubiquitous nature favor their colonization by many organisms, and their ability to be transported over long distances increases the risk of introducing toxic and/or invasive organisms into new environments (Velzeboer et al. 2014; Brennecke et al. 2016). Also, during subsequent aging processes, the composition of the corona could influence the interactions of the particle with the surrounding environment, in particular the microbial communities (Benchrifa et al. 2022) A priori, strangulation seems unlikely or so on rare microorganisms. The ingestion of microplastics is possible by two routes: directly by filtration, respiration or predation, or indirectly via trophic transfers (Halle et al. 2017; Barboza et al. 2018;

Benchrifia et al. 2022). Direct ingestion can be achieved by the smallest individuals and has been observed in the laboratory and in the field for many species (Fattah et al. 2021). Indirect ingestion has only been observed in the laboratory (Sebille et al. 2015; Kim et al. 2017). Moreover, it is unlikely in the natural environment because MPs are excreted rapidly, in a few hours (Mabrouki et al. 2019). Microplastics are therefore theoretically available for the entire food web. Moreover, once inside, the smallest particles ($<1 \mu\text{m}$) can be transferred through the tissues (Mabrouki et al. 2022a; Frère et al. 2018; Bakir et al. 2016). MPs can also obstruct digestive organs (Rehse et al. 2016). The pollutants that make up plastics (polymers and additives) and those adsorbed on their surfaces are potentially the same for PM and macroplastics (toxicity), but can be adsorbed or released in greater quantity due to a surface area to volume ratio. Larger (Kim et al. 2017). Finally, Galgani et al. suspect that MPs can:

- Disrupt the production of certain essential compounds (enzymes, hormones),
- Decrease appetite and suppress nutrition,
- Reduce growth rate,
- Suppress ovulation and hinder reproduction effects

due to the ingestion of MPs have already been observed, at all scales, from DNA to the organism. Avio et al. observed DNA fragmentation after exposing mussels to PE and PS powder. They suspected oxidative stress, through the production of free radicals, but the responses of the biomarkers used did not confirm this hypothesis. This result nevertheless emphasizes the genotoxic potential of MPs. This same study detected a decrease in the granulocytes/hyalinocytes ratio (hemocytes crucial for the maintenance of immune defenses in bivalves) indicating an immune response, but no change in phagocytic activity, just like Browne et al. on another species of mussel. Avio et al. also observed a reduction in the membrane stability of lysosomes, as did Von Moos et al. suggesting the production of free radicals, but the two markers of damage by oxidative stress tested (lipodosis and lipofiscinosis) were not found (Alouani et al. 2022; Fossi et al. 2014; Moore et al. 2002; Arthur et al. 2009; Goldstein et al. 2012). At the neurological level, the activity of acetylcholinesterase, an enzyme involved in the neurotransmission of fundamental physiological processes, seems to be reduced, as in fish (Ramesh et al. 2015). Rocheman et al. (2013) observed reduced glycogen, fat vacuolation, and tissue-level bond formation after feeding fish (*Oryzias latipes*) with PE microbeads. Von Moos et al. reported the formation of granulocytomas suggesting tissue inflammation. Rodriguez-Seijo et al. found atrophies and detachments of the epithelial wall in *Eisenia andrei* earthworms exposed to very high concentrations of MPs ($> 125 \text{ mg kg}^{-1}$, PE of 0.25–1 mm) (Cauwenberghe et al. 2015; Ziajahromi et al. 2016). This same study also observed other physical damage, inflammation sometimes leading to the development of fibrosis or congestion, but also an immune system response, with an increase in proteins, lipids and polysaccharides but no effect on reproduction., survival and mass of individuals. Rodriguez-Seijo et al. observed the development of necrosis and bleaching after exposing different coral species to 4000 L–1 microparticles (PE of 37–163 μm). They find that contact can be internal (by ingestion) or external, that it can elicit protective responses, such as increased mucus production, and that the effects are different depending on the species. So far no signs of autophagy, apoptosis, neoplasm, or tumor have been found or studied. At the organism level, Von Moos et al. did not report any effect on physical abilities,

(Weltje and Sumpter 2017) did not observe any impact on food capacity. Cauwenberghé et al. (Cauwenberghé et al. 2015) found an impact of MPs on cellular energy allocation.

10.4 Treatment

Several pilot studies have been carried out to assess the load of microplastics in wastewater treatment plants (in Europe, Russia and the United States), the example of a study demonstrates that with mechanical, biological and chemical, 99% of microplastics out of 15,000 particles/L in the influent at 8 particles/L are removed in the effluent (Mabrouki et al. 2022a, 2022b; Kim et al. 2017; Ziajahromi et al. 2016). Although WWTPs are not currently designed to specifically eliminate MPs, we note, with recent studies, that a large part is removed following primary treatment. During these phases, the density of the MPs can make the difference during their elimination, it makes them buoyant and easily removed by surface skimming. Some studies have shown that tertiary treatment is more effective than primary and secondary. One can add the fact that the physico-chemical properties of MPs can be transformed during the treatment process. This is possible due to the presence of biofilms on the MPs in the wastewater. The influence is on the surface properties and the density of the MPs. It was concluded that these biofilms changed the physicochemical properties of plastic debris, making them less hydrophobic and more dynamic. Microplastics can also be captured and trapped in sludge (Ziajahromi et al. 2016).

10.5 Conclusion

The presence of microplastics in the environment has aroused growing interest in recent years among the scientific community, the general public and public authorities. It is in this context that this review was carried out. The danger of microplastics is not limited to their presence but also depends on several parameters either present or characteristic of the environment or other natural parameters such as uv and time (aging) which can aggravate and amplify their effects on the ecosystem.

References

- Abrouki Y, Mabrouki J, Anouzla A, Rifi SK, Zahiri Y, Nehhal S, Souabi S (2021) Optimization and modeling of a fixed-bed biosorption of textile dye using agricultural biomass from the moroccan sahara. *Desalin Water Treat* 240:144–151
- Alimi OS, Farnier Budarz J, Hernandez LM, Tufenkji N (2018) Microplastics and nanoplastics in aquatic environments: aggregation, deposition, and enhanced contaminant transport. *Environ Sci Technol* 52:1704–1724

- Andrady AL (2011) Microplastics in the marine environment. *Mar Pollut Bull* 62:1596–1605
- Arthur C, Baker J, Bamford H (2009) Proceedings of the international research workshop on the occurrence, effects, and fate of microplastic marine debris. NOAA Tech Memo 49:9–11
- Bakir A, O'Connor IA, Rowland SJ, Hendriks AJ, Thompson RC (2016) Relative importance of microplastics as a pathway for the transfer of hydrophobic organic chemicals to marine life. *Environ Pollut* 219:56–65
- Barboza LGA, Vieira LR, Branco V, Carvalho C, Guilhermino L (2018) Microplastics increase mercury bioconcentration in gills and bioaccumulation in the liver, and cause oxidative stress and damage in *dicentrarchus labrax* juveniles. *Sci Rep* 8:15655
- Benchrifra M, Mabrouki J (2022) Simulation, sizing, economic evaluation and environmental impact assessment of a photovoltaic power plant for the electrification of an establishment. *Adv Build Energy Res* :1–18.
- Benchrifra M, Mabrouki J, Elouardi M, Azrou M, Tadili R (2022) Detailed study of dimensioning and simulating a grid-connected PV power station and analysis of its environmental and economic effect, case study. *Model Earth Syst Environ* :1–9.
- Brennecke D, Duarte B, Paiva F, Caçador I, Canning-Clode J (2016) Microplastics as vector for heavy metal contamination from the marine environment. *Estuar Coast Shelf Sci* 178:189–195
- Cole M, Lindeque P, Halsband C, Galloway TS (2011) Microplastics as contaminants in the marine environment : a review. *Mar Pollut Bull* 62:2588–2597
- De Tender C, Devriese LI, Haegeman A, Maes S, Vangeyte J, Cattrijsse A (2017) Temporal dynamics of bacterial and fungal colonization on plastic debris in the north sea. *Environ Sci Technol* 51:7350–7360
- De Tender CA, Devriese LI, Haegeman A, Maes S, Ruttink T, Dawyndt P, Regraguy B, Ellouzi I, Mabrouki J, Rahmani M, Drhimer F, Mahmoud C, El Hajjaji S (2022). Zinc doping of different nanoparticles of TiO₂ sachtopore for improved elimination of the methyl orange by photocatalysis. *Emergent Mater* :1–14.
- Ekvall MT, Lundqvist M, Kelpsiene E, Šileikis E, Gunnarsson SB, Cedervall T (2019) Nanoplastics formed during the mechanical breakdown of daily-use polystyrene products. *Nanoscale Adv*. 1:1055–1061
- El Alouani M, Aouan B, Rachdi Y, Alehyen S, El Herradi EH, Saufi H, Barka N (2022) Porous geopolymers as innovative adsorbents for the removal of organic and inorganic hazardous substances: a mini-review. *Int J Environ Anal Chem* :1–13.
- Eriksen M, Lebreton LCM, Carson HS, Thiel M, Moore CJ, Borerro JC (2014) Plastic pollution in the world's oceans: more than 5 trillion plastic pieces weighing over 250,000 tons afloat at sea. *PLoS ONE* 9:1–15
- Fattah G, Ghrissi F, Mabrouki J, Kabriti M (2021) Control of physicochemical parameters of spring waters near quarries exploiting limestone rock. In: *E3S Web of Conferences*, vol 234. EDP Sciences, p 00018.
- Fossi MC, Coppola D, Bainsi M, Giannetti M, Guerranti C, Marsili L (2014) Large filter feeding marine organisms as indicators of microplastic in the pelagic environment: the case studies of the Mediterranean basking shark (*Cetorhinus maximus*) and fin whale (*Balaenoptera physalus*). *Mar Environ Res* 100:17–24
- Fotopoulou KN, Karapanagioti HK (2012) Surface properties of beached plastic pellets. *Mar Environ Res* 81:70–77
- Frère L, Maignien L, Chalopin M, Huvet A, Rinnert E, Morrison H (2018) Microplastic bacterial communities in the bay of brest: influence of polymer type and size. *Environ Pollut* 242:614–625
- Galloway TS, Cole M, Lewis C (2017) Interactions of microplastic debris throughout the marine ecosystem. *Nat. Ecol. Evol.* 1:0116
- Gewert B, Plassmann MM, MacLeod M (2015) Pathways for degradation of plastic polymers floating in the marine environment. *Environ Sci Process Impacts* 17:1513–1521
- Ghizlane F, Mabrouki J, Ghrissi F, Azrou M (2022) Proposal for a high-resolution particulate matter (PM₁₀ and PM_{2.5}) capture system, comparable with hybrid system-based internet of things: case of quarries in the western rif, Morocco. *Pollut* 8(1), 169–180.

- Gigault J, Ter Halle A, Baudrimont M, Pascal P, Gauffre F, Phi T-L (2018) Current opinion: what is a nanoplastic? *Environ Pollut* 235:1030–1034
- Goldstein MC, Rosenberg M, Cheng L (2012) Increased oceanic microplastic debris enhances oviposition in an endemic pelagic insect. *Biol Lett* 8:817–820
- Hu Y, Gong M, Wang J, Bassi A (2019) Current research trends on microplastic pollution from wastewater systems: a critical review. *Rev Environ Sci Bio/Technol* 18:207–230
- Kim HY, Lee IS, Oh JE (2017) Human and veterinary pharmaceuticals in the marine environment including fish farms in Korea. *Sci Total Environ* 9:579–940
- Kooi M, Van Nes EH, Scheffer M, Koelmans AA (2017) Ups and downs in the ocean: effects of biofouling on vertical transport of microplastics. *Environ Sci Technol* 51:7963–7971
- Long M, Moriceau B, Gallinari M, Lambert C, Huvet A, Raffray J (2015) Interactions between microplastics and phytoplankton aggregates: impact on their respective fates. *Mar Chem* 175:39–46
- Loukili H, Anouzla A, Jioui I, Achiou B, Alami Younssi S, Azoulay K, Riadi Y (2022) Combining multiple regression and principal component analysis to evaluate the effects of ambient air pollution on children's respiratory diseases. *Int J Inf Technol* 14(3):1305–1310
- Loukilia H, Mabroukic J, Anouzlab A, Kouzia Y, Younssia SA, Diguab K, Abroukic Y (2021) Pre-treated Moroccan natural clays: application to the wastewater treatment of textile industry. *DESALINATION AND WATER TREATMENT* 240:124–136
- Lowry GV, Gregory KB, Apte SC, Lead JR (2012) Transformations of nanomaterials in the environment. *Environ Sci Technol* 46:6893–6899
- Lundqvist M, Stigler J, Elia G, Lynch I, Cedervall T, Dawson KA (2008) Nanoparticle size and surface properties determine the protein corona with possible implications for biological impacts. *Proc Natl Acad Sci* 105:14265–14270
- Mabrouki J, Azrou M, Hajjaji SE (2021) Use of internet of things for monitoring and evaluating water's quality: a comparative study. *Int J Cloud Comput* 10(5–6):633–644
- Mabrouki J, Fattah G, Al-Jadabi N, Abrouki Y, Dhiba D, Azrou M, Hajjaji SE (2022a) Study, simulation and modulation of solar thermal domestic hot water production systems. *Model Earth Syst Environ* 8(2):2853–2862
- Mabrouki J, El Yadini A, Bencheikh I, Azoulay K, Moufti A, El Hajjaji S (2018) Hydrogeological and hydrochemical study of underground waters of the tablecloth in the vicinity of the controlled city dump Mohammedia (Morocco). In: *International Conference on Advanced Intelligent Systems for Sustainable Development*. Springer, Cham, pp 22–33.
- Mabrouki J, Bencheikh I, Azoulay K, Es-Soufy M, El Hajjaji S (2019). Smart monitoring system for the long-term control of aerobic leachate treatment: dumping case Mohammedia (Morocco). In: *International Conference on Big Data and Networks Technologies*. Springer, Cham, pp 220–230.
- Mabrouki J, Benbouzid M, Dhiba D, El Hajjaji S (2020) Simulation of wastewater treatment processes with bioreactor membrane reactor (MBR) treatment versus conventional the adsorbent layer-based filtration system (LAFS). *Int J Environ Anal Chem* :1–11.
- Mabrouki J, Azoulay K, Elfanssi S, Bouhachlaf L, Mousli F, Azrou M, Hajjaji SE (2022b) Smart system for monitoring and controlling of agricultural production by the IoT. IoT and smart devices for sustainable environment. Springer, Cham, pp 103–115.
- Mai H, Morin B, Cachot J (2013) Toxic effects of copper and cadmium on fertilization potency of gametes of Pacific oyster (*Crassostrea gigas*). *J Xenobiotics* 3:9
- McCormick A, Hoellein TJ, Mason SA, Schluep J, Kelly JJ (2014) Microplastic is an abundant and distinct microbial habitat in an urban river. *Environ Sci Technol* 48:11863–11871
- Mgalaa S, Mabrouki J, Elouardi M, El Azzouzi L, Moufti A, El Hajjaji S, El Belghiti MA (2022) Study and evaluation of the degradation of procion blue dye by the ozonation method: parametric and isothermal study. *Nanotechnol Environ Eng* :1–7.
- Michels J, Stippkugel A, Lenz M, Wirtz K, Engel A (2018) Rapid aggregation of biofilm-covered microplastics with marine biogenic particles. *Proc R Soc B Biol Sci*. 285:20181203
- Moore C, Moore S, Weisberg S, Lattin G, Zellers A (2002) A comparison of neustonic plastic and zooplankton abundance in southern California's coastal waters. *Mar Pollut Bull* 44:1035–1038

- Paul-Pont I, Tallec K, Gonzalez-Fernandez C, Lambert C, Vincent D, Mazurais D (2018) Constraints and priorities for conducting experimental exposures of marine organisms to microplastics. *Front Mar Sci* 5:1–22
- Peeken I, Primpke S, Beyer B, Gütermann J, Katlein C, Krumpen T (2018) Arctic sea ice is an important temporal sink and means of transport for microplastic. *Nat Commun* 9:1505
- Porter A, Lyons BP, Galloway TS, Lewis C (2018) Role of marine snows in microplastic fate and bioavailability. *Environ Sci Technol* 52:7111–7119
- Prunier J, Maurice L, Perez E, Gigault J, Pierson Wickmann A-C, Davranche M (2019) Trace metals in polyethylene debris from the North Atlantic subtropical gyre. *Environ Pollut* 245:371–379
- Rahmani M, Mabrouki J, Regraguy B, Moufti A, El'Mrabet M, Dahchour A, El Hajjaji S (2021) Adsorption of (methylene blue) onto natural oil shale: kinetics of adsorption, isotherm and thermodynamic studies. *Int J Environ Anal Chem* :1–15.
- Ramesh R, Chen Z, Cummins V (2015) Land-ocean interactions in the coastal zone : past, present and future. *Anthropocene* 12:85–98
- Rehse S, Kloas W, Zarfl C (2016) Short-term exposure with high concentrations of pristine microplastic particles leads to immobilisation of *Daphnia magna*. *Chemosphere* 153:91–99
- Rochman CM, Hoh E, Hentschel BT, Kaye S (2013) Long-term field measurement of sorption of organic contaminants to five types of plastic pellets: implications for plastic marine debris. *environ sci technol* 47:130109073312009
- Samghouli N, Bencheikh I, Azoulay K, Abahdou FZ, Mabrouki J, Hajjaji SE (2022) Study of piroxicam removal from wastewater by artichoke waste using nemrodW® software: statistical analysis. IoT and smart devices for sustainable environment. Springer, Cham, pp 29–42.
- Ter Halle A, Jeanneau L, Martignac M, Jardé E, Pedrono B, Brach L (2017) Nanoplastic in the north atlantic subtropical gyre. *Environ Sci Technol* 51:13689–13697
- Van Cauwenbergh L, Devriese L, Galgani F, Robbens J, Janssen CR (2015) Microplastics in sediments: a review of techniques, occurrence and effects. *Mar Environ Res* 111:5–17
- Van Sebille E, Wilcox C, Lebreton L, Maximenko N, Hardesty BD, van Franeker JA (2015) A Glob Inven Small Float 10:124006
- Velzeboer I, Kwadijk CJAF, Koelmans AA (2014) Strong sorption of PCBs to nanoplastics, microplastics, carbon nanotubes, and fullerenes. *Environ Sci Technol* 48:4869–4876
- Wegner A, Besseling E, Foekema EM, Kamermans P, Koelmans AA (2012) Effects of nanoplastics on the feeding behavior of the blue mussel (*Mytilus edulis* L.). *Environ Toxicol Chem* 31:2490–2497.
- Weltje L, Sumpter JP (2017) What makes a concentration environmentally relevant? critique and a proposal. *Environ Sci Technol* 51:11520–11521
- Wu X, Cobbina SJ, Mao G, Xu H, Zhang Z, Yang L (2016) A review of toxicity and mechanisms of individual and mixtures of heavy metals in the environment. *Environ Sci Pollut Res* 23:8244–8259
- Zettler ER, Mincer TJ, Amaral-Zettler LA (2013) Life in the “plastisphere”: microbial communities on plastic marine debris. *Environ Sci Technol* 47:130619162220002
- Ziajahromi S, Neale PA, Leusch FDL (2016) Wastewater treatment plant effluent as a source of microplastics: review of the fate, chemical interactions and potential risks to aquatic organisms. *Water Sci Technol J Int Assoc Water Pollut Res* 74(10):2253–2269.

Chapter 11

An Effective Ensemble Learning Model to Predict Smart Grid Stability Using Genetic Algorithms



Mohamed Khalifa Boutahir, Abdelaaziz Hessane, Yousef Farhaoui, and Mourade Azrou

Abstract The term “smart grid” refers to an innovative network for electricity distribution that employs demand-and-response and bidirectional data exchanges. Therefore, predicting the grid’s stability is crucial to make the smart grid more dependable and the electricity supply more efficient and consistent. This study’s primary objective and contribution were to develop a highly accurate XGBoost model that leverages the Genetic Algorithm as a parameters tuner to predict the stability of smart grids. The proposed model outperformed the other models (Artificial Neural Network, Random Forest, and LightGBM) with a precision of 98.02%.

Keywords Solar energy · Smart grid stability · Neural networks · Deep learning

11.1 Introduction

The standard power grid consists of basic fossil fuel-based power production units. However, due to increasing energy costs, the demand for renewable resources, and climate change, the current power system is becoming antiquated and is hampered by cyberattacks, anonymity, and power damage (Gharavi and Ghafurian 2011). To address this issue and enhance the sustainability and dependability of renewable energy sources. Therefore, the smart grid is proposed. The smart grid system is a technological electricity supply of the future that enables bidirectional connection between devices and the control center.

One of the numerous dimensions that must be handled is the stability of smart grids. The strength relies on the balance between the supply and demand of energy (Ackermann et al. 2001). Due to a constant transition from fossil-based to renewable energy sources, their penetration at low voltage, and the distribution level of electrical power systems, grid architectures are getting more decentralized, and energy transfer is becoming more bidirectional (Ackermann et al. 2001).

M. K. Boutahir (✉) · A. Hessane · Y. Farhaoui · M. Azrou
STI Laboratory, IDMS Team, Faculty of Sciences and Techniques, Moulay Ismail University of Meknès, Meknès, Morocco
e-mail: moha.boutahir@edu.umi.ac.ma

In the past few years, academia and industry have supplied related investments for addressing the requirements of such a novel issue. Several researches have been conducted in the field of Smart Grid stability (Shi et al. 2020). Artificial Intelligence in general and Machine Learning and Deep learning led to proposal solutions and predictions for various issues Boutahir et al. (2022), Rajasekhar et al. (2022), Azroul et al. (2022) especially the grid's stability. However, most of these strategies rely on supervised models, which need substantial data sources. Annotating big datasets for energy applications is difficult, time-consuming, and costly, as well as requiring subject expertise.

Several studies have looked into and provided solutions for the smart grid stability. In Khalid et al. (2019), the authors developed a Long Short Term Memory, Recurrent Neural Network models for sales forecasts and power price estimation. The researchers diligently tried to create a revolutionary forecasting model. This model has both single and multiple input variables. Researchers found that using many factors improves prediction performance in their investigation. In Omar et al. (2022), an improved forecasting model for predicting the stability of smart grids was developed utilizing neural networks to carry out with the missing data. In order to train the suggested models, the Levenberg–Marquardt method is utilized. As transfer functions, the authors employed Tansig and Purelin in the hidden and output layers. The model's performance was tested using the MSE and R2 values on a four-node star network. Their models exhibit excellent performance and the finest training and prediction capabilities. In Gorzałczany et al. (2020), the authors want to examine the hierarchy of influence of certain input qualities on the decentralized smart grid control stability, as well as the effect of probable “overlapping” of some input attributes. In order to do this, the authors describe a methodology for generating fuzzy rule-based classifiers from data using multi-objective evolutionary optimization methods. In addition, a comparison with 39 alternative methodologies was conducted to demonstrate the strengths of their methods. In Bingi and Prusty (2021) the authors compared the performance of Feedforward neural network, cascade, and recurrent neural-network-based models for predicting the stability of smart grids. The findings of MSE and R² values show that the Feedforward neural network outperformed cascade and recurrent neural networks. In Sattari et al. (2021), it is demonstrated that the performance of forecasting the smart grid's stability may be enhanced by adding extra hidden layers in a Feedforward neural network. With a multilayer network, this performance fluctuation is minimal. The authors determined that their strategy improved the performance but increased the network's complexity. In Malbasa et al. (2017), the prediction of voltage stability in transmission networks using active machine learning was presented. The authors used pool-based active learning approaches to power system metrics, such as synchro phasor data, which determines voltage stability. Their research used machine learning approaches to predict the margins of voltage stability in a transmission network.

This study evaluates the accuracy and performance of four models for smart grid stability, including XGboost with a genetic algorithm as the parameter optimizer, an artificial neural network, a random forest, and LightGBM.

The remaining of this paper describes the datasets utilized in Sect. 11.2. Section 11.3, describes the recommended methodology. Section 11.4, describes the experiment's outcomes and results. The final section sums up the paper.

11.2 Data Source

In our paper, we utilized an enhanced version (PAULO BREVIGLIERI 2020) of the “Electrical Grid Stability Simulated Dataset” generated by Vadim Arzamasov (Karlsruher Institut für Technologie, Karlsruhe, Germany) (Arzamasov 2018) and provided by the University of California (UCI) Machine Learning Repository 14. The dataset contains 60,000 occurrences and 12 primary predictive features and two dependent variables, of which 63.7 % are stable, whereas 36.2 % are unstable.

The dataset includes:

- Participants' price-change reaction times (**tau1, tau2, tau3, tau4**).
- Nominal power produced by customers (**p1, p2, p3, p4**).
- Consumers' proportional price elasticity (**g1, g2, g3, g4**).
- Target value **Stab**: positive indicates instability, while negative indicates stability.
- Target class **Stabf**: stable or unstable.

11.3 Methodology

The suggested methodology will address the difficulties associated with predicting smart grid stability. The dataset presented in the previous part has been preprocessed and normalized to obtain usable results and the most accurate findings possible utilizing various methodologies. After the data was preprocessed, our methodology and other models were employed, and their results were compared.

11.3.1 XGBoost with Genetic Algorithm

XGBoost offers outstanding results; generally, it has many parameters, and different **parameter** combinations generate varied scores. The genetic algorithm solves this issue and performs well in parameters tuning. In this research, the Genetic Algorithm is employed to optimize XGBoost's parameters tuning process.

a. XGBoost

Chen and Guestrin (2016) created XGBoost (Extreme Gradient Boosting), a boosting algorithm for classifying regression tree models. The boosting algorithm belongs to the category of methods for supervised learning. Boosting is a sequential technique for ensemble learning. XGBoost utilizes regularization parameters to minimize overfitting. In addition, it employs auto-pruning to prevent branches from not spreading beyond a certain level. The model was utilized in numerous industries to resolve several classification problems.

b. Genetic Algorithms

GA (Genetic Algorithm) is an adaptable and random search algorithm Jiang et al. (2019). It comprises group selection, crossing over, mutation, and extinction. In the genetic algorithm, the “*chromosome*” is comparable to the individuals in the population, such as a sample or a mixture of values, and each coding unit is referred to as a “*gene*”. The GA differentiates the merits of each chromosome or sample by comparing the values of the fitness function. and the algorithm is superior the larger the value. Each chromosome’s fitness value is determined by an evaluation function Boutahir et al. (2022).

Figure 11.1 illustrates the Genetic Algorithm. Initializing the population with random numbers and encoding the chromosomes come first. Then, individuals are selected according to their fitness levels. The fittest individuals can be retained to avert population decline. In the crossover step, it is necessary to establish a random threshold. The mutation step determines the number of algorithm iterations and modifies the gene’s position based on its probability. Finally, the termination step is utilized to determine whether or not genetic evolution is halted.

11.3.2 Artificial Neural Network

The artificial neural network (ANN) model represented in Fig. 11.2 is the one examined in our study for smart grid stability monitoring. It demonstrates a schema with one input layer (12 input nodes), three hidden layers (36, 36, and 24 nodes, sequentially), and one output layer with a single node. Due to the numerical nature of the characteristics, the selection of ‘*relu*’ as the activation function for hidden layers appears obvious. Since the output is binary (‘0’ for ‘unstable’ and ‘1’ for ‘stable’), ‘sigmoid’ is the optimal activation for the output layers. The same logic applies to compilation with ‘*adam*’ as the optimizer and ‘binary crossentropy’ as the loss function. The performance of the fitting will be evaluated using “accuracy” as the chosen metric.

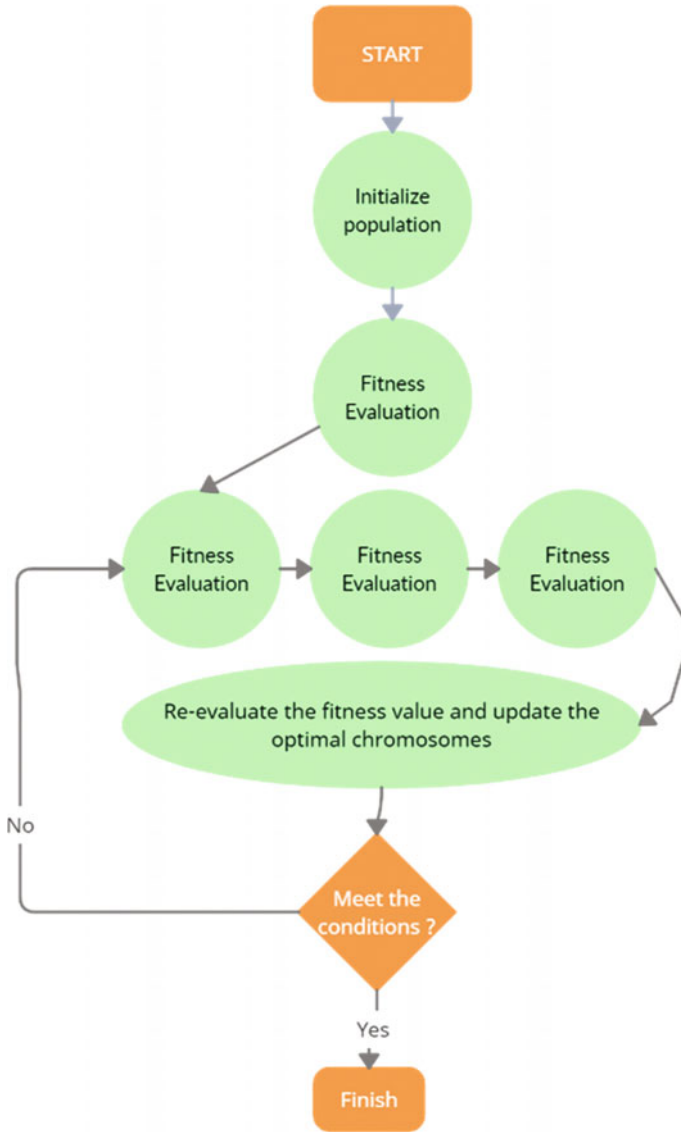


Fig. 11.1 The process of the genetic algorithm

11.3.3 LightGBM

LightGBM is a robust implementation of the boosting approach that is comparable to XGBoost but varies in a few pertinent aspects, such as how the tree or base learners are built. XGBoost is one of its primary inspirations. In contrast to other ensemble

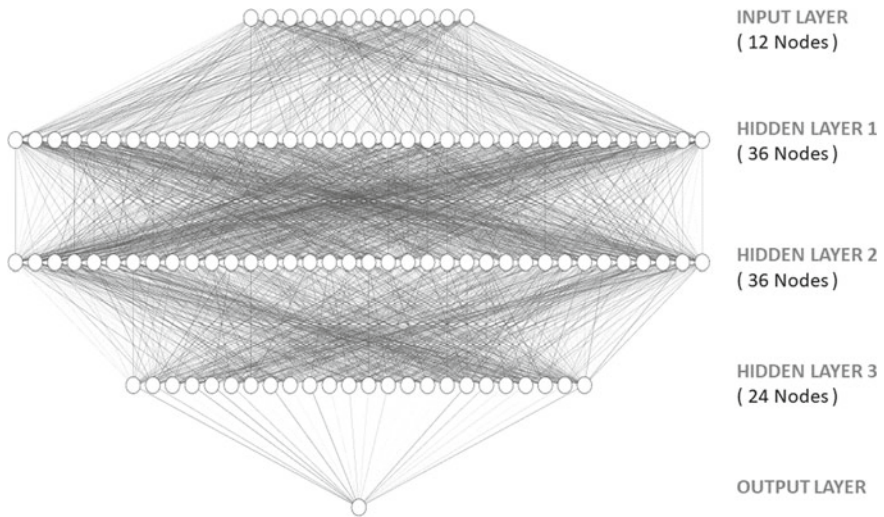


Fig. 11.2 The artificial neural network structure

algorithms, LGBM produces trees one leaf at a time, which helps to reduce the amount of information that is lost during the sequential boosting phase Boutahir et al. (2022).

11.3.4 *Random Forest*

Random forests are a method for supervised learning. It can be utilized for regression analysis in addition to classification. Additionally, it is the most adaptable and simple algorithm to implement. Trees are the fundamental building blocks of a forest. It is commonly believed that the greater the number of trees in a forest, the stronger it is. The random forest algorithm aims to construct decision trees based on randomly chosen data samples, obtain a prediction from each tree, and then vote on which answer is the most effective. In addition to this, it serves as a reasonably reliable indicator of the relevance of the feature.

11.4 Results and Discussions

Several models have been utilized to assess the Smart Grid stability prediction. The entire project was executed in a Google Colab environment using Jupyter Notebook and Python 3.8 (Google Colaboratory). The features dataset will have all 12 original predictive features, however, the labels will only contain the “stabf” characteristic. In

Table 11.1 Different models and their accuracy

Model	Accuracy
XGBoost with GA	98.02%
ANN	97.69%
Random forest	95.13%
LightGBM	96.17%

addition, the training set will contain all 54,000 initial data, and the testing set will contain all 6,000 recent observational data. Given that the dataset has already been mixed up, the original 54,000 observations, which were used to fit the model, will be included in the training set. In comparison, the most recent 6,000 observations will be included in the testing set.

XGBoost with GA outperformed the other models in predicting smart grid stability. As shown in Table 11.1, the XGBoost with GA model predicts with the highest accuracy with 98.02%. Tuning parameters is a crucial step in enhancing the performance of any ML algorithm, and the GA was utilized as a parameter’s tuner in this case. It entails establishing a grid of all potential parameters and testing them to determine the values that maximize the model’s performance.

In addition, ANN achieved an accuracy of 97.69% by adopting a multiple hidden layers composed of (36, 36, and 24 nodes), as shown in Fig. 11.2. Although Random Forest and LightGBM also displayed a high degree of accuracy (95.13% and 96.17%, respectively), Grid Search CV greatly enhanced both models’ performance by tuning the parameters.

As demonstrated in Table 11.2, our study and the various models utilized exceeded earlier research. Therefore, the approach can assist prevent power outages and greatly enhance smart grid efficiency.

Table 11.2 A comparison of previous works ensures the stability of the grid search

Reference	Year	Model = Accuracy
Ibrar et al. (2022)	2022	XGBoost = 96.8%
Bano et al. (2019)	2020	SVM = 70:40%
Yin et al. (2019)	2019	XGBoost = 91:40%
Moldovan and Salomie (2019)	2019	MLP = 93:8%
Baltas et al. (2018)	2018	ELM = 94:13%
Malbasa et al. (2017)	2018	RF = 90:01% ANN = 89:73

11.5 Conclusion

In this research, we describe a new method for predicting the stability of smart grids based on various machine learning and deep learning models. A stable power system is required to prevent blackouts and provide a steady electrical supply. The XGBoost method outperformed all other models in our analysis, including ANN, Random Forest, and LightGBM. Using the principles of genetic algorithm, the accuracy of XGBoost's prediction was enhanced to 98.02%. As future research, we wish to consider: (1) the incorporation of additional classifiers into the study, (2) the real-time identification of instability issues, and (3) the incorporation of a machine learning technique for predicting system stability based on feature extraction.

References

- Ackermann T, Andersson G, Söder L (2001) Distributed generation: a definition. *Electr Power Syst Res* 57:195–204
- Arzamasov V (2018) “Electrical grid stability simulated data set”. The UCI Machine Learning Repository
- Azrou M, Mabrouki J, Fattah G, Guezzaz A, Aziz F (2022) Machine learning algorithms for efficient water quality prediction. *Model Earth Syst Environ* 8(2):2793–2801. <https://doi.org/10.1007/s40808-021-01266-6>
- Baltas GN, Perales-González C, Mazidi P, Fernandez F, Rodríguez P (2018) “A novel ensemble approach for solving the transient stability classification problem”. In: 2018 7th International Conference on Renewable Energy Research and Applications (ICRERA). Paris, France, pp 1282–1286.
- Bano H, Tahir A, Ali I, Haseeb A, Javaid N (2020) “Electricity load and price forecasting using enhanced machine learning techniques,” in innovative mobile and internet services in ubiquitous computing. IMIS 2019. In: Barolli L, Xhafa F, Hussain O (Eds) *Of Advances in Intelligent Systems and Computing*, vol 994, Springer, Cham, pp 255–267.
- Bingi K, Prusty BR (2021) Neural network-based models for prediction of smart grid stability. In: *Proceedings of the 2021 Innovations in Power and Advanced Computing Technologies (i-PACT)*, Kuala Lumpur, Malaysia, pp 1–6.
- Boutahir MK, Farhaoui Y, Azrou M (2022) “Machine learning and deep learning applications for solar radiation predictions review: morocco as a case of study”. In: *Digital Economy, Business Analytics, and Big Data Analytics Applications*. Springer, Cham, pp 55–67.
- Boutahir MK, Farhaoui Y, Azrou M, Zeroual I, El Allaoui A (2022) Effect of feature selection on the prediction of direct normal irradiance. *Big Data Min Anal* 5(4):309–317. <https://doi.org/10.26599/BDMA.2022.9020003>
- Breviglieri P (2020) “Smart grid stability”, Kaggle. www.kaggle.com/datasets/pcbreviglieri/smart-grid-stability
- Chen T, Guestrin C (2016) “Xgboost: a scalable tree boosting system”. In: *Proceedings of the 22nd ACM SIGKDD International Conference on Knowledge Discovery and Data Mining*. San Francisco California, USA, pp 785–794.
- Gharavi H, Ghafurian R (2011) *Smart grid: the electric energy system of the future*, Vol 99. IEEE, Piscataway, NJ, USA
- Google Colaboratory. <https://colab.research.google.com>

- Gorzałczany MB, Piekoszewski J, Rudziński F (2020) A modern data-mining approach based on genetically optimized fuzzy systems for interpretable and accurate smart-grid stability prediction. *Energies* 13(10):2559. <https://doi.org/10.3390/en13102559>
- Ibrar M, Hassan MA, Shaukat K, Alam TM, Khurshid KS, Hameed IA, Aljuaid H, Luo S (2022) “A machine learning-based model for stability prediction of decentralized power grid linked with renewable energy resources”. *Wirel Commun Mob Comput* 2022: 15. Article ID 2697303. <https://doi.org/10.1155/2022/2697303>
- Jiang Y, Tong G, Yin H, Xiong N (2019) A pedestrian detection method based on genetic algorithm for optimize XGBoost training parameters. *IEEE Access* 7:118310–118321. <https://doi.org/10.1109/ACCESS.2019.2936454>
- Khalid R, Javaid N, Al-zahrani FA, Aurangzeb K, Qazi EH et al (2019) Electricity load and price forecasting using jaya-long short term memory (JLSTM) in smart grids. *Entropy* 22(1):10
- Malbasa V, Zheng C, Chen P-C, Popovic T, Kezunovic M (2017) Voltage stability prediction using active machine learning. *IEEE Trans Smart Grid* 8(6):3117–3124
- Moldovan D, Salomie I (2019) “Detection of sources of instability in smart grids using machine learning techniques”. In: 2019 IEEE 15th International Conference on Intelligent Computer Communication and Processing (ICCP). ClujNapoca, Romania, pp 175–182.
- Omar MB, Ibrahim R, Mantri R, Chaudhary J, Ram Selvaraj K, Bingi K (2022) Smart grid stability prediction model using neural networks to handle missing inputs. *Sensors* 22(12):4342. <https://doi.org/10.3390/s22124342>
- Rajasekhar C, Azroul M, Vinayakumar R et al (2022) A particle swarm optimization and deep learning approach for intrusion detection system in internet of medical things. *Sustainability* 14(19):12828
- Sattari MA, Roshani GH, Hanus R, Nazemi E (2021) Applicability of time-domain feature extraction methods and artificial intelligence in two-phase flow meters based on gamma-ray absorption technique. *Meas* 168:108474
- Shi Z, Yao W, Li Z, Zeng L, Zhao Y et al (2020) Artificial intelligence techniques for stability analysis and control in smart grids: methodologies, applications, challenges and future directions. *Appl Energy* 278(2015):115733
- Yin D, Yang Y, Yang M, Yang Z, Li C, Li L (2019) “A new distributed power system for stability prediction and analysis”. In: 2019 IEEE 10th International Conference on Software Engineering and Service Science (ICSESS). Beijing, China, pp 1–4

Chapter 12

Optimization of Performance the Waste in Treatment of Textile Wastewater Using Response Surface Methodology



Abdelkader Anouzla, Amina Khalidi Idrissi, Oussam Hartal, Malika Kastali, Hayat Loukili, Khalid Digua, Salah Souabi, Bachar Redouane, Ali Moussadik, Mohamed Elouardi, Karima Azoulay, Imane Bencheikh, Mohamed Benchrifa, Younes Abrouki, Jamal Mabrouki, Adnane El Hamidi, Mohammed Dahhou, Hicham Harhar, Ghizlane Fattah, and Mohammed Salah

Abstract Among all industrial waste, wastewater from the textile industry is the most contaminated. Textile industrial wastewater (TIWW) is challenging to manage due to the use of colors and complicated chemicals at different stages of the textile processing process. Therefore, traditional methods based on single unit treatment might not be sufficient to meet the stricter norms for zero discharge of dangerous substances and environmental quality discharge standards. The study described here concentrated on using FeCl₃-rich steel industrial wastewater (SIWW) as an initial coagulant to remove pollution of wastewater from textile manufacturing industry. With the central composite design (CCD) technique, the independent parameters, such as pH, coagulant dosage, and flocculant dosage, were optimized while considering the dependent variables, including turbidity, COD reduction, and color. ANOVA was used to evaluate the statistical fitness of the proposed model. At pH 9.2, SIWW 14 and 1 ml /L of Flocculant dose, the most significant reduction in turbidity (99%), COD (88%), and color (100%) was seen. For all three coagulants, the ultimate pH of the solution was below the disposal limitations.

Keywords Textile industrial wastewater · Optimization · Central composite design · Turbidity · COD reduction · Decolorization

A. Anouzla (✉) · A. K. Idrissi · O. Hartal · M. Kastali · H. Loukili · K. Digua · S. Souabi
FSTM, Hassan II University of Casablanca, Mohammedia, Morocco
e-mail: aanouzla@gmail.com

B. Redouane
FPBM, Sultan Moulay Slimane University, Béni Mellal, Morocco

A. Moussadik · M. Elouardi · K. Azoulay · I. Bencheikh · M. Benchrifa · Y. Abrouki ·
J. Mabrouki · A. E. Hamidi · M. Dahhou · H. Harhar · G. Fattah
FSR, Mohammed V University in Rabat, Rabat, Morocco

M. Salah
FSJ, Chouaib Doukkali University, El Jadida, Morocco

12.1 Introduction

Due to increasingly more significant discharge into water bodies due to technological advancements, interference of dyes in the environment has become an ecological issue (Moussadik 2022 and Ihaddaden 2022). According to reports, the textile industry primarily releases secondary effluents from various polluting industries into the environment at a rate of 7.5 105 metric tons a year (Loukili et al. 2021 and Kuleyin et al. 2022). Over 60% of all dyes used each year are consumed by the textile industry, according to research (Abrouki et al. 2021 and Altayb et al. 2021). Chemically, dyes have aromatic rings with various functional groups (Rachiq et al. 2021 and Anouzla et al. 2009a). Dyes have conjugatively extended electrons, which can absorb light with a spectrum between 400 and 700 nm (Anouzla 2020 and Abdallah et al. 2021). These have been identified as hydrocarbons from coal tar, such as toluene, naphthalene, xylene, and anthracene. They have been used to add color to various products, such as medications, paper, clothes, cosmetics, waxes, leather, and greases (Mabrouki et al. 2020a and Arce et al. 2021).

Various dyes have been used in the textile business to colorize raw cotton (Dadban et al. 2022 and Anouzla et al. 2009a). This property is caused by the inclusion of chromogens and chromophores in dye chemical structures, which render dye electron acceptors with potential dyeing capacities. As a result, over 100,000 pounds of dye are used in the textile industry, of which 20% are discharged into water bodies without any effluent treatment (Okur et al. 2022 and Anouzla et al. 2009a).

Industrial wastewater treatment methods frequently employ physical–chemical processes (Ab-Hamid et al. 2020 and Kastali et al. 2020). Coagulation/flocculation appears to be the most suitable procedure in these conditions, and it is frequently used to treat the textile industry (Mabrouki et al. 2020a and Kastali et al. 2021). The coagulation-flocculation process allows the removal of a large part of the organic matter and suspended matter and a good yield in decoloration. It presents a necessary first treatment before the biological treatment. This technique is less expensive, easy to apply, and does not require much space. It is undoubtedly advantageous even for the infrastructure of small industrial units (Rizvi et al. 2022 and Anouzla et al. 2014).

Numerous experimental designs, such as the central composite design (CCD), full factorial design (FFD), fractional factorial design, Box-Behnken design (BBD), and Doehlert matrix design (DMD), are fitted to all the circumstances that an investigator may experience (Chaymae et al. 2022 and Abrouki et al. 2014a). Each sort of experimental design considers the limitations of the experimental field under study and results from a trade-off between the number of tests and the required precision of the replies. Therefore, in order to realize the DOE experiments, it is first necessary to comprehend ANOVA and linear regression as statistical techniques (Zhang 2022 & Weissman and Anderson 2015). Appropriate statistical software can be used to plan and analyze experiments. Minitab, Design Expert, JMP, STATISTICA, (Loukili et al. 2021).

In this instance, the variances in features are the leading causes of the difficult-to-treat textile wastewater. This study's motivation was to better evaluate the

coagulation-flocculation treatment by determining the effects and interactions of various parameters. The most crucial goal of this study was to ascertain the impact of steel industrial wastewater (SIWW) on the effectiveness of treating textile wastewater, as well as to find their interactions with pH, coagulant dosages, and flocculant doses. The central composite design was used in planning process tests of coagulation-flocculation to accomplish this goal. With the help of this experimental design methodology, it was possible to determine the ideal conditions (favorable levels of factors) for decolorization and COD reduction. Important factors studied included pH, coagulant dosage, and flocculant dosage, as well as their effects and interactions on coagulation-flocculation performance.

12.2 Materials and Techniques

12.2.1 Materials

In this study, wastewater was taken from a textile manufacturer in Casablanca, Morocco. Manually obtained samples of textile wastewater were put in a special 25 L container. The samples were brought to the lab immediately and kept there at 4 °C.

Before analysis, these samples were left at standard condition for two hours. The conventional methods for determining water and wastewater were followed for all analytical procedures (APHA 2012). Table 12.1 summarizes these wastewater's primary physico-chemical parameters compared to Moroccan Wastewater Discharge Standards.

This table shows that the wastewater from the textile industry has a significant pollutant load and is a highly turbid liquid with a high pH. Unfortunately, Moroccan wastewater discharge standards do not allow these concentrations.

Table 12.1 Textile wastewater analysis

Parameters	Range	Mean	Discharge standards
pH	10.3–10.7	10.5	9
COD (mg/L)	3193–3274	3206	500
BOD ₅ (mg/L)	198–224	213	140
TNK (mg/L)	67–81	74	40
Turbidity (NTU)	426–438	430	–
Conductivity (mS/cm)	38–46	41	2.7
TSS (mg/L)	511–532	520	50

In addition, the COD/BOD5 ratio is greater than 4, indicating that this effluent is not readily biodegradable. As a result, a physicochemical treatment method such as coagulation-flocculation is required to combat the pollution of this discharge.

12.2.2 Methods

A pilot-scale laboratory test known as the “jar test” mimics the coagulation and flocculation processes used in wastewater treatment. (Kastali et al. 2020 and Mabrouki et al. 2020a, 2020b) The two steps of quick mixing and gradual mixing are often used to complete coagulation-flocculation operations (Kastali et al. 2021). Rapid mixing ensures a complete chemical reaction and distributes the coagulants uniformly throughout the water. A longer time of mild agitation is required to encourage particle collisions and improve floc development. The flocs were not disturbed once the mixing procedure was complete to allow for settling.

In this study, Coagulation-flocculation experiments were performed to determine the optimal effluent pH, doses of SIWW coagulant and Polysep 3000 flocculant. Removal efficiency of turbidity, COD and colour were obtained according to the following equation (Eq. 12.1).

$$Removal(\%) = \frac{C_i - C_f}{C_i} \times 100 \quad (12.1)$$

Knowing that, the initial and final concentrations of pollutants from textile wastewater are noted C_i and C_f , respectively.

12.2.3 Test

Based on the design of experiments, the Response Surface Methodology (RSM) is a set of statistical and mathematical tools for designing experiments and maximizing the impact of process factors (Mabrouki et al. 2020a, 2020b). Doing research in an objective, controlled manner such that accuracy is maximized and precise conclusions may be formed in relation to a hypothesis statement is known as experimental design (Anouzla 2020). Typically, the goal is to determine a factor, independent variable, or dependent variable's impact on another.

The most used model for fitting the response surface approach is the central composite design (CCD) (Abrouki et al. 2014a, 2014b). The global model that predicts the best operating conditions, was represented depending on the under-mentioned equation (Eq. 12.2).

$$Y = \beta_0 + \sum_{i=1}^n \beta_i X_i + \sum_{i=1}^n \beta_{ii} X_i^2 + \sum_{i=1}^n \sum_{j=1}^n \beta_{ij} X_i X_j + \epsilon \tag{12.2}$$

where the predicted response is represented by Y; the coefficients of the intercept, linear, quadratic and interaction terms among independent factors (X) are indicated respectively by β_0 , β_i , β_{ii} and β_{ij} ; and the model error is denoted by ϵ . Statgraphics-Plus statistical software was used in this study to evaluate and interpret the outcomes of this experimental design. In addition, multiple response processes have been simultaneously optimized using the desired function technique.

12.3 Results and Argumentation

12.3.1 Results

In this research, central composite design was utilized to optimize the operating conditions of coagulation-flocculation process for textile wastewater treatment, namely coagulant dose (X1), flocculant dose (X2) and effluent pH (X3). Whereas three responses, namely removal efficiency of turbidity (Y1), COD removal (Y2) and colour removal (Y3) are investigated in Table 12.2.

The experimental design matrix and the corresponding experimental parameters and response value were summarized in Table 12.3.

A regression analysis by least squares method was performed to fit the responses and predict the outcome of these responses. The final empirical models in term of coded factors after excluding the insignificant terms for removal efficiency pollution of textile wastewater by coagulation-flocculation process, are shown in equations (Eqs. 12.3–12.5), respectively:

Table 12.2 Factors and responses

Input	Factors			
	x _i	X _i		
		-1	0	+1
	x ₁ = Coagulant dose (mL/L)	10	15	20
	x ₁ = Flocculant dose (mL/L)	1	1.5	2
	x ₂ = Effluent pH	6	8	10
Output	Responses			
	Y ₁ = Turbidity removal (%)			
	Y ₂ = COD removal (%) Y ₃ = Colour removal (%)			

Table 12.3 Design matrix

Runs	Independent variables			Responses		
	X ₁	X ₂	X ₃	Y ₁	Y ₂	Y ₃
1	-1	-1	-1	88	79	92
2	+1	-1	-1	52	64	70
3	-1	+1	-1	87	80	88
4	+1	+1	-1	41	56	63
5	-1	-1	+1	82	75	89
6	+1	-1	+1	99	83	96
7	-1	+1	+1	91	84	95
8	+1	+1	+1	98	84	98
9	-1.4142	0	0	95	81	97
10	+1.4142	0	0	71	69	82
11	0	-1.4142	0	83	77	90
12	0	+1.4142	0	82	78	89
13	0	0	-1.4142	55	66	69
14	0	0	+1.4142	98	86	96
15	0	0	0	95	86	98
16	0	0	0	95	86	98

$$Y_1 = 94.51 - 7.2X_1 - 0.42X_2 + 12.76X_3 - 4.08X_1^2 - 4.26X_2^2 - 6.38X_3^2 - 2.5X_1X_2 + 13.25X_1X_3 + 2.5X_2X_3 \tag{12.3}$$

$$Y_2 = 85.99 - 3.75X_1 + 0.34X_2 + 5.9X_3 - 3.88X_1^2 - 2.99X_2^2 - 3.52X_3^2 - 2.13X_1X_2 + 5.88X_1X_3 + 2.13X_2X_3 \tag{12.4}$$

$$Y_3 = 98.01 - 4.56X_1 + 0.34X_2 + 8.09X_3 - 3.04X_1^2 - 3.04X_2^2 - 5.51X_3^2 - 0.88X_1X_2 + 7.13X_1X_3 + 2.38X_2X_3 \tag{12.5}$$

Analysis of variance (ANOVA) was used to support these models' suitability further, as shown in Table 12.4.

As a result of this ANOVA, we can deduce that the regression is statistically significant for all of these second order polynomial equations at a 95% confidence level because the model F-value was higher than the crucial value at the 5% level of significance. In addition, significant model terms larger than or equal to 95% at a confidence level for each answer included linear terms (X1 X2, and X3), squared terms (X1 X1, X2 X2, and X3 X3), and interaction terms (X1 X2, X1 X3, and X2 X3).

Table 12.4 ANOVA table

Response	Terms	Sum of squares	Df	Mean square	F _{exp}
Y ₁	Model	4856.237292	09	539.58	4607
	Errors	0.702708	06	0.117118	—
	Total	4856.94	15	—	—
Y ₂	Model	1205.265623	09	133.92	1658.86
	Errors	0.484377	06	0.0807294	—
	Total	1205.75	15	—	—
Y ₃	Model	1925.425021	09	213.94	3949.84
	Errors	0.324979	06	0.0541632	—
	Total	1925.75	15	—	—

12.3.2 Process Analysis

Turbidity is a term used to describe how much-dispersed particles have affected the water’s clarity. The water seems murkier and has higher turbidity when more total suspended solids are present. Turbidity is regarded as a reliable indicator of water quality. Figure 12.1a in this study illustrates the effects of the coagulant dosage, flocculant dose, and effluent pH on the removal of turbidity from textile wastewater by the coagulation-flocculation process.

From these response surface plots, it can be seen that after treatment of textile wastewater by coagulation-flocculation process, the residual turbidity of this wastewater is minimal for a pH greater than 9.2, for a coagulant dosage equal to 14 and 1.5 ml/l for flocculant dosage. In environmental chemistry, the chemical oxygen demand (COD) is an indicative measure of the amount of oxygen that can be consumed by reactions in a measured solution. In this work, the evolution of the COD reduction percentage, depending on the coagulant dosage and effluent pH with fixed concentration of flocculant dosage, is shown in Fig. 12.1b.

This geometric representation shows that for a fixed flocculant dosage, the increase in pH increases the COD reduction rate. In addition, the increase in coagulant dosage

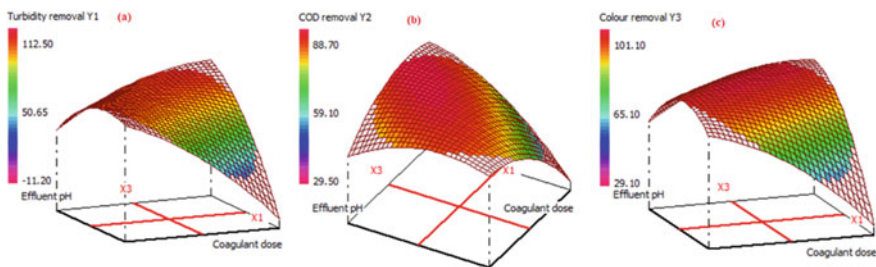


Fig. 12.1 Response surfaces

increases the rate of reduction to reach their minimum at the optimal dose of coagulant from 14 ml/l at a pH greater than 9.2. Increasing the dosage above this value does not improve the pollution elimination rate. Indeed, the color of textile wastewater is determined using a UV/Visible spectrophotometer (Model 7800 UV/VIS spectrophotometer) by measuring the absorbances at the three wavelengths 436, 525 and 620 nm and the color corresponds to the sum of these absorbances. In our case, the geometric representation of the effects of factors that control the operating conditions of the color removal by the coagulation-flocculation process for the treatment of textile wastewater, is shown in Fig. 12.1c. The analysis of these isoresponse curves shows that for a fixed coagulant concentration, the increase in pH increases the colour removal. Moreover, for a fixed pH, the increase in coagulant concentration decreases the colour reduction rate in the experimental domain.

12.3.3 Process Optimization

The existence of certain limits in the calculation of the optimal circumstances makes them more realistic. High and low values of the process parameters in the experimental design are invariably taken into account as explicit limitations to prevent extrapolation if the model employed in the optimization research is empirical. The main goal of this study is to identify the experimental conditions needed to clean up textile wastewater through the coagulation-flocculation process (Fig. 12.2). Using the methodology for experimental design mentioned above, the ranges of the parameters needed to achieve the best conditions were identified.

The graphical analysis of the model makes it possible to locate the ranges of the optimal conditions of the treatment. From the three isoresponse curves of turbidity reduction, COD elimination and color elimination, we deduce that for 14 ml /l of coagulant dose and 1 ml /l of flocculant dose at 9.2 of effluent pH, we manage to eliminate the almost all of the pollution from textile wastewater. The comparative study of our results with those of other coagulants cited in the literature, reveals that SIWW can be used as an efficient and alternative coagulant for pollution removal from textile wastewater.

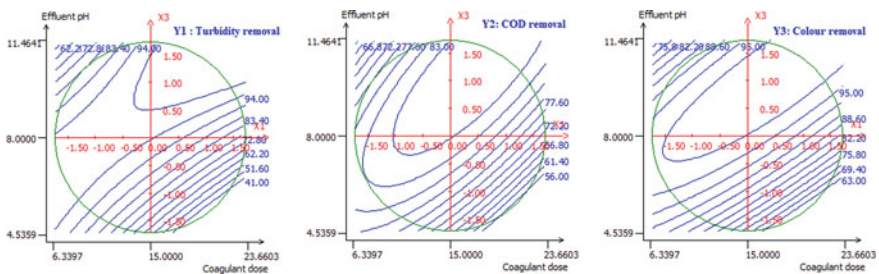


Fig. 12.2 Process optimization

12.4 Conclusion

In this study, a data-driven methodology was used to examine the optimal performance of coagulation-flocculation concerning turbidity removal, COD removal, and decolorization for the treatment of industrial textile wastewater.

This paper illustrated with success the employ of a central composite design by locating the best process parameters that yield the highest % elimination of pollution for this wastewater.

The results demonstrated that SIWW has performance in the treatment of textile wastewater and that SIWW has the advantages of more cost saving and less computational effort than classic coagulants.

The suggested model possessed better performance for use in wastewater treatment engineering due to the good control of turbidity removal, COD removal and discoloration based on experimental data.

References

- Abdallah R, Barkat D, Jawad AH, Abdulhameed AS, Al-Kahtani AA, Alotman ZA (2021) Parametric optimization by box-behnken design for synthesis of magnetic chitosan-benzil/ZnO/Fe₃O₄ nanocomposite and textile dye removal. *J Environ Chem Eng* 9(3):105166. <https://doi.org/10.1016/J.JECE.2021.105166>
- Ab-Hamid FH, Salim SA, Mat-Shayuti MS (2020) Optimization of progressive freeze concentration on stormwater purification via response surface methodology. *Asia-Pac J Chem Eng* 15(3):1–7. <https://doi.org/10.1002/apj.2419>
- Abrouki Y, Anouzla A, Loukili H, Bennazha J, Lotfi R, Rayadh A, Bahlaoui My A, Sebti S, Zakarya D, Zahouily M (2014a) Experimental design-based response surface methodology optimization for synthesis of β -mercapto carbonyl derivatives as antimycobacterial drugs catalyzed by calcium pyrophosphate. *Int J Med Chem* 4: 586437.
- Abrouki Y, Anouzla A, Loukili H, Lotfi R, Rayadh A, Bahlaoui My A, Sebti S, Zakarya D, Zahouily M (2014b) Experimental design and modeling of heterogeneous catalytic activity for synthetic phosphate in conjugate addition. *Am J Mater Res* 1:1–6.
- Abrouki Y, Mabrouki J, Anouzla A, Rifi SK, Zahiri Y, Nehhal S, El-Yadini A, Slimani R, El-Hajjaji S, Loukili H, Souabi S (2021) Optimization and modeling of a fixed-bed biosorption of textile dye using agricultural biomass from the moroccan sahara. *Desalin Water Treat* 240:144–151. <https://doi.org/10.5004/dwt.2021.27704>
- Ali M, Nour-eddine L, Driss M, Siro BF, Kitty B, Tom H, Abdellah B, Younes A, Mohamed K, Frederik T, Mohammed H, Adname EH (2022) Investigation of electronic and photocatalytic properties of AgTi₂(PO₄)₃ NASICON-type phosphate: combining experimental data and DFT calculations. *J Photochem Photobiol, A* 435:114289. <https://doi.org/10.1016/j.jphotochem.2022.114289>
- Altayb HN, Kouidhi B, Baothman OAS, Abdulhakim JA, Ayed L, Hager M, Chaieb K (2021) Mathematical modeling and optimization by the application of full factorial design and response surface methodology approach for decolourization of dyes by a newly isolated photobacterium ganghwense. *J Water Process Eng* 44:102429. <https://doi.org/10.1016/J.JWPE.2021.102429>
- Anouzla A, Abrouki Y, Souabi S, Safi M, Rhal H (2009a) Colour and COD removal of disperse dye solution by a novel coagulant: Application of statistical design for the optimization and regression analysis. *J Hazard Mater* 166:1302–1306. <https://doi.org/10.1016/j.jhazmat.2008.12.039>

- Anouzla A, Abrouki Y, Souabi S, Safi M, Rhbal H. (2009c) Valorisation of industrial rejection as an original coagulant for removal of textile wastewater. *Water Pract Technol.* 4 wpt2009c044. doi: <https://doi.org/10.2166/wpt.2009.044>.
- Anouzla A, Souabi S (2020) Treatment of industrial discharges loaded with dyes and surfactant, Scholar's Press
- Anouzla A, Souabi S, Safi M, Abrouki Y, Loukili H, Rhbal H (2014) Waste to treat waste of landfill leachates. *Int J Environ Prot Policy* 2:50-53. doi:<https://doi.org/10.11648/j.ijcpp.20140202.12>
- Anouzla A, Souabi S, Safi M, Aboulhassan A, Rhbal H, Abrouki Y (2009b) Valorization of steel industry wastewaters in the decolorization of dyes containing solutions. *Sci Study Res Chem Chem Eng Biotechnol Food Ind.* doi:10 277 284
- APHA 2012. Standard methods for the examination of water and wastewater, In: Rice EW, Baird RB, Eaton AD, Clesceri LS (eds) American Public Health Association (APHA), American Water Works Association (AWWA) and Water Environment Federation (WEF), 22nd edn. Washington, DC, USA
- Arce MM, Sanllorente S, Ruiz S, Sánchez MS, Sarabia LA, Ortiz MC (2021) Method operable design region obtained with a partial least squares model inversion in the determination of ten polycyclic aromatic hydrocarbons by liquid chromatography with fluorescence detection. *J Chromatogr A* 1657:462577. <https://doi.org/10.1016/J.CHROMA.2021.462577>
- Chaymae H, Ennaciri K, Driouch A, Digua K, Souabi S (2022) Optimization of the coagulation-flocculation process for vegetable oil refinery wastewater using a full factorial design. *Process Saf Environ Prot* 160:803–816. <https://doi.org/10.1016/J.PSEP.2022.02.068>
- Hayat L, Abdelkader A, Ilham J, Brahim A, Alami YS, Karima A, Imane B, Jamal M, Younes A, Saloua S, Ihame B, Abdelaziz S, Najoua L, Souad EH, Rachid A, Mourade A, Amine EGM, Mohammed S, Soufiane T, Yassine R (2022) Combining multiple regression and principal component analysis to evaluate the effects of ambient air pollution on children's respiratory diseases. *Int J Inf Technol* 14:1305–1310. <https://doi.org/10.1007/s41870-022-00906-z>
- Kastali M, Mouhir L, Assou M, Anouzla A, Abrouki Y (2020) Diagnosis of leachate from a closed landfill, impact on the soil, and treatment by coagulation flocculation with alginate and ferric chloride desalin. *Water Treat* 206: 307–314. doi:<https://doi.org/10.5004/dwt.2020.26303>
- Kastali M, Mouhir L, Chatoui M, Souabi S, Anouzla A (2021) Removal of turbidity and sludge production from industrial process wastewater treatment by a rejection of steel rich in FeCl₃ (SIWW). *Biointerface Res Appl Chem.* 11:13359-13376. doi:<https://doi.org/10.33263/BRIAC115.1335913376>
- Kuleyin A, Gök A, Eroğlu HA, Burcu Özkaraova E, Akbal F, Jada A, Duply J (2022) Combining electro-fenton and adsorption processes for reclamation of textile industry wastewater and modeling by artificial neural networks. *J Electroanal Chem* 921:116652. <https://doi.org/10.1016/J.JELECHEM.2022.116652>
- Loukili H, Mabrouki J, Anouzla A, Kouzi Y, Younsi SA, Digua K, Abrouki Y (2021) Pre-treated moroccan natural clays: application to the wastewater treatment of textile industry. *Desalin Water Treat* 240:124–136. <https://doi.org/10.5004/dwt.2021.27644>
- Mabrouki J, Bencheikh I, Azoulay K, Es-soufy M, El Hajjaji S (2020b) Smart monitoring system for the long-term control of aerobic leachate treatment: Dumping case Mohammedia (Morocco). In: Farhaoui Y (ed), Springer, Cham, pp 220–230
- Mabrouki J, Moufti A, Bencheikh I, Azoulay K, El Hamdouni Y, El Hajjaji S (2020a) Optimization of the coagulant flocculation process for treatment of leachate of the controlled discharge of the city mohammedia (Morocco), Springer, Cham, pp 200–212. doi: https://doi.org/10.1007/978-3-030-36475-5_19.
- Okur MC, Akyol A, Nayir TY, Kara S, Ozturk D, Civas A (2022) Performance of Ti/RuO₂-IrO₂ electrodes and comparison with BDD electrodes in the treatment of textile wastewater by electro-oxidation process. *Chem Eng Res Des* 183:398–410. <https://doi.org/10.1016/J.CHERD.2022.05.016>

- Rachiq T, Abrouki Y, Mabrouki J, Samghouli N, Fersi C, Rahal S, El-Hajjaji S (2021) Evaluation of the efficiency of different materials to remove specific pollutants from landfill leachate. *Desalin Water Treat* 238:240–250. <https://doi.org/10.5004/dwt.2021.27779>
- Rizvi OS, Ikhtlaq A, Ashar UU, Qazi UY, Akram A, Kalim I, Alazmi A, Ibn SM, Shamsah KA, Al-Sodani A, Javaid R, Qi F (2022) Application of poly aluminum chloride and alum as catalyst in catalytic ozonation process after coagulation for the treatment of textile wastewater. *J Environ Manage* 323:115977. <https://doi.org/10.1016/J.JENVMAN.2022.115977>
- Shahamat D, Yousef MM, Borghei P, Rahmati SH (2022) Removal of azo red-60 dye by advanced oxidation process O₃/UV from textile wastewaters using box-behnken design. *Inorg Chem Commun* 143:109785. <https://doi.org/10.1016/J.INOCHE.2022.109785>
- Soraya I, Aberkane D, Boukerroui A, Robert D (2022) Removal of methylene blue (basic dye) by coagulation-flocculation with biomaterials (bentonite and opuntia ficus indica). *J Water Process Eng* 49:102952. <https://doi.org/10.1016/J.JWPE.2022.102952>
- Weissman SA, Anderson NG (2015) Design of experiments (DoE) and process optimization. A review of recent publications. *Org Process Res Dev* 19(11):1605–1633. <https://doi.org/10.1021/OP500169M>
- Zhang A, Zhao R, Wang Y, Liu T, Tian H, Yin X, Yang L, Sui X (2022) Natural surfactant used as an additive in the homogenate-ultrasound-synergistic extraction of regaloside A and polysaccharides from liliium lancifolium bulbs using doehlert matrix design. *Ind Crops Prod* 188:115689. doi: 10.1016/J.INDCROP.2022.115689

Chapter 13

An Overview of the Security Challenges in IoT Environment



Souhayla Dargaoui, Mourade Azrou, Ahmed El Allaoui, Fatima Amounas, Azidine Guezzaz, Hanaa Attou, Chaimae Hazman, Said Benkirane, and Sara Haddou Bouazza

Abstract The internet of things (IoT) is a huge network of heterogeneous devices; sensors and actuators, which provide a better world of services such as smart cities, smart grid, health care, smart agriculture and so on. This novel concept represents a rich area of research challenges. Instead, the most important aspects of the IoT networks are security and privacy. Because of the potential augmentation of IoT devices number and their limitations in terms of computational power, energy and memory, those aspects become more and more difficult to be established. This chapter consists of an exhaustive study about IoT applications and security in such environment. Hence, we present IoT deployment issues and the existent attacks on IoT environment considering the IoT layers. Then, we discuss the requirement of IoT security as well as the actual solutions for remediation of the compromised security, such as authentication protocols, intrusion detection systems and machine learning.

Keywords Internet of things · Security · Attacks · IDS · Authentication · Machine learning

S. Dargaoui · M. Azrou (✉) · A. El Allaoui
STI Laboratory, IDMS Team, Faculty of Sciences and Techniques, Moulay Ismail University of Meknès, Meknes, Morocco
e-mail: mo.azrou@umi.ac.ma

F. Amounas
RO.AL&I Group, Computer Sciences Department, Faculty of Sciences and Technics, Moulay Ismail University of Meknes, Errachidia, Morocco

A. Guezzaz · H. Attou · C. Hazman · S. Benkirane
Technology Higher School Essaouira, Cadi Ayyad University, Marrakesh, Morocco

S. H. Bouazza
Physics Department, Faculty of Sciences Semlalia, Cadi Ayyad University, Marrakesh, Morocco

13.1 Introduction

In our days, the Internet of Things (IoT) has been brought to the attention of governments, businesses and universities, thanks to its wide application for commercial and private users. However, because of the continued miniaturization of electronic devices used in IoT networks, these devices become very limited in terms of computing power and storage capabilities and based on wireless communication technologies, the thing which causes poor security configurations (Mabrouki et al. 2021; Guezzaz et al. 2022; Fattah et al. 2022).

Moreover, security is the most important element to adopt IoT solutions on a large scale, and it must be conceived in a global way at different levels: sensors and peripherals, network infrastructures, application platforms, and data. In cases of absence of confidentiality and authenticity guarantees, relevant stakeholders are unlikely to adopt IoT solutions (Azroul et al. 2021a, 2021b, Azroul et al. 2017). Thus, it is necessary to provide very powerful security solutions, to ensure the security of the data streams generated by IoT networks. Subsequently, this paper consists of a detailed study on the security of IoT, since it is a major challenge in the implementation of IoT solutions in the various fields. It presents the results of an exhaustive survey of IoT applications, security issues and solutions.

The remainder of this chapter is organized as follows. The second section introduces some IoT applications. The third section addresses the IoT deployment and security difficulties. The security solutions are detailed in the fourth section. Finally, the paper is concluded in the fifth section.

13.2 Some Application of IoT

The term “Smart cities” is used to describe the emerging cyber physical ecosystem through the deployment of advanced communications infrastructure and new services on citywide scenarios. Thanks to advanced services, it is indeed possible to manage components such as transport, health, energy, homes and buildings and the environment in an intelligent and dynamic way. Traffic data is one of the most important data sources in a smart city. Good analysis of this data can help greatly in traffic management. Another form of IoT exploitation in smart cities is waste management. The waste container is equipped with a level sensor; when a certain threshold is reached, a road driver’s management platform receives a notification on the smartphone. The application domains of the Internet of Things in smart cities are diverse (Kim et al. 2017).

A Smart Grid is a system of infrastructure, hardware and software solutions for autonomous power distribution that allows two-way communication between the utility and its customers (Pandey and Kalra 2022). A smart grid generally offers: generation, distribution, use and control of Energy. The integration of IoT sensors into a smart grid has enabled the monitoring of energy consumption. After processing

the captured data it is possible to visualize the state of energy consumption in the house, calculate costs, remotely manage devices, make load distribution decisions and discover defects. IoT sensors are not only useful for electrical energy, they can also estimate the rate of gas consumption or any other type of energy and cross check all the data collected to provide predictive models to consumers.

In the healthcare sector, IoT has changed the way we collect, process, and store data, setting up networks of objects: embedded sensors and actuators, to improve patient care, learn more about their needs and preferences and optimize treatment processes (Mohanty et al. 2020). Indeed the Internet of Things with its advanced telemetry capabilities and its surveillance solutions, has made a remarkable change in the logistics sector. It allows the monitoring of almost all activities of the supply chain from the purchase of raw materials, production, transport, storage, distribution and sale of products, but also the processing of returns and after-sales service (Datta et al. 2016).

On the other hands, agriculture has undergone a number of technological transformations in recent decades, and through IoT sensors that collect environmental measurements, Farmers are able to make effective decisions and improve all aspects of their work, from livestock to agriculture. IoT has enabled better control of internal processes and improved product quality and quantity (Mabrouki et al. 2022).

13.3 IoT Security Challenges and Issues

13.3.1 IoT Security Challenges

In recent years, attacks on the Internet of Things are increasing and becoming increasingly sophisticated. Furthermore, the finance and transportation sectors have a maximum ranking in attack scenarios. According to recent studies and research, these increases have resulted from poor security configurations placed throughout the IoT ecosystem. Hence, IoT security challenges can be categorized into four types:

- **Device security.** IoT is an emerging and continuously developing market. For this reason, designers and manufacturers of IoT devices are more interested in getting their products on the market quickly than in taking the necessary measures and conducting sufficient tests to integrate safety from the outset. In addition, IoT system suppliers rarely provide the latest firmware upgrades to physical devices, leaving these devices vulnerable to attack.
- **Device heterogeneity.** Device manufacturers have neither a single view of IoT, nor consistent or agreed standards, so the Internet of Things is made up of heterogeneous devices in terms of resources, standards and communication standards. Indeed, this increases the complexity of designing secure unified schemas for the entire IoT ecosystem.
- **Unsecured networks.** Wireless networks such as Wi-Fi are the most common communication technologies used in the development of IoT solutions because

of their high availability, convenience and low cost. Unfortunately, this type of network presents significant vulnerabilities to various intrusions, including unauthorized access, brute force attacks and traffic injections.

- **High mobility and dynamic network topology.** In case IoT devices are very mobile, the sensor connects to different networks that do not have the same security configuration, requiring different threat mitigation approaches. In addition, the ability of IoT devices to exit IoT networks leads to introducing dynamics into the network with multiple real-time connections and disconnections. This increases the attack surface and further complicates the application of universal security solutions for these complex dynamic network topologies.

13.3.2 Main Attacks in the IoT Environment

IoT is vulnerable to a considerable number of attacks, and to build a better security environment, these attacks require special attention. In this section, we will detail the most common attacks on the IoT environment.

- **Sensor tracking.** Most IoT sensors are equipped with GPS functionality, especially in the case of the smart health, to send the patient's location in an emergency. In the case where the sensor is vulnerable, an attacker can exploit location maintenance devices to steal GPS data and locate it (Patel and Doshi 2019).
- **Side channel attack.** A side channel attack is any kind of attack based on information obtained using the hardware characteristics of the encryption circuit, rather than on weaknesses in the algorithm itself. There are several methods to extract the information needed to perform a lateral channel attack such as monitoring the electromagnetic activity around IoT devices, and analyzing energy consumption (Devi and Majumder 2021).
- **Forged node.** Inserting a forged or malicious node between the real nodes of an IoT network can help the attacker to access the IoT network, then modifies the data and transmits the wrong information to the other nodes. By injecting two malicious nodes that work together, the hacker can create a collision at a legitimate node and prevent it from receiving or relaying any packet (Na and Park 2021).
- **Man in the middle.** In this type of attack, the attacker seeks to intercept a communication between two separate IoT devices. This attack can be very dangerous, as the hacker can exploit a possible vulnerability to access confidential data, then secretly modify it while being able to trap the recipient into believing that the message he receives is legitimate (Saritha et al. 2022; Sivasankari and Kamalakkannan 2022).
- **Denial of service.** It is an attack that often targets the availability of IoT services, introducing significant response times, excessive losses and service interruptions. Since, IoT devices have very limited capacities and capabilities. So, if a service receives an enormous number of requests, it may cease to be available to legitimate users.

- **Distributed Denial of Service (DDoS).** It is a more aggressive form of denial of service attack, using more compromised nodes to flood the system. In this type of attack, it is often quite difficult to determinate the original source of the attack (Ali et al. 2022).
- **Impersonation.** The Internet of Things has made our lives much easier, but the more we use connected devices, the more our data becomes valuable to an opportunistic hacker. Therefore, we became our worst enemy in terms of security.
- **Routing attacks.** In this type of attack, the attacker affects how the data are routed. Therefore, it is possible to redirect, deflect, spoof or even drop packets on the network layer (Agiollo et al. 2021). The main forms of this attack are cloned ID attack, selective transmission attack and black hole attack.
- **SQL injection.** In this type of attack, from the insertion of malicious SQL statements, the attacker tries to attack the background database connected to the application. The SQL query is usually injected via the client input data to the application. A successful SQL attack allows the attacker to exploit all the data in the main database, modify it (Insert/Update/Delete), perform administrative operations and even send commands to the operating system.
- **Brute force attack.** The brute force attack is a very old method of attack, but it is still effective and popular. Because of the lower computing capacity of most IoT devices, a simple brute force attack can easily compromise the device's access control. As the name suggests, this type of attack uses excessive force attempts to "force" access to a private account.

13.3.3 Security Services Required for the IoT

In the following paragraphs, we list the most important security requirements that emerge in IoT applications (Azroul et al. 2021b).

- **Identification.** In IoT networks, it is very useful to use radio frequency identification (RFID) as a means to automate the identification and storage of information in RFID tags. These labels can be attached or integrated into an object to be identified and are read by an RFID reader.
- **Authentication.** A process allows verification or authentication of a user's identity. The actions performed by IoT devices are based on the data they receive. Hence, it is crucial to ensure that the data comes from a reliable source. If the authenticity of the data is not guaranteed, attackers could usurp false data in the system.
- **Integrity.** It is one of the most important information security requirements, which ensures protection against any illegitimate modification of the data, whether voluntary or accidental during transmission, processing or storage. Ensuring integrity is essential to ensure that the information provided by the source is the information received by the destination or destinations.
- **Non-repudiation.** This requirement consists in ensuring that an action on the data performed on behalf of a user (after authentication) cannot be repudiated by the

latter in the future. However, in the case of IoT systems, especially in the health and transport sectors, logs are kept for subsequent audits in the event of a fatal accident, so non-repudiation is necessary.

- **Confidentiality.** This security service ensures that only authorized entities can access data resources. In IoT systems and especially in communication, cryptographic mechanisms are used to guarantee the confidentiality of data.
- **Availability.** It is the security service used to ensure that the services and resources offered by the system are available at all times, and can be accessed by authenticated and authorized users, in order to maintain the proper functioning of the IoT system.

13.4 Solutions

13.4.1 Authentication Protocols

The first line of defense against security threats in IoT networks is the establishment of an authentication service (Fig. 13.1). The authentication phase is often a mandatory prerequisite for secure communication between devices (Azrour et al. 2021a,2021c, 2021d, 2017, 2020). As it mentioned previously authentication is a process that allows verification or authentication of a user's identity. It allows the legitimate user to access resources, yet it prevents malicious entities from accessing those resources.

Currently authentication is the most popular method (60%) to grant access to the user at the application layer and give access to the device in the IoT network. However, to fill the gaps in the existing authentication protocols, it's still there a lot of challenges and issues to be addressed like inconsideration of additional requirements of the IoT systems, lack of support for heterogeneous, lack of efficient mobility support, dependence on the IoT network architecture, and high computational requirements.

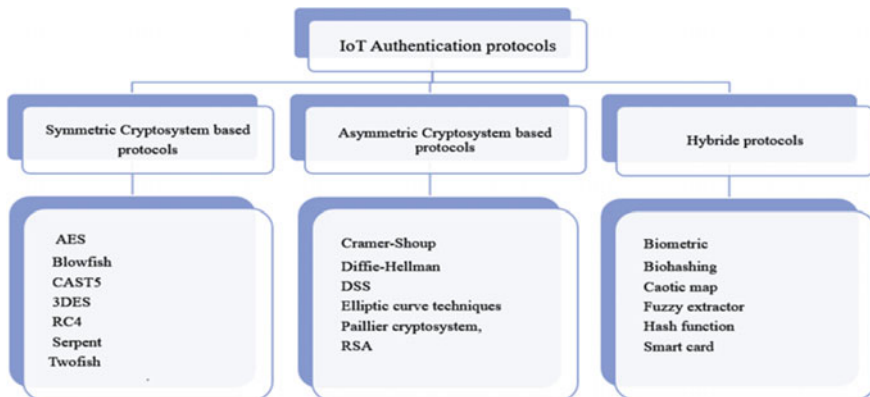


Fig. 13.1 Classification of authentication protocols

13.4.2 *Intrusion Detection Systems*

An intrusion in cybersecurity is typically an attacker gaining unauthorized access to a device, network, or system. Intrusion Detection System (IDS) is a monitoring system that recognize known threats and suspicious or malicious activities and generates alerts when they are detected. A security operations center (SOC) analyst or incident responder can investigate the issue and take the appropriate actions to remediate the threat, based upon these alerts. Most IDS solutions their role stops once when they detect an anomaly. However, some can go a step further by taking action after anomalous activity detection, such as blocking malicious or suspicious traffic. Based on the detection mechanism, we can classify intrusion detection systems in three categories; Anomaly-based systems, signature-based systems and hybrid systems (Guezzaz et al. 2022; Elhoseny et al. 2021, Guezzaz et al. 2021a, 2021b, 2021c, 2022).

- **Signature-based systems.** This terminology comes from antivirus software that monitors all packets on an IoT network and compares them with sequences of known malicious instructions used by malware «signatures». Despite their performance in detecting known attacks, they cannot detect new attacks, for which no model is known.
- **Anomaly-based systems.** In order to recover the uselessness of signature detection for new attacks, anomaly based systems were designed to detect unknown attacks. This method is based on the construction of a precise model of safe activity, using machine learning, which is then used in comparison with new behaviors.
- **Hybrid systems.** A hybrid intrusion detection system is a combination of the two approaches of the intrusion detection system, which enables a detection potential of attacks with a lower error rate than using either system in isolation (Guezzaz et al. 2020).

13.4.3 *Machine Learning*

Machine learning (ML) is a field of artificial intelligence that primarily uses data and algorithms to mimic the way humans learn, gradually improving its accuracy (Boutahir et al. 2022; Azroul et al. 2022, 2019; Ahajjam et al. 2022). Over the last few years, ML-based security solutions for IoT networks field has become one of the most attracting research areas (Fig. 13.2). With the machine learning methods that enable the IoT systems to make informed and intelligent decisions, the data generated by IoT devices becomes better utilized. Indeed, machine learning can be used as solutions for deferent IoT security issues such as authentication and authorization using face recognition and character recognition, anomaly and intrusion detection by identifying malicious code, attack detection and mitigation like DDoS attacks through behavior analysis, and malware analysis (Douiba et al. 2022a, 2022b; Chaganti et al. 2022).

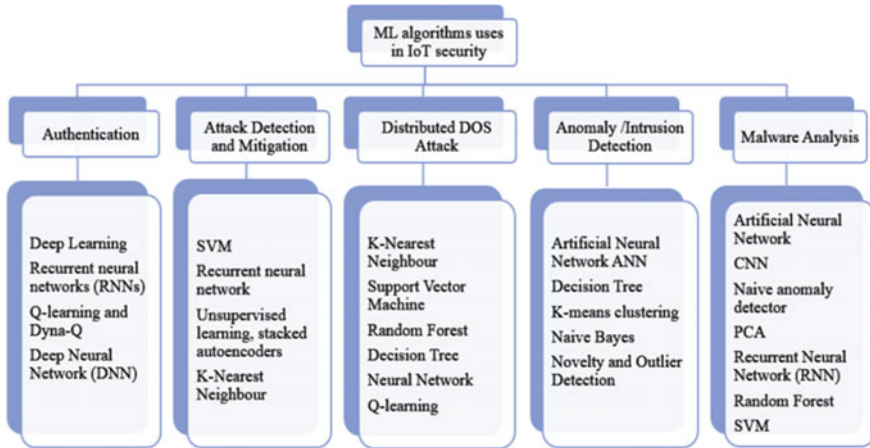


Fig. 13.2 Machine learning uses in IoT security

Even if machine learning provides new applications in IoT, it presents also new limitations and challenges. Because, the traditional machine learning methods need considerable modifications to be inherently efficient and scalable enough to manage IoT data. In the following, we present some challenges of using machine-learning techniques in IoT networks.

- **Processing power and energy.** Machine-learning methods cause some complexity issues such as memory and computational complexity, because of the fact that they cannot handle with high-dimensional problems.
- **Real-time update issue.** From day to day, IoT devices increase more and more rapidly, therefore they need software updating frequently, which is not easy to apply to millions of IoT devices. More than that, the dynamic nature of IoT systems, results in unknown new attacks. Thus, to detect unknown attacks IoT security must adopt more intelligent and real-time updated ML algorithms.
- **Data management and analytics.** IoT networks generate many data that present a syntactic and semantic heterogeneity (different types, formats...). In case of big data and various datasets, this difference causes problems in terms of efficient and unified generalization. Considering machine learning assumes that the statistical properties across the entire dataset remain the same, and not designed to handle semantically and syntactically diverse data.

13.5 Conclusion

IoT technology is the highly popular and most talked about paradigm in today's research community. It's trying to improve the quality of our daily life, on the basis of different technologies and devices, which are different in terms of energy, computational power and storage memory. This heterogeneity in technologies and limitation of devices causes security issues that spread across the three layers of IoT architecture: Perception, Network and Application. For this reason, security on IoT is still looking at how it can enhance network's reliability and protection against threats. Again, authentication protocols, intrusion detection systems and machine learning algorithms are some of the main important parts in security. Because authentication is the gateway of a user or device to introduce in a network, and IDS and ML algorithms can provide networks monitoring and the capability of resistance against the most popular attacks in IoT environment. Therefore, this chapter shows some issues and threats in IoT security and existing solutions to protect them.

References

- Agiollo A, Conti M, Kaliyar P et al (2021) DETONAR: detection of routing attacks in RPL-based IoT. *IEEE Trans Netw Serv Manage* 18:1178–1190
- Ahajjam T et al (2022) Predicting students' final performance using artificial neural networks. *Big Data Min Anal* 5:294–301
- Ali MH et al (2022) Threat analysis and distributed denial of service (DDoS) attack recognition in the internet of things (IoT). *Electronics* 11:494
- Azrou M, Farhaoui Y, Ouanan M et al (2019) SPIT detection in telephony over IP using K-means algorithm. *Procedia Comput Sci* 148:542–551
- Azrou M, Mabrouki J, Chaganti R (2021a) New efficient and secured authentication protocol for remote healthcare systems in cloud-IoT. *Secur Commun Netw* 2021:1–12
- Azrou M, Mabrouki J, Guezzaz A et al (2021b) Internet of things security: challenges and key issues. *Secur Commun Netw* 2021:1–11
- Azrou M, Mabrouki J, Guezzaz A et al (2021d) New enhanced authentication protocol for Internet of Things. *Big Data Min Anal* 4:1–9
- Azrou M et al (2022) Machine-learning algorithms for efficient water quality prediction model. *Model Earth Syst Environ* 8(2):2793–2801. <https://doi.org/10.1007/s40808-021-01266-6>
- Azrou M, Ouanan M, Farhaoui Y et al (2017) Security analysis of Ye et al. authentication protocol for internet of things. In: Farhaoui Y, Moussaid L (eds) *Big data and smart digital environment*, vol 53. Springer International Publishing, pp 67–74
- Azrou M, Farhaoui Y, Guezzaz A (2020) Experimental validation of new SIP authentication protocol. In: Farhaoui Y (ed) *Big data and networks technologies*, vol 81. Springer International Publishing, pp 1–11
- Azrou M, Mabrouki J, Farhaoui Y et al (2021c) Security analysis of Nikooghadam et al.'s authentication protocol for cloud-IoT. In: Gherabi N, Kacprzyk J (eds) *Intelligent systems in big data, semantic web and machine learning*, vol 1344. Springer International Publishing, pp 261–269
- Boutahir MK, Farhaoui Y, Azrou M (2022) Machine learning and deep learning applications for solar radiation predictions review: morocco as a case of study. In: Yaseen SG (ed) *Digital economy, business analytics, and big data analytics applications*, vol 1010. Springer International Publishing, pp 55–67

- Chaganti R et al (2022) A Particle swarm optimization and deep learning approach for intrusion detection system in internet of medical things. *Sustainability* 14(19):12828
- Datta SK, Da Costa RPF, Harri J et al (2016) Integrating connected vehicles in Internet of Things ecosystems: challenges and solutions. In: 2016 IEEE 17th international symposium on a world of wireless, mobile and multimedia networks (WoWMoM). IEEE, pp 1–6. <https://doi.org/10.1109/WoWMoM.2016.7523574>
- Devi M, Majumder A (2021) Side-channel attack in Internet of Things: a survey. In: *Applications of Internet of Things*. Springer, pp 213–222
- Douiba M, Benkirane S, Guezzaz A et al (2022a) Anomaly detection model based on gradient boosting and decision tree for IoT environments security. *J Reliab Intell Environ* 1–12
- Douiba M, Benkirane S, Guezzaz A et al (2022b) An improved anomaly detection model for IoT security using decision tree and gradient boosting. *J Supercomput* 1–20
- Elhoseny M et al (2021) Security and privacy issues in medical internet of things: overview, countermeasures, challenges and future directions. *Sustainability* 13:11645
- Fattah G, Mabrouki J, Ghriissi F et al (2022) Multi-sensor system and internet of things (IoT) technologies for air pollution monitoring. In: *Futuristic research trends and applications of internet of things*. CRC Press, pp 101–116
- Guezzaz A, Benkirane S, Azrou M et al (2021a) A reliable network intrusion detection approach using decision tree with enhanced data quality. *Secur Commun Netw* 2021:1–8
- Guezzaz A et al (2021b) A Mathematical validation of proposed machine learning classifier for heterogeneous traffic and anomaly detection. *Big Data Min Anal* 4:18–24
- Guezzaz A, Asimi A, Asimi et al (2021c) A distributed intrusion detection approach based on machine leaning techniques for a cloud security. In: *Intelligent systems in big data, semantic web and machine learning*. Springer, pp 85–94
- Guezzaz A, Asimi A, Mourade et al (2020) A multilayer perceptron classifier for monitoring network traffic. In: Farhaoui Y (ed) *Big data and networks technologies*. Springer International Publishing, pp 262–270. https://doi.org/10.1007/978-3-030-23672-4_19
- Guezzaz A, Benkirane S, Azrou M (2022) A novel anomaly network intrusion detection system for internet of things security. In: *IoT and smart devices for sustainable environment*. Springer, pp 129–138
- Guezzaz A et al (2022) A lightweight hybrid intrusion detection framework using machine learning for edge-based iiot security. *Int Arab J Inf Technol* 19
- Kim T, Ramos C, Mohammed S (2017) Smart city and IoT. *Futur Gener Comput Syst* 76:159–162
- Mabrouki J, Azrou M, El Hajjaji S (2021) Use of internet of things for monitoring and evaluation water's quality: comparative study. *Int J Cloud Comput* 10(5–6):633–644
- Mabrouki J et al (2022) Smart system for monitoring and controlling of agricultural production by the IoT. In: *IoT and smart devices for sustainable environment*. Springer, pp 103–115
- Mohanty S, Mohanty S, Pattnaik PK (2020) Smart healthcare analytics: an overview. In: Pattnaik PK, Mohanty S, Mohanty S (eds) *Smart healthcare analytics in IoT enabled environment*. Springer International Publishing, pp 1–8. https://doi.org/10.1007/978-3-030-37551-5_1
- Na D, Park S (2021) Lightweight blockchain to solve forgery and privacy issues of vehicle image data. In: 2021 22nd Asia-Pacific network operations and management symposium (APNOMS). IEEE, pp 37–40
- Pandey JC, Kalra M (2022) A review of security concerns in smart grid. In: Raj JS, Kamel K, Lafata P (eds) *Innovative data communication technologies and application*. Springer Nature, pp 125–140. https://doi.org/10.1007/978-981-16-7167-8_10
- Patel C, Doshi N (2019) Security challenges in IoT cyber world. In: *Security in smart cities: models, applications, and challenges*. Springer, pp 171–191
- Saritha K, Sarasvathi V, Singh A et al (2022) Detection and mitigation of man-in-the-middle attack in IoT through alternate routing. In: 2022 6th international conference on computing methodologies and communication (ICCMC). IEEE, pp 341–345
- Sivasankari N, Kamalakkannan S (2022) Detection and prevention of man-in-the-middle attack in iot network using regression modeling. *Adv Eng Softw* 169:103126

Chapter 14

Modeling of the Coagulation System for Treatment of Real Water Rejects



Ghizlane Fattah, Mohamed Elouardi, Mohammed Benchrif, Fouzia Ghrissi, and Jamal Mabrouki

Abstract The process of coagulation is a critical phase in the production of drinking water from raw water. From raw water, it allows to remove colloidal particles, source of contamination, later on of contamination. The consumption of coagulant agent makes this step the most expensive step in the costly operation in the treatment chain. Usually the dose of coagulant is determined by trials. This type of process also has the disadvantage of having a relatively long delay time delay. Indeed, the coagulant is only modified once the event has occurred. event has occurred. Furthermore, it does not allow for a fine control of the quality of the raw water. This study is to prove that the coagulant dose is a factor explained by various variables. The model of method by the identification of the dose of clotting agent by adopting the coagulant dose by adopting the neuronal approach, which is based on the modeling of the data through a network of through a neuronal network.

Keywords Modeling · Coagulation-flocculation · Réseau de neurones · Water treatment

14.1 Introduction

Water use is increasing substantially and shortages are being felt in many regions of the country (Mabrouki et al. 2022a; Benchrif et al. 2022). This is going to have an impact on the socio-economic development as well as the environment (Benchrif and Mabrouki 2022). Economic development as well as the conservation of the natural

G. Fattah (✉) · F. Ghrissi

Water Treatment and Reuse Structure, Civil Hydraulic and Environmental Engineering Laboratory, Mohammadia School of Engineers, Mohammed V University in Rabat, Avenue Ibn Sina B.P 765 Agdal Rabat, 10090 Rabat, Morocco
e-mail: ghizlane_fattah@um5.ac.ma

M. Elouardi · M. Benchrif · J. Mabrouki

Laboratory of Spectroscopy, Molecular Modelling, Materials, Nanomaterial, Water and Environment, Faculty of Science, CERNE2D, Mohammed V, University in Rabat, Avenue Ibn Battouta, Agdal, BP1014 Rabat, Morocco

environment. This strong Demand for water is rising because of the population growth and the increase in living standard. In the face of these challenges. The large effort of harnessing its potential water in facing these problems. Water purification plants are one of the facilities to which great significance has been given (Mabrouki et al. 2021a; Hassan El Ouazzani 2020; Loukilia et al. 2021).

The administration and functioning of a water treatment plant focused on improving quality and cutting costs. The major progress made in the last few years in the field of intellectual property has made it possible to reduce the problems and limitations of linear networks. Models based on the technology of artificial neurons networks have been perfected (Mousli et al. 2022). This type of modeling has been included in order to establish the optimal coagulant dose depending on different aspects of the raw water quality such as cloudiness, pH, conductivity... etc.

Not almost all water in the natural world is good to drink. Even apparently, crystal-clear water carries with it all sorts of inert and living substances, some of which may be detrimental to the human body. These materials come from either from the physical milieu in which the water has grown, or from the discharges of certain human activities for which the water has become the container. Of which the water has been made the receptacle (Samghouli et al. 2022; Lkima et al. 2022). The water is thus the preferred vector of the transmission of diseases (cholera, typhoid, lead pollution, mosquito's transmitting different diseases, diabetes, etc.). In conclusion, in order to be safe for consumption, water must be treated, be processed to be safe for consummation (Samghouli et al. 2022).

The treatment system of a water plant will depend on the one side on the raw water supply itself and on the other hand on the legislation and regulations regulating drinking water. On the other hand, the regulatory framework of drinking water. On their side, the treatment processes must meet special conditions that will assure their proper performance (Lkima et al. 2022). All these issues must be taken into accounts in the decision to choose the right processes for a water treatment plant. This holistic approach applies to the planning of new plants as well as for the expansion or upgrade of existing ones. Coagulation is a dynamic process that consists, firstly, in the destabilization of a collisional suspension and, in the second place, in the assembly of the particles in small clusters or flakes, with agitation and movement under the impact of a moderate stirring, by addition of a chemical product called "coagulant", most often metal salts, based on Aluminum or iron (Loukili et al. 2022; Fattah et al. 2022; Ghizlane et al. 2022).

The purpose of this method is to destabilize the organic particles and colloids in order to promote their agglomeration and removal by a solid-liquid separating process and, on the other side, to minimizing the concentration of the remaining coagulant. A process of coagulation that is considered optimum does the cost minimization of the treatment. It corresponds to the proportion of coagulant that to ensure that all required quality objectives are met (Mgalaa et al. 2022). In assessing the optimal conditions for clotting and flocculation, the coagulation and flocculation. Those, carried out in a range of operating conditions, allow identifying the type of coagulant, its dosage, the pH and the agitating conditions that maximize the reduced turbidity. In this study, we will try to create a neural model that integrates the different

physic-chemical properties of the raw water using a neuronal network to determine the optimal dose of coagulant for a good quality and service at the treatment plant, while keeping in mind the case of low turbidization of the raw water.

14.2 Materials and Methods

14.2.1 Coagulation Process

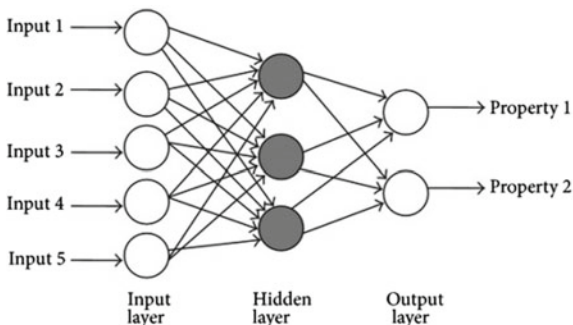
In a classical water treatment system, a coagulation-flocculation-settling procedure is used to remove very small colloidal particles. These particles can stay in suspension in the water for very long times, can even pass through a very fine filter. Moreover, because of their high stability they do not tend to cling to each other (Azroul et al. 2021a; Rahmani et al. 2021; Regraguy et al. 2022). They are also responsible for the turbidity and color of the water. To eliminate these particles, coagulation and flocculation procedures are used. The word coagulation comes from the Latin “coagulare” which means “to clump”. The coagulation consists in destabilizing them. It is a matter of neutralizing their charges of repulsion to allow them to meet. The flocculation gives an idea of their agglomerate into aggregates eliminated by settling and/or filtration.

14.2.2 Artificial Neural Networks (ANNs)

The artificial neural network models are functions of universal approximations between expected and observed values used to map a non-linear function between input and output vectors that have an unknown relationship and are therefore hard to fit during the learning phase without the overriding hypotheses about the original data. Multilayer networks are made of several layers arranged one after the other. There is no interconnection between neurons of the same layer, the connection is only made with neurons of the layers below, each input unit is followed by a succession of hidden layers, and each unit of a given layer receives its input from the previous layer only. The activation function used in such a network is usually of the sigmoid type generally of the Sigmoid type, which gives them a non-linear characteristic. We distinguish two types: the multilayer perceptron (MPL) and the radial basis function (RBF) networks (Bencheikh et al. 2019; Fattah et al. 2021; Abrouki et al. 2021; Mabrouki et al. 2019a).

The network family mostly used, this type covers more than 95% of the applications in science and industry. Scientific and industrial applications. MLPs were first used to solve complex classification problems. Complex clustering problems. However, because of their property of universal approximation, they were quickly universal property, they were quickly used as models for nonlinear regression, and

Fig. 14.1 Diagram of a multilayer network



then for linear models, and then for time series and forecasting modeling. When developing PMCs, it is very important to specify the number of layers hidden in the model and the number of cells in these layers but it is also important to choose the activating the activation feature and the learning methods (Mabrouki et al. 2022b).

The type of network most used after the PMC, the structure is the same as for the PMC however, the basic function used here are Gaussian functions (Fig. 14.1).

La loi de Widrow-Hoff:

It is a learning function that allows to adjust the weights of a neural network to reduce at each step the error made by the neural network (provided that the learning factor is well chosen) (Mabrouki et al. 2018). A given weight is modified using the following equation:

$$W_{ij}(t + 1) = W_{ij}(t) + \alpha \delta_k x_k \tag{14.1}$$

where: $W_{ij}(t)$ is the weight at time t

$W_{ij}(t+1)$ the weight at time $t+1$

α is the learning factor

δ_k characterizes the difference between the expected output and the actual output of the neuron at time t .

x_k the value of the input with which the weight w is associated at time t .

Neural networks offer a promising approach for different scientific problems like the identification of nonlinear systems.

Model validation:

Validation is used to judge the model’s ability to reproduce the modeled variables (Mabrouki et al. 2021b). Several criteria have been selected. In our case, we based ourselves on the coefficient of determination (R^2), the root of the mean square error (RMSE).

Correlation coefficient (R^2):

$$R^2 = \left[\frac{\frac{1}{N_i} \sum_{i=1}^N (Y_{iobs} - \bar{Y}_{obs})(Y_{ical} - \bar{Y}_{cal})}{\sigma_{obs}\sigma_{cal}} \right]^2 \quad (14.2)$$

with:

Y_{iobs} and Y_{ical} : correspond respectively to the values observed and calculated by the model of the dose of the coagulant for the day (i).

\bar{Y}_{obs} and \bar{Y}_{cal} : are the means of the observed values calculated by the model.

σ_{obs} and σ_{cal} : standard deviations of observed and calculated values.

Root of the mean square error (RMSE):

The error function is used to assess the performance of a neural network during process.

$$RMSE = \sqrt{\frac{\sum (Y_{obs} - Y_{cal})^2}{N}} \quad (14.3)$$

N: represents the number of values used. The model is well optimised if the RMSE value is close to zero.

14.3 Results and Discussions

14.3.1 Analysis of the Results

The objective of our research is to evaluate the coagulant dose to be injected into the water as a function of the raw water quality descriptors. Our understanding of the process is limited to logged data (Mabrouki et al. 2020; Azoulay et al. 2021; Bencheikh et al. 2021). The mean values of the coagulant dose are usually between 10 and 20 mg/l. The information available comes from the results of tests carried out on a daily basis. Several parameters that describe the quality of the raw water are monitored. The following descriptive parameters are continuously available: temperature, PH, organic matter, conductivity, turbidity, hardness, TAC, ammonium and bicarbonate. The statistics of the selected variables are shown in Table 14.1.

From the analyses carried out, we note that the water treatment quality is quite good, but it does not meet the norms in terms of cloudiness, organic matter and the concentration of ammonium, which requires a light treatment (Azroul et al. 2021b).

Table 14.1 Statistics of descriptive variables of water

	Min	Max	Medium	Type deviation
T (°C)	8	12	10,00	2,5350
pH	6.83	7,83	7,60	0,4659
Turbidity (NTU)	6.5	22.55	15,10	5,3151
SS (mg/l)	2	6,65	4,30	1,2224
Conductivity ($\mu\text{S}/\text{cm}$)	433	563	491,30	27,7310
HCO_3^- (mg/l)	134	170	154,2 0	12,3260
OM (mg/l)	2	6,65	4,30	1,2224
Ammonium (mg/l)	0,01	0.095	0,06	0,0451

Table 14.2 Prediction of descriptive statistical analyses

	RBF	MLP
Min prediction	14,58	14,13
Max prediction	22,10	22,60
Min test prediction	15,83	14,05
Max test prediction	16,51	18,91
Min validation prediction	15,85	17,79
Max prediction validation	15,85	17,79

14.3.2 RNA Models

The construction of the ANN templates is based on a composite of input parameters. Each of the quality parameters studied is modeled by the concentration at the outlet of the station, which will be used as a target data during the learning and validation phase of the ANR model (Bencheikh et al. 2020) (Table 14.2).

14.3.3 Model Validation

The coagulant dose prediction performances are given in the figures. For the comparison of the capacities of the different variants tested, we have used two digital criteria mentioned earlier: the correlation index (R^2) and the Mean Square Root Error (RMSE). The variables are introduced gradually and the qualitative criteria are computed at each step. Let us recall, among other things, that the root mean square error (RMSE) represents the average gap between the predicted (simulated) results and the observed results, while the determination coefficient R^2 is a simple measure of the rate of explanation of the phenomena by the adopted model. About 100 networks were constructed and we kept the best one: the one showing a good compromise between the learning and testing capacities. The error minimize procedure is used to

obtain an optimal network architecture. The selection of the error distribution used for the training of the neural networks (Bencheikh et al. 2020; Mabrouki et al. 2019b; Azroul et al. 2022).

The decision of the error function used for the learning of multi-layer neural networks has some bearing on the speed of learning and the generalization quality of the network. The best candidate in terms of performance indices was visualized at the machine learning level is the (MLP). The testing and calibration data alone may not be enough evidence of a good generalization power of a trained neural model. In the calibration step, the RMSE is equal to 0.4 mg/l and the R^2 is equal to 0.98 (Figs. 14.2, 14.3).

The failure function shows how close the network’s prediction is to the target values and therefore, what the learning algorithm needs to do to adjust the weights at each repetition. The mistake function thus acts as the eyes and ears of the learning algorithm to determine if the network is efficient or not given the actual state of learning (and thus, what correction should be made to the value of its individual

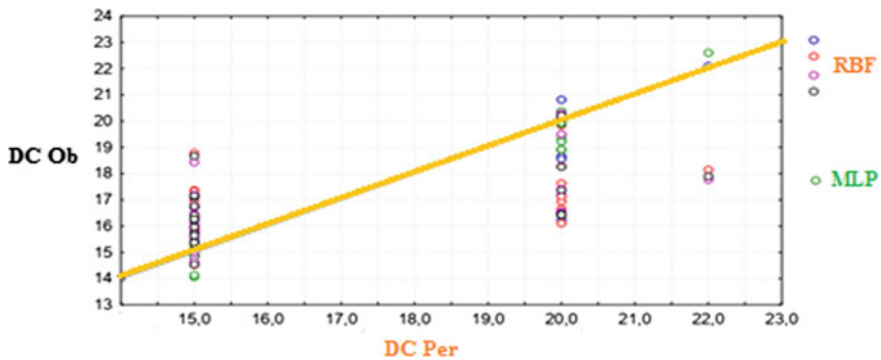


Fig. 14.2 Learning results, model testing

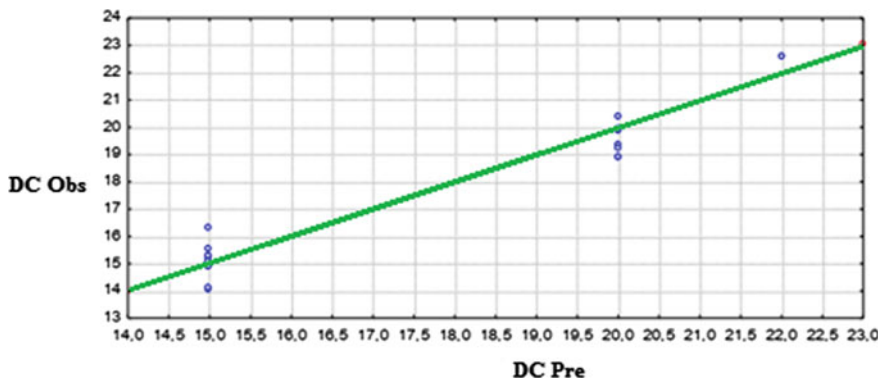
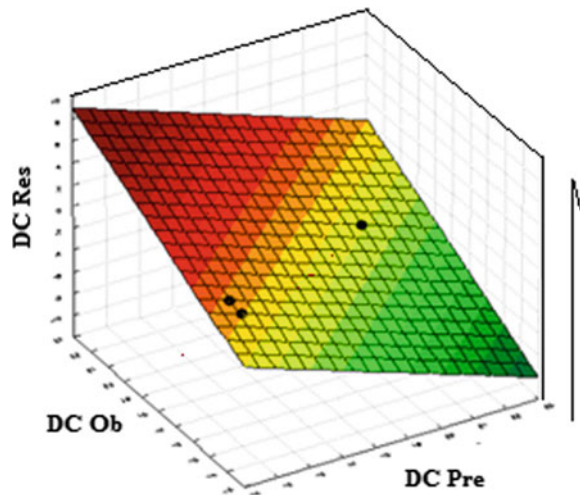


Fig. 14.3 Learning results of the MLP model

Fig. 14.4 MLP model error results



weights) (Mabrouki et al. 2019c; Rahmania et al. 2021; Bencheikh et al. 2022; Azoulay et al. 2022).

In view of validating this design, the error was approximated on a 5% validation dataset. The validation sample is never used for the training of the neural network. However, we use it after training as an extra check on the performance of the model. If the network's performance is completely correct on the test sample and on the validation sample, we can consider that the network has a good capacity to generalize on unknown data. The learning error is a measure of the quality of a model, and we can see that our neural network shows interesting performance (error rate below 7.9%) (Fig. 14.4).

Neural network are often compared to a kind of black box because, in fact, it is very difficult to comprehend the computing done during the teaching process. Nevertheless, because of these operations, it is important to estimate the sensitivity of the input variables the sensitivity of the input parameters and thus to find out which are the most explanatory variables of the concept to be modeled.

14.4 Conclusion

The main problem in the coagulation process is to determine the right amount of coagulate to be added according to the raw material's properties. Poor process control can lead to a large increase in running costs and failure to meet the plant's outlet standards. This chapter shows the results of the use of artificial neural networks with a multilayer perceptron (MLP). The attempts to model were able to link the optimum dose of coagulant (aluminum sulfate) to the values of the characteristic parameters of the raw water quality at the inlet of the water treatment plant. By making this, we

could also furnish a preparatory tool for the automated control of the said station, therefore improving its quality of life.

References

- Abrouki Y, Mabrouki J, Anouzla A, Rifi SK, Zahiri Y, Nehhal S, ... Souabi S (2021) Optimization and modeling of a fixed-bed biosorption of textile dye using agricultural biomass from the Moroccan Sahara. *Desalin Water Treat* 240:144–151
- Azoulay K, Bencheikh I, Mabrouki J, Samghouli N, Moufti A, Dahchour A, El Hajjaji S (2021) Adsorption mechanisms of azo dyes binary mixture onto different raw palm wastes. *Int J Environ Anal Chem* 1–20
- Azoulay K, Bencheikh I, Samghouli N, Mabrouki J, Moufti A, Hajjaji SE (2022) Modeling and design of water treatment processes by biosorption method using JMP® 11 software. In: *IoT and smart devices for sustainable environment*. Springer, Cham, pp 53–69
- Azrou M, Mabrouki J, Guezzaz A, Kanwal A (2021b) Internet of things security: challenges and key issues. *Secur Commun Netw* 2021:1–11
- Azrou M, Mabrouki J, Fattah G, Guezzaz A, Aziz F (2022) Machine learning algorithms for efficient water quality prediction. *Model Earth Syst Environ* 8(2):2793–2801
- Azrou M, Mabrouki J, Farhaoui Y, Guezzaz A (2021a) Experimental evaluation of proposed algorithm for identifying abnormal messages in SIP network. In: *Intelligent systems in big data, semantic web and machine learning*. Springer, Cham, pp 1–10
- Bencheikh I, Azoulay K, Mabrouki J, El Hajjaji S, Dahchour A, Moufti A, Dhiba D (2020) The adsorptive removal of MB using chemically treated artichoke leaves: parametric, kinetic, isotherm and thermodynamic study. *Sci Afr* 9:e00509
- Bencheikh I, Azoulay K, Mabrouki J, El Hajjaji S, Moufti A, Labjar N (2021) The use and the performance of chemically treated artichoke leaves for textile industrial effluents treatment. *Chem Data Collect* 31:100597
- Bencheikh I, Mabrouki J, Azoulay K, Moufti A, El Hajjaji S (2019) Predictive analytics and optimization of wastewater treatment efficiency using statistic approach. In: *International conference on big data and networks technologies*. Springer, Cham, pp 310–319
- Bencheikh I, Azoulay K, Samghouli N, Mabrouki J, Bouhachlaf L, Moufti A, Hajjaji SE (2022) Mathematical and statistical study for the wastewater adsorbent regeneration using the central composite design. In: *IoT and smart devices for sustainable environment*. Springer, Cham, pp 71–83
- Benchrifa M, Mabrouki J (2022) Simulation, sizing, economic evaluation and environmental impact assessment of a photovoltaic power plant for the electrification of an establishment. *Adv Build Energy Res* 1–18
- Benchrifa M, Mabrouki J, Elouardi M, Azrou M, Tadili R (2022) Detailed study of dimensioning and simulating a grid-connected PV power station and analysis of its environmental and economic effect, case study. *Model Earth Syst Environ* 1–9
- Fattah G, Ghrissi F, Mabrouki J, ... Kabriti M (2021) Control of physicochemical parameters of spring waters near quarries exploiting limestone rock. In: *E3S web of conferences*, vol 234, p 00018. EDP Sciences
- Fattah G, Ghrissi F, Mabrouki J, Cherifi H (2022) Impact of limestone deposit operation on the yield of surrounding agricultural land: case of the western Rif, Morocco. In: *E3S web of conferences*, vol 337, p 02005. EDP Sciences
- Ghizlane F, Mabrouki J, Ghrissi F, Azrou M (2022) Proposal for a high-resolution particulate matter (PM10 and PM2.5) capture system, comparable with hybrid system-based internet of things: case of quarries in the western Rif, Morocco. *Pollution* 8(1):169–180

- Hassan El Ouazzani BP (2020) Study of the efficacy of coagulation-flocculation process in domestic wastewater treatment plant (WWTP) from the city of hattane (MOROCCO). *J Adv Res Dyn Control Syst* 12(7)
- Lkima K, Salcedo FP, Mabrouki J, Aziz F (2022) Precision agriculture: assessing water status in plants using unmanned aerial vehicle. In: *IoT and Smart Devices for Sustainable Environment*. Springer, Cham, pp 139–153
- Loukili H, Anouzla A, Jioui I, Achiou B, Alami Younssi S, Azoulay K, ... Riadi Y (2022) Combining multiple regression and principal component analysis to evaluate the effects of ambient air pollution on children's respiratory diseases. *Int J Inf Technol* 14(3):1305–1310
- Loukilia H, Mabroukic J, Anouzlab A, Kouzia Y, Younssia SA, Diguab K, Abroukic Y (2021) Pre-treated Moroccan natural clays: application to the wastewater treatment of textile industry. *Desalination Water Treat* 240:124–136
- Mabrouki J, Azrou M, Hajjaji SE (2021b) Use of internet of things for monitoring and evaluating water's quality: a comparative study. *Int J Cloud Comput* 10(5–6):633–644
- Mabrouki J, Fattah G, Al-Jadabi N, Abrouki Y, Dhiba D, Azrou M, Hajjaji SE (2022b) Study, simulation and modulation of solar thermal domestic hot water production systems. *Model Earth Syst Environ* 8(2):2853–2862
- Mabrouki J, El Yadini A, Bencheikh I, Azoulay K, Moufti A, El Hajjaji S (2018) Hydrogeological and hydrochemical study of underground waters of the tablecloth in the vicinity of the controlled city dump mohammedia (Morocco). In: *International conference on advanced intelligent systems for sustainable development*. Springer, Cham, pp 22–33
- Mabrouki J, Bencheikh I, Azoulay K, Es-Soufy M, El Hajjaji S (2019a) Smart monitoring system for the long-term control of aerobic leachate treatment: dumping case Mohammedia (Morocco). In: *International conference on big data and networks technologies*. Springer, Cham, pp 220–230
- Mabrouki J, Moufti A, Bencheikh I, Azoulay K, El Hamdouni Y, El Hajjaji S (2019b) Optimization of the coagulant flocculation process for treatment of leachate of the controlled discharge of the city Mohammedia (Morocco). In: *International conference on advanced intelligent systems for sustainable development*. Springer, Cham, pp 200–212
- Mabrouki J, Azrou M, Farhaoui Y, El Hajjaji S (2019c) Intelligent system for monitoring and detecting water quality. In: *International conference on big data and networks technologies*. Springer, Cham, pp 172–182
- Mabrouki J, Benbouzid M, Dhiba D, El Hajjaji S (2020) Simulation of wastewater treatment processes with bioreactor membrane reactor (MBR) treatment versus conventional the adsorbent layer-based filtration system (LAFS). *Int J Environ Anal Chem* 1–11
- Mabrouki J, Benbouzid M, Dhiba D, Hajjaji SE (2021a) Internet of things for monitoring and detection of agricultural production. In: *Intelligent systems in big data, semantic web and machine learning*. Springer, Cham, pp 271–282
- Mabrouki J, Azoulay K, Elfanssi S, Bouhachlaf L, Mousli F, Azrou M, Hajjaji SE (2022a) Smart system for monitoring and controlling of agricultural production by the IoT. In: *IoT and smart devices for sustainable environment*. Springer, Cham, pp 103–115
- Mgalaa S, Mabrouki J, Elouardi M, El Azzouzi L, Moufti A, El Hajjaji S, ... El Belghiti MA (2022) Study and evaluation of the degradation of procion blue dye by the ozonation method: parametric and isothermal study. *Nanotechnol Environ Eng* 1–7
- Mousli F, Mabrouki J, Bouhachlaf L, Azrou M, Hajjaji SE (2022) Detection of some water elements based on IoT: review study. In: *IoT and Smart Devices for Sustainable Environment*, pp 1–17
- Rahmani M, Mabrouki J, Regraguy B, Moufti A, El'Mrabet M, Dahchour A, El Hajjaji S (2021) Adsorption of (methylene blue) onto natural oil shale: kinetics of adsorption, isotherm and thermodynamic studies. *Int J Environ Anal Chem* 1–15
- Rahmania M, Regraguya B, Mabroukia J, Mouftib A, El'Mrabet M, Dahchourd A, El Hajjajia S (2021) Response surface modeling of methylene blue dye removal from wastewater on natural oil shale. *Desalination Water Treat* 244:253–262

- Regraguy B, Rahmani M, Mabrouki J, Drhimer F, Ellouzi I, Mahmou C, ... Hajjaji SE (2022) Photocatalytic degradation of methyl orange in the presence of nanoparticles $\text{NiSO}_4/\text{TiO}_2$. *Nanotechnol Environ Eng* 7(1):157–171
- Samghouli N, Bencheikh I, Azoulay K, Abahdou FZ, Mabrouki J, Hajjaji SE (2022) Study of piroxicam removal from wastewater by artichoke waste using NemrodW® software: statistical analysis. In: *IoT and smart devices for sustainable environment*. Springer, Cham, pp 29–42

Chapter 15

Effects of Heat Stress and Chemical Pollutants on Sheep Reproduction and Strategies to Mitigate Them



Abdellatif Rahim and Bouchra El Amiri

Abstract Nowadays, climate change and the accumulation of chemical pollutants have become major environmental challenges. Natural and anthropogenic activities have certainly caused environmental pollution and a dramatic increase in ambient temperature. Sheep, are considered among the species susceptible to these environmental challenges. Previous findings indicate that sheep exposure to heat stress and chemical pollutants lead to several toxic effects. Therefore, these specific environmental problems have a direct impact on the reproductive performances. More precisely, heat stress and acute or chronic exposure to chemical pollutants, such as endocrine disruptors and heavy metals, significantly impair sheep's reproduction and influence milk and meat production. In this chapter, we discuss in detail the impact of heat stress and chemical pollutants on sheep sexual behavior, ram sperm quality, cycling ewes, and pregnancy. Also, mitigation strategies available to improve sheep reproduction parameters under the scenario of climate change and increasing chemical pollutants were elaborated.

Keywords Heat stress · Chemical pollutants · Sheep reproduction

15.1 Introduction

Sheep farming is a significant activity in many countries around the world. It is one of the first animals that have been domesticated by humans. The primary characteristics that rendered this species favorable to domestication were their body size, which made them easier to control, early puberty and maturity, higher rate of reproduction, sociable nature, and obedient nature (Mazinani and Rude 2020). Sheep are considered a major source of meat and milk (Swanepoel et al. 2010). Because of the increase in population in recent years, the growing global demand

A. Rahim · B. El Amiri (✉)

Animal Production Unit, Regional Center Agricultural Research of Settat, National Institute for Agricultural Research (INRA), Avenue Ennasr, Rabat Principal, P.O. Box 415, 10090 Rabat, Morocco

e-mail: bouchraelamiri@hotmail.com; bouchra.elamiri@inra.ma

for meat and milk has also increased. However, given the natural geological mechanisms and anthropogenic inputs, several environmental challenges mainly climate change and chemical pollutants had direct and indirect effects on sheep production (Wettere et al. 2021; Castillo et al. 2021). Therefore, these specific environmental problems have a direct impact on the reproductive performances (Castillo et al. 2021; Rhind et al. 2010; George et al. 2020). Assuredly, it was reported that these environmental challenges have a negative impact on ewe and ram fertility, pregnancy, fetal growth, and lactation (Wettere et al. 2021; Dado-Senn et al. 2019). This paper covers in detail the impact of heat stress and chemical pollutants on male and female reproductive systems in sheep. Moreover, mitigation strategies available to improve sheep reproduction parameters under the scenario of climate change and increasing chemical pollutants were elaborated.

15.2 Climate Change and Chemical Pollutants as Major Environmental Challenges

Climate change and chemical pollutants are one of the most significant aspects, which cause a threat to all species living on the planet earth (Akhtar et al. 2021; Abbas 2022). Natural geological processes and anthropogenic inputs are the two variables resulting in these concerns (Karimi et al. 2018).

In recent years, several scientific evidence documented a reciprocal interaction between climate change and pollution originated from chemical pollutants (Akhtar et al. 2021; Schiedek et al. 2007). Precisely, persistent and emerging chemical pollutants to a certain extent cause climate change, and the environmental changes associated with global warming have the potential to increase species' susceptibility to chemical pollutants' toxicities (Noyes and Lema 2015). Hence, climate changes and air pollution caused by chemical pollutants can interact to amplify risks to human and animal health via several intoxications (Sillmann et al. 2021). In several arid and semi-arid areas in the world, sheep farming is crucially important to the economy. However, several toxic effects caused by chemical pollutants mainly endocrine disruptor chemicals (EDC) and heavy metals (HM) such as fluoride, lead, arsenic, and cadmium were observed in sheep (Rahim et al. 2022a). In addition, climate change particularly heat stress had negative health impacts on this species (Lacetera 2019). More precisely, both climate change and chemical pollutants severely impact reproductive processes (Fig. 15.1).

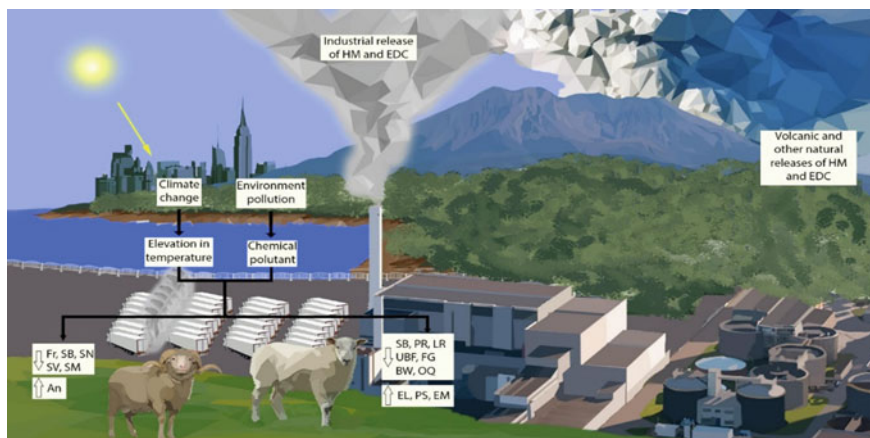


Fig. 15.1 Schematic diagram displaying the impact of heat stress and chemical pollutants on sheep reproduction. HM: heavy metals; EDC: endocrine disruptor chemicals; Fr: fertility; SB: sexual behavior; SN: sperm number; SV: sperm volume; SM: sperm motility; An: anomalies; PR: pregnancy rate; LR: lambing rate; UBF: uterine blood flow; FG: fetal growth; BW: birth weight; OQ: oocyte quality; EL: embryo loss; PS: placental stunting; EM: embryo mortality

15.3 Impact of Heat Stress on Sheep Reproductive Performances

15.3.1 Thermoregulation

In sheep, as a result of heat stress, the hypothalamic–pituitary–adrenal axis (HPA) and sympathoadrenal system are known to be activated. This causes the release of glucocorticoids and catecholamines (Bouroutzika et al. 2022). Adrenocorticotrophic hormone, on the other hand, promotes the release of glucocorticoids and has an inhibitory effect on the reproductive axis. In addition, a variety of hematological factors as well as physiological and behavioral characteristics, such as variations in respiration, heart rate, ruminal motility, body temperature, and perspiration, are expressed differently under stress (Terrien et al. 2011; Mota-Rojas et al. 2021). Unlike the ewes, the physiological process of thermoregulation of the ram reproductive system is well documented. Under normothermic conditions, the pampini-form plexus provides crosscurrent heat exchange between arterial blood entering the scrotum and cooler venous blood exiting (Wettere et al. 2021). Through fluctuations in scrotal surface area and degree of contraction toward the body as well as the release of scrotal sweat glands, the tunica dartos and cremaster muscles play a critical role in the scrotal reactions to temperature change. The woolled ram's respiration rate increases when the scrotum is heated over 36 °C (Maloney et al. 2003), and cutaneous scrotal thermoreceptors regulate the tunica dartos, sweat gland, and respiratory responses to heat (Wettere et al. 2021; Maloney and Mitchell 1996; Gibson et al.

2002). However, under heat stress situations, these thermoregulatory mechanisms are unable to function at their full potential, which causes large rises in testicular temperature linked to a number of reproductive disorders. The latter are influenced mainly by breed, temperature rise degree, and duration of exposure (Wettere et al. 2021; Barragán Sierra et al. 2021).

15.3.2 Semen Quality and Spermatogenesis

Extensive experimental studies offer convincing proof of heat stress's impact on the quality of ram semen (Barragán Sierra et al. 2021; Sejian et al. 2012). Maurya et al. (2016) reported that scrotal circumference, sperm concentration, mass motility, and serum testosterone were reduced in adult Malpura rams exposed to hyperthermia. Another study reported that the experimental exposition of Awassi breed to high testicular and ambient temperature decreased concentration and sperm progressive motility, and increased abnormalities mainly in the acrosomal part (Abi Saab and Sleiman 1995). However, this breed showed the capacity for heat stress adaptability after subsequent heat stress events (Abi Saab and Sleiman 1995). Moreover, it was shown that heating the scrotum of Merino rams and using their sperm in artificial insemination, led to dramatic embryonic mortality between 17 and 65 days of pregnancy (Mieusset et al. 1992). On the other hand, in several arid and semi-arid areas in the world, studies investigated the effects of seasonal variations on ram sperm quality to determine their capacity to adapt to warm environments. Depending on the breed, and the environmental temperature, contradictory results have been obtained. It was reported that the semen quality of Old Djellal (Algeria), Dorper (Thailand), Hamari (Sudan), Suffolk (Egypt), Persian Karakul (Iran), Friesian, and Chios (Greece) rams was higher during summer and/or spring compared to the other seasons (Karagianidis et al. 2000; Kafi et al. 2004; Marai et al. 2006; Suhair and Abdalla 2013; Panyaboriban et al. 2016; Belkadi et al. 2017). Whereas other studies reported that the season did not influence ram semen quality. In Morocco, it was reported that D'Man × Timahdit crossbred rams (INRA 180) have the capacity to produce high semen quality throughout the year (Benmoula et al. 2017). In Brazil, it was reported that Morada Nova and Santa Inês rams are able to deal with thermal problems without compromising the quality of their semen throughout the year, making them resistant to tropical climates (Kahwage et al. 2017).

15.3.3 Male and Female Behaviors

Heat stress can negatively affect the reproduction of the ram by different mechanisms, mainly the decrease in testosterone concentrations, and direct damage in the morphometry and content of genetic material of the sperm leading finally to failures in the sexual behavior of animals (Barragán Sierra et al. 2021; Soravia et al. 2021).

Previous studies reported that rams are susceptible to reduce their sexual behavior induced by heat stress (Maurya et al. 2018). In arid Algerian areas, it was reported that the Rembi rams exhibited lower libido during the summer when the temperature reaches 39.5 °C (Benia et al. 2013). In addition, it was reported in several sheep breeds that heat stress, reduces the reaction time first ejaculation (RTFE), the total time taken for first ejaculation (TTFE), the latency period (LP), the number of mounts first ejaculation (NMFE), the reaction time second ejaculation (RTSE), the total time taken for second ejaculation (TTSE), and/ or the number of mounts second ejaculation (NMSE) (Maurya et al. 2016; Magaña-Monforte et al. 2015; Kumar et al. 2017). On the contrary, another study performed on crossbred rams showed that these aforementioned parameters did not change between the group chronically exposed to elevated temperature in a climatic chamber and the control (De et al. 2017). On the other hand, the effect of heat stress on ewes' sexual behavior was also reported. Indeed, it was revealed that sexual behavior parameters such as circling, tail-fanning, head-turning, standing, and approaching to ram were reduced in Bharat Merino ewes exposed to hyperthermia (Maurya et al. 2005).

15.3.4 Heat Stress Effects During Mating on Ewe Fertility

Recently, a study conducted by Narayan et al. (2018) found that summer heat waves can affect the results of artificial insemination and embryo transfer by causing physiological stress and early embryo loss in ewes suffering from hyperthermia. Studies on heat stress and its impact on reproductive wastage conducted in the 1960 and 1970s provided evidence that environmental stress has a significant impact on the ewes' ability to reproduce. Oocyte and/or embryo quality is most altered when ewes are exposed to hyperthermia during the first 3 days after artificial insemination (Thwaites 1971; Sawyer 1979; Sawyer and Narayan 2019). For instance, exposure of ewes to hyperthermia during the twelfth day of the cycle and mating at estrus decreased the fertility rate and also caused early embryo mortality as 69.2% of cleaved ovules (Dutt 1963). However, a Mexican study indicated that Pelibuey ewes reduced their estrous activity from January to June under arid conditions, but high environmental temperatures in summer are not affecting the estrus for this sheep breed (Gastelum-Delgado et al. 2015). Heat stress in ewes decreased behavioral estrus, luteinizing hormone preovulatory surge during the anticipated estrous cycle period, and plasma progesterone between days 7 and 13 of the cycle (Hill and Alliston 1981). In another study, Sejian et al. (2012) documented that hyperthermia and restricted fed reduced body weight, estrus duration, birth weight of lambs, and estradiol 17- β , whereas, significantly increased estrus cycle length and progesterone Malpura ewes compared to the control.

15.3.5 Pregnancy

Studies addressing the impact of heat stress on ewes' pregnancy proved that hyperthermia reduces birth weight, placenta weight, and total blood flow to the uterus, increases embryo mortality and placental stunting (Alexander and Williams 1971; Ali et al. 2009; Romo-Barron et al. 2019). Moreover, it was reported that heat stress decreased progesterone secretion, and placental lactogen resulted in placental stunting (Bell et al. 1989). Similarly, there are negative correlations between ewe rectal temperature during extreme heat and birth weight (McCrabb and Bortolussi 1996; Brown et al. 1977; Andrianakis and Walker 1994). These different harmful effects are influenced by several factors such as breed, temperature, and exposure time. For example, it was reported that chronic exposure of pregnant ewes to hyperthermia, induced gradual increases in uterine blood flow, boosting prostaglandin production in the uterus and/or placenta to protect the developing fetus (Andrianakis et al. 1989). However, severe heat stress reduced uterine and umbilical blood flow (Gilbert et al. 1985). In this context, Van Wettere et al. (2021) suggested that severe hyperthermia could suppress the fetal metabolic rate to reduce heat generation, which may contribute to impaired fetal growth. Recently, it was documented that the placenta serves as a conduit between the mother and the growing fetus (Sawyer and Narayan 2019). Glover (2015) showed that heat stress appears to activate the mother's HPA and causes the release of glucocorticoids, which cross the placenta and reach the fetus. Furthermore, the maternal-fetal connection is regulated by complex mechanisms of hormones, such as glucocorticoids, growth factors similar to insulin-IGF, and hormones expressed along the brain-gut axis, which may cause long-lasting endocrine changes that affect behavior and health outcomes in offspring (Glover 2015). Consequently, hyperthermia that increases glucocorticoid secretion has the potential to alter epigenetic patterns in future offspring (Sawyer and Narayan 2019).

15.3.6 Mitigation Strategies for Heat Stress

To maintain the productivity of sheep in a hot environment, several strategies have been developed (Krishnan et al. 2017). Sheep can adapt morphologically to climate by their size, the color of their coat and skin, the type of hair, and the fat (Berihulay et al. 2019). For instance, the loose and open fleece of hair and wool of Awassi sheep, as well as their reserves of fatty tissue, allow them to adapt to the unfavorable conditions of the Middle East (Gootwine 2011). Pourlis (2011) indicated that Damara sheep can adapt by their fat tail. Furthermore, Soay, Massese, and Xalda sheep adapt because of their coat color (Krishnan et al. 2017; Fontanesi et al. 2011).

Scientific studies were oriented toward the genetic development of breeds that are adaptable to heat stress (Krishnan et al. 2017; Collier et al. 2019). A study realized on Baraki desert in Egypt, discovered sheep chromosome 10 (OAR10), which

included multiple genes linked to stress, including those controlling angiogenesis, wound healing, and tumor suppressors (Kim et al. 2016). Other scientific studies were focalized on nutritional strategies in order to mitigate heat stress. In this context, it was shown that antioxidants like vitamin E, selenium, betaine, and melatonin counteracted the negative effects of heat stress on the productive performances of sheep (Bouroutzika et al. 2022; Krishnan et al. 2017; DiGiacomo et al. 2012).

Shearing sheep completely during the summer is a common practice in wool breeds to regulate their body temperatures (Barragán Sierra et al. 2021). However, in Argentina, it was discovered that when Australian Merino rams were completely sheared in a hyperthermic environment, the incidence of elliptical sperm heads increased (Armengol et al. 2015). Similar research has demonstrated that shearing Desert Hamari hair breed rams improve their thermoregulation but have the opposite effect on seminal quality during the summer (Barragán Sierra et al. 2021). Additionally, installing shade improves the thermoregulation capability in sheep (Kahwage et al. 2017; Hassanin et al. 1996).

15.4 Impact of Chemical Pollutants on Sheep Reproductive Performances

The main chemical pollutants attacking sheep are pesticides, Endocrine-Disrupting Chemicals (Rhind et al. 2010), heavy metals (cadmium, arsenic, and lead) (Rahim et al. 2022a), and fluoride (Rahim et al. 2022b). According to their chemical properties, these compounds exert toxic effects on the HPA, and male and female fertility.

15.4.1 *Endocrine Disruptor Chemicals*

Some chemical pollutants act as endocrine disruptors, mainly in the hypothalamus and pituitary gland which stimulate endogenous gonad activity (Rhind et al. 2010). Exposure to excess synthetic, or natural hormonally active compounds may disrupt the normal function of endocrine systems and tissues, particularly the reproductive endocrine axis. In sheep, Sweeney et al. (2007) reported that maternal exposure to octyl-phenol from birth to weaning increased the number and percentage of sperm abnormalities in the ejaculates of their rams after 1 year of age. In addition, pregnant ewes exposed to the same dose of octyl-phenol from days 110–115 of gestation, inhibited the normal FSH profile of the fetus in utero, with a resultant decrease in testis size and Sertoli cell number at birth (Sweeney et al. 2000). In another study exposure to octyl-phenol advanced the onset of puberty, without effect on endocrine status, and subsequent ovarian follicular dynamics of ewe lambs (Wright et al. 2002). On the other hand, prenatal Bisphenol A inhibited LH secretion in female ewes either when

the exposure occurred during development (Savabieasfahani et al. 2006) or during the prepubertal period (Evans et al. 2004). An utero exposure of pregnant ewes to environmentally relevant concentrations of polychlorinated biphenyls disrupt fetal testis development in sheep, and had minor effects on the fetal testis proteome, but had little impact on testis shape or testosterone production (Krogenæs et al. 2014).

15.4.2 Effects of Heavy Metals and Fluoride on Sheep Reproductive Parameters

In Baraki sheep, oral administration of cadmium chloride for 4 weeks reduced the levels of LH, FSH, and testosterone compared to the control (Zaki et al. 2013). Moreover, Leoni et al. (2002) investigated the influence of cadmium exposure on in vitro ovine gamete dysfunction, they observed that in vitro exposure to 0.2 μM decreases the viability of spermatozoa, the maturation of oocytes and fertilization, and causes an acrosome reaction of spermatozoa, abnormal activation and fertilization of mature oocytes. While in vitro exposure to 20 μM is lethal (Leoni et al. 2002). Recently, it has been showed that Kermani sheep reared in Iranian industrial areas and exposed to endocrine-disrupting chemicals, presented severe damage to testicular histology, sperm production, and sperm quality (Heidari et al. 2021).

In several areas where fluorosis is endemic, the effect of fluoride on reproduction parameters in ruminants has been well investigated (Rahim et al. 2022b). However, till now a limited number of studies have investigated the effect of this halogen in sheep. In a literature review, it was reported that the first research conducted in the 1950s, revealed that fluoride had no noticeable effect on the fetus, fertility rate, or the number of lambs born (Rahim et al. 2022b). However, recently it was declared that fluoride excess in water was shown to significantly decrease serum progesterone, estrogen, and triiodothyronine (Abdel-Rahman et al. 2018). Moreover, smooth ovaries with an atrophied uterus and fibroleiomyomas, cystic follicular ovaries associated with chronic cystic endometritis, and apoptosis in uterine tissue were revealed (Abdel-Rahman et al. 2018).

15.4.3 Mitigation Strategies for Chemical Pollutants

Several studies focused on the addition of antioxidants to alleviate oxidative stress caused by chemical pollutants (Rahim et al. 2022b; Najarnezhad et al. 2008; Vasant and Narasimhacharya, 2011; Piras et al. 2022). However, a few of them have been performed on sheep. In Moroccan endemic areas (El Amiri et al. 2022), selenium administration to Sardi ewes a month before lambing, followed by the addition of aluminum to lambs' diets, allowed for a live weight gain of 11.4 kg per animal over the course of a year and a 20% drop in blood fluoride levels when compared to

the control (Dahri 1990). A recent in vivo study showed that Resveratrol recovered the impaired meiotic competence of ovine oocytes caused by cadmium exposure. It also maintained normal oocyte fertility. Furthermore, resveratrol protects against cadmium-induced changes in oocyte cytoplasmic maturation (Piras et al. 2022). In another study, oral coadministration of lead acetate and *Allium sativum*, reduced ovary lead contents in ewes compared to the group administered by lead acetate only (Najarnezhad et al. 2008).

15.5 Conclusion

It is clear that hyperthermia due to climate change and chemical pollutants could lead to toxic effects on the reproductive system of sheep, disruption of sexual behavior, and fertility in rams and ewes. However, researches focusing on mitigation strategies are still limited. Therefore, it is more likely that various stages of the reproductive cycle will be impacted as a result of global warming and the ongoing buildup of chemical contaminants in the environment. Further studies focusing on mitigation strategies toward the impact of these two environmental challenges are needed. Precisely, studies on the nutritional side to compensate for animal stress, as well as genetic studies to select breeds adaptable to climate change are needed.

References

- Abbas S (2022) Climate change and major crop production: evidence from Pakistan. *Environ Sci Pollut Res* 29:5406–5414
- Abdel-Rahman GH, El-Hallawany HA, Dohreig RA (2018) Effect of excess fluoride on reproductive potentials in farm animals (ovine). *AJVS* 57:41–57
- Abi Saab S, Sleiman FT (1995) Physiological responses to stress of filial crosses compared to local Awassi sheep. *Small Rumin Res* 16:55–59
- Akhtar E, Roy AK, Haq MA, von Ehrenstein OS, Ahmed S, Vahter M, Ekstrom E-C, Kippler M, Wagatsuma Y, Raqib R (2021) A longitudinal study of rural Bangladeshi children with long-term arsenic and cadmium exposures and biomarkers of cardiometabolic diseases. *Environ Pollut* 271:116333
- Alexander G, Williams D (1971) Heat stress and development of the conceptus in domestic sheep. *J Agric Sci* 76:53–72
- Ali A, Hayder M, Derar R (2009) Reproductive performance of Farafra ewes in the subtropics. *Anim Reprod Sci* 114:356–361
- Andrianakis P, Walker D (1994) Effect of hyperthermia on uterine and umbilical blood flows in pregnant sheep. *Exp Physiol: Transl Integr* 79:1–13
- Andrianakis P, Walker DW, Ralph MM, Thorburn GD (1989) Effects of hyperthermia on fetal and maternal plasma prostaglandin concentrations and uterine activity in sheep. *Prostaglandins* 38:541–555
- Armengol ML, Sabino GA, Forquera JC, de La Casa A, Aisen EG (2015) Sperm head ellipticity as a heat stress indicator in Australian Merino rams (*Ovis aries*) in Northern Patagonia, Argentina. *Theriogenology* 83:553–559

- Barragán Sierra A, Avendaño-Reyes L, Hernández Rivera JA, Vicente-Pérez R, Correa-Calderón A, Mellado M, Meza-Herrera CA, Macías-Cruz U (2021) Thermoregulation and reproductive responses of rams under heat stress review. *Rev Mex De Cienc Pecu* 12:910–931
- Belkadi S, Safsaf B, Heleili N, Tlijdane M, Belkacem L, Oucheriah Y (2017) Seasonal influence on sperm parameters, scrotal measurements, and serum testosterone in Ouled Djellal breed rams in Algeria. *Vet World* 10:1486
- Bell AW, McBride BW, Slepetic R, Early RJ, Currie WB (1989) Chronic heat stress and prenatal development in sheep: I. Conceptus growth and maternal plasma hormones and metabolites. *J Anim Sci* 67:3289–3299
- Benia AR, Taibi K, Ait-Amrane A, Belhamiti T, Hammoudi SM, Kaidi R (2013) Study of seasonal sexual activity variations in Algerian rams: sexual behaviour, testosterone concentration control and environmental factors. *Afr J Biotechnol* 12
- Benmoula A, Badi A, Fadili ME, Khalil KE, Allai L, Hilali AE, Amiri BE (2017) Effect of season on scrotal circumference, semen characteristics, seminal plasma composition and spermatozoa motility during liquid storage in INRA180 rams. *Anim Reprod Sci* 180:17–22
- Berihulay H, Abied A, He X, Jiang L, Ma Y (2019) Adaptation mechanisms of small ruminants to environmental heat stress. *Animals* 9:75
- Bouroutzika EV, Theodosiadou EK, Barbagianni MS, Papadopoulos S, Kalogiannis D, Chadio S, Skaperda Z, Kouretas D, Katsogiannou EG, Valasi I (2022) Redox status and hematological variables in melatonin-treated ewes during early pregnancy under heat stress. *Vet Sci* 9:499
- Brown DE, Harrison PC, Hinds FC, Lewis JA, Wallace MH (1977) Heat stress effects on fetal development during late gestation in the ewe. *J Anim Sci* 44
- Castillo DA, Gaitan JJ, Villagra ES (2021) Direct and indirect effects of climate and vegetation on sheep production across Patagonian rangelands (Argentina). *Ecol Ind* 124:107417
- Collier RJ, Baumgard LH, Zimbelman RB, Xiao Y (2019) Heat stress: physiology of acclimation and adaptation. *Anim Front* 9:12–19
- Dado-Senn B, Skibiél AL, Fabris TF, Dahl GE, Laporta J (2019) Dry period heat stress induces microstructural changes in the lactating mammary gland. *PLoS One* 14
- Dahri M (1990) Aspects nutritionnels et toxicologiques des oligoéléments: prévention de la carence en sélénium et de l'intoxication fluorée chez les ovins. Thèse Doct Vét IAV Hassan II, Maroc
- De K, Kumar D, Balaganur K, Saxena VK, Thirumurugan P, Naqi SMK (2017) Effect of thermal exposure on physiological adaptability and seminal attributes of rams under semi-arid environment. *J Therm Biol* 65:113–118
- DiGiacomo K, Simpson S, Leury BJ, Dunshea FR (2012) Dietary betaine improves physiological responses in sheep under chronic heat load in a dose dependent manner. *J Anim Sci* 90:269
- Dutt RH (1963) Critical period for early embryo mortality in ewes exposed to high ambient temperature. *J Anim Sci* 22:713–719
- El Amiri B, Abdellatif R, Mounia S (2022) Perception et pratiques d'élevage pour atténuer la fluorose chez les ovins dans trois communes de la province de Khouribga-Maroc. *AFRIMED Agric J-Al Awamia* 135:1–17
- Evans NP, North T, Dye S, Sweeney T (2004) Differential effects of the endocrine-disrupting compounds bisphenol-A and octylphenol on gonadotropin secretion, in prepubertal ewe lambs. *Domest Anim Endocrinol* 26:61–73
- Fontanesi L, Dall'Olio S, Beretti F, Portolano B, Russo V (2011) Coat colours in the Massese sheep breed are associated with mutations in the agouti signalling protein (ASIP) and melanocortin 1 receptor (MC1R) genes. *Animal* 5:8–17
- Gastelum-Delgado MA, Avendaño-Reyes L, Álvarez-Valenzuela FD, Correa-Calderón A, Meza-Herrera CA, Mellado M, Macías-Cruz U (2015) Circannual estrous behavior in Pelibuey ewes under arid conditions of Northwestern of Mexico. *Rev Mex De Cienc Pecu* 6:109–118
- George W, Zoltán B, András J, Szilvia K (2020) Impacts of climate change on sheep genetic diversity: a review. *Sustainable Development*, vol 10
- Gibson A, Akinrinsola A, Patel T, Ray A, Tucker J, McFadzean I (2002) Pharmacology and thermosensitivity of the dartos muscle isolated from rat scrotum. *Br J Pharmacol* 136:1194–1200

- Gilbert RD, Schroder H, Kawamura T, Dale PS, Power GG (1985) Heat transfer pathways between fetal lamb and ewe. *J Appl Physiol* 59:634–638
- Glover V (2015) Prenatal stress and its effects on the fetus and the child: possible underlying biological mechanisms. In: *Perinatal programming of neurodevelopment*. Springer, Berlin, pp 269–283
- Gootwine E (2011) Mini review: breeding Awassi and Assaf sheep for diverse management conditions. *Trop Anim Health Prod* 43:1289–1296
- Hassanin SH, Abdalla EB, Kotby EA, Abd-Elaziz AMS, El-Fouly MA (1996) Efficiency of asbestos shading for growth of Barki rams during hot summer. *Small Rumin Res* 20:199–203
- Heidari AH, Zamiri MJ, Nazem MN, Jafarzadeh Shirazi MR, Akhlaghi A, Ansari Pirsaraei Z (2021) Detrimental effects of long-term exposure to heavy metals on histology, size and trace elements of testes and sperm parameters in Kermani Sheep. *Ecotoxicol Environ Saf* 207:111563
- Hill TG, Alliston CW (1981) Effects of thermal stress on plasma concentrations of luteinizing hormone, progesterone, prolactin and testosterone in the cycling ewe. *Theriogenology* 15:201–209
- Kafi M, Safdarian M, Hashemi M (2004) Seasonal variation in semen characteristics, scrotal circumference and libido of Persian Karakul rams. *Small Rumin Res* 53:133–139
- Kahwage PR, Esteves SN, Jacinto MAC, Junior WB, Pezzopane JRM, de Andrade Pantoja MH, Bosi C, Miguel MCV, Mahlmeister K, Garcia AR (2017) High systemic and testicular thermolytic efficiency during heat tolerance test reflects better semen quality in rams of tropical breeds. *Int J Biometeorol* 61:1819–1829
- Karagiannidis A, Varsakeli S, Alexopoulos C, Amaratidis I (2000) Seasonal variation in semen characteristics of Chios and Friesian rams in Greece. *Small Rumin Res* 37:125–130
- Karimi V, Karami E, Keshavarz M (2018) Climate change and agriculture: impacts and adaptive responses in Iran. *J Integr Agric* 17:1–15
- Kim E-S, Elbeltagy AR, Aboul-Naga AM, Rischkowsky B, Sayre B, Mwacharo JM, Rothschild MF (2016) Multiple genomic signatures of selection in goats and sheep indigenous to a hot arid environment. *Heredity* 116:255–264
- Krishnan G, Bagath M, Pragna P, Vidya MK, Aleena J, Archana PR, Sejian V, Bhatta R (2017) Mitigation of the heat stress impact in livestock reproduction. *Theriogenology* 8:8–9
- Krogenæs AK, Ropstad E, Gutleb AC, Hårdnes N, Berg V, Dahl E, Fowler PA (2014) In: Utero exposure to environmentally relevant concentrations of PCB 153 and PCB 118 disrupts fetal testis development in sheep. *J Toxicol Environ Health Part A* 77:628–649
- Kumar D, Sejian V, Gaughan JB, Naqvi SMK (2017) Biological functions as affected by summer season-related multiple environmental stressors (heat, nutritional and walking stress) in Malpura rams under semi-arid tropical environment. *Biol Rhythm Res* 48:593–606
- Lacetera N (2019) Impact of climate change on animal health and welfare. *Anim Front* 9:26–31
- Leoni G, Bogliolo L, Deiana G, Berlinguer F, Rosati I, Pintus PP, Ledda S, Naitana S (2002) Influence of cadmium exposure on *in vitro* ovine gamete dysfunction. *Reprod Toxicol* 16:371–377
- Magaña-Monforte JG, Centurión-Castro FG, Aké-López JR, Cárdenas-Gallegos MA (2015) Libido and serving capacity of mature hair rams under tropical environmental conditions. *Arch De Med VetIa* 47:39–44
- Maloney SK, Mitchell D (1996) Regulation of ram scrotal temperature during heat exposure, cold exposure, fever and exercise. *J Physiol* 496:421–430
- Maloney SK, Bonomelli JM, DeSouza J (2003) Scrotal heating stimulates panting and reduces body temperature similarly in febrile and non-febrile rams (*Ovis aries*). *Comp Biochem Physiol a: Mol Integr Physiol* 135:565–573
- Marai IF, El-Darawany A-HA, Ismail ESAF, Abdelhafez MA (2006) Tunica dartos index as a parameter for measurement of adaptability of rams to subtropical conditions of Egypt. *Anim Sci J* 77:487–494
- Maurya VP, Naqvi SMK, Gulyani R, Joshi A, Mittal JP (2005) Effect of Thermal Stress on Sexual Behaviour of Superovulated Bharat Merino Ewes. *Asian Australas J Anim Sci* 18:1403–1406

- Maurya VP, Sejian V, Kumar D, Naqvi SMK (2016) Impact of heat stress, nutritional restriction and combined stresses (heat and nutritional) on growth and reproductive performance of Malpura rams under semi-arid tropical environment. *J Anim Physiol Anim Nutr* 100:938–946
- Maurya VP, Sejian V, Kumar D, Naqvi SMK (2018) Biological ability of Malpura rams to counter heat stress challenges and its consequences on production performance in a semi-arid tropical environment. *Biol Rhythm Res* 49:479–493
- Mazinani M, Rude B (2020) Population, world production and quality of sheep and goat products. *Am J Anim Vet Sci* 15:291–299
- McCrabb GJ, Bortolussi G (1996) Placental growth and the ability of sheep to thermoregulate in hot environment. *Small Rumin Res* 20:121–127
- Mieusset R, Casares PQ, Partida LS, Sowerbutts SF, Zupp JL, Setchell BP (1992) Effects of heating the testes and epididymides of rams by scrotal insulation on fertility and embryonic mortality in ewes inseminated with frozen semen. *Reproduction* 94:337–343
- Mota-Rojas D, Titto CG, de Mira Geraldo A, Martínez-Burnes J, Gómez J, Hernández-Ávalos I, Casas A, Domínguez A, José N, Bertoni A (2021) Efficacy and function of feathers, hair, and glabrous skin in the thermoregulation strategies of domestic animals. *Animals* 11:3472
- Najarezhad V, Aslani MR, Balali-Mood M (2008) Evaluation of allicin for the treatment of experimentally induced subacute lead poisoning in sheep. *Biol Trace Elem Res* 126:141–147
- Narayan E, Sawyer G, Parisella S (2018) Faecal glucocorticoid metabolites and body temperature in Australian merino ewes (*Ovis aries*) during summer artificial insemination (AI) program. *PLoS ONE* 13:e0191961
- Noyes PD, Lema SC (2015) Forecasting the impacts of chemical pollution and climate change interactions on the health of wildlife. *Curr Zool* 61:669–689
- Panyaboriban S, Suwimonteerabutr J, Swangchan-Uthai T, Tharasanit T, Phutikanit N, Techakumphu M (2016) Effect of heat stress on reproductive performance of an imported dorper ram: a case study in Thailand. *Thai J Vet Med* 46:671
- Piras AR, Ariu F, Maltana A, Leoni GG, Martino NA, Mastrorocco A, Del AME, Bogliolo L (2022) Protective effect of resveratrol against cadmium-induced toxicity on ovine oocyte *in vitro* maturation and fertilization. *J Anim Sci Biotechnol* 13:83
- Pourlis AF (2011) A review of morphological characteristics relating to the production and reproduction of fat-tailed sheep breeds. *Trop Anim Health Prod* 43:1267–1287
- Rahim A, Aydogmus-Öztürk F, Çakir C, Essamadi A, El Amiri B (2022a) Mitigating fluoride, lead, arsenic and cadmium toxicities in laboratory animals and ruminants through natural products. *Rec Agric Food Chem* 2:1–17
- Rahim A, Essamadi A, El Amiri B (2022b) A comprehensive review on endemic and experimental fluorosis in sheep: Its diverse effects and prevention. *Toxicology* 465:153025
- Rhind SM, Evans NP, Bellingham M, Sharpe RM, Cotinot C, Mandon-Pepin B, Loup B, Sinclair KD, Lea RG, Pocar P (2010) Effects of environmental pollutants on the reproduction and welfare of ruminants. *Animal* 4:1227–1239
- Romo-Barron CB, Diaz D, Portillo-Loera JJ, Romo-Rubio JA, Jimenez-Trejo F, Montero-Pardo A (2019) Impact of heat stress on the reproductive performance and physiology of ewes: a systematic review and meta-analyses. *Int J Biometeorol* 63
- Savabieasfahani M, Kannan K, Astapova O, Evans NP, Padmanabhan V (2006) Developmental programming: differential effects of prenatal exposure to bisphenol-A or methoxychlor on reproductive function. *Endocrinology* 147:5956–5966
- Sawyer GJ (1979) The influence of radiant heat load on reproduction in the Merino ewe. The relative effects of heating before and after insemination. *Aust J Agric Res* 30
- Sawyer G, Narayan EJ (2019) A review on the influence of climate change on sheep reproduction. *Comp Endocrinol Anim* 10
- Schiedek D, Sundelin B, Readman JW, Macdonald RW (2007) Interactions between climate change and contaminants. *Mar Pollut Bull* 54:1845–1856
- Sejian V, Maurya VP, Kumar K, Naqvi SMK (2012) Effect of multiple stresses (thermal, nutritional, and walking stress) on the reproductive performance of Malpura ewes. *Vet Med Int* 2012

- Sillmann J, Aunan K, Emberson L, Bükler P, Van Oort B, O'Neill C, Otero N, Pandey D, Brisebois A (2021) Combined impacts of climate and air pollution on human health and agricultural productivity. *Environ Res Lett* 16:093004
- Soravia C, Ashton BJ, Thornton A, Ridley AR (2021) The impacts of heat stress on animal cognition: implications for adaptation to a changing climate. *Wiley Interdiscip Rev: Clim Chang* 12:e713
- Suhair SM, Abdalla MA (2013) Effects of seasonal changes and shearing on thermoregulation, blood constituents and semen characteristics of desert rams (*Ovis aries*). *Pak J Biol Sci: PJBS* 16:1884–1893
- Swanepoel FJC, Stroebel A, Moyo S (2010) The role of livestock in developing communities: enhancing multifunctionality. University of the Free State/CTA
- Sweeney T, Nicol L, Roche JF, Brooks AN (2000) Maternal exposure to octylphenol suppresses ovine fetal follicle-stimulating hormone secretion, testis size, and sertoli cell number. *Endocrinology* 141:2667–2673
- Sweeney T, Fox J, Robertson L, Kelly G, Duffy P, Lonergan P, O'doherty J, Roche JF, Evans NP (2007) Postnatal exposure to octylphenol decreases semen quality in the adult ram. *Theriogenology* 67:1068–1075
- Terrien J, Perret M, Aujard F (2011) Behavioral thermoregulation in mammals: a review. *Front Biosci-Landmark* 16:1428–1444
- Thwaites CJ (1971) Short term heat stress and embryo mortality in the ewe. *Aust J Exp Agric* 11:265–267
- van Wettere WH, Kind KL, Gatford KL, Swinbourne AM, Leu ST, Hayman PT, Kelly JM, Weaver AC, Kleemann DO, Walker SK (2021) Review of impact of heat stress on reproductive performance of sheep. *J Anim Sci Biotechnol* 12:1–18
- Vasant R, Narasimhacharya A (2011) Amelioration of fluoride-induced oxidative stress by *Mangifera indica* L. fruit. *Spatula DD* 1:181–188
- Wright C, Evans ACO, Evans NP, Duffy P, Fox J, Boland MP, Roche JF, Sweeney T (2002) Effect of maternal exposure to the environmental estrogen, octylphenol, during fetal and/or postnatal life on onset of puberty, endocrine status, and ovarian follicular dynamics in ewe lambs. *Biol Reprod* 67:1734–1740
- Zaki MS, Abd El-Rahman HH, Mohamed MI, Abd El-Magid SS (2013) Some studies in Barki sheep intoxicated with cadmium. *Life Sci J* 10:1202–1204

Chapter 16

Dynamics of Tree Cover on the Adaptive Genetic Variation and Evolutionary Power of the Argan Forests from the Essaouira Region of Morocco Facing Climate Change



Mohammed Alami, Bouchra Belkadi, Chaimaa Yatrib, Leila Medraoui, Ouafae Pakhrou, Karim Rabeh, and Abdelkarim Filali-Maltouf

Abstract Ecosystems are increasingly facing severe environmental conditions as a result of climate change. For this, the species continues to evolve to better adapt to this changing environment, especially plant species that have an essential adaptive power. Understanding these processes will help us to protect nature and lead conservation and management programs of biodiversity. The argan forest is one of the unique ecosystems in the world with the presence of an endemic tree in Morocco, *Argania spinosa* L. unfortunately it is subjected to high anthropic pressure in addition to the effect of global warming, which causes a serious regression of its area. This study aimed to understand the evolutionary power of Argan tree by detecting the evolution of tree cover dynamics in the Essaouira region and evaluate its impact on adaptive genetic variation during two epochs between 2010 and 2020. Our approach is to use remote sensing methods (GIS) with Landsat satellite maps and MODIS land products coupled with genetic marking by microsatellite molecular markers (SSR). The study showed a positive evolution with a small increase in argan trees occupancy rate and vegetation indices in most populations of the region. This dynamic seems to positively impact genetic diversity ($r^2 = 0.73$, $P < 0.01$). This variation in allelic richness, generated by the natural selection of alleles, shows a great adaptive power leading to genetic evolution. This adaptation, which remains to be determined, is due to the effect of climate change and the positive genetic impact of argan forest protection plans and to establish more effective conservation strategies against climate change.

Keywords Argan forests · Vegetation dynamics · Adaptive power · Genetic variability · Climate change · Morocco

M. Alami · B. Belkadi · C. Yatrib · L. Medraoui · O. Pakhrou · K. Rabeh · A. Filali-Maltouf (✉)
Laboratory of Microbiology and Molecular Biology, Faculty of Sciences, Mohammed V
University, Rabat, Morocco
e-mail: a.filalimaltouf@gmail.com

16.1 Introduction

The argan forests of Essaouira province cover an area of 136,430 ha, accounting for 20% of the national argan plantations. It represents the first forest species in this region from which it takes the name “Argan zone” with 60% of the argan tree (HCEFLCD 2013). Furthermore, the argan forest forms a very particular ecosystem and argan tree plays an important role in protecting the soil from erosion and against desertification. It is also known for the multiple virtues of its oil extracted from its seeds. However, over the last century, these argan plantations have lost much of their land and their average density has decreased from 200 to 30 trees per hectare (Nouaim et al. 1991), which necessarily means a loss of diversity. For this reason, several national and international projects are interested in protecting this millennial tree. This was realized by the creation of the Argan forests Biosphere Reserve (RBA) since 1998; the first biosphere reserve in Morocco has declared a world heritage of humanity.

However, we still have a relative knowledge of argan forest extent and evolution. As well as the degradation of the argan forests has often been overvalued for strictly financial purposes. Several studies mention the degradation of the argan forests but are not based on precise scientific research. Most of these studies start from an alarmist observation but do not rely on scientific reference points to assess objectively the degree of degradation.

Satellite sensors today make it possible to map forests and to measure the evolution of their surface reliably (Diao et al. 2020). Climate change and deforestation have led to the development of sensitive and specific maps of forest cover change (FCC). Several studies have mentioned that climate change and deforestation remain the most dangerous because it affects the global carbon cycle, the hydrological cycle and changes in the biodiversity of ecosystems (Band 1993; Parker et al. 2000; Townshend et al. 2012). A study conducted by Guarino et al. (2001) shows the importance of the uses of remote sensing in the management of plant genetic resources and its potential benefits. Other studies have combined molecular analysis and remote sensing for the management and conservation of genetic resources, illustrating the power of this technique, which highlights a better understanding of the impact of vegetation dynamics on adaptation (Elliott et al. 2014; Gomez et al. 2010).

For molecular analysis, microsatellite markers are particularly relevant for this approach because they provide information on the origin of genetic variation and are also a tool for detecting and analyzing genotypes. Various molecular genetic markers have been used to assess the genetic diversity and relationships between the populations of *Argania spinosa* L. such as Restriction Fragment Length Polymorphism (RFLP) of chloroplast DNA (Mousadik and Petit 1996), Random Amplified Polymorphic DNA (RAPD) (Majourhat et al. 2008), Amplified Fragment Length Polymorphism (AFLP) (Pakhrou et al. 2016), Inter-Simple Sequence Repeat (ISSR) (Yatrib et al. 2015) and Simple Sequence Repeat (SSR) (Majourhat et al. 2008). For the argan tree, the specific markers recently developed by Bahloul et al. (2014) were used to characterize the natural genetic diversity detected in this species by Yatrib

et al. (2017), and they proved sufficiently informative to discriminate against argan trees.

In addition, the availability of Landsat global datasets and MODIS land products has considerably improved the characterization of vegetation cover. Landsat Vegetation Continuous Fields (LVCF) is a multi-temporal representation of long-term to detect the global forest dynamics at a high resolution of 30 m per pixel (Feng et al. 2016). For the monitoring and characterization of the vegetation dynamics, several vegetative indicators are developed in MODIS land products (Sakamoto et al. 2005). These include the Normalized Difference Vegetation Index (NDVI), the Enhanced Vegetation Index (EVI), the Fraction of Photo-synthetically Active Radiation (FPAR) and the Leaf Area Index (LAI). These variables are the most frequently used to characterize the state of plant growth (Xu et al. 2018; Sun and Schulz 2017).

To this end, 13 Simple Sequence Repeat (SSR) markers were used to determine genetic diversity and allelic richness of argan tree as well as the study of their evolution over 11 years subdivided into two epochs, by remote sensing techniques, which determine the presence or absence of argan trees. This study will contribute to a better understanding of the adaptation of genotypes to climate change and essential facts to conservation programs.

16.2 Material and Methods

16.2.1 Study Area

The study area is located in Essaouira region, in the south-west of Morocco, bordered on the north by Safi city and on the south by Agadir city (31°28' N, 9°27' W). This region has an arid to semi-arid Mediterranean climate, with hot to temperate winter and under oceanic influence. We have concentrated on ten argan forests and the tree covers have already been identified (Fig. 16.1). Other characteristics of each site are given in Table 16.1.

16.2.2 Genetic Analysis of Argan Trees

Plant Sampling and DNA Isolation. Fresh leaves were sampled for the genetic analyses from 10 sites collected at the rate of 20 trees per site, for a total of 200 adult trees geo-referenced of *Argania spinosa* L. stored at -80°C before lyophilisation and Vibro-grinding. The extraction of genomic DNA was carried out by the protocol of the ISOLATE II Plant DNA Kit. The quality and quantity of the DNA were determined using a NanoDrop 2000 (NanoDrop Technologies Inc., USA) and a visual assessment on a 1% agarose gel. DNA concentration was adjusted to 50 ng/ μL and samples were stored at -20°C .

Fig. 16.1 Distribution of Essaouira argan populations

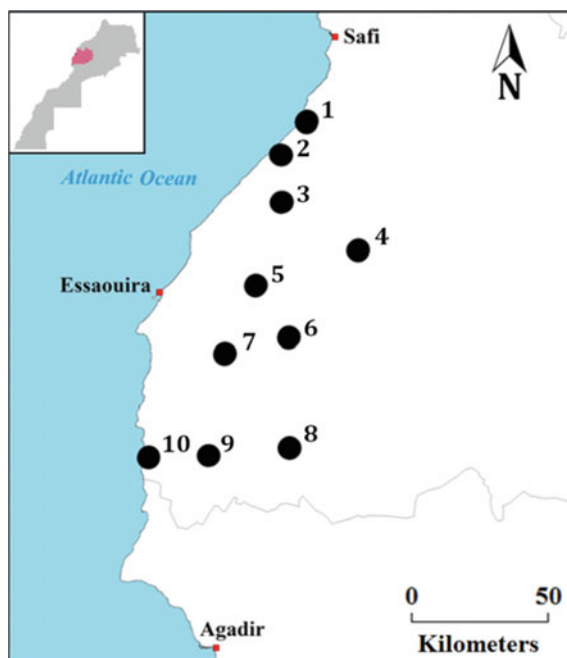


Table 16.1 Basic information regarding 10 sampling populations

Sampling population	Code	Longitude	Latitude	Altitude (m)	Date of sampling	Sampling area (ha)
Retmana	1	−9°19′	32°02′	58	23/12/2012	56.34
Ouled Lhaj	2	−9°24′	31°56′	120	23/12/2012	56.25
Jbel kourati	3	−9°24′	31°47′	360	23/12/2012	56.16
Mramer	4	−9°10′	31°38′	396	24/12/2012	54.00
Rbaï	5	−9°28′	31°32′	269	24/12/2012	51.75
Tamesrart	6	−9°22′	31°21′	540	24/12/2012	91.08
Neknafa	7	−9°33′	31°19′	242	24/12/2012	51.30
Ait Issi	8	−9°22′	31°02′	980	28/12/2012	92.16
Tmanar	9	−9°37′	31°00′	576	25/12/2012	51.12
Timzgidah Oufetass	10	−9°48′	31°00′	231	25/12/2012	53.01

SSR Analysis. A total of 13 SSR primer pairs were selected for this study labelled with 6-FAM, Atto 565, or HEX fluorescent dyes (Table 16.2). Primer information was obtained from Majourhat et al. (2008) and (El Bahloul et al. 2014).

Based on the protocol given by Zietkiewicz et al. (1994) modified for optimizing the PCR reaction, the final volume was performed in 20 μ L reaction mixtures: 1X

Table 16.2 Characteristics of 13 SSR markers

Locus	Primer sequences (5' → 3')	Repeat motifs	Ta	Fluorescent label dyes	Sequence reference
ASMS01	GTTTCTTGCAGTTTGAGAATTGAAAGGACAACG CCTCCCATCTAATAATTTCTAGTTCCATCC	(CT) ₁₁ (CA) ₁₇	57	6-FAM	El Bahloul et al. (2014)
ASMS20	GTTTCTTAATACTTCAATGCGAAGGTCGTG ATTACTCCCAACCTCAGTCAGC	(CT) ₁₄	53.8	ATTO565	El Bahloul et al. (2014)
ASMS2012_04	CCAATAATAGAAAACACCCGGAA GTTTCTTACTTAGCCACCTTCTCTTCT	(CTT) ₇	55	HEX	El Bahloul et al. (2014)
ASMS2012_34	CCCATTGTAGACTTCCGCTTAC GTTTCTTAAACCACAGAGAGCAGCAACTTT	(AG) ₁₆	55	6-FAM	El Bahloul et al. (2014)
ASMS2012_37	CGGAAAGGAATTAGGATTTGG GTTTCTTCGGTTCGTCTCTTCTCCAGTAT	(AG) ₁₅	55	HEX	El Bahloul et al. (2014)
MH07	ATTGCAGCATATCCACACCA GC AAAAGGTGATGGGTTAGA	(CT) ₂₃	56	6-FAM	Majourhat et al. (2008)
MH04	GCACCTCTCCATGGTTCCAGT AAAGAGTCAATGGCGTGAGC	(CT) ₁₂	52	6-FAM	Majourhat et al. (2008)
MH06	ACACGCACAAAAACAAACCAA TTCTTGAAGGAGGGTTGCTC	(GA) ₁₄	56	HEX	Majourhat et al. (2008)

(continued)

Table 16.2 (continued)

Locus	Primer sequences (5' → 3')	Repeat motifs	Ta	Fluorescent label dyes	Sequence reference
ME11	TTGCTATTTGCCTGTT TTCATCACCTTCCCTCTC	(GT) ₁₀	48	HEX	Majourhat et al. (2008)
MH20	GAAAGTTTTGACCAATTTGGGAAT GACATAACACTAACCCCTCACGA	(GA) ₁₃	56	6-FAM	Majourhat et al. (2008)
MH08	GTAATGGGAGCCGTTTGAGA CTGGGTAGCAATTTGTTGCAT	(CT) ₁₁	56	6-FAM	Majourhat et al. (2008)
ME05	GTTTGTATGGTTTCGGTT CTTCGTTTTTCAGTAGGTCTC	(TG) ₇	52	6-FAM	Majourhat et al. (2008)
MH12	TGCGGAAGTGTGGAAAGAGT ATCCACACAATGACTGACG	(CT) ₉ (AC) ₆	56	HEX	Majourhat et al. (2008)

PCR buffer, 2.5 mM MgCl₂, 0.1 mM dNTP, 0.2 μM forward and reverse primers, 0.6 U Taq polymerase (GoTaq[®] DNA Polymerase, Promega), 2 μl DNA, and completing the volume with sterile double-distilled water. PCR conditions optimized as an initial step of 2 min at 94 °C for initial denaturation, 35 cycles with 30 s at 94 °C, 30 s at 48–59 °C as annealing temperature (depending on primer pair), 30 s at 72 °C for the extension and a final extension step of 7 min at 72 °C. Amplification of DNA has been performed with GenAmp[®] thermal cycler (Applied Biosystem, CA, USA).

After DNA amplification, DNA fragments were separated via ABI 3130xl DNA analyser by capillary electrophoresis using 1.5 μl of amplification products mixed with 9.5 μl of formamide and 0.5 μl GeneScan[™] 500 ROX[®] as internal size standard (Applied Biosystems, Foster City, USA). The deposits are made by multiplexing.

Identification of Genetic Diversity. SSR alleles are visualized in the form of peaks and data matrices were scored with GeneMapper v5.0 software (Applied Biosystems, Foster City, CA, USA) for each year of this study. The allelic richness (Ar), Shannon's information index (I) and the percentage of polymorphic bands (%P) were calculated for each of the ten argan forests using the GenALEX v6.5 Software (Peakall and Smouse 2006; 2012). The coefficient of genetic differentiation (F_{st}), and gene flow (Nm) were calculated using POPGENE v1.32 (Yeh et al. 1997).

16.2.3 Data Sources

Our choice was based first on Landsat Vegetation Continuous Fields (LVCF), tree cover maps specific to woody vegetation over 5 m in height and with a good resolution of 30 m per pixel (Sexton et al. 2013) and the Terra MODIS Vegetation Continuous Fields (VCF) to detect the tree cover. Furthermore, to measure the density of Argan trees, we used four databases from the Moderate Resolution Imaging Spectroradiometer (MODIS): The Normalized Difference Vegetation Index (NDVI), The Enhanced Vegetation Index (EVI), The Fraction of Photo-synthetically Active Radiation (FPAR) and Leaf Area Index (LAI) (Table 16.3).

Landsat Images. The Landsat Vegetation Continuous Fields (LVCF) tree cover maps for the two years (2010 and 2015) in the study area were extracted from the site: Earth Science Data Interface "ESDI" and the University of Maryland's Global Land Cover Facility (GLCF) (<http://glcf.umd.edu/>). The satellite map of study zone from Essaouira region is located on path 203, row 38. The Forest Cover dataset includes Landsat ETM + images with 30 m spatial resolution.

MODIS Datasets. The MOD44B v6 Terra MODIS Vegetation Continuous Fields (VCF) product is generated yearly and produced using monthly composites of Terra MODIS 250 and 500 m Land Surface Reflectance data. Designed to continuously represent Earth's terrestrial surface as a proportion of basic vegetation traits, it provides a gradation of three surface cover components: per cent tree cover, per

Table 16.3 The characteristics of the used satellite data

Satellite data	Product type	Spatial resolution (m)	Temporal resolution
Landsat	LVCF	30	Yearly
MOD44B	PTC	250	Yearly
MOD13Q1	NDVI EVI	250	16-day composite
MOD15A2H	LAI FPAR	500	8-day composite

LVCF: Landsat Vegetation Continuous Field; **PTC:** Percentage of Tree Cover; **NDVI:** the Normalized Difference Vegetation Index; **EVI:** the Enhanced Vegetation Index; **FPAR:** the Fraction of Photo-synthetically Active Radiation; **LAI:** the Leaf Area Index

cent non-tree cover, and per cent bare. VCF products provide a continuous, quantitative portrayal of land surface cover with improved spatial detail, and hence, are widely used in environmental modelling and monitoring applications (DiMiceli et al. 2015).

In the MOD13Q1 data, the NDVI product is provided every 16 days at 250 m spatial resolution and designed to offer a consistent spatial and temporal comparison of vegetation conditions (Didan 2015). The Normalized Difference Vegetation Index (NDVI) obtained from the ratio of red (RED) and near-infrared (NIR) of vegetation reflectance in the electromagnetic spectrum ($NDVI = (NIR - RED)/(NIR + RED)$); (Myneni et al. 1995)). The second vegetation layer is the Enhanced Vegetation Index (EVI), which has improved sensitivity over high biomass regions. The EVI uses the blue band to remove residual atmosphere contamination caused by smoke and sub-pixel thin clouds that minimizes canopy background variations (Sakamoto et al. 2005). The significance of the NDVI index was fixed at 0.3 while for EVI index was at 0.2.

In the MOD15A2H data, the Leaf Area Index (LAI) of a broadleaf canopy corresponds to one-half of the total intercepting area per unit ground surface (Chen and Black 1992). The 8-day composite dataset together with the quality criteria (QC) layer is retrieved from the Terra MODIS platform with a 500 m pixel size (Myneni 2015). The MOD15A2H data also includes the Fraction of Photo-synthetically Active Radiation (FPAR) defined as the fraction of incident photo-synthetically active radiation (400–700 nm) absorbed by the green elements of a vegetation canopy (Myneni 2015). We fixed the significance of the LAI value at 0.5 and for FPAR at 0.25.

It is worth mentioning that the satellite maps of the study area are located on horizontal line 17 and vertical line 05. After extraction of satellite maps of each vegetation index by the ENVI program (v4.5) (Research Systems 2008), it was also used to generate three matrices of these vegetation indices for the three years studied (2010, 2015 and 2020) from each argan forest.

Maps Creation. Two maps for the evolution of tree cover: 2010–2015 and 2015–2020 for each argan forest were carried out with LVCF and MOD44B images using

the ENVI program (v4.5) (Research Systems 2008) and the evolution of occupancy rate calculated for each argan forest. It is interesting to note that the Landsat ETM + images have the same spatial and spectral characteristics so there is no difference between them if we respect the procedure of the pre-treatment of forest cover images.

Model Validation. Evaluation and validation are very important to ensure the results of Spatio-temporal dynamics of tree cover. The performance of the distribution model of tree cover was tested using the cross-validation between generated matrices and high-resolution satellite maps from Google Earth. Also, the model accuracy was assessed by calculating the Kappa coefficient (K) (Cohen 1960) using STATISTICA Software (StatSoft 2011). The classification is supposed to be excellent if $K > 0.8$, good if $0.6 < K < 0.8$, moderate when $0.2 < K < 0.6$ and bad when $K < 0.2$ (Landis and Koch 1977).

16.3 Results

16.3.1 Evolution of Tree Cover

The vegetation cover of the Essaouira region has especially covered by argan trees and some agriculture plantations. The occupancy rate of Essaouira argan forests has increased over 11 years in the study area. The total average of the evolution of argan tree occupation rate is 3.22 and 0.92% between 2010–2015 and 2015–2020, respectively with a total of 4.14% (Table 16.4).

Over the years between 2010 and 2015, the tree occupancy rate increased only for the studied area of Ait Issi (21.58%), Ouled Lhaj (19.84%), Retmana (13.74%), Timzgidah Oufetass (8.49%) and Jbel Kourati with only 1.60%. While, the studied

Table 16.4 Evolution of tree occupation rate during the 4 epochs studied

Population	2010–2015 (%)	2015–2020 (%)	Total (%)
<i>Retmana</i>	13.74	0.23	13.97
<i>Ouled Lhaj</i>	19.84	1.00	20.84
<i>Jbel kourati</i>	1.60	3.39	4.99
<i>Mramer</i>	–16.33	0.86	–15.47
<i>Rbaï</i>	–8.17	0.40	–7.77
<i>Tamesart</i>	–0.79	0.03	–0.76
<i>Neknafa</i>	–1.93	0.08	–1.85
<i>Ait Issi</i>	21.58	1.25	22.83
<i>Tmanar</i>	–5.81	0.54	–5.27
<i>Timzgidah Oufetass</i>	8.49	1.43	9.92
<i>Average</i>	3.22	0.92	4.14

area in the other populations has decreased; especially from the argan forest of Mramer; which severely decreased by 16.33%.

While during the epoch between 2015 and 2020, the tree occupancy rate remained practically unchanged in the studied area with a very slight increase, especially for the population of Jbel Kourati (only 3.39%).

Finally, between the 11 years of our study, the tree occupancy rate increased for five studied areas (Ait Issi (22.83%), Ouled Lhaj (20.84%), Retmana (13.97%), Timzgidah Oufetass (9.92%) and Jbel Kourati with only 4.99%) and decrease for the other five areas (Tamesrart (−0.76%), Neknafa (−1.85%), Tmanar (−5.27%), Rbai (−7.77%) and especially from the argan forest of Mramer (−15.47%).

This result is approved by the kappa coefficient calculated from a contingency table with 440 references checked in Landsat maps and high-resolution satellite maps from Google Earth. The kappa coefficient is equal to 0.73, which is supposedly a good classification generated by our study.

16.3.2 Vegetation Indices

The vegetation indices have evolved between the three years studied for all the populations, which reflect a change of density and a dynamic within these argan forests (Table 16.5, Figs. 16.2 and 16.6.3).

Table 16.5 Evolution of vegetation indices between 2000 and 2020 of each argan forest

Population	2010				2015				2020			
	NDVI	EVI	FPAR	LAI	NDVI	EVI	FPAR	LAI	NDVI	EVI	FPAR	LAI
<i>Retmana</i>	0.49	0.33	0.42	0.93	0.44	0.26	0.38	0.81	0.43	0.28	0.38	0.78
<i>Ouled Lhaj</i>	0.55	0.39	0.39	0.84	0.43	0.25	0.31	0.67	0.43	0.28	0.30	0.62
<i>Jbel kourati</i>	0.57	0.32	0.44	0.96	0.50	0.29	0.45	0.97	0.47	0.27	0.36	0.74
<i>Mramer</i>	0.57	0.42	0.42	0.97	0.45	0.31	0.40	0.87	0.42	0.31	0.33	0.72
<i>Rbai</i>	0.48	0.33	0.49	1.09	0.39	0.24	0.38	0.85	0.38	0.25	0.34	0.71
<i>Tamesrart</i>	0.45	0.33	0.47	1.04	0.36	0.27	0.41	0.93	0.32	0.24	0.32	0.68
<i>Neknafa</i>	0.50	0.39	0.42	0.90	0.36	0.27	0.30	0.59	0.34	0.26	0.29	0.58
<i>Ait Issi</i>	0.40	0.22	0.37	0.70	0.37	0.20	0.31	0.60	0.35	0.21	0.31	0.58
<i>Tmanar</i>	0.32	0.22	0.30	0.60	0.25	0.14	0.22	0.40	0.23	0.15	0.22	0.38
<i>Timzgidah Oufetass</i>	0.50	0.33	0.34	0.69	0.43	0.26	0.22	0.40	0.38	0.25	0.32	0.72
<i>Average</i>	0.48	0.33	0.40	0.87	0.40	0.25	0.34	0.71	0.37	0.25	0.32	0.65

NDVI: the Normalized Difference Vegetation Index; **EVI:** the Enhanced Vegetation Index; **FPAR:** the Fraction of Photo-synthetically Active Radiation; **LAI:** the Leaf Area Index

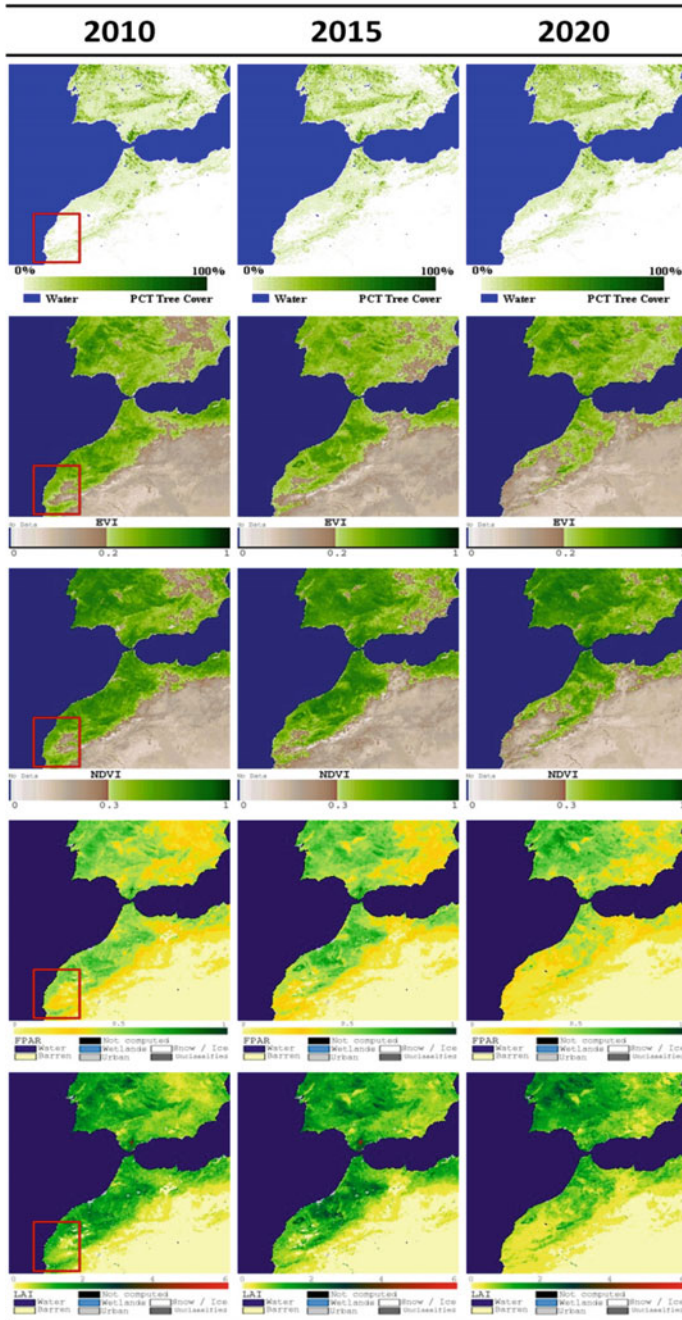


Fig. 16.2 Evolution of tree cover and the four vegetation indices (EVI, NDVI, FPAR and LAI) from h17 v05 map between 2010 and 2020

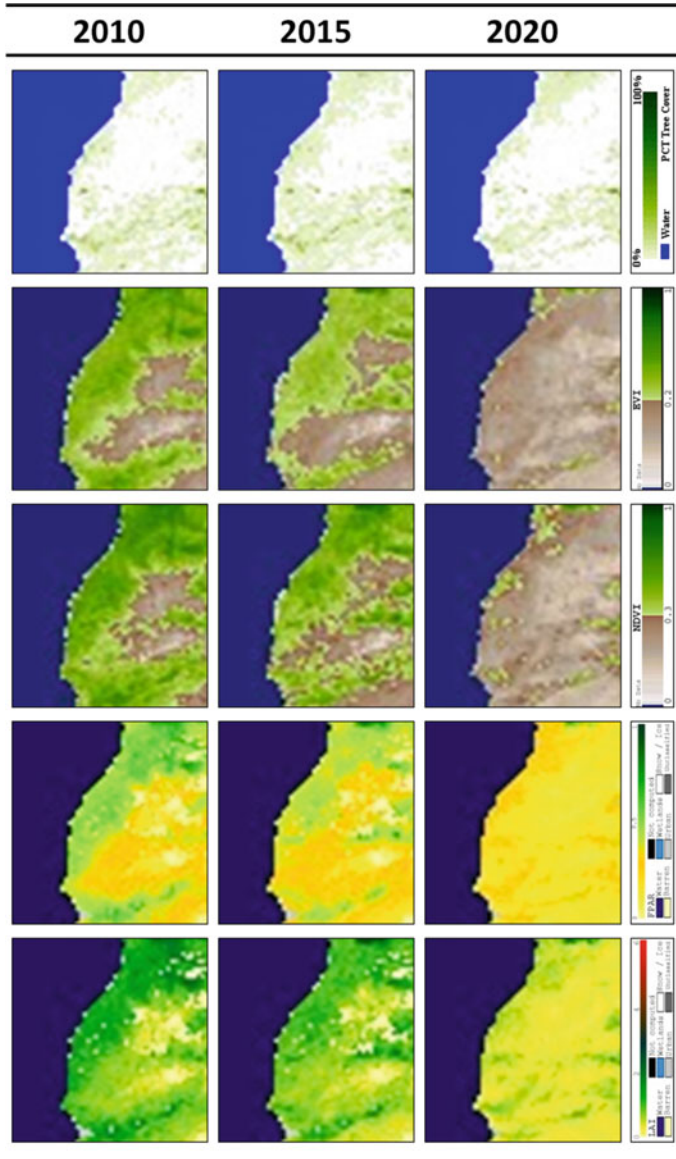


Fig. 16.3 Evolution of tree cover and the four vegetation indices (EVI, NDVI, FPAR and LAI) of study area between 2010 and 2020

The peak values of all vegetation indices were found in 2010. All populations have presented a significant value of NDVI and EVI indices with an average of 0.48 and 0.33 respectively. Also, the LAI and FPAR indices were significant for all populations with an average of 0.87 and 0.40 respectively. The NDVI and EVI indices have a good correlation ($r^2 = 0.70$; $P < 0.01$) and an excellent correlation between LAI and FPAR index ($r^2 = 0.96$; $P < 0.01$).

While in 2015, the values of NDVI and EVI indices decreased but remain significant for all populations except the population of Tmanar. Also, this population and Timzguidah Oufetass have no significant value for the indices of leaf density. We observe a good correlation between NDVI and EVI index ($r^2 = 0.66$; $P < 0.01$) and an excellent correlation between LAI and FPAR index ($r^2 = 0.98$; $P < 0.01$).

Finally, in 2020, the values of NDVI and EVI indices decreased but remained significant for all populations except the population of Tmanar. We observe a good correlation between NDVI and EVI index ($r^2 = 0.73$; $P < 0.01$) and an excellent correlation between LAI and FPAR index ($r^2 = 0.97$; $P < 0.01$).

The results showed by the vegetation indices during the past 11 years confirm the dynamic found in the tree cover of the study area of all argan forests from the Essaouira region. This vegetation dynamics will affect necessarily the genetics of these forests.

16.3.3 Genetic Indices

In the three years of this study (2010, 2015 and 2020), the adaptive power was estimated by the genetic diversity shown in the study area of argan forests. The presence or absence of the 200 trees studied was searched in the Landsat maps (LVCF) and confirmed by their presence in the high-resolution satellite maps from Google Earth.

The estimates of the genetic diversity of *Argania spinosa* L. varied among populations in the Essaouira region during the past 11 years. The averages of genetic diversity indices for 13 microsatellite *loci* calculated on the presence or absence of each tree for each year are given in Table 16.6.

Table 16.6 Evolution of genetic indices between 2010 and 2020

Genetic index	2010	2015	2020
<i>Ar</i>	180	178	176
<i>%P</i>	92.31	96.58	94.45
<i>I</i>	1.48	1.48	1.48
<i>Fst</i>	0.139	0.138	0.139
<i>Nm</i>	1.797	1.770	1.784

Ar: Allelic richness; **%P:** Percentage of polymorphic bands; **I:** Shannon’s information index; **Fst:** Coefficient of gene differentiation; **Nm:** Gene flow

The argan forests of Essaouira have presented a large allelic richness (A_r). A total of 180 alleles in 2010 with an excellent correlation with the evolution of tree cover in the study area. In 2015, the allelic richness has little decreased with 178 alleles and continued to decrease in 2020 with 176 alleles.

Similarly, the measure of Shannon's information index (I) also indicated a high genetic diversity in the populations of argan trees. In 2010, the value of Shannon's information index (I) was 1.48 and remained stable in 2015 and in 2020; suggesting that argan forests are significantly impacted by vegetation dynamics.

In connection, the percentage of polymorphic bands ($\%P$) increased from 92.31% (2010) to reach its maximum of 96.58% in 2015 and slightly decreased in 2020 to 94.45%. On the opposite, the coefficient of gene differentiation (F_{st}) was considerably low and practically unchanged in 2010, 2015 and 2020 with 0.139, 0.138 and 0.139 respectively. Finally, the gene flow (N_m) was also practically unchanged from with 1.797, 1.770 and 1.784 in 2010, 2015 and 2020 respectively.

16.4 Discussion

Environmental change is expected to have a significant impact on species persistence in their current distribution areas and especially the species that can neither accommodate them physiologically nor migrate to a more favourable site, such as forest trees (Pluess et al. 2016; Wan et al. 2016). Its last are known for their great adaptive potential to have local persistence under climate change. However, because of constraints of time, species with long life cycles cannot adapt rapidly through the accumulation of novel mutations (Potvin and Tousignant 1996). Instead, trees can adapt via changes in allele frequencies or genotypic recombination, this microevolution process is probably the key method for locally trees persistence (Bell and Gonzalez 2009). The expected responses of forests to climate change and especially the Mediterranean forests are no insignificant issue, the analysis of which is further complicated by many problems like the fragmentation of existing landscapes (Fibbi et al. 2019).

Our study of an endemic tree species of Mediterranean forests, *Argania spinosa* L., has highlighted associations between genetic diversity and Spatio-temporal dynamics of tree cover over 11 years. This suggests great evolutionary power and natural selection of this species in response to climate change; our results provide indirect evidence of the adaptive power of this tree.

Our analysis of the SSR molecular markers suggests that the argan tree maintained moderate genetic diversity during the two epochs of study, with a coefficient of differentiation among the ten populations estimated at 0.139 in 2010 and 2020, which is lower than previous results for the argan forest based on allozymes ($F_{st} = 0.24$) (Mousadik and Petit 1996), based on ISSR markers ($G_{st} = 0.40$ and $G_{st} = 0.39$) (Yatrib et al. 2015; Mouhaddab et al. 2015) and based on the two combined IRAP and ISSR markers ($G_{st} = 0.5391$) (Pakhrou et al. 2017). However, our result is comparable to that found using the SSR markers ($F_{st} = 0.170$) (Yatrib et al. 2017).

This suggests that, like most other woody species, maintains more variation within species and populations, but less variation among populations, especially since for this study, all ten populations belong to the same region. In addition, the slight decrease in the coefficient of differentiation between the two epochs is probably due to the decrease in allelic richness from 180 (2010) to 176 (2020), as reported by Caballero and Garcia-Dorado (2013); the high allelic richness influences negatively the coefficient of differentiation among populations.

Also, Shannon's information index reflects this high genetic diversity among populations of argan trees with 1.48 between 2010 and 2020 highlighting the importance of intra-specific genetic variation. Recently, Yatrib et al. (2017) have reported that genetic diversity plays a very important role in species evolution, allowing good adaptation to new environments. That is what we can see clearly for the argan forests, since during the two epochs of this study we notice a generally positive average evolution in the selected areas of the ten populations of *Argania spinosa* L. (3.22% (2010–2015) and 0.92% (2015–2020)), testifying of large evolutionary power. Several studies assume that the variation of the characters results from a great potential of plasticity and especially of genetic variation (Moran et al. 2016; Kramer et al. 2010; Valladares et al. 2014). This variation produces an adaptive model of global vegetation dynamics with novel communities of allelic combinations to filter the most competitive alleles and able to coexist in a new environment (Scheiter et al. 2013).

Moreover, the level of G_{st} -based gene flow was practically unchanged between 2010 (1.797) and 2020 (1.784), which suggests that the exchange of genes among populations in the same region was very high. Similar results were found by Yatrib et al. (2017) (1.294) using SSR markers and by Pakhrou et al. (2016) (1.709) using AFLP markers, hence the abundant gene flow among populations might be caused by the pollen and seed movement in particular. This increase in gene flow can suggest that climate change has a great impact on the gene flow among populations to conserve the diversity of the same region; especially since the Argan tree has an entomophilous breeding system. The results of this analysis confirm that the gene flow among populations throughout the entire distribution area is important to prevent population divergence (Wright 1931; Cornille et al. 2015; Martins et al. 2018). Other studies suggest that climate change is expected to impact the diversity and genetic distribution of species (Lyam et al. 2018; Costa e Silva et al. 2018; Razgour et al. 2019).

The density of argan forests showed a variation during the two epochs of the study. The NDVI and EVI indices are relatively high and exceed the thresholds of 0.3 and 0.2 respectively for the two indices, especially in 2010 where a peak of the indices is noted for all populations. This is probably due to climate change that knows the region during the epochs of the study. The study conducted by Hamel et al. (2009) affirmed that the NDVI is a powerful predictor of temporal variations in density in the timing of spring.

The same result was found for the leaf density of trees. The FPAR and LAI indices are moderately high for all argan forests. These two indices are perfectly used to determine leaf density and showed a high precision rate. According to several studies, the precision of FPAR and LAI exceeds 54% on average (reported accuracy

$r^2 = 0.47$, $r^2 = 0.73$, $r^2 = 0.68$ and $r^2 = 0.27$ in mountain areas (Fang et al. 2012; Camacho et al. 2013; Xiao et al. 2014; Jin et al. November 2016).

Finally, the correlation between these vegetation indices and genetic diversity was achieved by the combination of satellite data and molecular data. The two data were positively correlated ($r^2 = 0.73$, $P < 0.01$) suggesting that the argan forests of the Essaouira region have a great genetic diversity correlated with the dynamics of their occupancy rate. Many populations showed a moderate evolution of tree cover and share their alleles with neighbouring populations. Despite this still, the result is alarming in the population of Mramer with regression of -16.33% between 2010 and 2015, knowing that it's the only population differentiated in this region and presents a higher number of unique and rare fragments (Pakhrou et al. 2016). This population should have priority for conservation.

16.5 Conclusion

The novelty of our work lies in its determination of the relationship between genetic diversity and the evolution of the tree cover, which indirectly reflects the climate change in the Essaouira region during the two epochs of the study. The significant positive relationships we observed between vegetation dynamics Spatio-temporal and genetic diversity indicate that climate change plays an important role in shaping the genetic diversity of argan forests. Similarly, many studies suggest that climate change is expected to impact the diversity and genetic distribution of species. Therefore, *Argania spinosa* L. have presented a high genetic diversity with which it adapts remarkably to climate change and it evolved over time.

The occupancy rate of selected areas of natural argan forests has been positive for almost all the populations in the Essaouira region. In addition, appropriate genotypes of the Argan tree may exist that allow adaption to rapid climate change and persistence under global warming. Nevertheless, most of the populations have a moderate tree density and the population of Mramer have a disturbing situation, which requires more effort in terms of preservation and reforestation.

References

- Band LE (1993) Effect of land surface representation on forest water and carbon budgets. *J Hydrol* 150(2–4):749–772
- Bell G, Gonzalez A (2009) Evolutionary rescue can prevent extinction following environmental change. *Ecol Lett* 12(9):942–948
- Caballero A, Garcia-Dorado A (2013) Allelic diversity and its implications for the rate of adaptation. *Genetics* 195(4):1373–1384
- Camacho F, Cernicharo J, Lacaze R, Baret F, Weiss M (2013) GEOV1: LAI, FAPAR essential climate variables and FCOVER global time series capitalizing over existing products. Part 2: validation and intercomparison with reference products. *Remote Sens Environ* 137:310–329

- Chen JM, Black TA (1992) Defining leaf area index for non-flat leaves. *Plant, Cell Environ* 15(4):421–429
- Cohen J (1960) A coefficient of agreement for nominal scales. *Educ Psychol Meas* 20(1):37–46
- Cornille A, Feurtey A, G elin U, Ropars J, Misvanderbrugge K, Gladieux P et al (2015) Anthropogenic and natural drivers of gene flow in a temperate wild fruit tree: a basis for conservation and breeding programs in apples. *Evol Appl* 8(4):373–384
- Costa e Silva J, Harrison PA, Wiltshire R, Potts BM (2018) Evidence that divergent selection shapes a developmental cline in a forest tree species complex. *Ann Bot* 122(1):181–194
- Diao J, Feng T, Li M, Zhu Z, Liu J, Biging G et al (2020) Use of vegetation change tracker, spatial analysis, and random forest regression to assess the evolution of plantation stand age in Southeast China. *Ann for Sci* 77(2):27
- Didan K (2015) MOD13Q1 MODIS/Terra vegetation indices 16-Day L3 Global 250 m SIN grid V006
- DiMiceli CM, Carroll ML, Sohlberg RA, Kim DH, Kelly M, Townshend JRG (2015) MOD44B MODIS/Terra vegetation continuous fields yearly L3 global 250m SIN grid V006. NASA EOSDIS Land Process DAAC. <https://doi.org/10.5067/MODIS/MOD44B.006>
- El Bahloul Y, Dauchot N, Machtoun I, Gaboun F, Van CP (2014) Development and characterization of microsatellite loci for the moroccan endemic endangered species *Argania spinosa* (Sapotaceae). *Appl Plant Sci* 2(4):1300071
- Elliott LJ, Mason DC, Wilkinson MJ, Allainguillaume J, Norris C, Alexander M, et al (2004) Methodological insights: the role of satellite image-processing for national-scale estimates of gene flow from genetically modified crops: rapeseed in the UK as a model. *J Appl Ecol* 41(6):1174–1184
- El Mousadik A, Petit RJ (1996) High level of genetic differentiation for allelic richness among populations of the argan tree [*Argania spinosa* (L.) Skeels] endemic to Morocco. *Theor Appl Genet* 92(7):832–839
- Fang H, Wei S, Liang S (2012) Validation of MODIS and CYCLOPES LAI products using global field measurement data. *Remote Sens Environ* 119:43–54
- Feng M, Sexton JO, Huang C, Anand A, Channan S, Song X-P et al (2016) Earth science data records of global forest cover and change: assessment of accuracy in 1990, 2000, and 2005 epochs. *Remote Sens Environ* 184:73–85
- Fibbi L, Moriondo M, Chiesi M, Bindi M, Maselli F (2019) Impacts of climate change on the gross primary production of Italian forests. *Ann for Sci* 76(2):59
- Gomez C, Batti A, Le Pierri s D, Campa C, Hamon S, de Kochko A et al (2010) Favourable habitats for *Coffea* inter-specific hybridization in central New Caledonia: combined genetic and spatial analyses. *J Appl Ecol* 47(1):85–95
- Guarino L, Jarvis A, Hijmans RJ, Maxted N (2001) Geographic information systems (GIS) and the conservation and use of plant genetic resources. In: International conference on science and technology for managing plant genetic diversity in the 21st century (SAT21). Kuala Lumpur, Malaysia
- Hamel S, Garel M, Festa-Bianchet M, Gaillard J-M, C t  SD (2009) Spring normalized difference vegetation index (NDVI) predicts annual variation in timing of peak faecal crude protein in mountain ungulates. *J Appl Ecol* 46(3):582–589
- HCEFLCD (2013) Le Programme d'Action National de Lutte Contre la D sertification: actualisation et adaptation aux sp cificit s zonales
- Jin H, Li A, Bian J, Nan X, Zhao W, Zhang Z et al (2016) Intercomparison and validation of MODIS and GLASS leaf area index (LAI) products over mountain areas: a case study in southwestern China. *Int J Appl Earth Obs Geoinf* 2017(55):52–67
- Kramer K, Degen B, Buschbom J, Hickler T, Thuiller W, Sykes MT et al (2010) Modelling exploration of the future of European beech (*Fagus sylvatica* L.) under climate change—Range, abundance, genetic diversity and adaptive response. *For Ecol Manage* 259(11):2213–2222
- Landis JR, Koch GG (1977) The measurement of observer agreement for categorical data. *Biometrics* 33(1):159–174

- Lyam PT, Duque-Lazo J, Durka W, Hauenschild F, Schnitzler J, Michalak I et al (2018) Genetic diversity and distribution of *Senegalia senegal* (L.) Britton under climate change scenarios in West Africa. *PLoS One* 13(4):e0194726
- Majourhat K, Jabbar Y, Hafidi A, Martínez-Gómez P (2008) Molecular characterization and genetic relationships among most common identified morphotypes of critically endangered rare Moroccan species *Argania spinosa* (Sapotaceae) using RAPD and SSR markers. *Ann for Sci* 65(8):805–805
- Martins K, Gugger PF, Llanderal-Mendoza J, González-Rodríguez A, Fitz-Gibbon ST, Zhao J-L et al (2018) Landscape genomics provides evidence of climate-associated genetic variation in Mexican populations of *Quercus rugosa*. *Evol Appl* 11(10):1842–1858
- Moran EV, Hartig F, Bell DM (2016) Intraspecific trait variation across scales: implications for understanding global change responses. *Glob Chang Biol* 22(1):137–150
- Mouhaddab J, Ait Aabd N, Achtak H, Msanda F, Zahidi A, Filali-Maltouf A et al (2015) Patterns of genetic diversity and structure at fine scale of an endangered moroccan endemic tree (*Argania spinosa* l. skeels) based on ISSR polymorphism. *Not Bot Horti Agrobot Cluj-Napoca* 43(2):528–535
- Myneni RB, Hall FG, Sellers PJ, Marshak AL (1995) The interpretation of spectral vegetation indexes. *IEEE Trans Geosci Remote Sens* 33(2):481–486
- Nouaim R, Chaussod R, El Aboudi A, Schnabel C, Peltier J (1991) L'arganier. Essai de synthèse des connaissances sur cet arbre. In: Groupe d'Etude de l'arbre. Physiologie des arbres et arbustes en zones arides et semi arides. Paris. Eurotext, John Libbey, pp 373–388
- Pakhrou O, Medraoui L, Yatrib C, Alami M, Filali-maltouf A, Belkadi B (2017) Assessment of genetic diversity and population structure of an endemic Moroccan tree (*Argania spinosa* L.) based in IRAP and ISSR markers and implications for conservation. *Physiol Mol Biol Plants* 23(3):651–661
- Pakhrou O, Medraoui L, Yatrib C, Alami M, Souda-kouraichi SI, El mousadik A et al (2016) Study of genetic diversity and differentiation of argan tree population (*Argania spinosa* L.) using AFLP markers. *Aust J Crop Sci* 10(07):990–999
- Parker WC, Colombo SJ, Cherry ML, Flannigan MD, Greifenhagen S, McAlpine RS et al (2000) Third millennium forestry: what climate change might mean to forests and forest management in Ontario. *For Chron* 76(3):445–463
- Peakall R, Smouse PE (2012) GenALEX 6.5: genetic analysis in excel: population genetic software for teaching and research—an update. *Bioinformatics* 28(19):2537–2539
- Peakall R, Smouse PE (2006) genalex 6: genetic analysis in excel: population genetic software for teaching and research. *Mol Ecol Notes* 6(1):288–295
- Pluess AR, Frank A, Heiri C, Lalagüe H, Vendramin GG, Oddou-Muratorio S (2016) Genome-environment association study suggests local adaptation to climate at the regional scale in *Fagus sylvatica*. *New Phytol* 210(2):589–601
- Potvin C, Tousignant D (1996) Evolutionary consequences of simulated global change: genetic adaptation or adaptive phenotypic plasticity. *Oecologia* 108(4):683–693
- Myneni R, Knyazikhin Y (2015) MOD15A2H MODIS/Terra leaf area index/FPAR 8-Day L4 Global 500 m SIN Grid V006. <https://doi.org/10.5067/MODIS/MOD15A2H.006>
- Razzour O, Forester B, Taggart JB, Bekaert M, Juste J, Ibáñez C et al (2019) Considering adaptive genetic variation in climate change vulnerability assessment reduces species range loss projections. *Proc Natl Acad Sci* 116(21):10418–10423
- Research Systems (2008) ENVI 4.5 research systems, Inc. Boulder
- Sakamoto T, Yokozawa M, Toritani H, Shibayama M, Ishitsuka N, Ohno H (2005) A crop phenology detection method using time-series MODIS data. *Remote Sens Environ* 96(3–4):366–374
- Scheiter S, Langan L, Higgins SI (2013) Next-generation dynamic global vegetation models: learning from community ecology. *New Phytol* 198(3):957–969
- Sexton JO, Song X-P, Feng M, Noojipady P, Anand A, Huang C et al (2013) Global, 30-m resolution continuous fields of tree cover: landsat-based rescaling of MODIS vegetation continuous fields with lidar-based estimates of error. *Int J Digit Earth* 6(5):427–448

- StatSoft (2011) Statistica (data analysis software system), version 10. www.statsoft.com
- Sun L, Schulz K (2017) Spatio-temporal LAI modelling by integrating climate and MODIS LAI data in a mesoscale catchment. *Remote Sens* 9(2):144
- Townshend JR, Masek JG, Huang C, Vermote EF, Gao F, Channan S et al (2012) Global characterization and monitoring of forest cover using Landsat data: opportunities and challenges. *Int J Digit Earth*. 5(5):373–397
- Valladares F, Matesanz S, Guilhaumon F, Araújo MB, Balaguer L, Benito-Garzón M et al (2014) The effects of phenotypic plasticity and local adaptation on forecasts of species range shifts under climate change. *Ecol Lett* 17(11):1351–1364
- Wan J, Wang C, Liu C, Li H (2016) Climate change may alter genetic diversity of *Duchesnea indica*, a clonal plant species. *Biochem Syst Ecol* 66:114–122
- Wright S (1931) Evolution in Mendelian populations. *Genetics* 16(2):97–159
- Xiao Z, Liang S, Wang J, Chen P, Yin X, Zhang L et al (2014) Use of general regression neural networks for generating the GLASS leaf area index product from time-series MODIS surface reflectance. *IEEE Trans Geosci Remote Sens* 52(1):209–223
- Xu X, Du H, Zhou G, Mao F, Li X, Zhu D et al (2018) Remote estimation of canopy leaf area index and chlorophyll content in Moso bamboo (*Phyllostachys edulis* (Carrière) J. Houz.) forest using MODIS reflectance data. *Ann For Sci* 75(1):33
- Yatrib C, Belkadi B, Medraoui L, Pakhrou O, Alami M, El Mousadik A et al (2017) Genetic diversity and population structure of the endangered argan tree (*Argania spinosa* L. Skeels) in morocco as revealed by SSR markers: implication for conservation. *Aust J Crop Sci* 11(10):1304–1314
- Yatrib C, Belkadi B, Pakhrou O, Alami M, Medraoui L, El Mousadik A et al (2015) Assessment of genetic diversity of *Argania spinosa* L. growing in arid and semi-arid areas of Morocco as revealed by inter-simple sequence repeats. *J Agric Sci Technol B* 5(5):336–346
- Yeh F, Yang R, Boyle T, Ye Z, Mao J (1997) PopGene, the user-friendly shareware for population genetic analysis, molecular biology and biotechnology center. <https://www.scienceopen.com/document?vid=5db9fe1d-3632-465d-9e0a-5b2c7f417d08>. Accessed 25 July 2017
- Zietkiewicz E, Rafalski A, Labuda D (1994) Genome fingerprinting by simple sequence repeat (SSR)-anchored polymerase chain reaction amplification. *Genomics* 20(2):176–183

Chapter 17

Deep-PDSC: A Deep Learning-Based Model for a Stage-Wise Classification of Parlatoria Date Scale Disease



Abdelaaziz Hessane, Mohamed Khalifa Boutahir, Ahmed El Youssefi, Yousef Farhaoui, and Badraddine Aghoutane

Abstract Precision agriculture is one of the solutions that has garnered significant attention from specialists recently, as it enables automatic detection and classification of plant and crop diseases, thereby increasing crop quality and yield, and it is also viewed as a tool for taking proactive measures to mitigate natural disasters, whether related to climate change or damage caused by certain insects. In this regard, our current study intends to develop a model for the automatic identification and classification of date palm disease caused by the *Parlatoria* Date Scale insect using deep learning techniques. A novel approach based on the combination of two deep learning algorithms is proposed. The first is a VGG16-based backbone, which was used as a feature extractor, and the second is an improved Fully Connected Neural Network, which was used as a classifier. The proposed model was trained using date palm leaflet RGB images of four categories, three of which are damaged to varying degrees, and one of which is healthy. A comparative study was conducted and demonstrated that the proposed model outperformed with an average accuracy of 98.06%, outpacing existing solution and some state-of-the-art methods. This study is meant to help the development and improvement of oasis agriculture, which relies heavily on palms and dates. It can help farmers and farm owners take preventative measures quickly and thus ensure a high-quality crop.

Keywords *Parlatoria* date scale · Precision farming · Deep learning · CNN · FCNN · Oasis agriculture · Date palm diseases

A. Hessane (✉) · M. K. Boutahir · A. El Youssefi · Y. Farhaoui
STI Laboratory, T-IDMS, Department of Computer Sciences, Faculty of Sciences and Techniques of Errachidia, Moulay Ismail University of Meknès, Errachidia, Morocco
e-mail: a.hessane@edu.umi.ac.ma

B. Aghoutane
IA Laboratory, Department of Computer Science, Faculty of Sciences, Moulay Ismail University of Meknès, Meknes, Morocco

17.1 Introduction

Date palm cultivation is a crucial component of any oasis farming system due to the ability of date palms to be planted and grown in arid and semi-arid climates. In Morocco, the cultivated area of this valuable tree—renowned for its economic and nutritional worth—exceeds 50,000 acres, with about 5 million trees, accounting for 4.8 percent of the world’s date palm heritage. It is primarily concentrated along the Ziz and Drâa valleys (Les chiffres clés de la filière Phoeniculture—Fellah Trade 2022; Sedra et al. 2015; Bakouri et al. 2021). Palm trees, like all plants, are susceptible to a range of diseases, including those caused by certain destructive insects. In Moroccan palm groves, the white cochineal, or “white scale”, is the most prevalent pest (TourerN 1967). The sucking bug (*Parlatoria blanchardii* T) can inflict significant harm in some areas, particularly on young palms, up to the point of death. Crusting affects the chlorophyll assimilation process, resulting in a qualitative and quantitative reduction in yield (Moulay Hassan Sedra 2003). Figure 17.1 demonstrates the evolution of date palm white scale infestation degree over time (Gassouma 2003).

In traditional pest management systems (PMS), determining the disease’s degree of infestation requires regular monitoring and sometimes manual counting of insects in infected parts of the trees, which is laborious and time-consuming. Fortunately, this process can be automated thanks to recent technologies, namely, machine learning-based detection and classification of plant diseases (Sharma et al. 2021), computer vision (Tian et al. 2020), and other recent technologies such as the Internet of Things (Raj 2021). Recently, the rapid advancement that has taken place in the field of artificial intelligence, especially in the sub-field of deep learning, has pushed researchers to expand its applications to other areas, including but not limited to natural language processing (NLP) (Otter et al. 2018), healthcare (Jiang et al. 2017), and agriculture (Santos et al. 2020).

In this study, we propose a novel deep learning-based model for a stage-wise classification of the date palm disease caused by the *Parlatoria* Date Scale (PDS). The main contributions of this work are:

Fig. 17.1 Various infestation degrees by *parlatoria* date scale. Photo/illustration by: Gassouma S. (2003–07-22)



- The development and implementation of a new deep learning architecture for the automatic detection and classification of white scale disease in date palms by investigating images of leaflets according to the degree of the infestation.
- The test of the model's performance using several evaluation metrics.
- The performing of a comparative study which demonstrates the effectiveness of the proposed solution over some state-of-the-art methods and over existing approaches.

The remaining sections of this work are structured as follows. Section 17.2 covers the numerous ways now used to classify plant diseases automatically using deep learning. In Sect. 17.3, the dataset, techniques, and experiments are discussed. The outcomes were discussed in Sect. 17.4. The concluding section of this work is Sect. 17.5.

17.2 Related Works

The use of traditional image recognition has shown promising results in identifying plant and crop diseases (Vishnoi et al. 2022). However, these systems are based on cumbersome and time consuming steps such as images preprocessing and artificial features extraction, the latter is labor intensive as it requires a lot of experiments to find the appropriate characteristics vector (Li et al. 2021). As a result, it is critical to diagnose plant leaf diseases intelligently, rapidly, and accurately. In recent years, progress has been made in the field of plant disease recognition using deep learning techniques. Deep learning (DL) technology does not require a high level of expertise in plant protection or statistics and can be used to automatically extract image features and classify plant diseases, thus eliminating the time and effort required by traditional image recognition methods for feature extraction. These traits have prompted extensive interest in deep learning approaches for plant disease recognition, which has developed into a hot research topic.

Al-Wesabi et al. (2022) proposed a novel intelligent apple leaf disease classification method based on Capsule Network (CapsNet) and Bidirectional Long Short-Term Memory (BiLSTM). The CapsNet backbone was used for the feature's extraction process, and the BiLSTM for classification. The classification accuracy of the proposed method reached 99.20%. A deep learning segmentation approach is proposed by Kerkech et al. (2020) to detect mildew diseases in vine fields. In this study, visible and infrared images were captured using two sensors deployed on an unmanned aerial vehicle (UAV) and used to train a SegNet model, the latter reached about 92% of accuracy. Mishra et al. (2020) proposed a real time method based on a fine tuned deep convolutional neural network (DCNN) for corn leaf disease recognition. To create a lighter network for real time inference, layer-wise feature visualization was performed to decide which layers to keep and which one to remove which leads to the reduction of learning parameters. The accuracy of proposed approach reached 98.40% while the modified version of the DCNN mainly

designed for real time inference outperforms with an average accuracy of 88.66%. Pretrained VGG19 neural network and a pyramid histogram of oriented gradient (PHOG) contour feature-based approach were combined to extract features from the Fruit-360 dataset's images as reported by Nasir et al. (2020). For the classification phase, various classifiers were evaluated and the cubic SVM demonstrated the best result with an accuracy of 99.6%. Guo et al. (2020) suggested a three-module methodology for identifying diverse plant diseases. The region proposal network (RPN) was utilized to identify the region of interest (RoI). Following that, the Chan-Vese algorithm was used to extract the symptoms' features. Finally, a transfer learning model previously trained on a dataset of unhealthy leaves on a plain background is utilized to identify plant diseases in the surrounding environment. This approach produced an accuracy of 83.57%. Boulent et al. (2020) employed a fine-tuned ResNet-18 architecture as a pre-identification model and then converted it to a Fully Connected Network (FCN) that provided segmentation of areas showing Flavescence Dorée symptoms. The proposed approach performs admirably when it comes to classifying Chardonnay, with an accuracy of 98.48%. However, it failed to classify other varieties such as Ugni-Blanc. Schirrmann et al. (2021) proposed a deep residual neural network (ResNet) for early detection of stripe rust in winter wheat. The image classifier achieved a total accuracy of 90% at the patch level and 77% at the image level. Lee et al. (2020) investigated the limitations of convolutional neural networks (CNN) in detecting and classifying plant and crop diseases, intending to develop a new attention-based technique that considers only the unhealthy part of the plant and extracts features from those regions of interest. Their solution is based on a recurrent neural network (RNN), and it performs well on numerous datasets when tested. Nalini et al. (2021) developed a novel deep neural network (DNN) classification model for rice leaf disease detection utilizing plant image data. The Crow Search Algorithm (CSA) was used to optimize the proposed model throughout pre-training and fine-tuning procedures. This DNN-CSA architecture permits straightforward statistical learning techniques with a reduced computing load while maintaining good classification accuracy of about 96.96% compared experimentally with that of an SVM algorithm under multiple cross-fold validations.

In the context of the automatic detection and classification of the disease caused by PDS, Hessane et al. (2022) proposed a system based on feature extraction and machine learning to classify infected date palm leaflets according to the stage of infestation. They proposed the combination of HSV color descriptors and the gray level co-occurrence matrix-based texture properties and used them as inputs for a k-nearest neighbor classifier to perform the classification task. The developed framework's performance achieves about 97% accuracy. However, the proposed approach requires feature engineering, which is time-consuming.

17.3 Methods and Experiments

In this paper, we proposed a deep learning-based model to automatically classify the degree of infestation by PDS. For this purpose, we used multiclass images of healthy and infected date palm leaflets at varying stages. Firstly, a VGG16 backbone was utilized as a feature extractor. Then, a fine-tuned Fully Connected Network (FCNN) was mainly designed to perform the final classification task. In addition, dropout layers were introduced on the FCNN model to regularize it, and the leakyRelu activation function was employed to avoid the dying ReLU problem. In what follows, we briefly present the used dataset, the architecture of the proposed framework, the performed tests, and the metrics we used to evaluate the model.

17.3.1 Dataset

The dataset utilized in the context of this study is a subset of an existing open-access dataset (Date Palm data 2022). It contains date palm leaflets RGB images split into four categories: Healthy, low, medium, and high infestation degree as illustrated in Fig. 17.2. First, data augmentation is performed to avoid the underfitting problem. After that, a total of 6228 images are generated. 80% of the dataset is used for training purposes, and the rest 20% for validation. Finally, we performed some data preprocessing techniques such as resizing and scaling to guarantee that the data satisfied the input requirements of tested models.

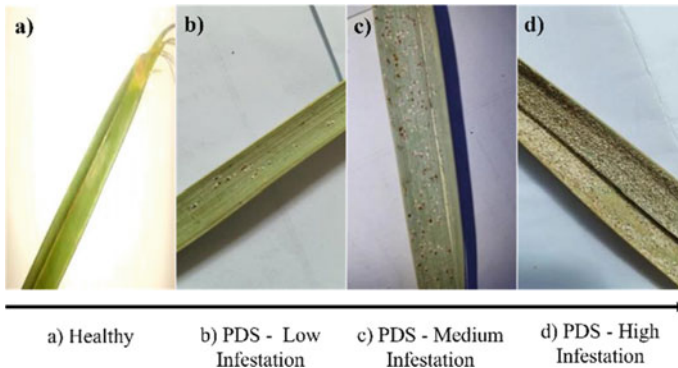


Fig. 17.2 Image samples from the used dataset

17.3.2 Proposed Framework

After data preparation, we evaluated multiple deep learning models. A few numbers of iterations were sufficient to notice that the generalization was unsatisfactory. To overcome this, we proposed to work on the final classification process. The objective is to improve the classification performance by alternating classifiers, finetuning, regularizing, and evaluating additional activation functions. Figure 17.3 depicts the suggested model’s general architecture.

Feature’s Extraction Process Using the VGG-16 Backbone

Initially designed for image recognition and classification tasks, Convolutional Neural Networks (CNNs) are architectures typically consist of two distinct components. The first, referred to as the backbone, is responsible for feature extraction based on the succession of convolution and sampling layers, while the final layer is responsible for classification. Figure 17.4 illustrates the general architecture of CNN (Gu et al. 2019).

In the context of this work, a VGG16 backbone is used as a feature extractor. VGG16 was proposed by Simonyan and Zisserman (2014) for object detection and image classification. Thanks to its sixteen learnable parameters layers, this CNN

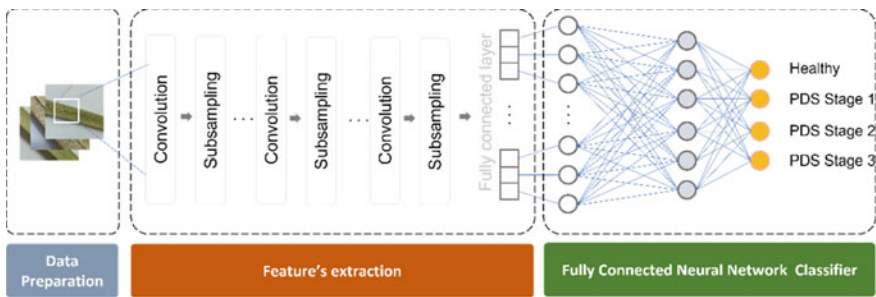


Fig. 17.3 Proposed framework

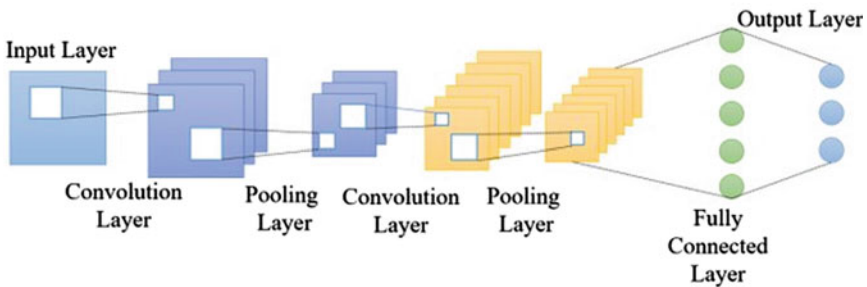


Fig. 17.4 Architecture of Convolutional Neural Network

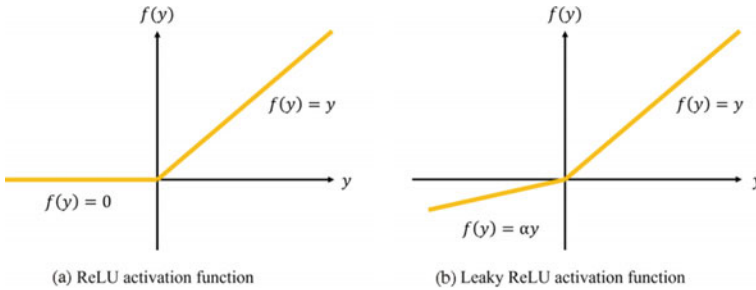


Fig. 17.5 Mean difference between ReLU and Leaky ReLU activation function

showed strong performance of abovementioned tasks. Moreover, the VGG16 architecture propose thirteen convolutional layers, five max pooling layers and three dense layers.

Classification Process Using Fully Connected Neural Network

In this work, a fine-tuned Fully Connected Neural Network (FCNN) classifier was considered. FCNN is a structure-agnostic model, which means that no specific assumptions about the input are required. Owing to the backpropagation technique, the model train and its parameters can be adjusted (i.e., weights and biases).

Activation function, finetuning and regularization

Leaky Rectified Linear Unit (Leaky ReLU) is utilized instead of Rectified Linear Unit (ReLU) as the activation function in this classification model to overcome the dying ReLU problem (Xu et al. 2015). The latter arises when the learning rate is very high or when there is a large negative bias. If a ReLU neuron is locked on the negative side and produces zero continuously, it is considered “dead”. The Leaky ReLU parameter alpha represents the negative slope of ReLU. Figure 17.5 depicts the distinction between the two functions.

In order to avoid overfitting issues, we incorporated dropout layers (Srivastava et al. 2014) within the FCNN classifier. The dropout mechanism arbitrarily neglects some neurons. On the forward pass, the influence of any weight updates on the activation of downstream neurons is momentarily nullified, and no weight updates are applied to the cell. Ultimately, the hyperparameters fine-tuning procedure yields ideal hyperparameters. The complete design of the improved FCNN classifier is depicted in Fig. 17.6. After obtaining the features from the features extraction step, we transformed them into a one-dimensional vector of 4096 values to represent the FCNN’s input layer. The latter is followed by three hidden layers with 100, 100, and 50 neurons, respectively. Each hidden layer is followed by a dropout layer of 50%, except for the last one where the rate of dropped neurons was reduced to 30%. In place of the ReLU activation function, the leaky ReLU activation function with parameter $\alpha = 0.3$ was employed after the drop out layers.

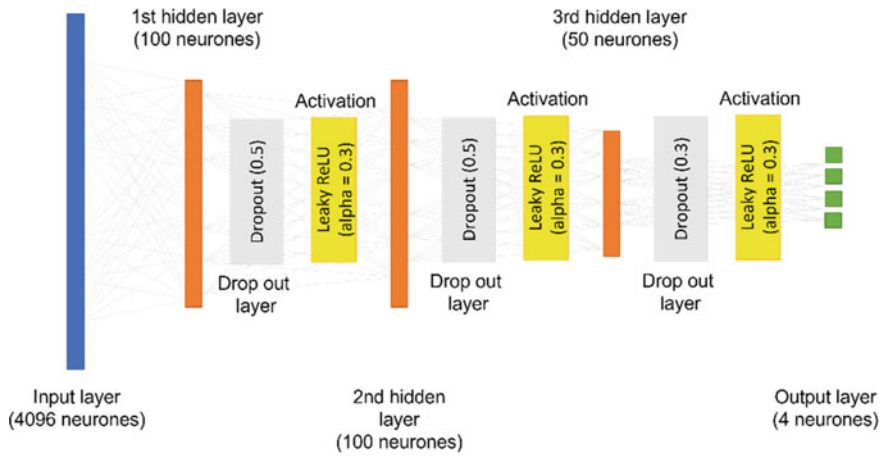


Fig. 17.6 Proposed classifier architecture

Table 17.1 Tested model's parameters

Batch size	32
Epochs	100
Learning rate	Adaptive
Optimizer algorithm	Adam
Loss function	Categorical_crossentropy

Table 17.2 Specs of used machine

GPU	GPU RAM	CPU	RAM	Storage
Nvidia M4000 and P5000 GPUs	8 Gb	8 × vCPU	30 Gb	5 Gb

17.3.3 Performed Tests

To determine the efficacy of the proposed adjustments, we conducted several experiments. First, we evaluated the performance of the proposed model with that of certain cutting-edge deep learning models, and secondly with transfer learning-based models. The comparison techniques emphasize the improvement of learning and validation accuracy over time. As reported in Table 17.1, parameters such as batch size, epochs, and optimizer were the same for all evaluated models.

All the experiments were performed using the gradient tools offered by paperspace¹ with the machine properties described in Table 17.2.

¹ <https://www.paperspace.com/gradient>.

17.3.4 Evaluation Metrics

Multiple metrics were employed to assess the performance of the suggested model. Initially, the accuracy, precision, recall, and f1 score were computed. In addition, we produced the confusion matrix since it provides a comprehensive yet exact perspective of the model's effectiveness per class. Precision is calculated by dividing the number of accurate predictions (TP) by the total number of predictions produced by the model. Recall is calculated by dividing the number of true positives (TP) by the sum of true positives and false negatives (FN). The F1 score is a weighted mean of recall and precision. The accuracy is determined by dividing the total number of correctly identified examples by the total number of samples. The precision, recall, f1 score, and accuracy formulas are provided in Eqs. 17.1, 17.2, 17.3, and 17.4, respectively.

$$precision = \frac{TP}{TP + FP} \quad (17.1)$$

$$recall = \frac{TP}{TP + FN} \quad (17.2)$$

$$accuracy = \frac{TP + TN}{TP + TN + FP + FN} \quad (17.3)$$

$$f1\ score = \frac{2(Recall \times Precision)}{Recall + Precision} \quad (17.4)$$

17.4 Results and Discussion

To evaluate the effect of introduced improvements on the classification process, we compared the training and validation accuracy of the proposed model with several CNN algorithms. We defined a set of callbacks to monitor the metrics and to stop the training process when no improvement is noted. Figures 17.7 illustrated the training and validation accuracy over time of tested models. VGG16-based model performances were not good enough when training from scratch, we obtained the best accuracy after only 22 epochs, and the performance didn't improve. The approach of transfer learning demonstrates an improvement in terms of inference. However, due to the similarity between the healthy samples and low infestation degree samples on the one hand, and between medium infestation and low infestation categories, on the other hand, it shows some poor generalization, as seen in Fig. 17.8b, c. The proposed model depicted in Fig. 17.8d shows a significant improvement in accuracy and generalization; the gap between training and validation accuracy is reduced. Moreover, the

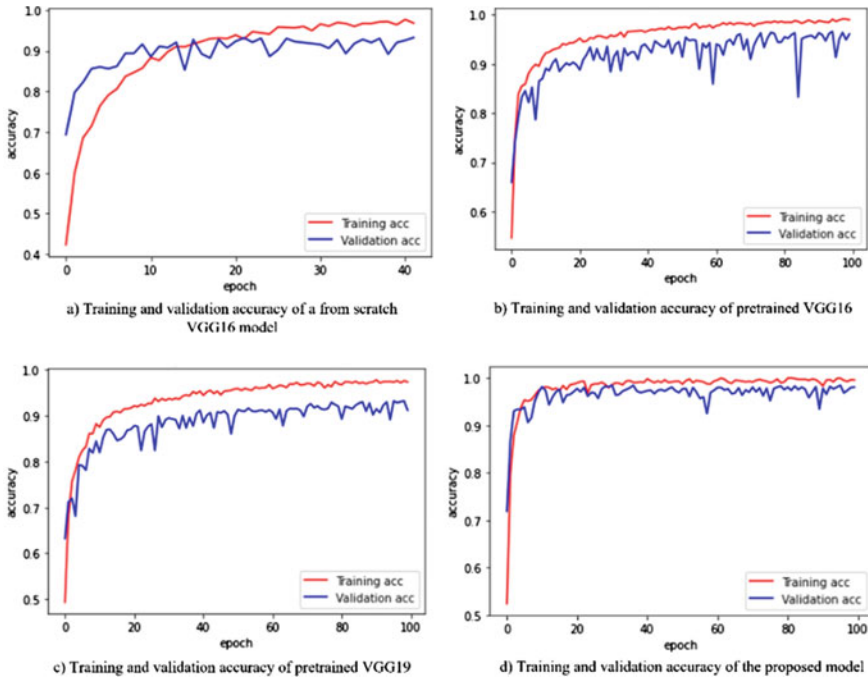


Fig. 17.7 Learning curves of tested models

proposed model outperforms some state-of-the-art deep learning models, as demonstrated in Table 17.3. The improvement ranges from 0.80 to 5.25% when compared with models from scratch, such as vgg16, DenseNet121, NasNetMobile, MobileNet, Xception and InceptionV3, and from 2,10 to 7,49% when compared with pre-trained models specifically pre-trained vgg16 and vgg19 models.

The results are supported by the confusion matrix depicted in Fig. 17.8, which displays considerable false negatives (FN) and false positives (FP) for the first three classes. Although the model accuracy is ideal for high infestation samples, this is to be expected given that the texture and color properties of the leaflets provided in this class are easily distinguishable.

Lastly, stage-wise metrics are reported in Table 17.4, illustrating and confirming the ability of the proposed model to accurately classify healthy and high infestation samples while presenting some misclassified samples for low and medium infestation samples.

Fig. 17.8 Confusion matrix of proposed model

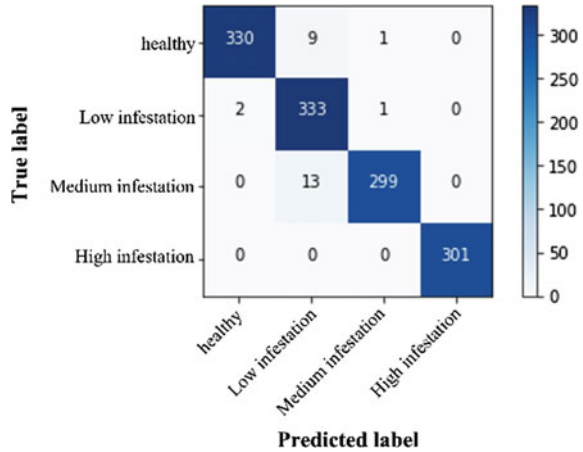


Table 17.3 Accuracy comparison

Model	Accuracy (%)
VGG16	93.17
DenseNet121	97.28
MobileNet	97.21
Xception	95.89
InceptionV3	95.11
NasNetMobile	94.80
Pretrained VGG16	96.04
Pretrained VGG19	91.23
Proposed model	98.06

Table 17.4 Stage-wise metrics

Class	Stage-wise evaluation metrics		
	Precision	Recall	F1 score
Healthy	1.00	0.97	0.99
Low infestation	0.94	0.99	0.96
Medium infestation	0.99	0.96	0.98
High infestation	1.00	1.00	1.00

17.5 Conclusion and Perspectives

This paper establishes a new deep learning model to classify the degree of infestation by the Parlatoria Date Scale. Images of date palm leaflets belonging to four classes: healthy, low, moderate, and high degree infection were used to train and to validate the proposed architecture. The latter consists of two modules; the first is the

feature extraction module, which employs the VGG16 backbone to extract a unidimensional vector of 4096 values. The second module is a refined FCNN developed and enhanced to perform classification tasks using the previously generated features as input. The suggested model outperforms the previous solution by 98.06% accuracy and outperforms other deep learning techniques. In addition, the proposed method is quasi-independent, as no human feature engineering is required. Despite this, it nonetheless contains engaging resources due to the complexity of its constituents. To circumvent this limitation, our future works will focus on developing and testing lightweight models by utilizing and developing pruning approaches. In addition, more models based on deep learning and transfer learning must be investigated for the automatic classification of date palm diseases which is a critical aspect of accurate oasis agriculture.

References

- Al-Wesabi FN, Abdulrahman Albraikan A, Mustafa Hilal A, Eltahir MM, Ahmed Hamza M, Sarwar Zamani A (2022) Artificial intelligence enabled apple leaf disease classification for precision agriculture. *Comput Mater Contin* 70(3):6223–6238. <https://doi.org/10.32604/cmc.2022.021299>
- Boulent J, St-Charles P-L, Foucher S, Théau J (2020) Automatic detection of flavescence Dorée symptoms across white grapevine varieties using deep learning. *Front Artif Intell* 3. <https://doi.org/10.3389/frai.2020.564878>
- Date Palm data | Kaggle (2022) <https://www.kaggle.com/hadjerhamaidi/date-palm-data>. Accessed 30 Jan 30 2022
- El Bakouri Z, Meziani R, Mazri MA, Chitt MA, Bouamri R, Jaiti F (2021) Estimation of the production cost of date fruits of cultivar majhoul (<i>Phoenix dactylifera</i> L.) and evaluation of the moroccan competitiveness towards the major exporting regions in the world. *Agric Sci* 12(11):1342–1351. <https://doi.org/10.4236/as.2021.1211086>
- Gassouma MS (2003) Parlatoria date scale infestation variations. <http://ecoport.org/>. <http://ecoport.org/ep?SearchType=pdb&PdbID=33531>
- Gu H, Wang Y, Hong S, Gui G (2019) Blind channel identification aided generalized automatic modulation recognition based on deep learning. *IEEE Access* 7:110722–110729. <https://doi.org/10.1109/ACCESS.2019.2934354>
- Guo Y et al (2020) Plant disease identification based on deep learning algorithm in smart farming. *Discret Dyn Nat Soc* 2020. <https://doi.org/10.1155/2020/2479172>
- Hessane A, El Youssefi A, Farhaoui Y, Aghoutane B (2022) Toward a stage-wise classification of date palm white scale disease using features extraction and machine learning techniques. In: 2022 international conference on intelligent systems and computer vision (ISCV), May 2022, pp 1–6. <https://doi.org/10.1109/ISCV54655.2022.9806134>
- Jiang F et al (Dec.2017) Artificial intelligence in healthcare: past, present and future. *Stroke Vasc Neurol* 2(4):230–243. <https://doi.org/10.1136/svn-2017-000101>
- Kerkech M, Hafiane A, Canals R (2020) Vine disease detection in UAV multispectral images using optimized image registration and deep learning segmentation approach. *Comput Electron Agric* 174. <https://doi.org/10.1016/j.compag.2020.105446>
- Les chiffres clés de la filière Phoeniculture—Fellah Trade. <https://www.fellah-trade.com/fr/filiere-vegetale/chiffres-cles-phoeniculture> . Accessed 13 Apr 2022
- Lee SH, Goëau H, Bonnet P, Joly A (2020) Attention-Based recurrent neural network for plant disease classification. *Front Plant Sci* 11. <https://doi.org/10.3389/fpls.2020.601250>

- Li L, Zhang S, Wang B (2021) Plant disease detection and classification by deep learning—a review. *IEEE Access* 9:56683–56698. <https://doi.org/10.1109/ACCESS.2021.3069646>
- Mishra S, Sachan R, Rajpal D (2020) Deep convolutional neural network based detection system for real-time corn plant disease recognition. *Procedia Comput Sci* 167:2003–2010. <https://doi.org/10.1016/j.procs.2020.03.236>
- Nalini S et al (2021) Paddy leaf disease detection using an optimized deep neural network. *Comput Mater Contin* 68(1):1117–1128. <https://doi.org/10.32604/cmc.2021.012431>
- Nasir IM et al (2020) Deep learning-based classification of fruit diseases: an application for precision agriculture. *Comput Mater Contin* 66(2):1949–1962. <https://doi.org/10.32604/cmc.2020.012945>
- Otter DW, Medina JR, Kalita JK (2018) A survey of the usages of deep learning in natural language processing, July 2018. <http://arxiv.org/abs/1807.10854>
- Raj M et al (2021) A survey on the role of Internet of Things for adopting and promoting Agriculture 4.0. *J Netw Comput Appl* 187. <https://doi.org/10.1016/j.jnca.2021.103107>
- Santos L, Santos FN, Oliveira PM, Shinde P (2020) Deep learning applications in agriculture: a short review, pp 139–151
- Schirmann M, Landwehr N, Giebel A, Garz A, Dammer K-H (2021) Early detection of stripe rust in winter wheat using deep residual neural networks. *Front Plant Sci* 12. <https://doi.org/10.3389/fpls.2021.469689>
- Sedra MH (2003) The date palm tree as base of oases development in Morocco: agricultural technics and oases creation
- Sedra MH (2015) Date palm status and perspective in Morocco. In: Al-Khayri JM, Jain SM, Johnson DV (eds) *Date palm genetic resources and utilization*, vol 1. Springer, Netherlands, Dordrecht, pp 257–323
- Sharma A, Jain A, Gupta P, Chowdary V (2021) Machine learning applications for precision agriculture: a comprehensive review. *IEEE Access* 9:4843–4873. <https://doi.org/10.1109/ACCESS.2020.3048415>
- Simonyan K, Zisserman A (2014) Very deep convolutional networks for large-scale image recognition, Sep 2014. <http://arxiv.org/abs/1409.1556>
- Srivastava N, Hinton G, Krizhevsky A, Salakhutdinov (2014) Dropout: a simple way to prevent neural networks from overfitting
- Tian H, Wang T, Liu Y, Qiao X, Li Y (Mar.2020) Computer vision technology in agricultural automation—a review. *Inf Process Agric* 7(1):1–19. <https://doi.org/10.1016/j.inpa.2019.09.006>
- TourerN G (1967) *Le palmier dattier culture et production*. Al awamia
- Vishnoi VK, Kumar K, Kumar B (Jan.2022) A comprehensive study of feature extraction techniques for plant leaf disease detection. *Multimed Tools Appl* 81(1):367–419. <https://doi.org/10.1007/s11042-021-11375-0>
- Xu B, Wang N, Chen T, Li M (2015) Empirical evaluation of rectified activations in convolutional network, May 2015. <http://arxiv.org/abs/1505.00853>

Chapter 18

Adsorption of Inorganic and Organic Pollutants in Urban Wastewater Treatment Using Pine Wood Activated Carbon



Karima Azoulay, Imane Bencheikh, Mohammed Benchrifa, Meryem Ben Baaziz, and Jamal Mabrouki

Abstract Water pollution is a physical, chemical, biological or bacteriological degradation of its natural qualities, caused by man and his activities. Also is caused by the discharge of water soiled by our domestic activities (washing and cleaning, evacuation of our urine and faeces, etc.) or by the various industrial and agricultural activities, necessary to provide the food and goods we need. During this work, we focused on reducing the abatement rate of urban wastewater by adsorption method using commercial activated carbon. Different experimental parameters were analyzed: contact time and adsorbent mass. The experimental results made it possible to determine the contact time and the optimal mass of activated carbon for BOD₅, COD and TSS ($t = 180$ min and $m = 1$ g). Kinetic study results show that equilibrium is established after 180 min and that the pseudo-second-order model describes our absorption phenomenon well.

Keywords Adsorption · Organic and inorganic pollutants · Urban wastewater

18.1 Introduction

Wastewater treatment plants are the receptacle for a very wide variety of wastewater to be treated. They can be from domestic, industrial or craft activities and from health care activities. These effluents contain numerous chemical substances, some of which are qualified as “micropollutants” because they are present in very low concentrations, in the order of nanograms to micrograms per liter. Micropollutants are inorganic or organic molecules that can have negative impacts on ecosystems and

K. Azoulay (✉) · I. Bencheikh · M. Benchrifa · J. Mabrouki
Mohammed V University in Rabat, Rabat, Morocco
e-mail: karima.azoulay@um5r.ac.ma

M. B. Baaziz

Laboratory of Materials Engineering for the Environment and Natural Resources, Department of Chemistry, Faculty of Science and Technology, Moulay Ismail University, 52000 Errachidia, Morocco

the environment. These micropollutants can contain toxic elements that are harmful to health, leading to the damage of the quality of water resources (Samuel 2010). And for the preservation of the latter, the discharge of wastewater must be authorized by the AHBT (Agency of the hydraulic basin of Oued Tensift) as stipulated in the law n°36–15 fixing the limit values of rejection to respect (Haytem and Boumenkar terek 2019). The protection of the environment includes all measures to safeguard the health of humans, animals and plants, preventing any pollution or alteration of the air, soil, surface and groundwater and avoiding the defacement of the landscape (Reporterre 2020). In a world where the demand for freshwater is steadily increasing, and where limited water resources are increasingly under stress from overexploitation, pollution, and climate change, it is simply unthinkable to overlook the opportunities that improved wastewater management offers. This is the conclusion of the World Water Development Report 2017, which highlights the critical importance of improved wastewater management to our shared future. To maintain our current habits is to encourage the worsening of already considerable neglect (WWAP 2017; Crini et al. 2007). European regulations, in particular through the Water Framework Directive (Directive 2000/60/EC or WFD) and the latest Directive 2013/39/EU, defines a list of 45 priority substances for which environmental quality standards must be respected. Environmental quality standards must be met. These substances include trace metals (TMEs) and trace organic compounds (TOCs). To date, Morocco has established a policy based on the participation of the representatives concerned to monitor the emissions of micropollutants in the natural environment and in the wastewater treatment plants (WWTP). For this reason, Morocco has decided to commit itself to carry out numerous studies to get an idea of the nature of the micropollutants found in surface waters or discarded from wastewater treatment plants (WWTPs). To this end, to monitor water quality, adequate instruments have to be developed. In addition, the treatment processes must be improved to treat the micropollutants found (Demirbas 2009; Bliefert and Perraud 2001). The adsorption technique is the most favorable method for the removal of inorganic and organic pollutants. It has become the analytical method of choice, very efficient and simple in its use (Azoulay et al. 2021). The principle of adsorption treatment is to trap pollutants in solid materials called adsorbents. In the literature, there are several solid materials (biomass, polymer, activated carbon, sludge, waste agricultural...) that can be used in wastewater removal processes (Bencheikh et al. 2021). The present study deals with the reduction of the abatement rate of urban wastewater by the adsorption method using activated carbon prepared from raw material (pine wood).

18.2 Materials and Methods

18.2.1 Materials

Preparation and characterization of activated carbon AC. Activated carbon (AC) is considered a reference material in water treatment due to its ability to remove a wide range of inorganic and organic pollutants. The activated carbon (AC) used in this study was recovered from LABOSI, France. It is prepared from the raw material (pine wood) but has undergone different treatments to acquire the properties described in Table 18.1.

Physico-chemical characteristics of urban wastewater. We chose purified water generated from an urban wastewater treatment plant to reduce the physico-chemical parameters by the adsorption method as a finishing method. Table 18.2 shows the physicochemical characteristics of raw and treated water on which the adsorption experiments will be performed.

Table 18.1 Characteristics of activated carbon used in our study (supplier data)

Properties	Carbon
Vendor	LABOSI, France
Particle size	~40 μm
BET specific surface	1050 $\text{m}^2 \text{g}^{-1}$
Raw material	Pinewood
Activation	Physics
Character	Basic
C in %	84.2
H in %	1
N in %	0.6
O in %	1.77

Table 18.2 Physico-chemical characterization of raw and purified water on which the adsorption experiments will be performed (Mabrouki et al. 2022)

Parameters	Raw water	Purified water	Standard Moroccan (Mabrouki et al. 2022)	Discharge Limit Values (Mabrouki et al. 2022)	
				Direct	Indirect
pH	7.91	7.89	5.5–9.5	6.5–8.51	6.5–8.51
T ($^{\circ}\text{C}$)	21	20	30	30	35
TSS (mg/L)	690	325	150	50	600
COD (mg O ₂ /L)	907	482	250	500	1000
BOD ₅ (mgO ₂ /L)	480	220	120	100	500

18.2.2 Experimental Methods

Determination of the hydrogen potential (pH). The pH was measured using the HACH model Sension 2 portable pH meter, with automatic temperature compensation. Before each measurement, a systematic calibration of the apparatus was carried out (accuracy ± 0.01).

Determination of the temperature. The temperature in $^{\circ}\text{C}$ was measured using a portable EUTECH instruments probe (Fisher Bioblock, France).

Determination of Chemical Oxygen Demand (COD). The organic pollutants were determined globally by COD measurement. The principle of this determination is based on the oxidation by an excess of potassium dichromate in an acid medium and boiling of the oxidizable materials contained in the aqueous solution analyzed, in the presence of silver sulfates as catalyst and mercury sulfate as complexing agent (Mabrouki et al. 2019).

Determination of the Biological Oxygen Demand after 5 days (BOD₅). The Biochemical Oxygen Demand determines the amount of oxygen, expressed in milligrams, that is consumed under the test conditions (incubation for five days, at 25 $^{\circ}\text{C}$ and in the dark) by certain materials present in a litre of water, in particular, to ensure their degradation (Mabrouki et al. 2019). The principle of this determination is based on the oxygen consumption of the medium under study compensated by a supply of pure oxygen. The measurement of the quantity of oxygen with time corresponds to the Biochemical Oxygen Demand of the medium under the given conditions. The measurement of COD and BOD₅ is carried out by a HACH-type oximeter model HQ10.

Suspended solids (SS). Total Suspended Solids (TSS) presents the amount of organic and inorganic pollutants and mineral pollutants not dissolved in water (EMabrouki et al. 2021). It is determined by quantitative analysis gravimetric method) according to the standard NF EN 1234-June 2014. For this purpose, a volume V (200 ml) of the water sample to be analyzed is taken and poured onto a previously weighed filter paper ($M1$). This filter paper containing the sample is then introduced into the oven at 105 $^{\circ}\text{C}$ for a period varying between one hour and two hours until total evaporation of the water and is then cooled in a desiccator for 20 min to 60 min and then weighed again ($M2$). Results are expressed in mg/l (Eq. 18.1).

$$TSS = (M1 - M2) / V * 1000 \quad (18.1)$$

Experimental batch adsorption. The adsorption experiments of the pollutants contained in water by activated carbon CA were carried out in the “batch method” in Erlenmeyer flasks of 100 ml, at room temperature (30 ± 2 $^{\circ}\text{C}$) and a stirring speed of 300 rpm. The effects of contact time and activated carbon mass were studied. After a contact time long enough to reach equilibrium, the solutions were filtered through Double Rings Filter Paper and the aqueous solution was analyzed for residual pollutant concentration. The removal efficiency was calculated according to Eq. (18.2):

$$R = \frac{C_i - C_e}{C_i} * 100 \quad (18.2)$$

C_i : Initial concentration of the organic compound tested (mg/L);

C_e : Concentration of organic compound tested at equilibrium (mg/L).

Influence of contact time. The experimental procedure followed consists of putting 1 g of powdered activated carbon in contact with a series of identical flasks each containing 250 ml of purified water at a given initial concentration. The whole is maintained in constant agitation at room temperature. At regular intervals, the content of one of the vials is emptied, filtered and the solution analyzed, and so on until the last vial. The content of adsorbed pollutants at each time Q_t (mg/g) was calculated by the Eq. 18.3:

$$Q = \frac{C_i - C_e}{m} * V \quad (18.3)$$

where:

C_0 and C_e (mg/L) represent the initial and equilibrium concentration in the solution, respectively;

V is the volume of the solution;

m is the mass of dry activated carbon used.

Influence of activated carbon dosage. The method consists in introducing in several Erlenmeyer flasks of variable masses of activated carbon, a volume (100 ml) of purified water. The whole is stirred under the same conditions for a period longer than the equilibrium time. At equilibrium, the solutions are filtered and the residual concentration of the pollutants is measured in the solution.

Description of the experimental procedure of adsorption kinetics. In the kinetic study of the adsorption of BOD₅, COD and TSS we take a volume of 600 ml of water discharged in a batch and a mass of 1.638 g of AC. Samples of the supernatant of the mixture (adsorbate/adsorbent) are taken every 10 min and filtered on Double Rings Filter Paper. The final concentration of BOD₅, COD and TSS is measured for each sample.

18.3 Results and Discussions

18.3.1 Evaluation of the Organic Pollution of Wastewater (Biodegradability)

Biodegradability reflects the ability of the effluent to decompose or oxidize Microorganisms involved in the biological water purification process (Metahri 2012). The

Table 18.3 Physico-chemical characterization of raw and treated water with the ratio COD/BOD₅

Parameters	Raw water	Purified water	Standard Moroccan (Mabrouki et al. 2022)	Discharge Limit Values (Mabrouki et al. 2022)	
				Direct	Indirect
pH	7.91	7.89	5.5–9.5	6.5–8.51	6.5–8.51
T (°C)	21	20	30	30	35
TSS (mg/L)	690	325	150	50	600
COD (mg O ₂ /L)	907	482	250	500	1000
BOD ₅ (mgO ₂ /L)	480	220	120	100	500
COD/BOD ₅	1.89	2.19	–	–	–
BOD ₅ /COD	0.53	0.46	–	–	–

value of the COD/BOD₅ ratio determines the choice of treatment approach. If the effluent is biodegradable, biological treatment should be applied. Otherwise, apply a physicochemical treatment (Mabrouki et al. 2018). We note that the estimation of the origin of the organic matter brought by the wastewater is done by the calculation of the average ratio COD/BOD₅. This COD/BOD₅ ratio also determines the degradability and expected yield of the biooxidative treatment (Table 18.3). The BOD₅/COD ratio provides very interesting information about the sources of wastewater loads and their treatment options (ISO 1994).

From Table 18.3 we observe that the ratio of COD/BOD₅ of the raw water, i.e. the inlet water, is between 1.5 and 2, so we can say that the effluent of the food industry is biodegradable. On the other hand, the ratio of COD/BOD₅ of the treated water, i.e. the outlet water, is between 2 and 3, so we can say that the predominantly domestic effluent is easily biodegradable. While the BOD₅/COD ratio is relatively high at about 0.53. This is the general case for emissions contaminated with organic matter. This organic load makes this effluent very unstable. It can quickly develop into a “digested” form that risks releasing odors. In fact, the effluent from this collector is mostly organic.

18.3.2 Parameters Effect

Influence of contact time on COD, BOD₅ and TSS removal. Figure 18.1 shows the evolution of the percentage of COD, BOD₅ and TSS abatement as a function of time at 30 °C for a solution of volume equal to 250 mL, containing respectively [COD]₀ = 220 mgO₂/L, [BOD₅]₀ = 482 mgO₂/L, [TSS]₀ = 325 mg/L and a mass of 1 g of activated carbon.

The graphs in Fig. 18.1 show maximum adsorption at 180 min for BOD₅, SS and COD. We observe that the first phase of adsorption takes place in a few tens of minutes (80 min). Thus a second slower phase can last from 80 to 180 min. After

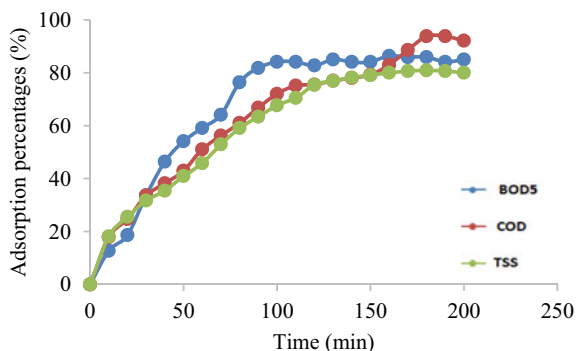


Fig. 18.1 Influence of contact time on COD, BOD₅ and TSS removal ($V = 250$ ml, $m(\text{AC}) = 1.25$ g, $[\text{BOD}_5]_0 = 220$ mgO₂/L, $[\text{COD}]_0 = 482$ mgO₂/L, $[\text{TSS}]_0 = 325$ mg/L)

180 min, the effect of the contact time does not affect the adsorption capacity of COD, BOD₅ and SS, so the adsorption equilibrium is reached at 180 min.

Influence of activated carbon mass on COD, BOD₅ and TSS removal.

Figure 18.2 shows the evolution of the percentage of COD, BOD₅ and TSS removal as a function of the mass of activated carbon used in the tests at 30 °C for a solution of volume equal to 250 mL, containing respectively $[\text{COD}]_0 = 220$ mgO₂/L, $[\text{BOD}_5]_0 = 482$ mgO₂/L, $[\text{TSS}]_0 = 325$ mg/L and a contact time of 200 min.

The analysis of these results shows that the adsorption efficiency of COD, BOD₅, and TSS increases with the mass of the adsorbent to stabilize at a value close to 1.25 g of activated carbon. Many authors (Mabrouki et al. 2020) have shown that the percentages of adsorption increase with the mass of activated carbon used, reaching here more than 80% of COD, BOD₅ and TSS removal.

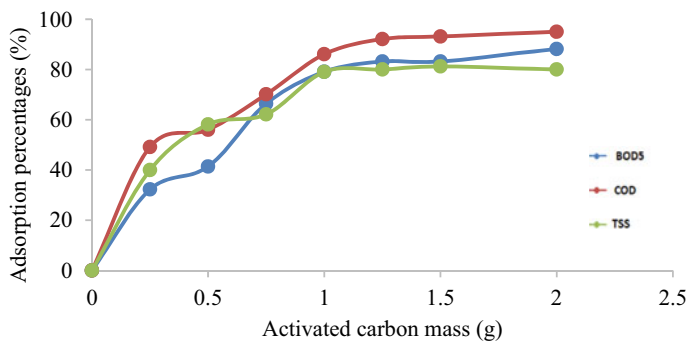


Fig. 18.2 Influence of commercial activated carbon dosage on COD, BOD₅ and TSS removal ($V = 250$ ml, $t = 2$ h, $[\text{BOD}_5]_0 = 220$ mgO₂/L, $[\text{COD}]_0 = 482$ mgO₂/L, $[\text{TSS}]_0 = 325$ mg/L)

18.3.3 Adsorption Kinetics

The results obtained from these experiments showed the existence of two trends over time.

- A first rapid trend between 0 and 80 min. The adsorbed quantities reach 37, 50 and 90 mg/g respectively for BOD₅, TSS and COD after 80 min of contact.
- A second slow trend after 80 min. The quantities adsorbed gradually until equilibrium. This can be explained on the one hand by the decrease of the concentration gradients as the adsorption proceeds, which has a direct impact on the kinetics. On the other hand, it can be attributed to the high availability of active sites on the surface of the AC.

Indeed we also notice in Fig. 18.3 that the amount of COD adsorbed is higher than that of BOD₅ and TSS. This remarkable difference is explained by the high affinity of activated carbons for organic compounds and a medium affinity for certain inorganic compounds. However, the BOD₅ only takes into account organic compounds.

Furthermore, the removal kinetics of BOD₅, COD and TSS on activated carbon was examined using pseudo-first-order and pseudo-second-order kinetic models.

Figures 18.4 and 18.5 represent the plots of the kinetic models (pseudo-1st-order and pseudo-2nd-order) applied to study the kinetic results.

The different kinetic constants extracted from the plotting equations of BOD₅, COD and TSS adsorption on AC (see Figs. 18.4 and 18.5) are grouped in Table 18.4.

From Table 18.4, the pseudo-second-order model describes the experimental data well since the corresponding correlation coefficient ($R^2_{\text{COD}} = 0.918$, $R^2_{\text{BOD}_5} = 0.9068$ and $R^2_{\text{TSS}} = 0.9333$) is higher than the pseudo-first-order model. In addition, the experimentally determined value of Q_{exp} in the equilibrium tests is closer to that of Q_{cal} determined theoretically with the pseudo-2nd-order model than to Q_{cal} determined with the pseudo-1st-order model. These two conditions would indicate

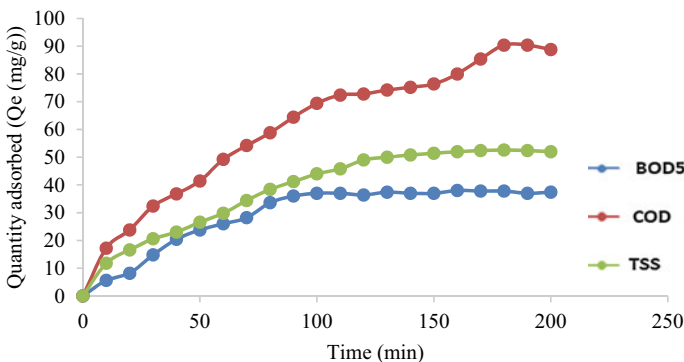


Fig. 18.3 The variation of the adsorbed quantity of BOD₅, COD and SS on AC as a function of time

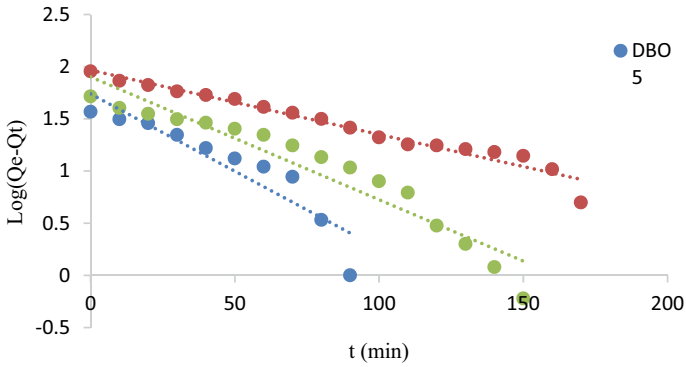


Fig. 18.4 Pseudo-1st-order kinetics model

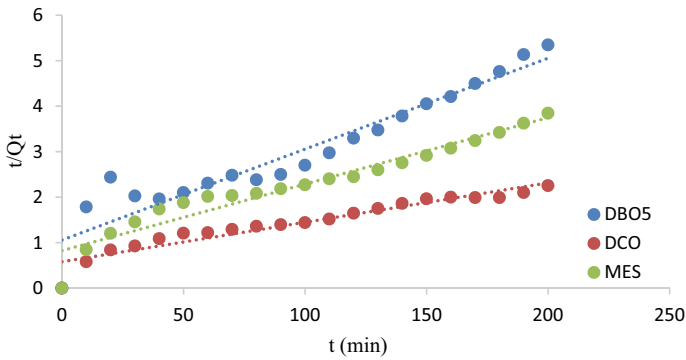


Fig. 18.5 Pseudo-second order kinetics model

Table 18.4 Kinetic constants of BOD₅, COD and SS adsorption on AC

Parameters	BOD ₅	COD	TSS
Pseudo-1st-order: $\text{Log}(Q_e - Q_t) = \text{log } Q_e - K_1 * t / 2.303$			
R ²	0.8493	0.9003	0.9146
Q _{cal} (mg/g)	5.697	7.123	6.707
Q _{exp} (mg/g)	37	90	50
K ₁ (min ⁻¹)	0.034	0.0143	0.027
Pseudo-2nd-order: $t/Q_t = Q_e / K_2 + 1/Q_e$			
R ²	0.9068	0.918	0.9333
Q _{cal} (mg/g)	40	114.94	68.49
Q _{exp} (mg/g)	37	90	50
K ₁ (g, mg ⁻¹ , min ⁻¹)	3.7.10 ⁻⁴	1.3.10 ⁻⁴	2.58.10 ⁻⁴

that the adsorption process is predominantly controlled by chemisorption (Azoulay et al. 2022; Bencheikh et al. 2020).

18.4 Conclusion

From this study, we can see that activated carbon is capable of retaining organic and inorganic matter in an aqueous medium. However, with a maximum adsorption capacity equal to 90 mg/g (for the adsorption of organic and inorganic pollutants estimated by global measurement of COD), 50 mg/g (for the adsorption of suspended solids TSS) and 37 mg/g for the adsorption of organic pollutants alone BOD₅). This work was carried out to determine the optimal conditions for the removal of BOD₅, COD and TSS on AC, we were led to carry out a parametric study, in which we took into account the influence of important factors such as the contact time and the mass of activated carbon used. The study of the influence of the mass and the contact time allowed us to determine the optimal conditions for BOD₅, COD and TSS, which are:

- To determine the optimal conditions for the removal of BOD₅, COD and TSS on AC, we were led to carry out a parametric study, in which we took into account the influence of important factors such as the contact time and the mass of activated carbon used. The study of the influence of the mass and the contact time allowed us to determine the optimal conditions for BOD₅, COD and TSS, which are:
 - Time = 180 min
 - masse = 1 g.

The results of the kinetic study showed that the equilibrium is established after 180 min and that the pseudo-second-order model writes well our adsorption phenomenon.

References

- Azoulay K, Bencheikh I, Mabrouki J, Samghouli N, Moufti A, Dahchour A, El Hajjaji S (2021) Adsorption mechanisms of azo dyes binary mixture onto different raw palm wastes. *Int J Environ Anal Chem* 1–20. <https://doi.org/10.1080/03067319.2021.1878165>
- Azoulay K, Bencheikh I, Moufti A, Dahchour A, Mabrouki J, El Hajjaji S (2022) Comparative study between static and dynamic adsorption efficiency of dyes by the mixture of palm waste using the central composite design. *Chem Data Collect* 27:100385. <https://doi.org/10.1016/j.cdc.2020.100385>
- Bencheikh I, Azoulay K, Mabrouki J, El Hajjaji S, Dahchour A, Moufti A, Dhiba D (2020) The adsorptive removal of MB using chemically treated artichoke leaves: parametric, kinetic, isotherm and thermodynamic study, *Scientific African*, vol 9, July, e00509. <https://doi.org/10.1016/j.sciaf.2020.e00509>.

- Bencheikh I, Azoulay K, Mabrouki J, El Hajjaji S, Moufti A, Labjar N (2021) The use and the performance of chemically treated artichoke leaves for textile industrial effluents treatment. *Chem Data Collect* 31:100597. DOI: <https://doi.org/doi:10.1016/j.cdc.2020.100597>
- Bliefert C, Perraud R (2001) *Chimie de l'environnement: air, eau, sols, déchets*. De Boeck Université
- Crini G, Badot PM, Morin-Crini GT (2007) Les principales techniques d'épuration des eaux industrielles polluées : une revue récente des méthodes proposées dans la littérature : traitement et épuration des eaux industrielles polluées. *Presse universitaire de Franche-Comté, Paris*, p 3
- Demirbas A (2009) Agricultural based activated carbons for the removal of dyes from aqueous solutions: a review. *J Hazard Mater* 167:1–9
- ISO 5667/3 (1994) *Qualité de l'eau et échantillonnage. Guide pour la conservation et la manipulation des échantillons* (1994)
- Labbaci Haytem et Boumenkar tarek, analyse des anomalies et redimensionnement de la STEP de la Wilaya de SKIKDA, mémoire de master, université Badji Mokhtar Annaba, Algérie (2019)
- Mabrouki J, El Yadini, A, Bencheikh I, Azoulay K, Moufti A, El Hajjaji S (2018) Hydrogeological and hydrochemical study of underground waters of the tablecloth in the vicinity of the controlled city dump mohammedia (Morocco). In: *International conference on advanced intelligent systems for sustainable development*. Springer, Cham
- Mabrouki J, Bencheikh I, Azoulay K, Es-Soufy M, El Hajjaji S (2019) Smart monitoring system for the long-term control of aerobic leachate treatment: dumping case Mohammedia (Morocco). In: *International conference on big data and networks technologies*. Springer, Cham, pp 220–230
- Mabrouki J, Benbouzid M, Dhiba D, El Hajjaji S (2020) Simulation of wastewater treatment processes with Bioreactor Membrane Reactor (MBR) treatment versus conventional the adsorbent layer-based filtration system (LAFS). *Int J Environ Anal Chem* 1–11
- Mabrouki J, Azrou M, Hajjaji SE (2021) Use of internet of things for monitoring and evaluating water's quality: a comparative study. *Int J Cloud Comput* 10(5–6):633–644
- Mabrouki J, Fattah G, Al-Jadabi N, Abrouki Y, Dhiba D, Azrou M, Hajjaji SE (2022) Study, simulation and modulation of solar thermal domestic hot water production systems. *Model Earth Syst Environ* 8(2):2853–2862
- Metahri, élimination simultanée de la pollution azotée et phosphatée des eaux traitées, par des procédés mixtes. Cas de la STEP Est de la ville de Tizi-Ouzou. P17, 20, 22, 27, 63, 72, 73 et 74 (2012)
- Reporterre (2020) 227 activistes de l'environnement assassinés en 2020, un record [archive], sur Reporterre, le quotidien de l'écologie (consulté le 16 septembre 2021)
- Samuel BAUMONT (2010) *Réutilisation des eaux usées épurées: risques sanitaires et faisabilité en Île-de-France*, Institut d'aménagement et d'urbanisme de la région Ile-de-France
- WWAP (Programme mondial pour l'évaluation des ressources en eau). *Rapport mondial des Nations Unies sur la mise en valeur des ressources en eau* (2017) *Les eaux usées – Une ressource inexploitée*. UNESCO, Paris, p 2017

Chapter 19

Control of COVID 19: Knowledge and Practices of Health Professionals in Hospitals Towards Patients and the Environment in Morocco (Meknes)



Karima El-Mouhdi , Smahane Mehanned, and Jawad Bouzid 

Abstract Coronavirus 2019 is considered the health disaster of the century and has caused a wave of global panic. Healthcare professionals were at the forefront of this pandemic to provide quality care respecting the safety of patients and the environment. The objective of this study is to determine the preventive measures applied by healthcare professionals towards patients and the environment to combat Covid19. The study was realized during April and May 2020 at the public hospital dedicated to the care of Covid patients in central Morocco in Meknes. Convenience sampling was used to collect the data. 104 people participated in the study, including 61 (58.7%) nurses and 12 (11.5%) doctors. Also, 73 (70.2%) of the healthcare professionals were men and 35 (33.7%) contracted the Coronavirus during their healthcare activity. According to the participants, the causes of this infection lie mainly in their interaction with their professional environment (71.4%). The main preventive measures applied by healthcare professionals were regular hand washing and wearing 104 masks (100%), of which 88 (84.6%) used the FFP2 mask and wore personal protective equipment. However, healthcare professionals were found to adopt other environmental practices, including surface disinfection 95 (91.3%), ventilation and sterilization of premises 46 (44.2%), maintenance and sterilization of equipment 78 (75%), and effective management of hospital waste 75 (72.1%). The study concluded that the preventive measures applied by the professionals were sufficient and complied with global recommendations to minimize the risk of contamination and maintain a healthy healthcare environment for themselves and their patients.

K. El-Mouhdi (✉)

Ministry of Health and Social Protection, Higher Institute of Nursing and Health Techniques,
50000 Meknes, Morocco

e-mail: k.elmouhdi@ispitsmeknes.ac.ma; karimaelmouhdi@gmail.com

K. El-Mouhdi · S. Mehanned

Faculty of Sciences, Moulay Ismail University, BP 298, Meknes, Morocco

J. Bouzid

Higher Institute of Health Sciences, Hassan I University, Settat, Morocco

Keywords Coronavirus · Environment · Healthcare professionals

19.1 Introduction

Since its emergence, the SARS-CoV-2 or COVID-19 Coronavirus has spread rapidly across countries and caused global panic. The virus was discovered in the Wuhan region of China in late 2019, when people were showing symptoms of pneumonia and spreading rapidly around the world causing a wave of panic that prompted the World Health Organization (WHO) to declare an international health emergency on 11 March 2020 (World Health Organization 2021a). To slow its spread and safeguard people's health, many countries resorted to preventive measures ranging from locking down borders to closing them (Mrazguia et al. 2021a). However, the pandemic claimed many lives and the global mortality rate reached 4.9% (Mrazguia et al. 2021a).

The SARS-CoV-2 pandemic has affected the whole world, but some populations are at high risk of infection, such as health workers, who constitute the first barrier to this pandemic. Indeed, infection among healthcare professionals is of great concern because of the risk of nosocomial spread, which can lead to a significant reduction in the already limited number of healthcare workers in developing countries (World Health Organization 2020a).

Scientific evidence has shown that environmental contamination in healthcare facilities increases the risk of transmission to the healthcare worker of contracting the disease (Chia et al. 2020). Environmental contamination is considered a route of transmission of coronavirus (Chia et al. 2020; Colaneri et al. 2020). Furthermore, the extent of COVID-19 contamination in the environment of infected patients has been proven by several research studies in healthcare settings (Colaneri et al. 2020; Ong et al. 2021, 2020). To limit the transmission of the coronavirus, the WHO has mandated that health services and populations adopt essential protective measures to prevent saturation of intensive care units, strengthen environmental hygiene and preventive practices such as promoting hand washing, mask-wearing, and avoiding physical contact, kissing and handshaking (World Health Organization 2021a, 2020a). The WHO guidelines state that caregivers directly caring for patients with COVID-19 should wear a medical mask, but in settings where aerosol-generating procedures are performed on patients with COVID-19, the WHO recommends that caregivers wear a respirator. In the absence of contact with COVID-19 patients, clinical care workers should wear a medical mask at all times for routine tasks (World Health Organization 2020a). Similarly, all facilities have implemented an infection control strategy at their level, with a dedicated team trained in measures to prevent nosocomial infections related to environmental contamination (World Health Organization 2021a, 2020a; Mrazguia et al. 2021a; Chia et al. 2020).

Despite the existence of all these measures, the greatest number of cases of contamination was recorded among health professionals. The WHO explains that this is due to the nature of their work and their presence in a risky environment

(International Council of Nurses 2020). The results of the International Council of Nurses report, which surveyed 50 countries, showed that infections among health-care workers accounted for between 1 and 32% of confirmed cases of COVID-19 (Davenne et al. 2020).

Knowledge of the severity of coronavirus and its control measures is a key step in the fight against this pandemic. However, the majority of studies realized on health-care workers in the context of COVID-19 have focused on the clinical, biological and epidemiological aspects of the disease. Few studies have been realized on the knowledge and preventive practices of health professionals against the COVID-19 during their care activities. It is in this context that we conducted this study to determine the knowledge and practices of healthcare professionals towards patients and towards the environment in the context of the fight against the pandemic COVID-19. To our knowledge, this is the first study carried out among health personnel in the central Moroccan city of Meknes which aims to describe the different measures applied by health professionals to protect themselves, others and the environment.

19.2 Materials and Methods

19.2.1 Study Area

The present study was conducted in central Morocco at the “Sidi Said” regional hospital in Meknes between April and May 2020. Its objective is to determine the preventive measures applied by healthcare professionals to fight against the Corona pandemic towards patients and the environment. The study was carried out at the time of the beginning of the containment in Morocco in a hospital designated exclusively as the pilot facility for the management of patients. The “Sidi Said” hospital, our choice for collecting information on the measures applied to protect patients and the environment, stands out for having played a strategic role since the beginning of the pandemic and even received the first suspect Moroccan cases returning from the Chinese city of Wuhan. This hospital has been equipped to receive patients from all regions of the Kingdom and has become known nationally as the “Corona Hospital”. Its total area is about 4.5 hectares and its capacity is 90 beds. It also offers inpatient, medical and nursing services. In 2020, more than 136 healthcare professionals, including 19 doctors, 67 nurses, 10 health technicians and 40 administrative staff, have been recruited to provide health services to patients.

19.2.2 Study Participants and Sampling

The participants in the study were healthcare professionals working at the “Sidi Said of Corona” hospital. The sample was selected according to specific criteria,

namely: the inclusion criteria required that the participant be a healthcare professional belonging to the category of doctors, nurses and health technicians or other healthcare professionals directly involved in the healthcare activities for Corona patients at the hospital. In contrast, the exclusion criteria included people working in the hospital but not performing the function of managing or providing health care. Also, healthcare professionals who refused to participate in our study were excluded.

19.2.3 Data Collection and Analysis

The data collection tool was a self-administered questionnaire with three main axes: (a) participants' socio-professional characteristics, (b) participants' knowledge of the emerging coronavirus, and (c) healthcare professionals' daily practices towards Covid-positive patients and the care environment.

The working team proceeded to check the validity of the tool and its understanding before its use with the participants. Therefore a pre-test of the questionnaire was carried out with seven healthcare professionals on whom it was refined and improved before its use in its final form. The research team endeavored to distribute the forms directly and in person to all healthcare professionals working at Corona Sidi Said Hospital. After collecting the forms that the healthcare professionals agreed to fill out, the data was entered and organized in an Excel file and statistically analyzed using SPSS.

19.2.4 Ethical Considerations

All ethical and moral considerations were respected throughout the realization of this work. As a result, verbal consent was obtained from all participants. Before administering each questionnaire, the objectives of the study were clearly explained to the participant. Similarly, the ethical principles of confidentiality and anonymity of information were respected in all stages of the study. Thus, it is important to say that only healthcare professionals who agreed to participate in our study were included.

19.3 Results

19.3.1 Socio-Professional Characteristics of Participants

Table 19.1 presents the socio-professional characteristics of the study participants. During the period of realization of this study, the total number of healthcare professionals working at the Sidi Said Hospital in Corona was 136, of whom 104 were

Table 19.1 Distribution of participants by socio-professional characteristics

Question	Answer	N = 104	%
Who are you?	Men	31	29.8
	Female	73	70.2
Age group	20–29 years old	26	25.0
	30–39 years old	22	21.2
	40 years and older	56	53.8
Professional category	Nurse	61	58.7
	Healthcare technician	15	14.4
	Doctor	12	11.5
	Midwife	9	8.7
	Healthcare administrator	7	6.7
Length of service in the health service	Less than 10 years	32	30.8
	10–20 years	18	17.3
	More than 20 years	54	51.9
Have you received any training on Covid 19?	Yes	104	100
	No	0	0.0
In your opinion, is there a national strategy for the fight against Covid 19 in Morocco?	Yes	77	74.0
	No	26	25.0
	No answer	1	1.0

accepted to participate voluntarily in our study. This means a participation rate of 76.5%. These 104 healthcare professionals were distributed as follows: 61 (58.7%) were nurses, 15 (14.4%) were healthcare technicians and 12 (11.5%) were doctors. Women were the largest number of participants 73 (70.2%) than men who accounted for only 31 (29.8%). In addition, healthcare professionals with more than 40 years of age represented 56 (53.8%) and those with more than 20 years of service in the health service were 89 (51.9%). On the other hand, all healthcare professionals confirmed that they were aware of the new coronavirus and had received training on the subject. Thus, 77 (74%) of healthcare professionals were aware of the existence of a national strategy for the management and control of the new coronavirus in Morocco.

19.3.2 Healthcare Professional History of Covid Infection

Working in a hospital dedicated solely to the care of Covid 19 positive patients means working in a highly risky environment. The healthcare professionals were aware that their constant contact with Covid patients increases the risk of contracting the disease. Table 19.2 shows the health status of the participants regarding their Covid19 infection, the causes of infection and their vaccination status against Coronavirus.

Table 19.2 Healthcare professional history of Covid infection

Question	Answer	N = 104	%
Have you ever had contact with Covid19?	Yes	35	33.7
	No	69	66.3
If so, what caused this contamination?	Contamination of the environment by polluted surfaces	25	71.4
	Contact with patients	8	22.9
	Shortage of PPE	2	5.7
During your Covid19 illness, what management modality did you receive?	Containment with home treatment	35	33.7
	Hospitalization	5	4.8
	Other	2	1.9
Are you vaccinated against the coronavirus?	Yes	84	80.8
	No	20	19.2
If not, what are your reasons for refusing vaccination?	Not convinced by Covid19 vaccine	11	55.0
	Pregnancy and breastfeeding	5	25.0
	Allergy to the vaccine	3	15.0
	Ever had Covid 19	1	5.0

* PPE: Personal Protective Equipment

Our results revealed that 35 (33.7%) of the healthcare professionals had contracted the Coronavirus during their healthcare activities and had to stop working. According to the participants, the causes of this infection lay mainly in their interaction with their professional environment (71.4%), contact with patients (22.9%) and lack of personal protective equipment (5.7%).

Concerning the vaccination status of healthcare professionals against coronavirus, the majority of respondents 84 (80.8%) confirmed having received the COVID-19 vaccine. However, 20 (19.2%) of them indicated that they had not received any dose of vaccine. The reasons for refusing to be vaccinated were mainly due to their lack of conviction about the importance of vaccination (55%), their sensitivity to vaccines (15%) or pregnancy and breastfeeding (25%).

19.3.3 Preventive Practices of Healthcare Professionals Towards Patients

The different preventive practices against Covid19 applied by healthcare professionals during their care activities with Covid patients have been illustrated in Table 19.3. Our results show that the wearing of masks and gloves is practised by all participants (100%). The most commonly used masks by healthcare professionals were FFP2 88 (84.6%). We also found that the majority of healthcare professionals wore protective equipment 88 (84.6%), wore face shields 55 (52.9%) and regularly washed

and disinfected their hands 100 (96.2%). Simple hand washing is always done by 76 (73.1%) of the caregivers, while antiseptic hand washing with hydro-alcoholic solution (HAS) is practised by 56 (53.8%). Similarly, the times at which washing and disinfection were used were determined successively before care 84 (80.8%), aftercare 71 (68.3%) and between two patients 57 (54.8%). While the moments of glove use were most frequent during any possible contact with a biological liquid (74%) and during the realization of aseptic care (66%). More details on the times and methods of use of these preventive measures are presented in Table 19.3.

19.3.4 Preventive Practices of Healthcare Professionals Towards the Environment

In our study, the question related to health and the environment was aimed at determining the measures taken by healthcare professionals (see Table 19.4). Almost all the participants (99%) stated that it is necessary to maintain and protect the healthcare environment to work in a healthy and unpolluted environment. As a result, the different practices adopted by healthcare professionals towards the environment were: (a) securing the workplace from potential contamination by disinfecting surfaces 95(91.3%), ventilating and sterilizing rooms 46(44.2%), (b) treating and sterilizing equipment 78(75%), as well as treating and managing hospital waste effectively 75(72.1%). More details on the use of these preventive measures are presented in Table 19.4.

19.4 Discussions

This study aims to determine the knowledge and preventive practices applied by healthcare professionals in the context of the fight against the Covid 19 pandemic. To our knowledge, this study is the first of its kind that reveals the preventive aspects and their application by healthcare professionals towards patients and the environment of the pandemic in hospitals in central Morocco.

Indeed, the results obtained revealed that 73 (70.2%) of the participants included in the research were women and that the category of nurses is the most participating 61 (58.7%). This is explained by the high number of nurses working in the Moroccan health care system represent the highest number of nurses compared to other categories (Ministry of Health and Social Protection. Health care supply 2022; El-Mouhdi et al. 2020). This category plays an important role in the provision of health care in cooperation with other professions (World Health Organization 2020b). The International Council of Nurses has indicated the importance of this category and the need to pay attention to it to ensure the success of health policies and programmers in countries (International Council of Nurses 2020).

Table 19.3 Preventive practices of healthcare professionals towards patients

Preventative method used		N = 104	%
Hand washing and disinfection	Yes	100	96.2
	No	4	3.8
Simple hand washing	Always	76	73.1
	Often	29	27.9
	Moderately	5	4.8
Hand disinfection (HAS)*	Always	56	53.8
	Often	33	31.7
	Moderately	20	19.2
	Rarely	3	2.9
Timing of hand washing and disinfection	Before the treatment	84	80.8
	After the treatment	71	68.3
	At the end of the treatment session	70	67.3
	Between two patients	57	54.8
Wearing of gloves	Yes	85	81.7
	No	19	18.3
Situations where gloves are used	During any possible contact with a biological liquid	77	74.0
	When realizing an aseptic care	69	66.3
	When performing all types of care	63	60.6
	For patients with a skin infection	63	60.6
	When there are lesions on the hands	61	58.7
Wearing of personal protective equipment	Yes	88	84.6
	No	16	15.4
Wearing masks	Yes	104	100.0
	No	0	0.0
Use of masks	FFP2** mask	88	84.6
	Surgical mask	27	26.0
Wearing face shields	Yes	55	52.9
	No	50	48.1
Physical distance	Between staff	89	85.6
	Between attendants	88	84.6
	Between patients	68	65.4

*HAS: Hydro-Alcoholic Solution; * FFP2: Filtering Face Piece

Table 19.4 Preventive practices of healthcare professionals towards patients

Question	Answer	N = 104	%
In your opinion, the maintenance of the care environment is mandatory	Yes	103	99.0
	No	1	1.0
In your daily practice, what procedures are applied in your department for the maintenance of the environment	Decontamination of surfaces	95	91.3
	Ventilation of patients' rooms	46	44.2
	Both	73	70.2
Do you systematically process and sterilise care equipment	Yes	78	75.0
	No	26	25.0
In your experience, how often is the treatment and sterilization of equipment used?	Always	78	75.0
	Often	16	15.4
	Rarely	5	4.8
	Never	2	1.9
	No answer	3	2.9
Other preventive measures for the care environment	Hygiene and routine cleaning of rooms	95	91.3
	Medical waste management and treatment	75	72.1
	Sterilization of deceased patients' rooms	46	44.2

Regarding the knowledge of healthcare professionals about the Covid19 virus, the study showed that all participants were aware of this emerging disease, and they all confirmed that they have received training on this subject. In this context, it can be said that the WHO has paid a lot of attention to healthcare professionals and considered that they should be supported in developing their capacities through effective and authentic continuous training such as simulation (World Health Organization 2020a).

In our study, we found that more than one-third of the participants (33.7%) had contracted coronavirus disease and stopped working. This figure is almost higher than that reported by the International Council of Nurses (International Council of Nurses 2020; International Council of Nurses 2020). The causes of infection according to most participants were mainly interaction with their work environment (71.4%), contact with patients (22.9%) and lack of personal protective equipment (5.7%). These results are consistent with those found by previous studies which also revealed that the nature of the virus makes it last a long time even on pure surfaces, leading to infection in the light of strict protective measures against it (Colaneri et al. 2020; Ong et al. 2021, 2020; Davenne et al. 2020; Mrazguia et al. 2021b).

According to the World Health Organization, health workers are living reservoirs of the virus, which means that they can transmit the infection to patients who are at risk of developing severe cases of the emerging coronavirus that can lead to death (World Health Organization 2021a). The organization stresses the need for vaccination as a mandatory preventive measure for healthcare professionals as it protects patients

and themselves (World Health Organization 2020c). In our study, we found that most healthcare professionals 84 (80.8%) were vaccinated against the corona virus. However, 20 (19.2%) of them indicated that they had not received any dose of the vaccine because they were not convinced of the usefulness of vaccination (55%) or because they were allergic to vaccines (15%). The refusal of the population to be vaccinated was already mentioned in several studies (Chazelet 2021).

It has been proven that the main element to preventing the occurrence of the Covid19 coronavirus is to reduce its transmission by respecting preventive measures that depend mainly on the application of hand hygiene measures, wearing medical masks, disinfection of the environment and maintenance of a healthy physical environment (Davenne et al. 2020). In this regard, the results of our study revealed that most healthcare professionals were aware of the need to comply with these procedures, as all participants (100%) stated that they are in the habit of washing their hands frequently and continuously, this percentage is higher than that reported in the study conducted among healthcare professionals at Nabeul Hospital in Tunis (Mrazguia et al. 2021b). In addition, the majority of participants expressed interest in hydro-alcoholic solutions and their use for hand disinfection, considering it the best way to sterilize hands due to its ease of use. In this context, the WHO indicated the importance of hand disinfection and sterilization in the control of the transmission of the Covid 19 Coronavirus infection (World Health Organization 2020c).

Analysis of the results regarding healthcare professionals' practices to prevent the risk of Covid 19 infection in their daily practice showed that all of them routinely wear gloves in all treatment and care activities they provide to patients with coronavirus, even in routine healthcare and in low-risk care activities. This behavior was also suggested by the WHO insofar as it insisted on the need to wear gloves in all care situations without exception (World Health Organization 2020b).

Regarding the use of protective masks by healthcare professionals in their daily practice, the results revealed that healthcare professionals are aware of the importance of this protective tool in offering the best protection against aerosols. However, despite the diversity of masks, the majority of respondents (84.6%) confirmed that they wear the "FFP2 mask". In addition, many studies have highlighted that healthcare professionals should wear protective masks at all times for routine tasks and even in severe cases such as intensive care units (World Health Organization 2021b; Chazelet 2021; Cochereau and Lamirel 2020; Hartman et al. 2020).

Concerning physical distancing, the majority of professionals affirmed their willingness to apply this procedure, especially towards each other (85.6%), towards companions (84.6%) and also towards patients (65.4%). This is in line with the WHO guidelines and recommendations, which stress that the physical distance within health facilities should be set at a distance of at least one meter between people to reduce the risk of transmission of the coronavirus19. In this context, the scientific community has argued that everyone in healthcare units should avoid physical contact unless the contact is part of the care (Liu et al. 2020; Watts et al. 2020; World Health Organization 2021c).

In contrast, much research has revealed the ability of the virus to survive for long periods on a range of inert surfaces such as steel, plastic and copper (Doremalen

et al. 2020). Environmental contamination by patients suggests that the environment is a potential means of transmission and supports the need for strict environmental hygiene (Chia et al. 2020). The extent of environmental contamination was due to direct tactile contamination by the patient or healthcare professionals (Ong et al. 2021). In this context, the results of our research revealed healthcare professionals' awareness of the environmental aspect of coronavirus transmission, as they all stressed the need to maintain a safe and healthy environment for patient care to prevent the transmission of the virus as a nosocomial infection through surface disinfection (91.3%), ventilation and disinfection of patient rooms (44.2%), sterilization of care equipment (75%), and effective treatment and management of hospital waste (72.1%).

In sum, it can be said that healthcare professional practices against the Covid19 pandemic differ from one place to another. In the case of the Toronto hospital, healthcare professionals focused on the systematic use of gloves, a white gown and overcoat, protective glasses and masks (Verma et al. 2021). In our case at Sidi Said Hospital in the city of Meknes in central Morocco, the majority of healthcare professionals ensured that they wore protective masks, gowns, gloves and face shields. They also used protective glasses, disinfected hands with alcoholic solutions and sterilized equipment. Indeed, according to the WHO, the use of all these measures contributes to the protection against the emerging Coronavirus (World Health Organization 2021a). Its control is not only limited to applying preventive measures while providing health care services, but also to taking into account the safety of the working environment and ensuring its quality to avoid the transmission of infections (Saunders-Hastings et al. 2017).

19.5 Conclusion

The present study revealed that healthcare professionals working at the Sidi Said Hospital, which is reserved for Covid patients, have a good knowledge of the Covid coronavirus. Similarly, the practices applied by healthcare professionals towards patients and the environment to fight the pandemic were fully in line with the recommendations of the World Health Organization. This is reinforced by their concern to systematically use personal protective equipment when caring for Covid patients and to respect the standards for working in an environment that is healthy and safe for them and patients.

Acknowledgements All the authors thank the assistance of the students Mbara Kaoutar and El Khloufi Oumayma during the data collection as well as the unconditional help of the healthcare professionals of Sidi Said Hospital who accepted to participate in this study.

Funding This work has not received any funding.

Conflicts of Interest None.

References

- Chazelet S (2021) Use of masks in the fight against Covid-19. *Environ Risques Santé* 20(3):317–320
- Chia PY, Coleman KK, Tan YK, Ong SWX, Gum M, Lau SK, Lim XF, Lim AS, Sutjipto S, Lee PH, Son TT, Young BE, Milton DK, Gray GC, Schuster S, Barkham T, De PP, Vasoo S, Chan M, ... Marimuthu K (2020) Detection of air and surface contamination by SARS-CoV-2 in hospital rooms of infected patients. *Nat Commun* 11(1):Art 1. <https://doi.org/10.1038/s41467-020-16670-2>
- Cochereau I, Lamirel C (2020) Hand hygiene and masks against COVID-19: daring the gradient? *J Fr Ophtalmol* 43(5):386–388
- Colaneri M, Seminari E, Novati S, Asperges E, Biscarini S, Piralla A, Percivalle E, Cassaniti I, Baldanti F, Bruno R, Mondelli MU, Bruno R, Mondelli MU, Brunetti E, Matteo AD, Seminari E, Maiocchi L, Zuccaro V, Pagnucco L, Vecchia M (2020) Severe acute respiratory syndrome coronavirus 2 RNA contamination of inanimate surfaces and virus viability in a health care emergency unit. *Clin Microbiol Infect* 26(8):1094.e1-1094.e5. <https://doi.org/10.1016/j.cmi.2020.05.009>
- Davenne E, Giot JB, Huynen P (2020) Coronavirus and COVID-19: an update on a rampant pandemic. *Rev Médicale Liège* 75. <https://orbi.uliege.be/handle/2268/252188>
- El-Mouhdi K, Chahlaoui A, Boussaa S, Fekhaoui M (2020). Sand flies control : a review of the knowledge of health professionals and the local community, Province of El Hajeb, Morocco. *Int J Environ Res Public Health* 17(22): Art. 22. <https://doi.org/10.3390/ijerph17228448>
- Hartman M, Martin AB, Washington B, Catlin A (2020) The NHEAT. National Health Care Spending In 2020: Growth Driven by Federal Spending In Response to the COVID-19 Pandemic. *Health Aff (Millwood)* 41(1):13-25 (2022)
- International Council of Nurses (2020a) Protecting nurses from COVID-19 a top priority: a survey of ICN's national nursing associations—INTERNATIONAL COUNCIL OF NURSES. International Council of Nurses. <https://www.readkong.com/page/protecting-nurses-from-covid-19-a-top-priority-a-survey-of-8979982>
- International Council of Nurses (2020b) The global nursing shortage and retention of nurses. https://www.icn.ch/sites/default/files/inline-files/ICN%20Policy%20Brief_Nurse%20Shortage%20and%20Retention_FR.pdf
- Liu J, Liao X, Qian S, Yuan J, Wang F, Liu Y et al (2020) Community transmission of severe acute respiratory syndrome coronavirus 2, Shenzhen, China. *Emerg Infect Dis* 26(6):1320–1323
- Ministry of Health and Social Protection. Health care supply. Health Map. <http://cartesanitaire.sante.gov.ma/offresoins/>
- Mrazguia C, Aloui H, Fenina E, Boujnah A, Azzez S, Hammami A (2021a) L'infection par le COVID-19 chez le personnel de santé à l'Hôpital Régional de Nabeul : épidémiologie et circonstances de transmission. *PAMJ—One Health* 4(11). <https://www.one-health.panafrican-med-journal.com/content/article/4/11/full>
- Mrazguia C, Aloui H, Fenina E, Boujnah A, Azzez S, Hammami A (2021b) COVID-19 infection among health personnel at the Regional Hospital of Nabeul: epidemiology and circumstances of transmission. *PAMJ—One Health* 4(11). <https://www.one-health.panafrican-med-journal.com/content/article/4/11/full>
- Ong SWX, Tan YK, Chia PY, Lee TH, Ng OT, Wong MSY, Marimuthu K (2020) Air, surface environmental, and personal protective equipment contamination by severe acute respiratory syndrome coronavirus 2 (SARS-CoV-2) from a symptomatic patient. *JAMA* 323(16):1610–1612. <https://doi.org/10.1001/jama.2020.3227>
- Ong SWX, Lee PH, Tan YK, Ling LM, Ho BCH, Ng CG, Wang DL, Tan BH, Leo Y-S, Ng O-T, Wong MSY, Marimuthu K (2021) Environmental contamination in a coronavirus disease 2019 (COVID-19) intensive care unit—what is the risk? *Infect Control Hosp Epidemiol* 42(6):669–677. <https://doi.org/10.1017/ice.2020.1278>
- Saunders-Hastings P, Crispo JAG, Sikora L, Krewski D (2017) Effectiveness of personal protective measures in reducing pandemic influenza transmission: a systematic review and meta-analysis. *Epidemics* 20:1–20

- Van Doremalen N, Bushmaker T, Morris DH, Holbrook MG, Gamble A, Williamson BN et al (2020) Aerosol and surface stability of SARS-CoV-2 as compared with SARS-CoV-1. *N Engl J Med* 382(16):1564-1567
- Verma AA, Hora T, Jung HY, Fralick M, Malecki SL, Lapointe-Shaw L et al (2021) Characteristics and outcomes of hospitalizations for COVID-19 and influenza cases in the Toronto area. *CMAJ* 193(23):E859-E869
- Watts E, Leck A, Hu V (2020) *Personal protective equipment* 17:6 (2020)
- World Health Organization (2020a) Prevention, identification and management of health worker infection in the context of COVID-19: interim guidance, 13 p. <https://apps.who.int/iris/handle/10665/336265>
- World Health Organization (2020b) Technical specifications of personal protective equipment for COVID-19: interim guidance. World Health Organization; Report No.: WHO/2019-nCoV/PPE_specifications/1. <https://apps.who.int/iris/handle/10665/336622>
- World Health Organization (2020c) Cleaning and Disinfection of Environmental Surfaces under COVID-19: Interim Guidance. Report No.: WHO/2019-nCoV/Disinfection/1. <https://apps.who.int/iris/handle/10665/332167>
- World Health Organization (2021a) Impact of COVID-19 on human resources for health and policy response: the case of Plurinational State of Bolivia, Chile, Colombia, Ecuador and Peru: overview of findings from five Latin American countries. Pan American Health Organization. <https://apps.who.int/iris/handle/10665/350640>
- World Health Organization (2021b) COVID-19: Occupational health and safety for health workers: interim guidance. https://www.who.int/publications-detail-redirect/WHO-2019-nCoV-HCW_advice-2021-1
- World Health Organization (2021c) WHO SAGE roadmap for prioritising the use of COVID-19 vaccines in a limited supply context. Report No: WHO/2019-nCoV/Vaccines/SAGE/Prioritization/1. <https://apps.who.int/iris/handle/10665/349451>

Chapter 20

The Evaluation of the Valorization of Cannabis Residues for the Production of Energy by Combustion



Mohamed Elouardi, Ghizlane Fattah, Mohammed Benchrifa,
Jamal Mabrouki, Touriya Zair, and Mohammed Alaoui El Belghiti

Abstract Our study is in the framework of the development of plant biomasses rich in cellulose and hemicelluloses, as a renewable energy source. The selection of plant material suitable for energy production requires a good understanding of their composition and their ability to be turned into bio methane or bioethanol by fermentation, or to be used as solid fuel. We studied an analytical method for the analysis of cellulose and energy conversion of plant biomasses. It is essentially based on neutral detergent extraction of interfering biomass components, acid hydrolysis of cellulose and hemicelluloses, and versatile analysis of the released monosaccharides. We showed that the valorization of cannabis waste as energy source is very significant.

Keywords Valorization of residues · Cannabis · Combustion · Energy

M. Elouardi (✉) · J. Mabrouki · M. A. E. Belghiti
Laboratory of Spectroscopy, Molecular Modelling, Materials, Nanomaterial, Water and Environment, CERNE2D, Faculty of Science, Mohammed V, University in Rabat, Avenue Ibn Battouta, BP 1014, Agdal, Rabat, Morocco
e-mail: elouardi-mohamed@um5r.ac.ma

G. Fattah
Water Treatment and Reuse Structure, Civil Hydraulic and Environmental Engineering Laboratory, Mohammadia School of Engineers, Mohammed V University in Rabat, Avenue Ibn Sina BP 765, Agdal, 10090 Rabat, Morocco

M. Benchrifa
Solar Energy and Environment Team, Faculty of Science, Mohammed V University in Rabat, Rabat, Morocco

T. Zair
Research Team of Chemistry Bioactive Molecules and the Environment, Laboratoire des Matériaux Innovants et Biothénologie des Ressources Naturelles, Faculty of Sciences, University Moulay Ismaïl of Meknes, BP 11201, Zitoune, 50003 Meknes, Morocco

20.1 Introduction

On the global scale, the current energy and environmental situations present several emerging problems (Kirchnerova et al. 1993; Agarwal and Pedler 1986; Liu et al. 2016). The steady growth in energy demand, the depletion of fossil fuel resources, air pollution and its effects on global warming and human health, are all major factors in a general awareness of energy use and environmental preservation (Azzouzi et al. 2022). This willingness has been translated into actions engaged in a policy of sustainable growth, which includes the optimization of existing technologies, but also the diversification and development of new procedures (Mabrouki et al. 2018). The development of alternative fuels “biofuels” is therefore one of the many solutions available within the framework of the overall renewable energy offer. The bioethanol is a liquid fuel produced from the transformation of biological matter. The organic matter is either sugar or starch in the first generation of bioethanol, or cellulose in the second generation. The latter generation is a response to the competition problems with the food chain faced by the first generation (Fattah et al. 2021). The second generation bioethanol is thus arousing a growing concern especially from the transport sector, because it offers several advantages: it is suitable for existing vehicle motorization systems, its combustion is cleaner than that of fossil fuels and it can be derived from the most abundant resource, which is the lignocellulosic biomass. The optimisation of the process of bioconverting lignocellulosic material into bioethanol presents a major problem (Elouardi et al. 2022; Samghouli et al. 2022; Benchrifa and Mabrouki 2022).

Cannabis is a widely used drug in the French population, particularly among young people. It is at the heart of a passionate discussion on its classification as a “hard” or “soft” drug, its legalization, tolerance, etc. The aim of this document is obviously not to enter into such controversies... Cannabis remains for many people, especially users, a great unknown as to its real effect (Benchrifa et al. 2022).

The oil extraction industry is constantly producing significant amounts of waste, most of which is not recycled and whose release into the environment is a major environmental threat (Regraguy et al. 2022). The recycling of these by-products would contribute to limiting the impact of this industry on the environment.

Waste Management has become a major priority of the environmental policy of our country. In the present context of sustainable growth involving energy diversification, the use of the biomass as a source of energy is becoming essential. The present political will encourages the use of waste as an alternative source. Economic, environmental and social reasons are in favor of this type of energy (Mabrouki et al. 2018, 2021; Alouani et al. 2022). Agricultural wastes constitute the most competitive source of renewable energy for the production of heat and power, this resource is widely available in Morocco. In the framework of this study, we are concerned with the valorization of cannabis residues for the production of thermal energy by combustion of compressed logs based on the plant roots.

20.2 Material and Method

20.2.1 Thermal Drying

The drying is a unitary process, which aims to remove by vaporization the water, which impregnates a product (liquid or solid) in order to convert it into a dry solid material with a very low residual humidity. Thermal drying is an intermediate treatment process of the waste that consists in evaporating the water they contain. This allows a significant reduction in the residue's volume and weight and promotes its valorization (Vaxelaire et al. 2000).

A straight drying is drying by direct contact with a hot gas. The extracted gases containing the evaporating water have a very high volume. The techniques that use the convection phenomenon are drum, single band, fluidized bed, hot air stream, cold air stream and solar driers. First, the dewatered waste can be mixed with a part of the dried recycled sludge. The recycling of the dried residues does not exist on all processes. However, it allows avoiding the problem of the plastic stage of the residue, since the residue is entering the dryer with a dryness of more than 60%. The residue is then pulverized in the drying chamber. It is entrained and dried by the liquid by convective action. At the dryer outlet, the gas–solid separator of cyclone or bag filter type makes it possible to extract on one side the dried slurry and on the other side the air charged with steam. After separation of the dried sludge and steam condensation, the medium is returned to the ambient air or partially recovered after heating in the heating boiler. In our case, we used the direct part of an oven on the roof of the laboratory (Fig. 20.1) for the residues drying (Mabrouki et al. 2020). These wastes are placed on a grid and then put inside the dryer exposed to the direct sunshine.

Fig. 20.1 Drying furnace



20.2.2 Measurement and Sampling

For the data collection and storage we used a data capture unit (CR10X) equipped with a storage module. With the help of a software program, we control the step of the measurements to 5 s and integrate the measures over one hour. This unit is connected to an infrared thermometer to measure the oven temperature, a probe to determine the relative moisture and temperature in the solar dryer and a pyranometer to measure the global solar radiation incident (Azoulay et al. 2021).

Measuring humidity

Moisture is essential to our comfort and health. But too much or not enough moisture can cause all kinds of difficulties for the occupant, as shown in the chart entitled “Moisture problems”. Some of these problems are just a nuisance, but others can be much more severe. Canadians are aware of many of these conditions, as they are often experienced in the heating season when it is cold outside.

Relative humidity.

Relative humidity is the ratio between the partial pressure of water vapour in a gas (P_v) and the maximum possible water vapour pressure, i.e. the saturation pressure (P_s), for a given temperature.

$$Hr = \frac{100 \times P_w}{P_s(t)} [\%] \quad (20.1)$$

Absolute humidity.

The absolute humidity (H) indicates the amount of water vapor contained in a given volume of air.

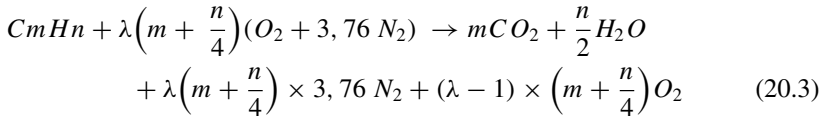
$$H = \frac{\text{Massed'elavapeur d'eau}}{\text{Volumed'air}} \quad (20.2)$$

The Model 6200 is a microprocessor controlled isoperibol oxygen can calorimeter, widely used for routine and occasional caloric testing. It utilizes the Parr 1108 style oxygen bomb and oval cup in a small, compact calorimeter, yielding reliable results with excellent repeatability.

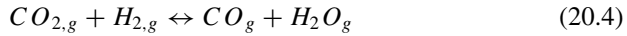
20.2.3 Data Collection

Burning can be defined as the chemical reactions that take place when oxygen and a combustible material combine. This reaction is overall exothermic, i.e. it takes place with a release of warmth. In the case of the building, this heat is mainly used to maintain a comfort temperature. There are many types of fuel (gas, oil, wood, coal,

etc.) but they have one thing in mind: they contain mainly hydrocarbon fuels, i.e. combinations of carbons and hydrogens.



Not a complete combustion



Law of mass action:

$$K_p \equiv \frac{[C O] \times [H_2 O]}{[C O_2] \times [H_2]} \quad (20.5)$$

20.3 Resultats and Discussion

20.3.1 *Physic Chemical Properties*

The analytical results of the proximal compositions of leaf, stem, and grain are shown in Table 20.1. The leaf showed a leaf moisture of 6.87% with a lipid content of 19.97%. The raw protein content gave a value of 23.78% protein, while the raw fibers were 18.95%. The ash level recorded a value of 11.18%; the stem had 17.20% of crude proteins, 23.14% of crude fibers, an aether extraction of 19.97%, ash of 11.18% and a moisture content of 6.87%. The proximal content of the stalk showed a crude protein value of 17.20%, crude fiber of 23.14%, ether extract of 8.02%, ash of 6.78% and a humidity content of 5.16% (Bencheikh et al. 2021). The results of the test on seeds reported a content of gross protein of 20.19%, gross fiber of 25.36%, ether extract of 9.31%, ash of 7.20% and a humidity value of 5.91% with nitrogen content free extract (NFE) values of 19.25, 39.70 and 32.03% for leaves, stem and grains, respectively, obtained by finding the differences between the summed proximal values with reference to a percent of 100 (Table 20.1).

20.3.2 *Realization of the Logs*

The materials used are the cannabis residues and the beeswax in order to maintain the flame as long as necessary for a better output. The cannabis residues are dried in the dryer for 4 days until moisture content lower or equals 10%. Then, these samples

Fig. 20.2 Poudre et brique



are crushed in order to have a homogeneous product (Fig. 20.2). Using sieves with different mesh sizes, only the particles with an average diameter of 2 mm were kept. Then we mixed this powder with the beeswax already melted in the water bath, until we have a homogeneous paste, which will be pressed inside a steel cylinder, maintaining the percentage of 20% of beeswax and 80% of waste material powder (Bencheikh et al. 2020; Mabrouki et al. 2019).

20.3.3 *Drying and Combustion Results*

In evaluating the functioning of the process, the variation of the operating temperature of the oven was measured (Fig. 20.3).

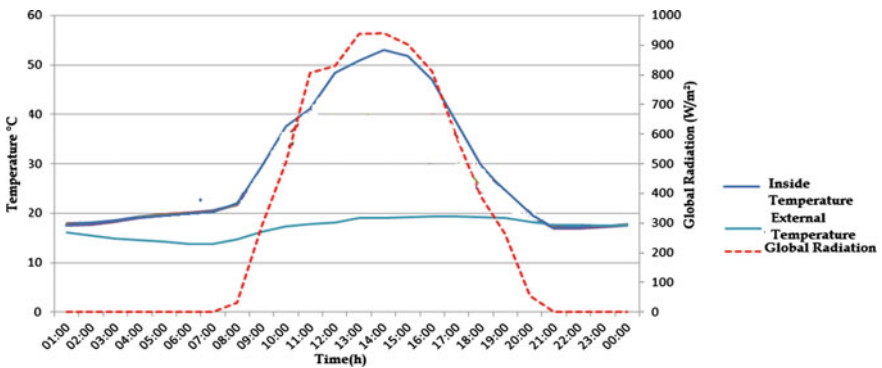
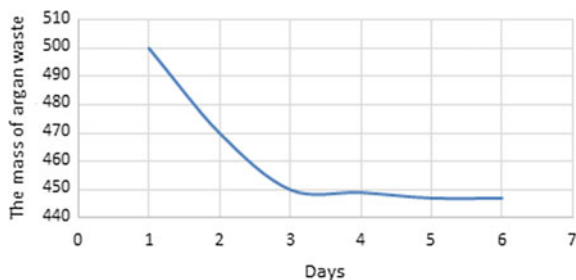


Fig. 20.3 Thermal variation as a result of time

Fig. 20.4 Variation in humidity of cannabis



According to the figure, it can be noticed that the internal temperature is close to 53 °C. This will make easier the drying of the plant remains and minimize the drying time as shown in the (Fig. 20.4).

The figure shows that the cannabis seeds have lost most of their humidity after 3 days of drying. The residue drying will facilitate the crushing of the residues and will increase their calorific power (Mujumdar and Zhonghua 2007; Gebreegziabher et al. 2013; Vorotinskienė et al. 2020; Kadioğlu and Varamaz 2003). To assess the quality of the furnace and the quality of the fuel, we have started the furnace by using the waste of the argan nuts as combustible. The result of this test is shown in the (Fig. 20.5).

From this test, we can see that after 45 min, the temperature of the oven has reached 420 °C, thanks to the high calorific power of the cannabis residues and also the beeswax contained in the logs, which has the purpose of maintaining the flames as long as possible (Abdulmalek et al. 2018; Sabarez 2018; Yuan and Wan 2002; Hassebrauck and Ermel 1996). On the other side this result showed that the insulation of the oven has increased its effectiveness since the time of temperature increase is short. Morocco as an oil producer country has the benefit and interest to make this kind of industry by marketing the waste as fuel and transform it into other by-products that will bring a plus to the domestic economy, and that thanks to the raw material availability and in very reduced count.

Fig. 20.5 Variation of the combustion temperature

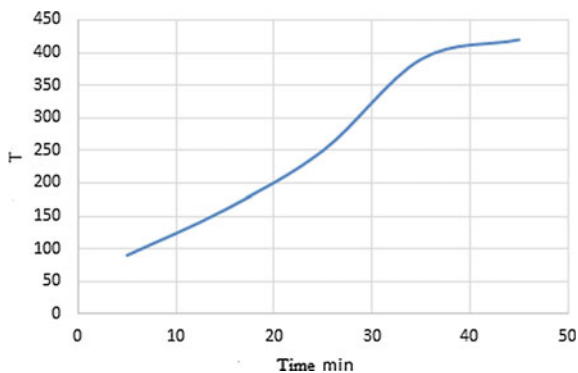


Table 20.1 Proximate analysis of Cannabis (wt.%)

Proximate (%)	Leaf	Stem	Seeds
Crude protein	23.08	17.10	20.09
Crude fibre	18.45	22.03	25.76
Ether extract	19.27	8.12	9.21
Ash	11.28	6.48	7.40
Moisture	6.17	5.36	5.21
NFE	19.05	39.10	31.03

20.4 Conclusion

Our research is in line with this sustainable management of the natural environment, as it enables the valorization of a widely available waste in our country. The experimental work enabled us to familiarize with the technique of adsorption and with the characterization methods via the latest equipment. The principal objective of our work was to demonstrate the absorbent qualities of a food by-product, cannabis, which we are seeking to valorize by using it as activated carbon. This valorization is part of an economic strategy in order to incite the maâsras not to spread the pomaces in the nature knowing that they strongly contribute to the contamination by the presence of pollutants such as phenol components but to consider them as valorizable sub-products of the cannabis extraction. The current study allows to reach the conclusion that further research is needed to identify the active components present in the plant extracts in order to develop biomass based on cannabis plants that are safe for energy generation and that present a minimal risk for the surrounding environment.

References

- Abdulmalek SH, Assadi MK, Al-Kayiem HH, Gitan AA (2018) A comparative analysis on the uniformity enhancement methods of solar thermal drying. *Energy* 148:1103–1115
- Agarwal PK, Pedler I (1986) Drying, devolatilisation and volatile combustion for single coal particles: a pseudo steady state approach. *Fuel* 65(5):640–643
- Azoulay K, Bencheikh I, Mabrouki J, Samghouli N, Moufti A, Dahchour A, El Hajjaji S (2021) Adsorption mechanisms of azo dyes binary mixture onto different raw palm wastes. *Int J Environ Anal Chem* 1–20
- Bencheikh I, Azoulay K, Mabrouki J, El Hajjaji S, Dahchour A, Moufti A, Dhiba D (2020) The adsorptive removal of MB using chemically treated artichoke leaves: parametric, kinetic, isotherm and thermodynamic study. *Scientific African* 9:e00509
- Bencheikh I, Azoulay K, Mabrouki J, El Hajjaji S, Moufti A, Labjar N (2021) The use and the performance of chemically treated artichoke leaves for textile industrial effluents treatment. *Chem Data Collect* 31:100597
- Benchrifa M, Mabrouki J (2022) Simulation, sizing, economic evaluation and environmental impact assessment of a photovoltaic power plant for the electrification of an establishment. *Adv Buil Energy Res* 1–18

- Benchrif M, Mabrouki J, Elouardi M, Azrou M, Tadili R (2022) Detailed study of dimensioning and simulating a grid-connected PV power station and analysis of its environmental and economic effect, case study. *Model Earth Syst Environ* 1–9
- El Alouani M, Aouan B, Rachdi Y, Alehyen S, El Herradi EH, Saufi H, ... Barka N (2022) Porous geopolymers as innovative adsorbents for the removal of organic and inorganic hazardous substances: a mini-review. *Int J Environ Anal Chem* 1–13.
- El Azzouzi L, El Hadki H, El Hadki A, El Alouani M, Mabrouki J, Tazi R, ... Kabbaj OK (2022) A computational investigation on the adsorption of amoxicillin on graphene oxide nanosheet. *Int J Environ Anal Chem* 1–9
- Elouardi M, Zair T, Mabrouki J, Fattah G, Benchrif M, Qisse N, El Belghiti MA (2022) A review of botanical, biogeographical phytochemical and toxicological aspects of the toxic plants in Morocco. *Toxicologie Analytique et Clinique*
- Fattah G, Ghrihi F, Mabrouki J, Al-Jadabi N (2021) Modeling and assessment of the impact of land use in the Western RIF Region, Morocco, on Water Quality. In: *International archives of the photogrammetry, remote sensing & spatial information sciences*, vol 46
- Gebreegziabher T, Oyedun AO, Hui CW (2013) Optimum biomass drying for combustion–A modeling approach. *Energy* 53:67–73
- Hassebrauck M, Ermel G (1996) Two examples of thermal drying of sewage sludge. *Water Sci Technol* 33(12):235–242
- Kadioğlu Y, Varamaz M (2003) The effect of moisture content and air-drying on spontaneous combustion characteristics of two Turkish lignites. *Fuel* 82(13):1685–1693
- Kirchnerova J, Klvana D, Vaillancourt J, Chaouki J (1993) Evaluation of some cobalt and nickel based perovskites prepared by freeze-drying as combustion catalysts. *Catal Lett* 21(1):77–87
- Liu HEJ, Ma X, Xie C (2016) Influence of microwave drying on the combustion characteristics of food waste. *Dry Technol* 34(12):1397–1405
- Mabrouki J, El Yadini A, Bencheikh I, Azoulay K, Moufti A, El Hajjaji S (2018) Hydrogeological and hydrochemical study of underground waters of the tablecloth in the vicinity of the controlled city dump mohammedia (Morocco). In: *International conference on advanced intelligent systems for sustainable development*. Springer, Cham, pp 22–33
- Mabrouki J, Moufti A, Bencheikh I, Azoulay K, El Hamdouni Y, El Hajjaji S (2019) Optimization of the coagulant flocculation process for treatment of leachate of the controlled discharge of the City Mohammedia (Morocco). In: *International conference on advanced intelligent systems for sustainable development*. Springer, Cham, pp. 200–212
- Mabrouki J, Benbouzid M, Dhiba D, El Hajjaji S (2020) Simulation of wastewater treatment processes with Bioreactor Membrane Reactor (MBR) treatment versus conventional the adsorbent layer-based filtration system (LAFS). *Int J Environ Anal Chem* 1–11
- Mabrouki J, Azrou M, Hajjaji SE (2021) Use of internet of things for monitoring and evaluating water's quality: a comparative study. *Int J Cloud Comput* 10(5–6):633–644
- Mujumdar AS, Zhonghua W (2007) Thermal drying technologies—Cost-effective innovation aided by mathematical modeling approach. *Drying Technol* 26(1):145–153
- Regragy B, Ellouzi I, Mabrouki J, Rahmani M, Drhimer F, Mahmoud C, ... El Hajjaji S (2022) Zinc doping of different nanoparticles of TiO₂ Sachtopore for improved elimination of the methyl orange by photocatalysis. *Emergent Mater* 1–14
- Sabarez HT (2018) Thermal drying of foods. In: *Fruit preservation*. Springer, New York, NY, pp 181–210
- Samghouli N, Regragy B, Abahdou FZ, Azoulay K, Bencheikh I, Mabrouki J, El Hajjaji S (2022) Removal of a non-steroidal anti-inflammatory drug (Piroxicam) in an aqueous medium by an agricultural by-product. In *E3S Web of Conferences*, vol 337, p 05001

- Vaxelaire J, Bongiovanni JM, Mousques P, Puiggali JR (2000) Thermal drying of residual sludge. *Water Res* 34(17):4318–4323
- Vorotinskienė L, Paulauskas R, Zakarauskas K, Navakas R, Skvorčinskienė R, Striūgas N (2020) Parameters influencing wet biofuel drying during combustion in grate furnaces. *Fuel* 265:117013
- Yuan Y, Wan ZL (2002) Prediction of cracking within early-age concrete due to thermal, drying and creep behavior. *Cem Concr Res* 32(7):1053–1059

Chapter 21

Delineation of Groundwater Potential Zones in a Semi-arid Region Using Remote Sensing and GIS: A Case Study of Argana Corridor (Morocco)



Mohamed Ait Haddou, Youssef Bouchriti, Mustapha Ikirri, Abderrahmane Wanaim, Ali Aydda, Salih Amarir, Rachid Amiha, and Youssef El Boudribili

Abstract Currently, the Argana corridor (Western High Atlas of Morocco) faced severe drought, desertification, and water and soil resources degradation. Due to many factors (climate change, rural practices, etc.) the level of satisfaction of water needs has been steadily decreased during last years in this semi-arid area. In general, delineation of potential aquifers is considered helpful to serve the water supply for population, especially in arid and semi-arid areas, but it is technically and economically limited as field investigations are expensive. Commonly, it can be easy to map and delineate groundwater potential areas by investigating the tectonic, lithologic, climatic and topographic data of an area. This study aims to map the potential groundwater areas in the Argana corridor using GIS and RS-based (Geographic Information System-Remote Sensing) multi-criteria analysis. The results show that the GIS and RS-based multi-criteria decision analysis plays a good role in identifying the groundwater potential areas. The areas of high groundwater potential are mainly located in the upstream part of the basin and in the eastern part of the Argana corridor. Whereas, the centrale and piedmont areas of the basin are of less interest due to the presence of Permo-Triassic continental terrain. In the western part of the basin, the main aquifers are linked to the Jurassic limestone-marlstones of the Ida-Ou-Tanane plateau boarding the western part of the Issen basin, and to the Triassic clay-sandstone terrain of Ait Khatab. The results obtained are in good agreement with water flow recorded from well points in the field (76% of accuracy). These finding emphasizes that the groundwater resources are very limited in the Argana basin.

Keywords GIS and RS multi-criteria analysis · Groundwater potentiality · Argana corridor · Issen basin

M. Ait Haddou (✉) · Y. Bouchriti · M. Ikirri · A. Wanaim · A. Aydda · S. Amarir · R. Amiha · Y. El Boudribili
Department of Earth Sciences, Faculty of Sciences, Ibn Zohr University, Agadir, Morocco
e-mail: mohamed.aithaddou@edu.uiz.ac.ma

21.1 Introduction

The water resources have been steadily declined in recent years, which probably due to global population growth pollution, affecting water quality and climate change (Knippertz et al. 2003; Kadi and Ziyad 2018; Yousif 2021; Azrour et al. 2022; Gougueni et al. 2021). In the Souss basin, Morocco, the expansion of intensive irrigated agriculture practices has led to a drastic decrease in groundwater resources and degradation of natural resources (Msanda et al. 2021). In this basin, surface water is limited and very irregular. The flows of the tributaries are irregular during the year. Runoff is only observed during the short winter and spring periods, where floods can be hitting and causing enormous damages. The Issen catchment, part of the Souss basin, is currently subject to severe drought, desertification and land degradation due to overgrazing, that causes considerable damage to the vegetation and soil quality. It is likely to face increased climate variability and water stress in the future (Ait Haddou et al. 2020, 2022c). It is strongly influenced by the altitude of the Atlas Mountains, which mitigates the effect of the ambient aridity by multiplying the contrasts on a local scale. Bouchaou et al. (2008), they established the link between the Triassic evaporites and the salinity anomaly of the Souss water table at the level of Issen Wadi. The key objective of this study is to map groundwater potential zones in the Issen catchment. Specifically, the study focuses on (i) providing a several potential indices maps (ii) identifying of groundwater potential zones and (iii) assessing certainty zones of the groundwater resources.

21.2 Study Area, Data and Methods

21.2.1 Study Area

The study area, Issen catchment, is an important catchment in the Souss basin, and a tributary of the Souss river in the central western of Morocco (Fig. 21.1). The Issen Wadi covers a drainage area of approximately 1300 km² (Ait Haddou et al. 2020, 2022a). Geologically, the Issen basin can be divided into three different zones (Tixeront 1974) (Fig. 21.2). The ancient primary massif consists of the schists and the quartzites. The Argana Permo-Triassic corridor comprises at least 2500 m of fluvial, lacustrine, and coarse to fine clastic floodplain deposits (Olsen et al. 2003). Forms broad troughs crisscrossed by sand-stone monoclinical ridges and controlled by an extensive fault system (Ben Mlih et al. 2004). The Jurassic limestone and marl-limestone plateaus corresponds to the northern cuestas which is classified as one of the meridional highlands. The tectonics, lithology, and external geodynamics characteristics of the Issen catchment indicate a strongly contrasted morphology (Ait Haddou et al. 2022b). The climate of the study area is warm and dry, where the mean annual temperature is approximately 21.85 °C, the mean annual rainfall is ~302 mm/year in the central parts, and the annual evaporation is 2278 mm/year.

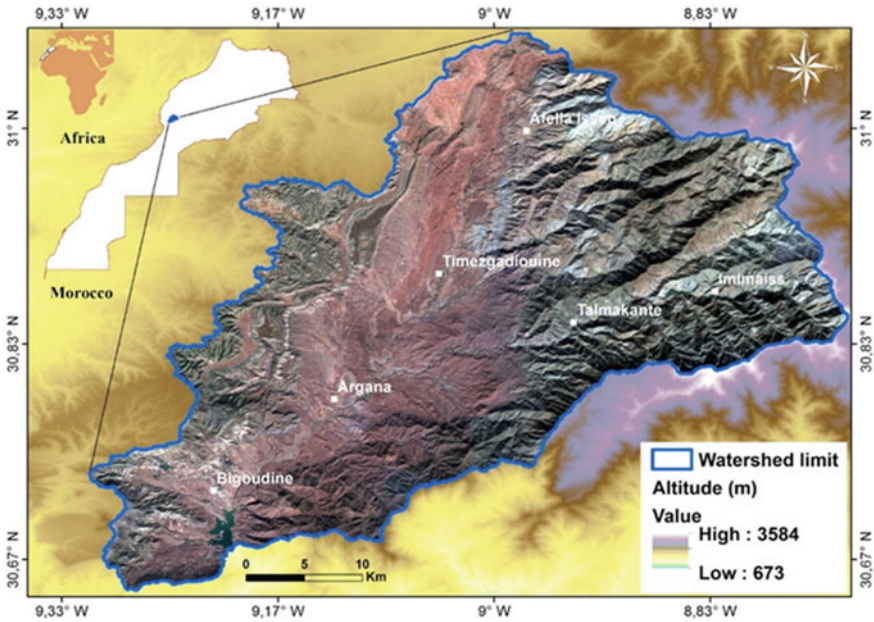


Fig. 21.1 Geographical location with elevation variation of the study area (Ait Haddou et al. 2020)

Commonly, the lithological facies heterogeneity, soil types, topography, climate, and fluvial system are the most and common parameters affecting the spatial hydrological flows variability.

The monthly and seasonal distribution of the flows of the Issen wadi is essentially conditioned by the winter rainfall contributions which are dependent on the Mediterranean climatic conditions, and by their physical stationary properties of a torrential nature. A hydrology that is characterized by a great spatio-temporal variability, with a succession of high and low water periods. The average interannual flow recorded over the observation period (1981/1982 to 2012/2013) is 1.81m³/s (Fig. 21.3), i.e. an average interannual input of 57.08 million m³. However, the supply of drinking water to douars is very low and the situation is alarming, as only 28% have direct access to surface water.

The correlation between the calculated interannual averages of the flows and the precipitation on the data set from 1981 to 2013 shows a value of the coefficient of determination $R^2 = 0.66$, it is about 70%. This reveals the large part of the contribution of the water linked essentially to precipitation in the flow of the Wadi Issen (Table 21.1). The Issen watershed receives an average annual rainfall of 302 mm. Its specific flow is 1.39 l/s/km² corresponding to a water flow of 43.90 mm.

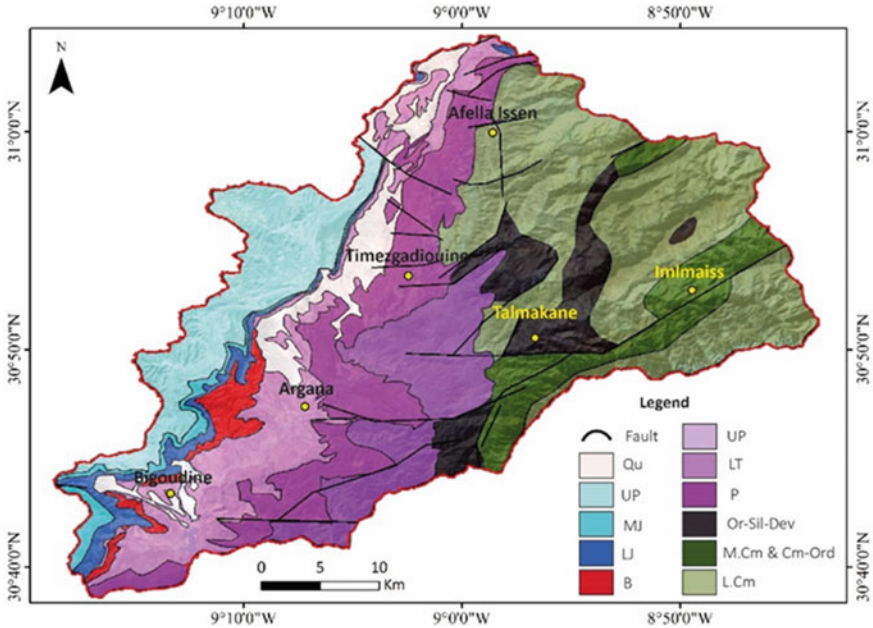


Fig. 21.2 Lithological units in the study area (1:100.000), digitalized from an assembly of two geologi-cal maps of Argana and Imi N'Tanoute (Tixeront 1974). (Of note the Palaeozoic massif completed as an approximation by the geological map of Imi N'Tanoute). Qu: Quaternary, UJ: Upper Jurassic, MJ: Middle Jurassic, LJ: Lower Jurassic, B: Basalt, UT: Upper Triassic, LT: Lower Triassic, P: Permian, Or-Si-Dev: Ordovician Silurian-Devonian, M. Cm & Cm-Ord: Middle Cambrian & Cambro-Ordovician, L.Cm: Lower Cambrian)

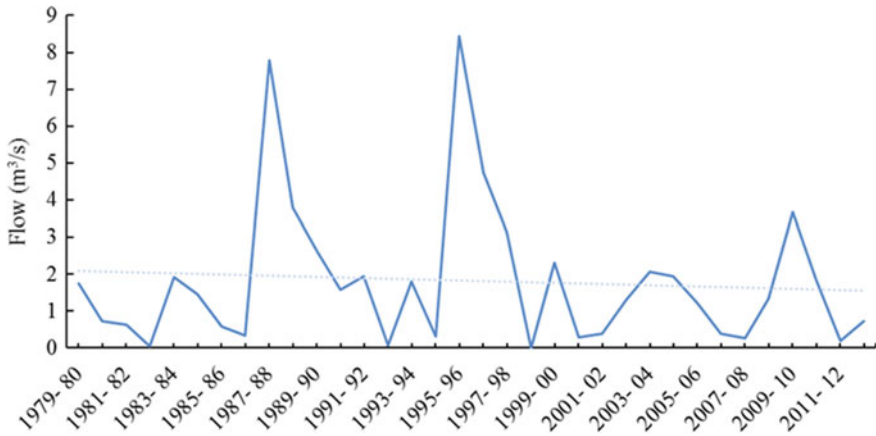


Fig. 21.3 Variation of the average interannual flows of the Wadi Issen recorded at the hydrometric station of Aгуenza from 1980 to 2013

Table 21.1 Comparison between the average flows (AF) of the Wadi Issen and the precipitation mean (PM) in the Issen basin

Parameter	Period	Mean	Standard deviation	Covariance %	Maximum (year)	Minimum (year)
PM (mm)	1980/2017	302	202.38	67	1995/96	2011/12
AF (m ³ /s)	1980/2013	1.81	1.98	109	1995/96	1998/1991 ^a

^aThe minimum liquid flow (Q) of the Wadi Issen has been recorded for several hydrological years.

21.2.2 Datasets

In this study, the annual rainfall data from 13 metrological stations with more than 37 years monthly data were collected and processed from the Hydrographic Basin Agency of Souss Massa (ABHSM) and the High Commission for Waters and Forests and the Fight against Desertification (HCEFLCD). In addition, A 12.5 m ALOS Digital Elevation Model (DEM) data was used to delineate the catchments and compute different hydrographic network. Further, the lithological units and the faults of the study area were digitalized from an assembly of two geological maps of Argana and Imi N'Tanoute (1:100.000). However, the lineaments were extracted from Landsat 8 OLI images.

21.2.3 Methods

The decision criteria are weights used based on linear combination to decide (Saaty 1977). These factors are frequently used for groundwater potential areas identification (Doumouya et al. 2012; Ta et al. 2011). It produces standardized weights whose sum is equal to 1.

Details of the application of The Analytic Hierarchy Process (AHP) are reported in the work of Saaty (2016). With the use of AHP, the relevant factor's relative significance was obtained after the construction of a pairwise comparison matrix (Mu and Pereyra-Rojas 2017). In the case of this study, the pairwise comparison matrices are presented in Table 21.2. The rating score of relative significance was set up from 0.05 to 0.24, indicating less importance to much more importance of the factor in that order.

In this study, eight factors affecting groundwater potential zones were considered, including permeability (Pe), lineament density (Ld), drainage density (Dd), precipitation (P), nodes density (Nd), distance to stream network (Ds), distance to lineament/Fault (Dl), and slope (S). The potential maps produced were then classified. The groundwater score index used to determine potential zones is expressed as shown in equation below (21.1).

Table 21.2 Comparison matrix of selected factors

Factors	Ld	Dd	P	Nd	Pe	Ds	Dl	S
Ld (km/km ²)	1	2	3	3	2	4	2	6
Dd (km/km ²)	1/2	1	2	3	3	5	2	6
P (mm)	1/2	1/2	1	4	2	3	1/4	4
Nd	1/3	1/3	1/2	1	6	4	1/2	3
Pe	1/4	1/4	1/3	1/2	1	6	1/2	3
Ds (m)	1/3	1/2	1/3	1/4	1/5	1	1/2	6
Dl (m)	1/2	1/2	3	6	5	6	1	6
S (degre)	1/3	1/3	1/4	1/2	1/3	1/3	1/4	1

$$DWPI = \sum_{i=1}^n (w_i * X_i) \tag{21.1}$$

$$DWPI = (Ld, \text{ km/km}^2 * 0.24) + (Dd, \text{ km/km}^2 * 0.19) + (P, \text{ mm} * 0.17) \\ + (Nd * 0.11) + (Pe * 0.09) + (Ds, \text{ m} * 0.06) \\ + (Dl, \text{ m} * 0.09) + (Slope * 0.05)$$

where w_i is the factor weight, x_i is the frequency ratio of the factor and n is a total number of the used factors.

After extraction of each influencing factor, from GIS and RS data, the model was performed in a GIS environment to produce groundwater potential zones map.

21.3 Results and Discussion

21.3.1 Conditioning Factors

Figures 21.4 and 21.5 show the importance of the outcrops of fairly impermeable and soft silt-sandstone and schistose terrains of the Permo-Triassic, totally drained by the Issen wadi and its tributaries. The Upper Permian and Triassic-Liassic terrains bear the traces of distensive geological events related to the onset of rifting. The basin is structured according to a system of large ENE—WSW faults which results in a varied topography and a morphologically dynamic relief. The main watercourse of the study area is of stream order 5, the drainage density is low, averaging 0.85 km/km² for the whole catchment. However, the density of the hydro-graphic network and its ramification are especially important from 1200 m altitude on the marl-limestone and friable schistose-gravel mountain slopes framing the Argana corridor. The mean annual precipitation sum at the total area of this basin (302 mm) in the upper section is about 600 mm.

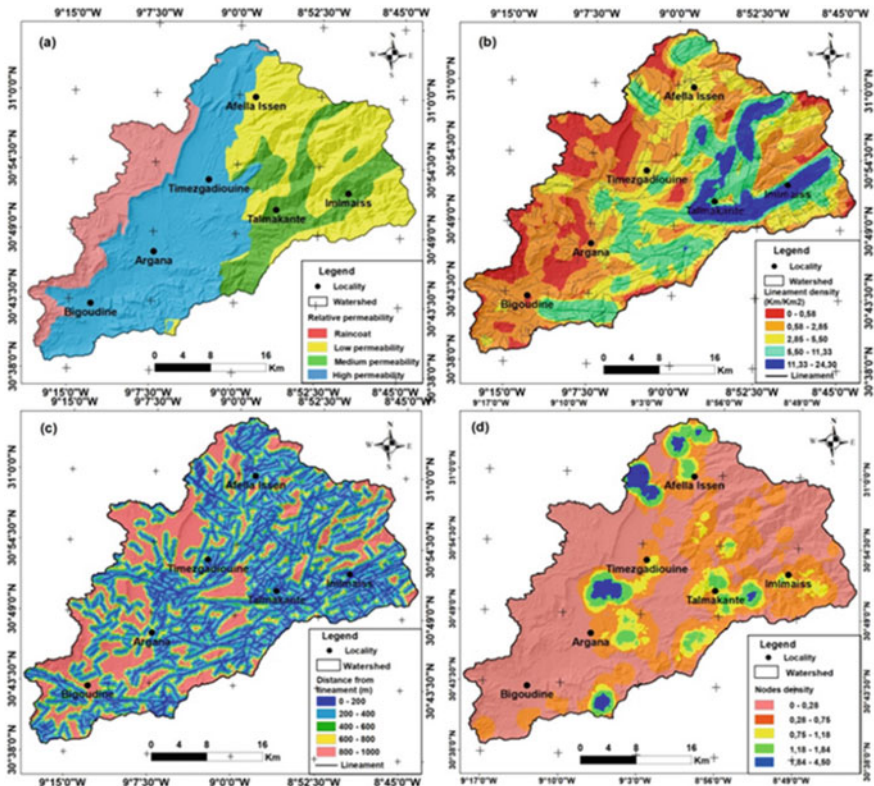


Fig. 21.4 Classification of lithological and structural factors influencing groundwater potential zones. Permeability map (a); Lineament density map (b); Distance to lineament/Fault map (c); Nodes density map (d)

The data available on the Triassic lands downstream of the catchment highlight several factors that are not in favor of a strong aquifer circulation:

- The very mountainous morphology in almost all the territory of the study area.
- The elevated topography.
- The impermeability of the schistose metamorphic substratum of the Paleozoic basement.
- The absence of watertight layers at shallow depths under the Permo-triassic, detrital facies soils which could constitute aquifer reservoirs.
- The presence of relatively permeable sandstone.

The area of the foothills of ancient primary massif, to the east of the Issen catchment, seems to be more interesting in terms of underground resources because of the presence of density of the hydrographic network and its ramification (Fig. 21.6).

However, the distance from stream networks had been considered as an important parameter in hydrogeological research because the local alluvial aquifers usually

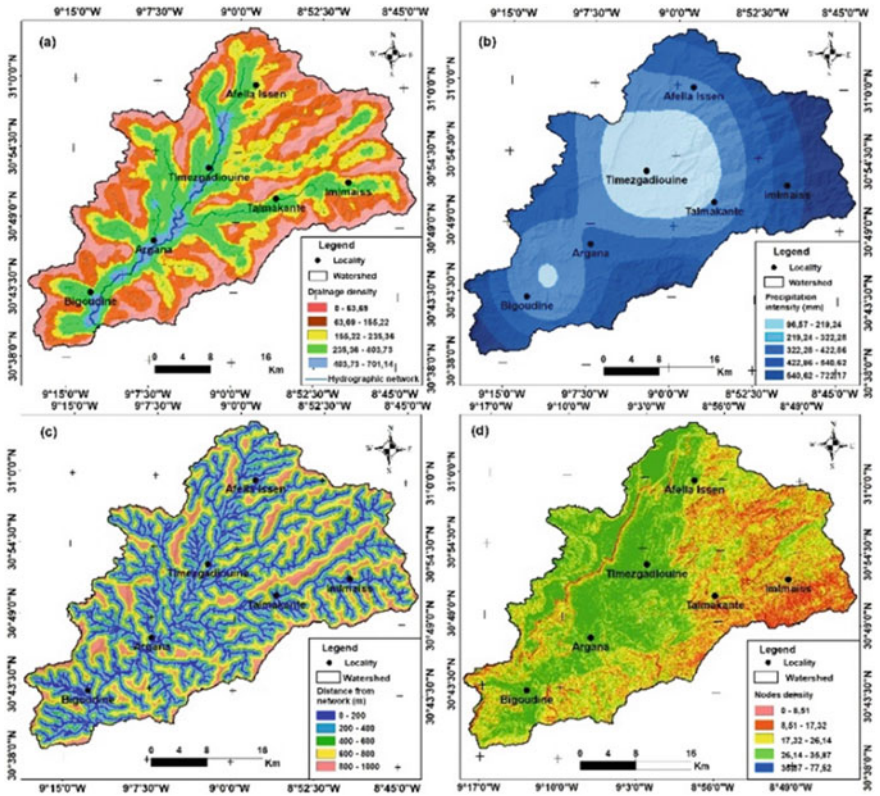


Fig. 21.5 Classification of hydrological, climatological, and topographical factors influencing groundwater potential zones. Drainage density map (a), Precipitation map (b), Distance to stream map (c), Slope gradient map (d)

prospect in areas near the rivers. The main aquifers are strictly linked to the Jurassic sandstone limestones and marls of the Mesozoic cover of the Ida-Ou-Tanane which border the south-western part of the Issen catchment. Additionally, the concentration of drainage also helps the streamflow recharge the groundwater system. The midstream region was less important and was influenced by the impermeability of fluvial, lacustrine, and coarse to fine clastic. The only existing water sources are characterized by very irregular flows that depend directly on the rainfall regime. The flows are less than 2 l/s. The areas of high and medium water potential cover about 51.40% of the total basin. Overall, these findings can be used as a tool to help prospecting groundwater resources in fractured environments.

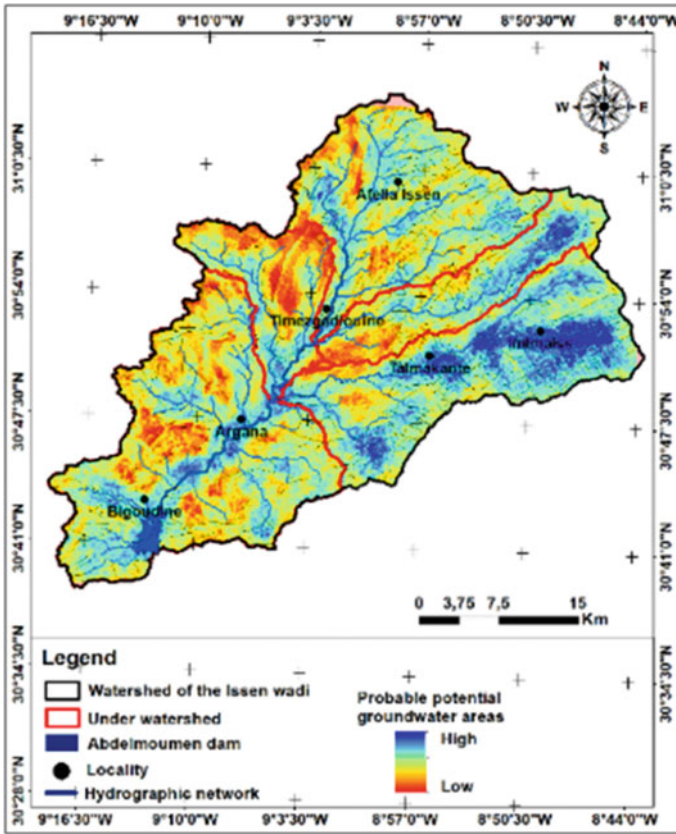


Fig. 21.6 Spatial distribution of groundwater potential zones

21.3.2 Validation of Groundwater Potential Map

Many models are used by researchers to delineate groundwater potential in various regions of the world, but it is essential to validate the results of the model in order to ensure that the tested model represents the true ground situation or the recorded observations sufficiently. Model calibration and validation can be done by comparing model output with observed data. For the study area there are many points available for the piezometer fluctuation. Therefore, the prediction accuracy results of the success rate were obtained using a local dataset.

The Water Resources Inventory (WRI) data for the Argana corridor is about 194 points (ABHSM 2004), of which only 82.5% are complete. They concern study and exploitation boreholes, hydrogeo-logical reconnaissance boreholes, wells, springs, and piezometers. Table 21.3 lists the number and the percentage of each inventory type.

Table 21.3 Distribution of water points in the Argana corridor

WRI	Borehole	Study boreholes	Wells	Piezometers	Total
Number	95	34	28	5	162 points
Percentage (%)	59	21	17	3	100%

According to the map of the Souss nappe (ABHSM 2008), the boundaries of its aquifer border the southern limit of the Issen basin without crossing it and extends into the alluvial cone of the right bank of the Souss, these recharging zones of the nappe over-hang the Souss plain. The water trapped behind the Abdelmomen dam feeds the Dkhila di-ersion dam, after rainfall infiltration into the ground to create a local water supply to the Issen perimeter water table. The depth of this water table is variable, fluctuating between 8 and 40 m with an average of 21.43 m. This groundwater leaches out the saliferous Triassic soils and is generally characterized by a high level of mineralization (dry residue >1 g/l). The foothills area, to the east of Issen, appears to be more interesting in terms of groundwater re-sources due to the presence of the Cretaceous cover. These reservoirs can give rise to interesting flows.

The ABHSM (ABHSM 2003) explained that the impermeability of the schistose metamorphic bedrock of the Paleozoic basement and the absence of watertight layers at shallow depths under the Permo-Triassic soils are not in favor of a strong aquifer circulation in the Issen watershed.

21.4 Conclusion

In this study, an integrated approach multi-criteria analysis, based GIS and RS technique, was proposed to delineate groundwater potential zones over the Issen catchment, Western High Atlas of Morocco. The areas of high groundwater potential are mainly located in the upstream part of the study area and in the eastern part of the Argana corridor. On the Permo-triassic continental terrain represented at the base by conglomerates, sandstones, clay-sandstones, red marls and by powerful clays crowned by basalts. Groundwater resources are very limited, only the sandstones can act, locally, as aquifers. The areas of high and medium groundwater potential cover about 51.40% of the total study area. The results obtained are in good agreement with water flow points (76% of accuracy) and in comparison, with other basins in the Western High Atlas. These findings emphasize that the groundwater resources are very limited in the Issen catchment.

References

- ABHSM (2003) Etude de synthèse des études géophysiques réalisées dans les plaines de Souss et Chtouka, ABHSM
- ABHSM (2004) Rapport de l'étude de la recharge artificielle des nappes dans les bassins hydrauliques du Souss Massa, mission I, étude de base par sous bassin, diagnostic et élaboration d'un programme de recharge artificielle
- ABHSM (2008) Demande en eau agricole », In ABHSM, « Étude de révision du Plan directeur d'aménagement intégré des ressources en eau (PDAIRE) des bassins du Souss-Massa. Mission I : Collecte des données, diagnostic et évaluation des ressources en eau et état de leur utilisation. Rapport définitif », ABHSM-Resing-Aquaplan, Agadir, vol 10, 45 p + annexes
- Azroum M, Mabrouki J, Fattah G et al (2022) Machine learning algorithms for efficient water quality prediction. *Model Earth Syst Environ* 8:2793–2801
- Ait Haddou M, Kabbachi B, Aydda A, Gougni H, Bouchriti Y (2020) Spatial and temporal rainfall variability and erosivity: case of the Issen watershed, SW-Morocco. *E3S Web Conf* 183:02003
- Ait Haddou M, Kabbachi B, Aydda A, Bouchriti Y, Gougueni H, En-Naciry M, Aichi A (2022a) Traditional practices: a window for water erosion management in the Argana basin (Western High Atlas Morocco). *E3S Web Conf* 337:02002
- Ait Haddou M, Wanaim A, Ikirri M et al (2022b) Digital elevation model-derived morphometric indices for physical characterization of the issen basin (Western High Atlas of Morocco). *Ecol Eng Environ Tech* 23(5):285–298
- Ait Haddou M, El Caid MB, Aydda A, Bouchriti Y, Wanaim A, Gougueni H, Ezaidi S (2022c) Fencing land impacts on plant biodiversity and argan trees dynamic in the Ida-Ou-Tanane (central western of Morocco). *IOP Conf Ser: Earth Environ Sci* 1090(1):012023
- Ben Mlih A, Laadila M, El Kochri A, El Youssi M, Nassili M (2004) Le remplissage synrift au permien et au trias du bassin de Tahanaout (Haut Atlas de Marrakech, Maroc) géodynamique et organisation sédimentaire. *Estud Geol* 60:123–138
- Bouchaou L, Michelot JL, Vengosh A, Hsissou Y, Qurtobi M, Gaye CB, Bullen TD, Zuppi GM (2008) Application of multiple isotopic and geochemical tracers for investigation of recharge, salinization, and residence time of water in the Souss-Massa aquifer, southwest of Morocco. *J Hydrol* 352:267–287
- Doumouya I, Dibi B, Kouame KI, Saley B, Jourda JP, Savane I, Biemi J (2012) Modelling of favourable zones for the establishment of water points by geographical information system (GIS) and multicriteria analysis (MCA) in the Aboisso area (South-east of Côte d'Ivoire). *Environ Earth Sci* 67(6):1763–1780
- Gougueni H, Ez-Zaher L, Bouchriti Y, Ait Haddou M, Ezaidi A (2021) Health effects of the consumed water from the traditional reservoirs on the population of Tiznit in Morocco. *E3S Web Conf* 234:00073
- Knippertz P, Christoph M, Speth P (2003) Long-term precipitation variability in Morocco and the link to the large-scale circulation in recent and future climates. *Meteorol Atmos Phys* 83(1):67–88
- Kadi MA, Ziyad A (2018) Integrated water resources management in Morocco. In: *Global water security; world water council*, Edn. Singapore, Springer, pp 143–163
- Mu E, Pereyra-Rojas M (2017) Understanding the analytic hierarchy process. In: *Practical decision making*. Springer, Cham, pp 7–22
- Msanda F, Mayad EH, Furze JN (2021) Floristic biodiversity, biogeographical significance, and importance of Morocco's Arganeraie Biosphere Reserve. *Environ Sci Pollut Res* 28:64156–64165
- Olsen PE, Kent DV, Touhami M, Puffer J (2003) Cyclo-magneto and bio-stratigraphic constraints on the duration of the CAMP event and its relationship to the Triassic–Jurassic boundary. In: Hames WE, McHone G, Renne PR, Ruppel C (eds) *The Central Atlantic magmatic province: insights from fragments of Pangea*. AGU Geophys Monogr 136:7–32
- Saaty TL (1977) A scaling method for priorities in hierarchical structures. *J Math Psychol* 15(3):234–281

- Saaty TL (2016) The analytic hierarchy and analytic network processes for the measurement of intangible criteria and for decision-making. In: Greco S, Ehrgott M, Figueira J (eds) Multiple criteria decision analysis. international series in operations research & management science, vol 233. Springer, New York, NY
- Ta MY, Lasm T, Adja GM, Kouamé KJ, Biémi J (2011) Cartographie des eaux souterraines en milieu fissuré par analyse multicritère. Cas de Bondoukou (Côte-d'Ivoire). *Rev Int Géomatique* 21(1):43–71
- Tixeront M (1974) Carte géologique et minéralisations du Couloir d'Argana. *Notes Mém Serv Géol Maroc* 1974:205
- Yousif M (2021) Une nouvelle théorie pour améliorer les décisions liées aux eaux souterraines basée sur le décryptage du régime paléohydrologique sous le changement climatique au Sahara. *Modèle. Terre Syst Environ* 1–11

Chapter 22

New Development in Renewable Energy Research



Tawaf Ali Shah, Li Zhihe, Li Zhiyu, and Andong Zhang

Abstract The depletion of fossil fuel sources and rising fuel costs together with releasing of harmful gases into the environment cause severe global warming and other crises around the world. Due to the two key characteristics of sustainability and renewability, biofuel research is now conducted on a global scale. There are numerous efficient biomass production methods, which are separated into 3 types, 1st generation, 2nd generation, and 3rd generation biofuel. The 1st generation, includes biomass connected to food crops, the 2nd generation includes waste organic residue, and the 3rd generation includes algal biomass, which represents potential renewable sources. Different processing methods for lignocellulosic and other biomass are reported to prepare it for biofuels production. Here the drawbacks of pretreatment methods with possible improvements are described. New technological applications in biorefineries to recycle waste biomass efficiently and cost-effectively are highlighted. In biorefineries, the role of microorganisms, enzymes, new catalysts, and different approaches than traditional ones are of great significance. The role of biochemical, physical, and thermal processes in the saccharification of the polysaccharides biomass to convert it into simple sugars monosaccharides that could be easily transformed into biofuels are discussed. New technologies, methods, biomass sources, relation with food security, biomass, water, environment, and advancements in the pretreatment of waste biomass for renewable energy production are included. The objective of this chapter is to briefly introduce the various biofuel sources, production methods, benefits, and sustainability of biofuels.

Keywords Waste · Biomass · Pretreatment · Hydrolysis · Energy · Lignin
Anaerobic digestion

T. A. Shah (✉) · L. Zhihe (✉) · L. Zhiyu · A. Zhang
College of Agriculture Engineering and Food Science, Shandong University of Technology, Zibo, China
e-mail: tawafbiotech@yahoo.com

L. Zhihe
e-mail: lizhihe@sdut.edu.cn

22.1 Introduction

Around 84 million barrels (Mb) of fossil fuels are needed globally per day, which was only 16 million barrels (Mb) in 2019 before the COVID-19 pandemic. The demand for fossil fuels is estimated to be increased further at a rate of 6–7 Kilos barrels per day in the near future (Johnsson et al. 2019). The most recent analysis makes it clear that the crude oil reserves may soon run out. Therefore, it is crucial to promote a reliable supply of renewable energy. By 2026, the production of biofuels in Asia will increase by almost 30%, surpassing that of Europe. The inflow of biofuel production from renewable sources is expected to increase by 24% (Rezania et al. 2020). In order to increase the production of biofuel, there is a need for innovative and cutting-edge technology to be commercialized (Yin et al. 2020a). Biomass to biofuels has notable benefits such as being cost-effective, readily available, and environmentally non-threatening, which results in a high output of biofuels. Only 2% of biofuels are currently employed in transportation. However, it is anticipated that biofuels will only account for around 27% of the demand for car fuel in 2050 (Murali et al. 2016). So far, the researchers are agreed that the greatest bases for the production of renewable energy and biofuels are lignocellulosic biomass, non-food crops, and leftover forest waste residue. It is critical to manage efficiently the environmental waste and keep the ecology safe from hazardous materials and pathogens (Shah and Zahra 2014). Nanotechnology may be able to help the biofuel industry implement efficient and well-organized procedures. The enzymes that were employed to hydrolyze the biomass can be immobilized using nanomaterials (Singh et al. 2020). To achieve the target of reaching 27% renewable energy production, there is a great need for novel methods for producing biofuels from waste materials. Further, obstacles in the production of ethanol, biodiesel, biogas, and other renewable energy should be resolved immediately to manage the energy crisis in the future. The drawbacks connected with the pretreatment methods, use of expensive chemicals, catalysts, complicated processes, and environmental damage are necessary to make right before large-scale operation. Thus, the disadvantages of each known aspect should be timely managed and new advanced technologies should be applied for biomass to sugar molecules, and biofuel production (Kassaye et al. 2017). The benefits of using forest leftovers and agricultural waste residue can be further improved by combining them with solid municipal waste. Thus, the process has the option to cover the process expenses and high energy yield.

22.2 Composition of Lignocellulosic Biomass

The lignocellulose found in the cell walls of agricultural plants is an organic form of carbon. Lignin, hemicellulose, and cellulose, the three major constituents, are collectively referred to as lignocellulosic material (Fig. 22.1) (Ali et al. 2018a). The composition of hemicellulose, cellulose, lignin, and other constituents may vary, but

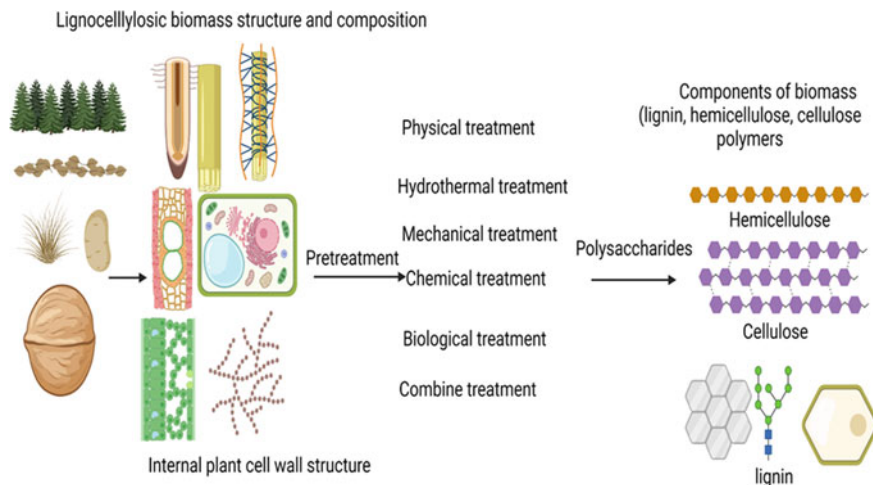


Fig. 22.1 Structure of lignocellulosic biomass contains the same basic components

overall the structure of plant biomass of different types is the same, the building materials are of similar nature as shown in Fig. 22.1.

22.2.1 Cellulose

Cellulose is the most predominant molecule on earth and makes up the majority of each plant's cell wall. The production of glucose and the polymerization of glucose units into long chains are the two main steps in photosynthesis. Cellobiose, a long chain of $(C_6H_{10}O_5)_n$ units in plant cell walls, and 4-O-D-glucopyranosyl-D-glucose are both structural components of cellulose. In highly concentrated acid and water at high temperatures, cellulose is soluble. While it is insoluble in weak acid and water, cellulose swells in a mild alkali solution and reduces the degree of polymerization, which aids in enhancing solubility and separation (Shah et al. 2018a).

22.2.2 Hemicellulose

Hemicellulose ranks as the second-highest molecule in plant cell walls. Heterogeneous polymers, such as xylan, arabinan, manan, glucans, galactans, glucomannan, and glucuronoxylan, as well as trace amounts of other polysaccharides, make up hemicellulose. Through a 1, 4-linked backbone, the unit molecules are joined together. The hemicellulose polymer is made of xylan with 1–4 connections of xylopyranosyl units, a glucose molecule with 4-O-methyl-D-glucuronopyranosyl,

and additional glucose monomers. Hemicellulose is insoluble in water at room temperature, but can be rendered soluble by thermal heating at high temperatures. It is significant to note that hemicellulose is readily soluble in both weak and strong acidic solutions, and that raising the temperature or acid concentration can increase this solubility. The polymeric structure of hemicellulose comes in a variety of sizes, shapes, and polymerizations. Hemicellulose forms a strong backbone for agricultural biomass by crosslinking cellulose, lignin, and non-covalent linkages (Anwar et al. 2014).

22.2.3 Lignin

Lignin, which derives from the word *lignum*, is the third major chemical in the cell wall of plants. Phenyl-propane units make up the long aromatic heterogeneous polymer known as lignin. Ether bonds bind the phenyl-propane units to one another. Lignin serves as a strong bond between the hemicellulose and cellulose in plant biomass. By bridging each crevice in the cell wall, the lignin strengthened and rigidified the entire structure. As a result, the breakdown is made more difficult by the lignin (Shah and Raheem 2019). Lignin is not soluble in acid at room temperature, but it can be heated to a high enough acid concentration to make it soluble. But lignin is easily soluble in basic alkali solutions at both normal and high temperatures. Heating plant biomass to temperatures between 160 and 320 °C can cause the linkages in the lignin polymer to disintegrate. The aromatic phenyl-propane units in lignin polymer are p-coumaryl (H), coniferyl (G), and sinapyl (S). The aromatic heterogeneous polymer includes guaiacyl units, phenolic methoxyl, hydroxyl, and aldehyde groups. Some of the prevalent links between phenolic groups in the lignin aromatic structure include the α -O-4, β -O-4, β - β , β -5 and β -1 linkages. Whereas some usual carbon-carbon bonds, carbon-oxygen bonds, carbon-oxygen and carbon-carbon bonds are present in the polymer (Abdelaziz et al. 2016).

22.3 Processing Methods

The waste agriculture biomass residue is targeted to be a hidden carbon material for biofuel because it contains good carbon polymers stored in the form of hemicellulose, lignin and cellulose. Different methods for lignocellulosic biomass pretreatment are discussed below and a list is displayed in (Fig. 22.2).

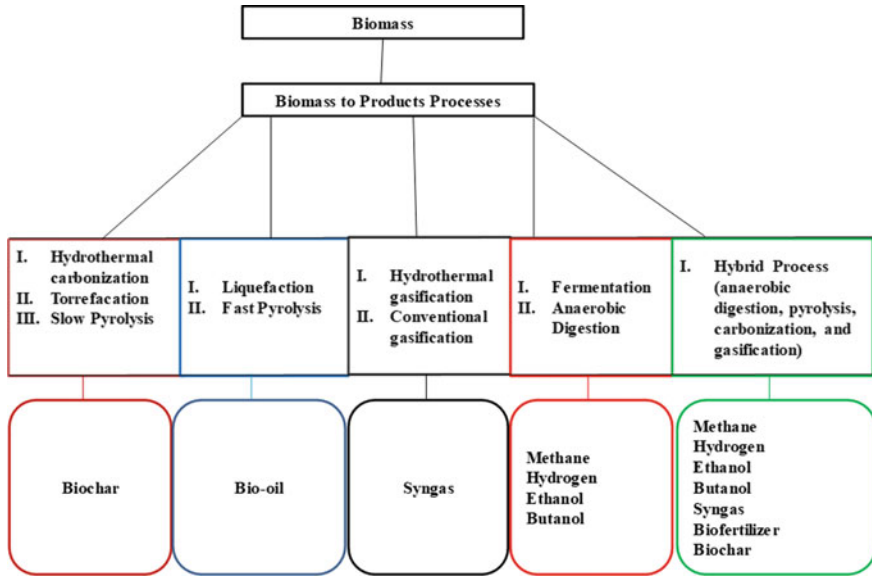


Fig. 22.2 Pretreatment methods and types of biofuels produced in the process

22.3.1 Physical and Thermal Process

The physical breakdown of lignocellulosic biomass comprises mechanical degradation (grinding, soaking or pelleting, mechanical extrusion), various radiation types, and ultrasonic pretreatments (microwave, ultrasound, pulsed electric field, freezing).

22.3.2 Grinding

Grinding of biomass reduced the size, crystallinity, and polymerization of the biomass before pyrolysis, which had an additional impact on the generation of bio-oil, and bio-crude molecules (Brandt et al. 2018).

22.3.3 Soaking

It increases the digestion of biomass, which can lower cellulose crystallinity and increase the effectiveness of enzymatic hydrolysis. Soaking also improves lignin removal, digestibility and rate of sugar release from the waste lignocellulosic biomass (Brandt et al. 2018).

22.3.4 Mechanical Extrusion

In mechanical extrusion, a high temperature above 300 °C is used to blend the waste lignocellulosic biomass for biomass hydrolysis. The process is costly because it demands a lot of shear force and energy. The pretreatment procedure is influenced by the pressure ratio, screw type, and screw speed, however, the reaction proved an enhancement of the enzymatic hydrolysis and sugar synthesis (Gu et al. 2020).

22.3.5 Microwave

In the microwave method, low-energy waves combine with irradiation produce high temperatures, in less time to degrade the biomass substrate with the least amount of inhibitor formation. Atomic collisions in this approach are caused by dielectric polarization, and the interruption of the biomass substrate is supported by thermal power generation. The microwave treatment can also specifically dissolve the lignin molecules of the biomass treated and thus improve subsequent hydrolysis to sugar molecules (Camani et al. 2020).

22.3.6 Ultrasound

The ultrasonic waves used in this procedure have an impact on both physical and chemical processes. The biomass's hemicellulose and cellulose content are destroyed by the formation of tiny bubble cavities. The ultrasonic waves and UV irradiation both decrease the cellulose crystallinity of the softwood and hardwood additionally, they increase the holocellulose content and providing less damage to sugar morphology in softwood and hardwood (Yang et al. 2020).

22.3.7 Pulsed Electric Field

With this technique, the lignocellulosic biomass is treated for a shorter amount of time at high voltage (between 5 and 20 kV/cm) (Yang et al. 2020). The plasma membrane's pores are opened during this process, exposing the cellulose, which the catalysts subsequently begin to hydrolyze. Following pretreatment, significant increases in sugar content were seen in woodchips and switchgrass (Rehman et al. 2013).

22.3.8 Freezing

This process involved submerging the lignocellulosic biomass in water initially, followed by a period of ice cube storage at a temperature of 18 °C. Finally, the frozen biomass is then kept at room temperature to do the freeze-thaw pretreatment process. This method also helps in the hydrolysis of lignocellulosic biomass to remove hemicellulose and cellulose (Rooni et al. 2017).

22.3.9 Pyrolysis

Pyrolysis is a high temperature pretreatment method under 400–550 °C without an oxygen environment in the reaction process to convert the lignocellulosic biomass into a variety of gaseous products including char, H₂, and CO. The gases, char, and bio-oil are produced from the heated lignocellulosic biomass. Both fast pyrolysis and slow pyrolysis with high and low temperatures in anaerobic (without oxygen) conditions are used to transform the lignocellulosic biomass into syngas, and other liquid fuels (Sun and Cheng 2002).

22.3.10 Carbonization

The process of gradual pyrolysis is known as carbonization, and it is primarily employed nowadays to produce charcoal. The three main ways to complete the reaction are, controlled combustion used for internal raw material heating, fuelwood or fossil fuels used for external heating, and hot circulating gas used in retorts or converters to produce chemicals (Sun and Cheng 2002).

22.3.11 Combustion

Boiling biomass in the air is the process of combustion, which is then used to transform chemical energy into temperature/ heat, electricity, and mechanical power. Stoves, boilers, furnaces, turbo-generators, steam turbines, and other kinds of machines are used to carry out the process of combustion. Through a series of heterogeneous and homogeneous reactions, the major combustion yields are power, and heat (Baskar et al. 2012).

22.3.12 Gasification

Another thermochemical process that heats the biomass feedstock to produce gaseous products containing high energy is gasification. The two main byproducts of gasification are fuel gas (methanol, hydrogen) and syngas (hydrogen, carbon monoxide, and carbon dioxide). The gasification process and conversion technology systems have the capacity to clean, purify the gas and compact the gas volume before combustion in the turbine (Baskar et al. 2012).

22.3.13 Liquefaction

Under conditions of controlled high hydrogen pressure and temperature, liquefaction transforms waste carbon sources or other organic biomass into constant melted hydrocarbons. Bio-oils made from a multifaceted blend of alcohols, volatile organic acids, ketones, ethers, aldehydes, esters, and hydrocarbons are produced by the liquefaction method from dried wood. An effective method for creating goods with a higher energy concentration in the liquid phase is catalytic liquefaction. However, the technique presents a number of technical issues and has restricted the use of the procedure (Pandey et al. 2019).

22.3.14 Steam Explosion

Compared to other techniques like grinding and soaking, flash vaporizing water applied at elevated pressure and temperature dissolves the biomass during this process, producing holes in the lignocellulosic biomass. In the pretreatment process, the combined steam explosion and hydrothermal explosion pretreat the biomass and reduce the content of lignin in the substrate (Bhutto et al. 2017).

22.3.15 Liquid Hot Water

The lignocellulosic biomass is treated at 200–350 °C temperature, 50–200 bar pressure, and with liquid hot water for the digestibility of the substrate. The pretreatment process is recorded to reduce the content of xylan and lignin up to 19, and 13% respectively. The process showed improvement by more than 50% of the glucose, ethanol, and xylose production yields after liquid hot water pretreatment (Matsakas et al. 2018).

22.3.16 *Wet Oxidation*

It is a general process that frequently takes place at high pressures and temperatures, involving an oxidation reaction to release the organic acids that solubilize the hemicellulose content of biomass, and delignify the lignin content. The reaction of the wet oxidation approach be combined with enzymes for biomass saccharification to improve the digestibility of the lignocellulose biomass for releasing hemicellulose and cellulose components (Bhutto et al. 2017).

22.3.17 *Carbon Dioxide Explosion Pretreatment*

This procedure requires a low-temperature, fully pressurized explosive CO₂ in a safe, and incombustible hydrolysis process to open up the surface area and penetrate the lignocellulosic biomass substrate. The reaction process proceeds at pressure (7.4 MPa), temperature (31°C), and supercritical CO₂ (sCO₂) to show gaseous appearances and liquid density to pretreat the biomass tested. The result of this reaction process yields higher cellulose content and faster enzymatic hydrolysis compared to untreated biomass (Zhang and Li 2020).

22.3.18 *Acid Pretreatment*

The pretreatment of agricultural wastes such as poplar grass, switchgrass, and maize by sulfuric acid or any other acid in dilute or high concentration, release sugar contents of the biomass in the liquid hydrolysate. The reaction of acid severity depends on the concentration of acid, temperature and nature of the substrate tested in a particular reaction process. However, this pretreatment enhances the enzymatic hydrolysis, production of sugars, and yield of biofuels (Shah et al. 2018a).

22.3.19 *Alkaline Pretreatment*

For waste biomass residue pretreatment, this method uses alkalis including calcium hydroxide, potassium hydroxide, sodium hydroxide, and other alkalis at various thermal conditions (Shah et al. 2018a). The result of the alkalis reaction is mostly on the lignin content of the lignocellulosic biomass, thus reported a high reduction of this lignin component, swelling of the substrate, and decreasing of the crystallinity of the biomass. The pretreatment is reported to enhance the biomass digestibility, sugars release, and increasing of the fermentation process for ethanol, methanol, and hydrogen (Shah et al. 2017).

22.3.20 *Ozonolysis Pretreatment*

In ozonolysis pretreatment process, using of ozone catalyst in the pretreatment reaction, the lignin content of the lignocellulosic biomass was dramatically reduced and a higher release of monolignol compounds. Thus the ozone pretreatment is particularly helps in the delignification of the lignocellulosic biomass (Bay et al. 2020).

22.3.21 *Ionic Liquids Pretreatment*

Ionic liquids used in the pretreatment of lignocellulosic biomass are those solvents that possess important qualities such as low vapor pressure, low liquefaction point, high levels of stable heat energy, and high levels of polarization. Fighting with the hydrogen bonds that already exist in the complex, it disturbs the lignocellulosic biomass structure. Ionic liquids recycle the expensive ionic liquids for additional processing while also separating the cellulose from lignocellulose contained in hardwood, softwood, poplar, and other similar forest waste (Bay et al. 2020).

22.3.22 *Ammonia Pretreatment*

Ammonia is employed as a key ingredient in a number of pretreatment methods, including aqueous ammonia soaking, ammonia fiber explosion, and ammonia recycling percolation. The alkaline ammonia fiber explosion method decreases the content of hemicellulose and lignin, additionally reduce the cellulose crystallinity of the substrate. Their distinct benefits include minimal inhibitor production, waste water discharge, high solids storage, and minimal modification to lignin's original structure (Ali et al. 2018b).

22.3.23 *Organosolv Pretreatment*

In this process, lignin and hemicellulose are broken down using solvents and acid catalysts such as sulfuric acid or hydrogen chloride. In the organosolvents method a variety of organic acids and solvents, such as ethanol, ethylene glycol, tetrahydrofurfuryl alcohol, acetylsalicylic acid, acetone, and triethylene glycol. The organosolvents combine with organic acids are tested for the pretreating of softwood, grasses, hardwood, and other lignocellulosic raw materials, and recover more than 80% of the cellulose content with high purity (Behera et al. 2014).

22.3.24 Multiple Solvents

This procedure uses a combination made up of two or three inexpensive components. Choline chloride is widely used because it is biodegradable, and has the capacity to generate deep eutectic solvents (DESs) including polyols, carboxylic acid, and urea. The combination of cost-effective solvents for the pretreatment of biomass reported an increase in glucose and xylose yield for biofuel production (Agbor et al. 2011).

22.3.25 Biological Pretreatment

The biotic/biological pretreatment approach is acknowledged as an efficient, environmentally friendly, and very low energy consumption process, in contrast to conventional physical and chemical pretreatment strategies (Shah and Ullah 2019). Microbes such as brown fungi, white rot fungi, and bacterial strains having capacity of breakdown of lignin, hemicellulose, and cellulose, are responsible for pretreatment of lignocellulosic biomass. The biological pretreatment with fungi and bacteria both have showed the enhancement of biomass digestibility and improvement in the fermentation process of biomass after pretreatment (Shah et al. 2018b).

22.3.26 Combined Pretreatment

The combination of pretreatments exhibits notable benefits, including a decrease in processing time, a reduction in inhibitor generation, and an improvement in sugar production efficiency. To recover the lignin and hemicellulose, the combination technique is very effective and scalable. The combine pretreatment may be of base-acid combination, organic acid-organosolvent, alkali-biological, acid-biological, alkali-ionic liquid, thermolysis, and biological and many more. The overall target is the same to disintegrate the crystalline structure of lignocellulosic biomass to separate lignin from hemicellulose, and cellulose matrix. The pretreatment effectively enhances the sugar content released from the cellulose of the biomass treated (Shah et al. 2018c).

22.3.27 Nanoscale Pretreatment Methods

Pretreatment techniques based on nanotechnology are currently being investigated broadly. This method primarily relies on the nanoparticles' capacity for penetration, which aids in entering the lignocellulosic biomass cell membrane. Under extreme circumstances, the associations of nanoparticles with the other major constituents can discharge the desired compounds, such as hemicellulose or lignin. This procedure

creates a high amount of mixing in the reacting vessel that breaks down the lignocellulosic biomass resistance in order to increase the activity of the chemical catalyst (Mood et al. 2013). This procedure is economical and has unique characteristics, including volume to surface area ratio, nanoscale size, good reactivity, high thermal stability, stability to chemicals, high discrimination, high catalytic power, and better adsorption capacity that take part in various reactions. The creation of biofuels is significantly influenced by all of the unique features of nanoparticles (Mood et al. 2013).

22.4 Biofuel and Energy Production

Based on the feedstock used to produce them, biofuels are broadly classified into different categories. They are divided into the following categories based on the biomass source, Biofuel of the 1st generation, 2nd generation, 3rd generation, and 4th generation.

22.4.1 Biofuel of the 1st Generation

The primary sources of the 1st generation biofuels are human food materials or grain/crops used as animal feed. These fuels are known as “conventional biofuels” since they are produced using different kinds of established processes and technologies, such as fermentation, and transesterification (Kassaye et al. 2017).

22.4.2 Biofuel of 2nd Generation

All of the non-food feedstocks, such as agricultural waste, waste lignocellulosic feedstock and forest waste are used to make 2nd-generation biofuels. The 2nd generation of biofuel production is an advancement over the 1st generation since it focuses on extra cheap biofuel and the synthesis of secondary waste carbon that can be utilized value-added material (Kassaye et al. 2017).

22.4.3 Biofuels of the 3rd Generation

3rd generation biofuels are made from microalgae. This method is important because it don't disrupt the food chain and microalgae is a simple, and easily digestible substrate for biofuel production (Kassaye et al. 2017).

22.4.4 Biofuels of the 4th Generation

Synthetic microalgae, solar energy, and hybrid electro-fuels are used to process the fourth generation of biofuels. By providing solar energy and heat, synthetic engineering of microalgal biomass has a prospective use in oil extraction methods. Genetic engineering and new cultivation for microalgae species could further open up new methods and technology for better biofuels and industrial biochemicals in the future (Paul et al. 2021). Examples of biofuels are.

Solid biofuels

Solid biofuels can be used to generate electricity, heat homes, or cook food since they are made from non-fossil, organic materials including plant biomass, animal waste, fuelwood, charcoal, wood pellets, wood scraps, and municipal garbage (Ghosh 2016).

Liquids biofuels

All liquids derived from natural biomass or biodegradable fractions are included in these biofuels. Due to their high energy density, liquid biofuels are superior to solid and gaseous biofuels in many ways, making them the best choice for transportation, storage, and retrofitting. Bioethanol, biodiesel, and bio-oil are a few of the most important primary examples of liquid biofuels. Other types of liquid biofuels are triglycerides, such as vegetable oil, hydrogenated oil, biodiesel, pyrolytic oil, and bio-gasoline (Ghosh 2016).

Gaseous biofuels

The low-density gaseous biofuels are gaseous by nature. Biogas, biohydrogen, and biosyngas are a few notable examples. The bio-wastes are pyrolyzed, gasified or fermented by an anaerobic digestion process to produce gaseous biofuels (biohydrogen and biomethane) (Aimen et al. 2020).

Ethanol

Fermentation of sugars, starch, corn, sweet sorghum, or sugarcane by microorganisms specially yeast *saccharomyces cerevisiae* is known to produce ethanol. Beside grains, sugar, starch, and other cellulosic raw carbon sources are also tested for ethanol production through the fermentation process.

Biodiesel

Transesterification is a method applied to the conversion of fats or oils into biodiesel. Biodiesel can be utilized in pure form for vehicle transportation (Verma et al. 2013). Biodiesel is more environmentally benign than conventional fossil fuels, since it significantly reduces atmospheric sulfate and carbon dioxide levels (Verma et al. 2013).

Biomethane

Another potential biofuel that could replace other traditional engine fuels is methane (Ali et al. 2017). The anaerobic digestion process is divided into four phases, hydrolysis, acetogenesis, acidogenesis, and methanogenesis (Shah et al. 2016). Methane, hydrogen, and organic acids are the products that can be used for energy and biomolecule synthesis (Afzal et al. 2019).

22.5 Advancement and Sustainability in Future

The production of biofuels is essential to the water-food-energy nexus for sustainable development. These biofuels play a vital role in the various nexuses by utilizing natural resources and services (Shah et al. 2016). The advancement of biofuels creates a seamless connection between food, water, land, and energy. Since first-generation biofuels are made from agricultural crops, they may have a negative effect on the environment (Boutahir et al. 2022a, b). Food waste generation is a social issue that impacts society internationally and has an impact on both the environment and social justice. The situation grew worse with the inclusion of using food crops for the production of biofuels, which not only put the food supply in direct competition but also led to an increase in food waste (Boutahir et al. 2022a, b). The technology of a hybrid system which can combine multiple process into single frame to get different kinds of energy in a single process is a sustainable approach in future energy systems. A schematic diagram of this idea is shown in (Fig. 2.3) below, which states that using a hybrid approach of the solar system, anaerobic digestion, gasification, and pyrolysis can play a vital role in the complete utilization of waste carbon into energy (Ali et al. 2020). The global energy shortage will be reduced, need less water, cultivation land, and agrochemicals. Thus, to sustain future energy demands around the globe, better and advanced technologies are needed to control energy, water, and food scarcity (Bhutto et al. 2017).

22.6 Summery

The production of biofuel is steadily rising in the modern era. When compared to edible plant sources, the energy output is more promising from non-edible and microalgal sources. The production of second-generation biofuels involves lignocellulosic raw materials, which don't interfere with food production, and agriculture land. A superior choice for producing biofuels is also offered by the third and fourth generation, but the study expedition is time-consuming and needs experienced handling. The triangle of water, food and energy on the globe needed to be manage carefully to meet the energy demands and food hunger in the future. Any technology

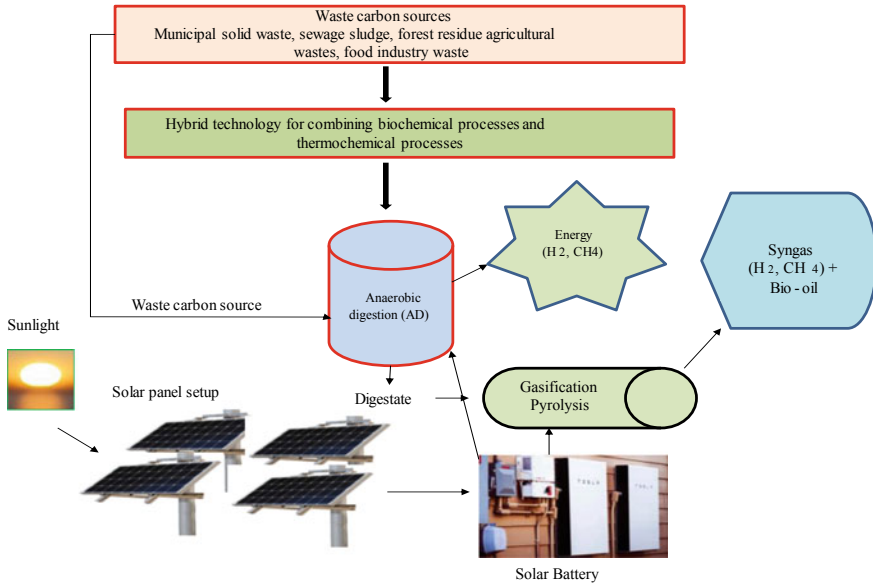


Fig. 22.3 A hybrid process of combining anaerobic digestion, gasification, pyrolysis and solar energy for production of various energy types

and process meeting all the three demands will ensure a sustainable future and global management of food and energy shortage.

Acknowledgements The author is thankful to Prof. Li Zhihe for providing postdoctoral fellowship, guidance and support in writing of this book chapter.

References

Abdelaziz OY, Brink DP, Prothmann J, Ravi K, Sun M, García-Hidalgo J et al (2016) Biological valorization of low molecular weight lignin. *Biotechnol Adv* 34(8):1318–1346

Agbor VB, Cicek N, Sparling R, Berlin A, Levin DB (2011) Biomass pretreatment: fundamentals toward application. *Biotechnol Adv* 29:675–685. <https://doi.org/10.1016/j.biotechadv.2011.05.005>

Aimen S, Hafiz Umar TA, Shah R, Tabassum, (2020) Fermentation of simple and complex substrates to biohydrogen using pure *Bacillus cereus* strains. *Environ Technol Innovat* 24:100704. <https://doi.org/10.1016/j.eti.2020.100704>

Ali S, Shah TA, Afzal A, Tabbassum R (2017) Evaluating the co-digestion effects on chicken manure and rotten potatoes in batch experiments. *Int J Biosci.* 10:150–159

Ali ST, Raheem U, Mustafa M, and Rashida (2020) Reprocessing of NaOH black liquor for pretreatment of agribiomass. *Int J Agri Sci Vet Med* 8:1–10

Anwar Z, Gulfranz M, Irshad M (2014) Agro-industrial lignocellulosic biomass a key to unlock the future bio-energy: a brief review. *J Radiat Res Appl Sci* 7(2):163–173. <https://doi.org/10.1016/j.jrras.2014.02.003>

- Afzal A, Shah TA, Ali S, Tabassum R (2019) Phylogenetic analysis of methanogenic archaea by *mcrA* gene in anaerobic digester. *Int J Agric Biol* 22(3):413–19 <https://doi.org/10.17957/ijab/15.1080>.
- Ali S, Shah TA, Afzal A, Tabassum R (2018a) Analysis of agricultural substrates for nutritive values and biomethane potential. *Curr Sci* 115(2):292. <https://www.currentscience.ac.in/Volumes/115/02/0292>
- Ali S, Shah TA, Afzal A, Tabassum R (2018b) Exploring lignocellulosic biomass for bio-methane potential by anaerobic digestion and its economic feasibility. *Energy Environ* 29:742–751. <https://doi.org/10.1177/0958305X18759009>
- Baskar C, Baskar S, Dhillon RS (2012) Biomass conversion: The interface of biotechnology, chemistry and materials science. Springer Sci & Business Media. DOI: <https://doi.org/10.1007/978-3-642-28418-2>
- Bay MS, Karimi K, Esfahany MN, Kumar R (2020) Structural modification of pine and poplar wood by alkali pretreatment to improve ethanol production. *Ind Crop Prod* 152:112506. <https://doi.org/10.1016/j.indcrop.2020.112506>
- Behera S, Arora R, Nandhagopal N, Kumar S (2014) Importance of chemical pretreatment for bioconversion of lignocellulosic biomass. *Renew Sust Energ Rev* 36:91–106. <https://doi.org/10.1016/j.energy.2017.01.005>
- Bhutto AW, Qureshi K, Harijan K, Abro R, Abbas T, Bazmi AA et al (2017) Insight into progress in pre-treatment of lignocellulosic biomass. *Energy* 122:724–745. <https://doi.org/10.1016/j.energy.2017.01.005>
- Boutahir MK, Farhaoui Y, Azroum M (2022a) Machine learning and deep learning applications for solar radiation predictions review: morocco as a case of study. In: Yaseen SG (ed) digital economy, business analytics, and big data analytics applications. Studies in computational intelligence, vol 1010. Springer, Cham. https://doi.org/10.1007/978-3-031-05258-3_6.
- Boutahir MK, Farhaoui Y, Azroum M, Zeroual I, El Allaoui A (2022b) Effect of feature selection on the prediction of direct normal irradiance. *Big Data Mining Anal* 5(4):309–317. <https://doi.org/10.26599/BDMA.2022.9020003>
- Brandt KL, Gao J, Wang J, Wooley RJ, Wolcott M (2018) Techno-economic analysis of forest residue conversion to sugar using three-stage milling as pretreatment. *Front Energy Res* 6:77. <https://doi.org/10.3389/fenrg.2018.00077>
- Camani PH, Anholon BF, Toder RR, Rosa DS (2020) Microwave-assisted pretreatment of eucalyptus waste to obtain cellulose fibers. *Cellulose* 27:3591–3609. <https://doi.org/10.1007/s10570-020-03019-7>
- Ghosh SK (2016) Biomass & bio-waste supply chain sustainability for bio-energy and bio-fuel production. *Procedia Environ Sci* 31:31–39. <https://doi.org/10.1016/j.proenv.2016.02.005>
- Gu BJ, Wolcott MP, Ganjyal GM (2020) Optimized screw profile design proved to inhibit re-agglomeration that occurs during extrusion of fine-milled forest residuals for producing fermentable sugars. *Ind Crop Prod* 154:112730. <https://doi.org/10.1016/j.indcrop.2020.112730>
- Johnsson F, Kjärstad J, Rootzén J (2019) The threat to climate change mitigation posed by the abundance of fossil fuels. *Clim Policy* 19(2):258–274. <https://doi.org/10.1080/14693062.2018.1483885>
- Kassaye S, Pant KK, Jain S (2017) Hydrolysis of cellulosic bamboo biomass into reducing sugars via a combined alkaline solution and Ionic liquid pretreatment steps. *Renew Energy* 104:177–184. <https://doi.org/10.1016/j.renene.2016.12.033>
- Mood SH, Golfeshan AH, Tabatabaei M, Jouzani GS, Najafi GH, Gholami M, et al (2013) Lignocellulosic biomass to bioethanol, a comprehensive review with a focus on pretreatment. *Renew Sust Energ Rev* 27:77–93. <https://doi.org/10.1016/j.rser.2013.06.033>
- Murali P, Hari K, Puthira Prathap D (2016) An economic analysis of biofuel production and food security in India. *Sugar Tech* 18(5):447–56. <https://doi.org/10.1007/s12355-015-0412-z>
- Matsakas L, Nitsos C, Raghavendran V, Yakimenko O, Persson G, Olsson E et al (2018) A novel hybrid organosolv: steam explosion method for the efficient fractionation and pretreatment of birch biomass. *Biotechnol Biofuels* 11:160. <https://doi.org/10.1186/s13068-018-1163-3>

- Pandey B, Prajapati YK, Sheth PN (2019) Recent progress in thermochemical techniques to produce hydrogen gas from biomass: a state of the art review. *Int J Hydrog Energy* 44:25384–25415. <https://doi.org/10.1016/j.ijhydene.2019.08.031>
- Paul D, Arora A, Verma ML (2021) Advances in microbial biofuel production. *Front Microbiol* 12:2768. <https://doi.org/10.3389/fmicb.2021.746216>
- Rehman MSU, Kim I, Chisti Y, Han JI (2013) Use of ultrasound in the production of bioethanol from lignocellulosic biomass. *Energy Edu Sci Technol* 30:1931–1410 <https://koasas.kaist.ac.kr/handle/10203/187385>.
- Rooni V, Raud M, Kikas T (2017) The freezing pre-treatment of lignocellulosic material: a cheap alternative for Nordic countries. *Energy* 139:1–7. <https://doi.org/10.1016/j.energy.2017.07.146>
- Rezania S, Oryani B, Cho J, Talaiekhosani A, Sabbagh F, Hashemi B et al (2020) Different pretreatment technologies of lignocellulosic biomass for bioethanol production: an overview. *Energy* 199:117457. <https://doi.org/10.1016/j.energy.2020.117457>
- Shah TA, Zahra R (2014) Screening of environment water for the presence of bla.NDM-1 microorganisms. *J Coll Physicians Surg Pak* 24(9):695–7. PMID: 25233980. <https://pubmed.ncbi.nlm.nih.gov/25233980/>
- Singh N, Dhanya B, Verma ML (2020) Nano-immobilized biocatalysts and their potential biotechnological applications in bioenergy production. *Mater Sci Energy Technol* 3:808–824. <https://doi.org/10.1016/j.mset.2020.09.006>
- Shah TA, Raheem U, Asifa A, Romana, Tabassum (2018a) Effect of alkalis pretreatment on lignocellulosic waste biomass for biogas production. *Int J Renewabl Energ Res* 8:1318–1326. <https://doi.org/10.20508/ijrer.v8i3.7725.g7431>
- Shah TA, Raheem U (2019) Pretreatment of wheat straw with ligninolytic fungi for increased biogas productivity. *Int J Environ Sci Technol* 19:1–12. <https://doi.org/10.1007/s13762-019-02277-8>
- Sun Y, Cheng J (2002) Hydrolysis of lignocellulosic materials for ethanol production: a review. *Bioresour Technol* 83:1–11. [https://doi.org/10.1016/s0960-8524\(01\)00212-7](https://doi.org/10.1016/s0960-8524(01)00212-7) 38
- Shah TA, Asifa A, Shehbaz A, Rahim U, Romana T (2017) A review on biohydrogen as a prospective renewable energy. *Int J Biosci* 11: 106–130. <https://doi.org/10.12692/ijb/11.1.106-130>
- Shah T, Ullah R (2019) Pretreatment of wheat straw with ligninolytic fungi for increased biogas productivity. *Int J Environ Sci Technol* 16:1–12. <https://doi.org/10.1007/s13762-019-02277-8>
- Shah TA, Lee C, Orts WJ, Tabassum R (2018b) Biological pretreatment of rice straw by ligninolytic *Bacillus* sp. strains for enhancing biogas production. *Environ Prog Sustainbl Energ* 38:1–9. <https://doi.org/10.1002/ep.13036>
- Shah TA, Ali S, Afzal A, Tabassum R (2018c) Simultaneous pretreatment and biohydrogen production from wheat straw by newly isolated ligninolytic *Bacillus* Sp. Strains with two-stage batch fermentation system. *Bioenerg Res* 11:835–849. <https://doi.org/10.1007/s12155-018-9936-x>
- Shah A, Favaro L, Alibardi L, Cagnin L, Sandon A, Cossu R et al (2016) *Bacillus* sp. strains to produce bio-hydrogen from the organic fraction of municipal solid waste. *Appl Energy* 176:116–124. <https://doi.org/10.1016/j.apenergy.2016.05.054>
- Verma ML, Barrow CJ, Puri M (2013) Nanobiotechnology as a novel paradigm for enzyme immobilisation and stabilisation with potential applications in biodiesel production. *Appl Microbiol Biotechnol* 97(1):23–39
- Yang X, Cui C, Zheng A, Zhao Z, Wang C, Xia S et al (2020) Ultrasonic and microwave assisted organosolv pretreatment of pine wood for producing pyrolytic sugars and phenols. *Ind Crops Prod* 157:112921. <https://doi.org/10.1016/j.indcrop.2020.112921>
- Yin Z, Zhu L, Li S, Hu T, Chu R, Mo F et al (2020a) comprehensive review on cultivation and harvesting of microalgae for biodiesel production: environmental pollution control and future directions. *Bioresour Technol* 301:122804. <https://doi.org/10.1016/j.biortech.2020.122804>
- Zhang L, Li Z (2020) Pretreatment of bamboo by ammonium sulfite for efficient enzymatic hydrolysis. *J Biobased Mater Bio-Energy* 14:265–272. <https://doi.org/10.1166/jbmb.2020.19522>

Chapter 23

Building an Intelligent Anomaly Detection Model with Ensemble Learning for IoT-Based Smart Cities



Chaimae Hazman, Said Benkirane, Azidine Guezzaz, Mourade Azrou, and Mohamed Abdedaïme

Abstract Internet of Things (IoT) solutions are enabling smart cities across the planet. A smart city concept demands the incorporation of communication and information technologies and devices across an infrastructure in to enhance customer services. They are becoming more tempting to attackers due to their rising number and mobility. To safeguard IoT, numerous solutions, such as encryption, authentication, availability, and data integrity, have been coupled. IDSs are a strong security instrument that could be enhanced by adding machine learning (ML) and deep learning (DL) approaches. The present work introduces an anomaly detection, a robust intrusion detection system for IoT-based smart settings that uses Ensemble Learning. Generally, the framework offered an optimum anomaly detection model that combines AdaBoost, as well as incorporating several feature selection approaches Boruta, mutual information, and correlation. The suggested model was tested using the GPU on the IoT-23, BoT-IoT, and Edge-IIoT datasets. After a lightweight comparison with recent IDS, our technique offers excellent rating performance attributes of ACC, recall, and precision, with 99.9% on recording detection and computation times approximately 33.68 s during training and 0.02156 s during detection.

Keywords Intrusion Detection · Smart environments · IoT · ML · Ensemble Learning · Edge-IIoT · BoT-IoT · IoT-23

C. Hazman · S. Benkirane · A. Guezzaz (✉)
Technology Higher School Essaouira, Cadi Ayyad University, Marrakesh, Morocco
e-mail: a.guezzaz@gmail.com

M. Azrou
STI Laboratory, IDMS Team, Faculty of Sciences and Techniques, Moulay Ismail University of Meknès, Meknes, Morocco

M. Abdedaïme
Faculty of Economics and Management, Ibn Tofail University, Kenitra, Morocco

23.1 Introduction

The Internet of Things (IoT) refers to the Network of the Tomorrow (Salim et al. 2019). IoT refers to the data network of physical items (including vehicles, devices, robots, structures, and other items) which enables different items to connect and cooperate in order to accomplish broad goals (Mabrouki et al. 2021). IoT sensor systems often gather and interpret both spatial and temporal data for specific occasions and locations confronting diverse problems. Smarter IoT item or object creation have simplified interactions simpler (Haabouni et al. 2019). Smart items become more efficient by combining IoT technologies and smart environments. Nonetheless, IoT applications are susceptible to a variety of network threats, including Investigation, Users to Root (U2R), denial-of-service (DoS) assaults, Remotes to Local (R2L) (Rathore and Park 2018), and distributed denial-of-service (DDoS) (Kimani et al. 2019). The following attacks have the potential to disrupt IoT services as well as smart ecosystem solutions on an IoT network. As a result, security IoT systems has become a concern (Sathesh 2019). Different security mechanisms (for example, encryption, biometrics, and anonymity) are widely used in a variety of application fields (Azroul et al. 2021a, b, c). Unfortunately, these are insufficient for the environment of smart cities.

Our research is focused on network intrusion detection systems (NIDS), and alerting system administrator. It is positioned outside of infrastructure and evaluates a copy of incoming data traffic. As a reason, the true automated network capability stays unaffected. It starts by analysing the packets obtained from hosts or networks. As a result, it seeks to automatically extract using feature engineering. The next step is to run classification techniques on the gathered information to identify the intrusion or anomaly. As a consequence, intrusion detection maintains a field of research since it is a dependable solution that offers protection and security of IoT settings against a wide range of attacks such as network scanning, key logger disruption of service (DoS), and distributed DoS (DDoS). A variety of ML, ensemble learning, and DL techniques have been coupled to suggest better IDS. Regardless of these efforts, other difficulties remain unresolved, including detection in real time, imbalanced data, quality enhancement, high three-dimensionality, massive data, and time efficiency (Thaseen and Kumar 2013).

This study offers a novel intrusion detection system (IDS) for IoT-based smart environments that employs ensemble learning to improve detection rate and make trustworthy conclusions. The suggested architecture typically incorporates an optimal ensemble-based intrusion detection strategy that makes use of AdaBoost and numerous feature selection algorithms. Experiment results using NSL KDD, Bot-IoT, and edgeIIoT datasets demonstrate that our technique outperforms in terms of ACC, Precision, F1-score, Recall, and Roc-auc. Two important contributions were confirmed in this research.

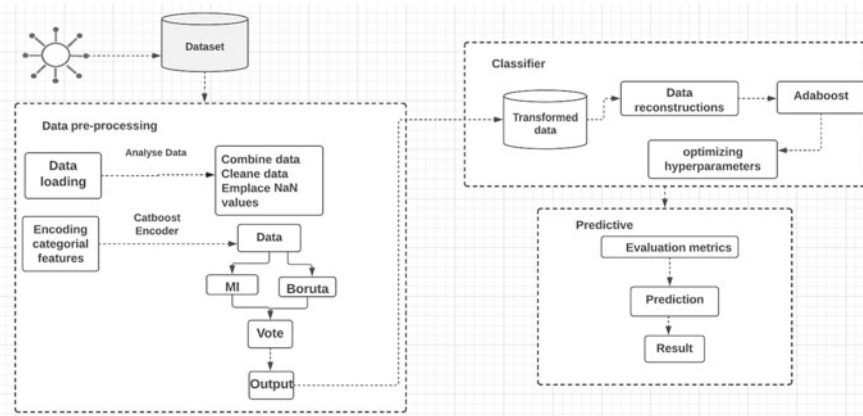


Fig. 23.1 Scheme of our Anomaly detection framework

- First, we improve data quality by employing PCA, Boruta, Mutual information, and Pearson correlation.
- Second, in order to create an efficient IDS, a classifier design based on the Adaboost model is built. As seen in Fig. 23.1, our suggested model is composed of three major components: data preparation, classifier model, and prediction.

The rest of this work is organized as following. The section two summarizes important IDS attempts that use ML and DL to defend IoT settings. The part is completed by a detailed comparison of many systems. The novel framework is described in full in the section three. The section four presents the research findings and matches it to previous attempts. Finally, the last section concludes our work and highlights the suggestions for further research.

23.2 Literature Survey

Given the variety of Iot network and the inadequacy of network security integrated in equipment, IoT security is a critical issue (Costa et al. 2019). For handle IoT security concerns, conventional and modern security controls including authenticating, secure routing, encrypting, access control protocols, permission systems, detection systems, and other techniques are employed (Guezzaz et al. 2019a, b; Chaganti et al. 2022). Therefore, they are inadequate to improve IoT security. Furthermore, the absence of controls needs to must consider the restricted power and memory resources. As a consequence, prior to actually connected to the Internet, devices and sensors must interact and summarize data, and then connect to the network via gateway using the authenticate header protocol (Azroul et al. 2021b). Intrusion detection, on the other hand, is a defensive measure that monitors traffic and detects flaws in network

Table 23.1 The results of performance indicators on BoT-IoT, Edge-IIoT, and IoT-23

Dataset	ACC	Precision	Recall	AUC	F1-score	Training (s)	Detection (s)
Edge-IIoT	100	100	100	100	100	0.6941	0.02156
BoTEdge-IoT	99.99	99.99	100	100	99.99	19.68	0.714
IoT-23	99.98	99.98	99.91	100	99.99	15.5	0.815

architecture. It can detect and prevent harmful activity (Guezzaz and Benkirane 2022; Douiba et al. 2022a; Guezzaz 2022; Guezzaz et al. 2017).

As shown in Table 23.1, several researchers studied their attempts to improve intrusion detection to secure the IoT environment in the literature study.

In 2019, Verma et al. (2019) investigate and incorporate the results of several supervised machine learning techniques in addition to select a trustworthy classifier model for IoT security. They recommended IDSs model focused on ensemble learning that indicated that the GBM has the strongest effect 99.53%. Pajouh et al. (2016) proposed an ID model based on 2-layer feature reduction (DR) and 2-tier classification to detect malicious activity (R2L or U2R). This model used linear discriminate and DR component analysis to batch the higher dimension dataset onto a smaller dimension dataset with minimal characteristics. Furthermore, Shakeel et al. (2018) focused on a learning-centric Deep-Q-Network for reducing malware (attacks) while handling health-related data. Initially, the IoT device was investigated based on the DNN, which checks every single feature to authenticate the device. Each query traffic characteristic was then taken from the request and saved in the database. The quality value of such extracted features was scrutinized based on the feature state and activities, which assisted in determining the quality of the secured data (Selvakumar et al. 2019). In this case, the LDQN technique achieved the lowest mistake rate (0.120), which improved the malware detection rate (98.790%). In 2021, Abu Al-Haija and Al-Dala'ien (2022) introduced an ensemble learning approach for botnet attack detection in IoT networks, which examines IoT network activity characteristics and use ensemble methods to detect anomalous network traffic from infected IoT devices. Furthermore, the IoT-based botnet detection system evaluates three alternative machine learning algorithms that are part of decision tree techniques RUSBoosted, AdaBoosted and bagged. To evaluate ELBA-IoT, we used the N-BaIoT-2021 dataset, which comprises records of both conventional IoT network traffic and botnet assault traffic from compromised IoT devices. The results of the experiments show that the ELBA-IoT could identify botnet assaults launched from hacked IoT devices with accuracy 99.6% and minimum calculation. Moreover, Guezzaz et al. (2021) proposed a network intrusion detection model based on DT, which compare their model to others that utilized the very same data sets as theirs for increased data quality using the NSL-KDD and CICIDS2017 datasets. Their model has an accuracy rate of 99.42 with the NSL-KDD dataset and 98.80% with CICIDS2017. Guezzaz et al. (2022) develop an IDS approach that captures network traffic using PcapSocks and an MLP classifier. The PcapSocks sniffer and MLP are used to determine and classify activities as normal or intrusive. In 2022, Douiba et al. (2022b)

developed an effective intrusion detection technique IoT security based on GBand deand DT through the Catboost. The proposed model was evaluated on the improved NSL-KDD, BoT-IoT, and IoT-23 datasets (Mohy-eddine et al. in press). The GPU is employed to enhance the experimental framework. In regards of ACC, recall, accuracy, and F1-score metrics with record detection and calculation time, our technique outperforms existing IDS by more than 99.9%.

23.3 Proposed Intrusion Detection Framework

23.3.1 Proposed Model

This section describes different solutions that have been used to test our intrusion detection technique for smart environment security. The purpose of our approach is to enhance detection rate, accuracy, and time consumption by proposing an optimal model. Figure 23.1 depicts the structure of the proposed framework. The objectives of this model are to verify optimal IDS based on the Adaboost model and feature selection algorithms. The GPU is used to perform the training stage. The optimized model procedure is split into four steps:

Data preprocessing component: Our proposed methodology relies on pre-processing and features engineering that are designed to increase data quality. Preprocessing is a beneficial operation that aims to remove noise and tidy data. Furthermore, the data are encoded with the catboostencoder to prevent the unfavorable impact of high weight of values features. We suggest extracting information samples to minimize several limitations such as processing and a large number of data. There are several ways for reducing the variety of features before using a dataset for training and validation of a classifier model. In this scenario, we apply PCA to do this assignment. The PCA is a statistical approach that aims to generate a reduced dimensional representation of the previous data by lowering high and complicated dimensionality while retaining all important information. Then, using real network data received through network traffic, we apply tree-based feature selection methods including Boruta, mutual information, and Pearson correlation to build a better training set while lowering training time and processing costs. Based on the bagging approach, our feature selection methods identify the most important attributes from the dataset to be used during the classification stage.

Classifier component: During classification, Adaboost, which assigns a class to each instance, was utilized. The goal of this component is to create a binary classifier. Using current data obtained from the preparation component as input. The classification process is divided into two parts: training stage and validation stage. In the first step, 60% of the data is used to train an Adaboost classifier, which is employed in our suggested technique; in the second stage, the rest of data is applied to validate our model.

Predictive data component: The test and train data are reconstructed, then hyperparameters such as max depth, iterations, task type, estimation technique, loss function, and evaluation metric are calculated, as shown in Table 23.2. As shown in Table 23.3, all hyperparameters have been fine-tuned to deliver the best possible performance. In the training process, Adaboost, an ML ensemble classifier, and GPU computing are employed. As a result, we assigned numerical numbers to both categories, with 0 signifying ordinary activity and 1 indicating incursion. It is crucial to remember that the number of variables must be specified in advance. For the validation step of our model, we used a variety of methods to partition the data into a learning and a test set. We presented the k-fold technique in this situation.

23.3.2 *Description of Solution*

The AdaBoost algorithm is built on the concept of “boosting.” The principle underlying boosting is that a number of “weak” classifiers may be joined to build a robust classifier by using a voting procedure. A poor classifier delivers outcomes that are only marginally better than throwing a (fair) ball. In other words, if we forecast a binary label at random and get it right about half of the time, a worse classification would get it right around 55% of the time [28]. To tackle a binary classification problem, our AdaBoost strategy will fit a series of weak classifiers (stumps) across a number of boosting rounds. These classifiers will be used to form a meta-classifier that will forecast using a weighted majority vote approach. In each boosting round, we will give more weight to observations that were misclassified in the prior iteration. As seen in the algorithm below, this technique may be codified. It is feasible to show that the formulas for α and W are the consequence of decreasing the exponential loss function.

23.4 Experimental Assessment and Results

The experimental assessment of our approach is carried out on a kaggle machine with GPU memory of 15 GB and a 64-bit system. The model is built with Jupyter Lab and Python 3.9.7, pandas, numpy, and sklearn modules. The evaluation of IDS is a critical issue. Moreover, the dataset utilized in model training and testing determines the optimum performance parameters of any classifier.

Following pre-processing and feature engineering on gathered traffic, the efficiency of the Adaboost classifier model is evaluated using Accuracy, Precision, FAR, and f-score measurements.

The ACC is the proportion of occurrences successfully predicted as normal or attack to the total number of occasions in the test set. Equation 23.1 yields this result.:

$$Accuracy = \frac{TP + TN}{TP + TN + FP + FN} \tag{23.1}$$

Precision denotes the percentage of occurrences properly recognized as attack to the overall number of attack occurrences in the test set. Equation 23.2 is used to compute it.

$$Precision = \frac{TP}{TP + FN} \tag{23.2}$$

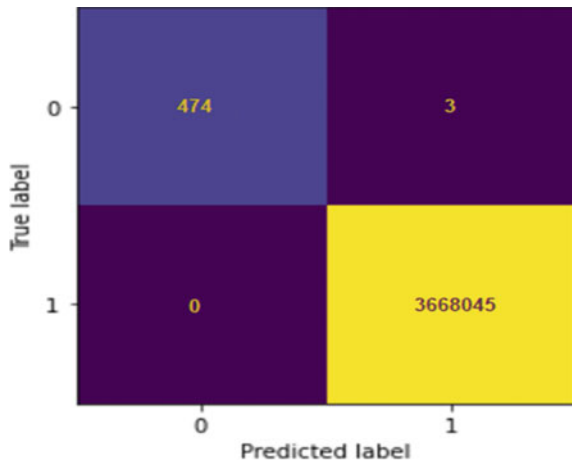
FAR is the percentage of instances classified as assault to the total number of incidents classified as normal activity. It is calculated using Eq. 23.3:

$$FAR = \frac{FP}{TP + FN} \tag{23.3}$$

Utilizing the BoT-IoT dataset, we achieve excellent outcomes. Table 23.1 and Figs. 23.2, 23.3, 23.4, and 23.10 show that our model has the best effectiveness of threat detection in terms of accuracy, precision, and recall. The confusion matrices in Fig. 23.3 illustrate that the model is recently attained with $8,17e-7$ FPR and 0 FNR. The table shows the learning and detection times. the performance time 19.68 s by modifying the model on GPU and 0.714 s to identify intrusions on the complete data Fig. 23.4 depicts the significance of attributes in the identification of attacks on the BoT-IoT dataset.

We evaluated our model with Edge-IIoT then employed only 30 features, as shown in Figs. 23.5, 23.6, 23.7, and 23.10, to improve the results. Table 23.2 summarizes the findings that validate the model efficiency. The accuracy, precision, and recall ratings are excellent. The confusion matrix in Fig. 23.4 indicates that the loss is with

Fig. 23.2 Confusion matrix of dataset Bot-IoT



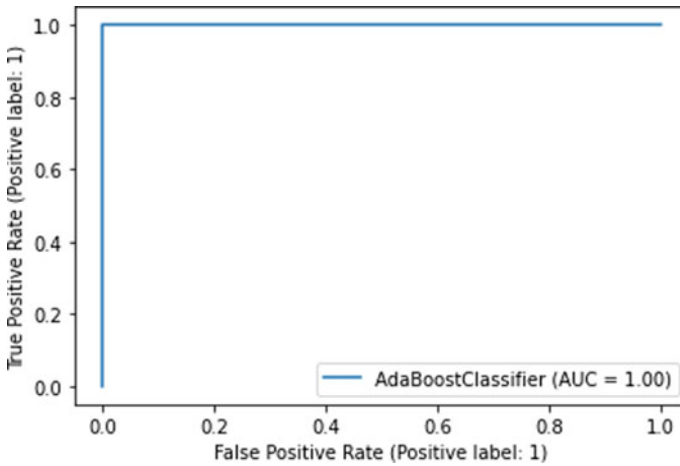


Fig. 23.3 AUC curve for BoT-IoT

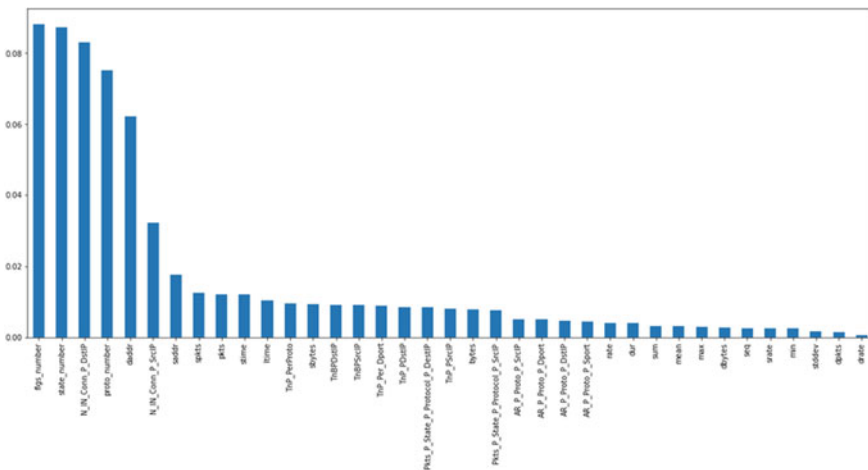


Fig. 23.4 Importance of features for detection attack on BoT-IoT dataset

zero. Table 23.2 also demonstrates that it takes 0.6941 s to build the model using GPU and 0.02156 s threat detection across all datasets.

As previously stated, the results collected validate the model’s performance in accuracy, precision, and recall with 99.80%, 0.00068 FPR, and 0.00082 FNR. Table 23.2 shows the results of testing the model using IoT-23. The obtained findings validate the effectiveness of the algorithm anomaly detection. All accuracy, precision, and recall values are almost 99.9%. In comparison, the error is nearly 0 with 0.00002 FNR and 0.00018 FPR, as shown in the confusion matrix in Fig. 23.8. Additionally,

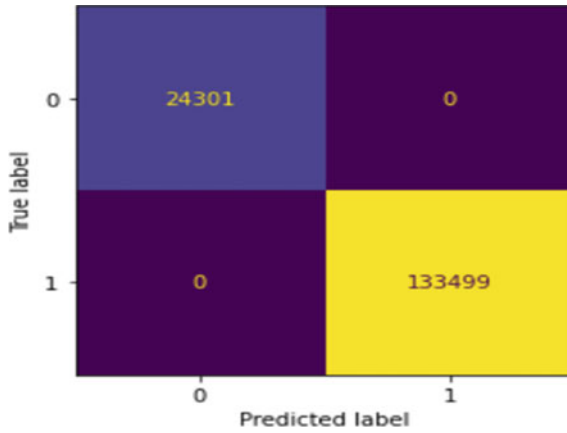


Fig. 23.5 Confusion matrix of for Edge-IIoT dataset

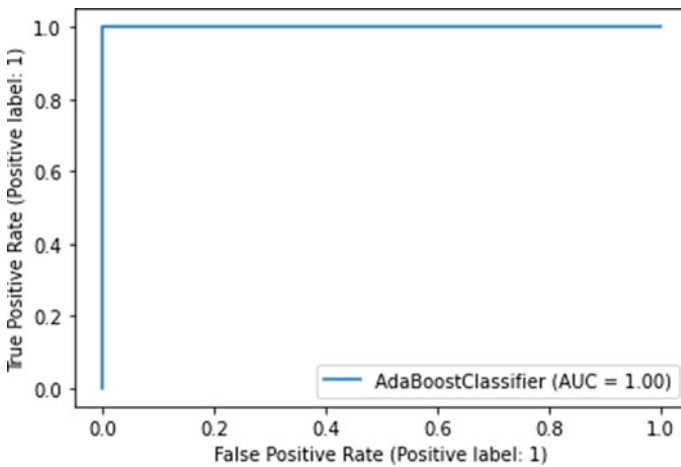


Fig. 23.6 AUC curve for Edge-IIoT

the model fits in GPU in around 15.5 s and recognizes all attacks in 0.815 s. Furthermore, we used 15 features to achieve these excellent results, despite the fact that only 12 influenced detecting features (Figs. 23.9 and 23.10).

We compared our model to several current techniques based on the IoT-23 and Bot-IoT. The findings produced utilizing the Bot-IoT and IoT-23 datasets show that our model more suitable outcomes than previous offered ways. Our method produces considerable results, which were aided by feature selection techniques.

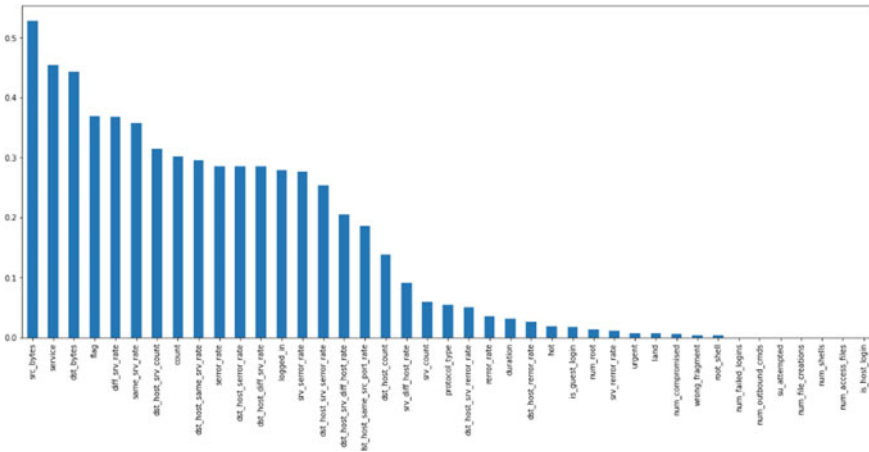
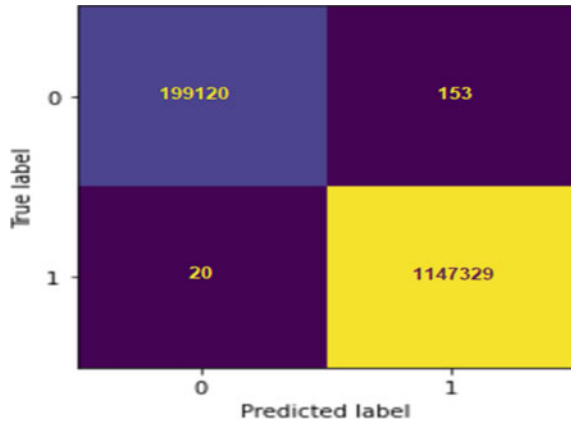


Fig. 23.7 Importance of features for detection attack on Edge-IIoT dataset

Fig. 23.8 Confusion matrix of dataset IoT-23



23.5 Conclusion

IDS is a mechanism for improving Security capabilities against attacks, notably before integration IDS in smart environment. This study offers an intrusion detection model optimized for IoT security based on detection of anomalies that enhances IDS accuracy while decreasing processing time. The results of research on numerous datasets, as well as performance evaluations, have shown that our approach provides the most efficient and resilient, with the lowest cost over time. The model improves from the Adaboost boosting technique, while we employed a variety of feature selection techniques to improve the data quality (MI, Boruta Pearson correlation). The model benefits by GPU performance. Based on the findings of this study, the proposed model would assist in the development of a successful IoT NIDS system that achieves

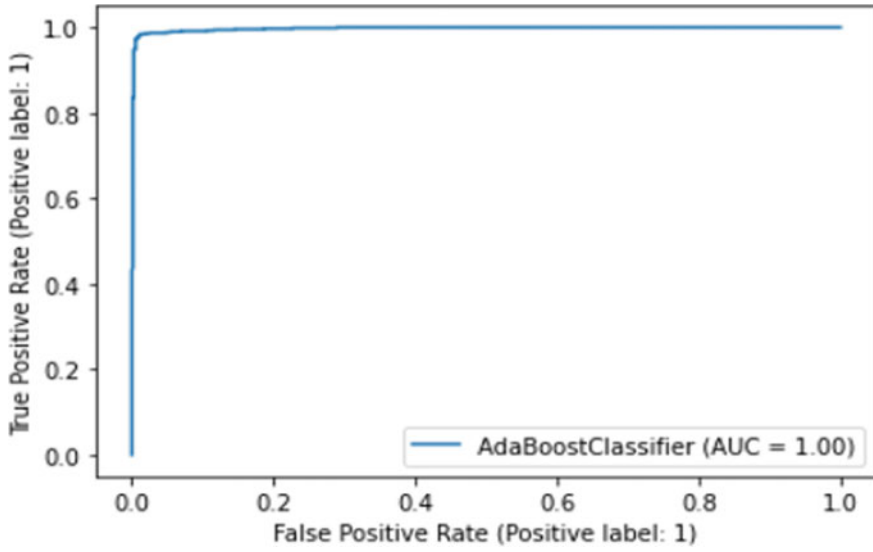


Fig. 23.9 AUC curve for IoT-23

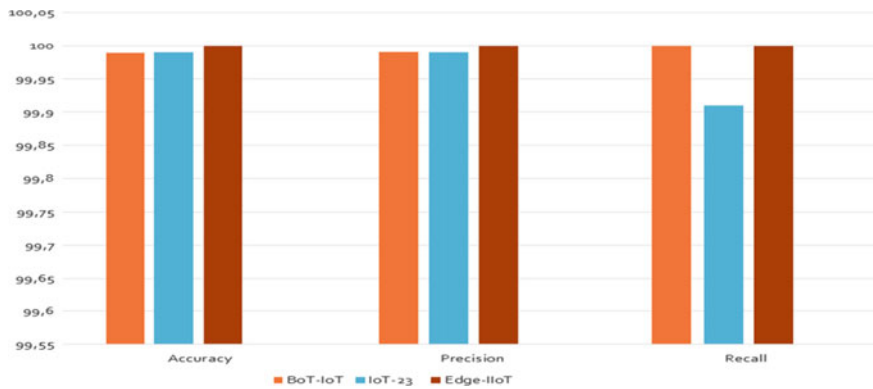


Fig. 23.10 Performance evaluation of our model

a high percentage of detection. Additionally, this research confirms Adaboost’s role as a strong ML. Our future research will involve multi-class classification and an anomaly detection model based on DL methods.

References

- Abu Al-Haija Q, Al-Dala'ien M (2022) ELBA-IoT: an ensemble learning model for botnet attack detection in IoT networks. *J Sens Actuator Netw* 11(1):18. <https://doi.org/10.3390/jsan11010018>
- Azrou M, Mabrouki J, Guezzaz A, Farhaoui Y (2021a) New enhanced authentication protocol for internet of things. *Big Data Mining Anal* 4(1):1–9
- Azrou M, Mabrouki J, Chaganti R (2021b) New efficient and secured authentication protocol for remote healthcare systems in cloud-IoT. *Secur Commun Netw* 2021. <https://doi.org/10.1155/2021/5546334>
- Azrou M, Mabrouki J, Guezzaz A et al (2021c) Internet of things security: challenges and key issues. *Secur Commun Netw* 2021:1–11
- Chaganti R, Mourade A, Ravi V, Vemprala N, Dua A, Bhushan B (2022) A particle swarm optimization and deep learning approach for intrusion detection system in internet of medical things. *Sustainability* 14(19):12828
- Douiba M et al (2022a) An improved anomaly detection model for IoT security using decision tree and gradient boosting. *J Supercomput* 1–20
- Douiba M, Benkirane S, Guezzaz A, Azrou M (2022b) Anomaly detection model based on gradient boosting and decision tree for IoT environments security. *J Reliab Intell Environ* 1–12
- da Costa KA, Papa JP, Lisboa CO, Munoz R, de Albuquerque VHC (2019) Internet of Things: a survey on machine learning-based intrusion detection approaches. *Comput Netw* 151:147–157
- Guezzaz A, Asimi A, Asimi Y, Tbatou Z, Sadqi Y (2017) A lightweight neural classifier for intrusion detection. *Gen Lett Math* 2(2):57–66
- Guezzaz A, Asimi Z, Batou YA, Sadqi Y (2019a) A global intrusion detection system using PcapSockS Sniffer and multilayer perceptron classifier. *Int J Netw Secur (IJNS)* 21(3):438–450
- Guezzaz A, Asimi A, Mourade A, Tbatou Z, Asimi Y (2019b) A multilayer perceptron classifier for monitoring network traffic. In: *International conference on big data and networks technologies*. Springer, Cham, pp 262–270
- Guezzaz A, Benkirane S, Azrou M, Khurram S (2021) A reliable network intrusion detection approach using decision tree with enhanced data quality. *Secur Commun Netw* 2021. <https://doi.org/10.1155/2021/1230593>
- Guezzaz SB, Azrou M (2022) A novel anomaly network intrusion detection system for internet of things security. *iot and smart devices for sustainable environment*. EAI/ Springer Innovations in Communication and Computing. Springer
- Guezzaz A et al (2022) A lightweight hybrid intrusion detection framework using machine learning for edge-based IIoT security. *Int Arab J Inf Technol* 19(5)
- Haabouni N, Mosbah M, Zemmari A, Sauvignac C, Faruki P (2019) Network intrusion detection for IoT security based on learning techniques. *IEEE Commun Surv Tutor* 21:2671–2701
- Kimani K, Oduol V, Langat K (2019) Cyber security challenges for IoT-based smart grid networks. *Int J Crit Infrastruct Prot* 25:36–49
- Mabrouki J, Azrou M, El Hajjaji S (2021) Use of internet of things for monitoring and evaluation water's quality: comparative study. *Int J Cloud Comput* 10(5–6):633–644
- Mohy-eddine M, Benkirane S, Guezzaz A, Azrou M (in press) Random forest-based IDS for IIoT edge computing security using ensemble learning for dimensionality reduction order a copy of this article. *Int J Embed Syst*
- Pajouh HH et al (2016) A two-layer dimension reduction and two-tier classification model for anomaly-based intrusion detection in IoT backbone networks. *IEEE Trans Emerg Top Comput* 7(2):314–323
- Rathore S, Park JH (2018) Semi-supervised learning based distributed attack detection framework for IoT. *Appl Soft Comput* 72:79–89
- Salim MM, Rathore S, Park JH (2019) Distributed denial of service attacks and its defenses in IoT: a survey. *J Supercomput* 2019:1–44
- Sathesh A (2019) Enhanced soft computing approaches for intrusion detection schemes in social media networks. *J Soft Comput Parad* 1:69–79

- Selvakumar K et al (2019) Intelligent temporal classification and fuzzy rough set-based feature selection algorithm for intrusion detection system in WSNs. *Inf Sci* 497:77–90
- Shakeel PM et al (2018) Maintaining security and privacy in health care system using learning based deep-Q-networks. *J Med Syst* 42(10):186.30
- Thaseen S, Kumar CA (2013) An analysis of supervised tree based classifiers for intrusion detection system. In: 2013 international conference on pattern recognition, informatics and Mobile engineering. IEEE, pp 294–299
- Verma A, Ranga V (2019) ELNIDS: ensemble learning based network intrusion detection system for RPL based Internet of Things. In: 2019 4th international conference on internet of things: smart innovation and usages (IoT-SIU). IEEE, pp 1–6

Chapter 24

Embedded Web Server Implementation for Real-Time Water Monitoring



Mouaad Mohy-Eddine, Mourade Azrou, Jamal Mabrouki, Fatima Amounas, Azidine Guezzaz, and Said Benkirane

Abstract Water is particularly essential for the healthy continuation of all living. Nevertheless, water resources are exposed to several issues, including pollution, dearth, increasing demand, etc. Accordingly, real-time water quality monitoring plays an important role in water management operation. In the present study, we have designed an embedded web server system for displaying water quality. The proposed system is founded on the Internet of Things solution. Hence, it allows to survey and control water quality remotely and in real-time. Our system contains four sensors for gathering water parameters mainly temperature, turbidity, conductivity and pH. Besides, it has two actuators. The measured values can be displayed in a specific web page by connecting to server in any browser.

Keywords Internet of Things · Water · IoT · Water quality · Server · Smart system

24.1 Introduction

Water is an essential element for well-being, as it has a considerable and determining influence on the quality of life and health of individuals. It is an important resource required for the main human activities such as feeding, breathing, navigation, excretion and reproduction. In additional, it provides a living environment and

M. Mohy-Eddine · A. Guezzaz · S. Benkirane
Technology Higher School Essaouira, Cadi Ayyad University, Marrakesh, Morocco

M. Azrou (✉)
STI Laboratory, IDMS Team, Faculty of Sciences and Techniques, Moulay Ismail University of Meknès, Meknes, Morocco
e-mail: mo.azrou@umi.ac.ma

J. Mabrouki
Laboratory of Spectroscopy, Molecular Modeling, Materials, Nanomaterial, Water and Environment, CERNE2D, Faculty of Science, Mohammed V University in Rabat, Rabat, Morocco

F. Amounas
RO.AL&I Group, Computer Sciences Department, Faculty of Sciences and Technics, Moulay Ismail University of Meknes, Errachidia, Morocco

a fundamental component in the creation of the living conditions of people (Kılıç 2020).

Generally, the operation for testing water quality requires transporting water samples directly into a laboratory to be analyzed day-by-day. However, this conventional approach is particularly difficult to control mainly when the water source is located very distant away to the laboratory. Furthermore, its efficiency is usually reduced due to the fact that some water values might change during the transporting (Mabrouki et al. 2020, 2021). On the other hand, the deployment of the Internet of Things has influenced entirely quotidian actions (Guezzaz et al. 2022). Henceforth, it was integrated vastly in various domains such as transport (Douiba et al. 2022a; Guezzaz et al. 2020; Cirillo et al. 2020), smart city (Lv et al. 2021; Wang et al. 2021; Douiba et al. 2022b), energy (Mabrouki et al. 2022; Khan, et al. 2020; Mehmood et al. 2021; Boutahir et al. 2022), healthcare (Azroul et al. 2021a; Chaganti et al. 2022; Dimitrievski et al. 2021), environment (Mabrouki, et al. 2022; Alaoui et al. 2019; Azroul et al. 2022, 2019; Guezzaz et al. 2022) and so ones (Ghizlane et al. 2022). Formally, water monitoring area is also affected. Consequently, innovative solutions have been proposed to control, monitor and manage water quality. The usage of various sensors and specific devices, scientists and water controllers are able to gather several water parameters in real-time. Despite the fact that some systems communicate the collected data to the user via several networking technologies, the others are limited to presenting gathered statistics on a simple local screen.

Normally, the employment of sensors to sense and to collect statistics on the water quality allows the water managers to control the process of water management according to the actual conditions. The Internet of Things (IoT) (Guezzaz et al. 2021a, b, c; Azroul et al. 2021b) has offered an innovative view totally different to traditional methods: the new approach is in form of one system that can be connected to the network and which can integrate smart policies. Consequently, one can visualize water parameters and interact with the system in real-time. However, to synchronize the operations of various users the development of a central server is required.

On the other side, an embedded system is an autonomous system that integrates two distinct parts: electronics and computing. This system is devoted to perform a well specified task by processing the information received from its environment. Basically, the embedded system represents a significant research field since it allows programming and customizing the system according to the user's requirements. Besides, it also provides solutions to real-time, online and remote applications. Hence, it occupies a very important position in the conception of embedded web solutions. In the present research study, we have developed an embedded web server for water quality monitoring. The developed server is responsible for acquisition and illustrating water parameters using the tables and graphics. It allows also to the water managers to interact in real-time with installed actuators.

The rest of this paper is organized as following. The second section summaries some recent related works. In the section three, the proposed system is detailed. The obtained results and discussions are illustrated in the fourth section. Finally, the section five concludes the paper.

24.2 Related Works

The main role of an embedded web server is to receive information collected by sensors and simplify the structure of the control system. Therefore, it uses standard interfaces of web and the standard communication protocols, to provide operation and control interface for users (Karia et al. 2021). In the literature the embedded Web server is deployed in many dynamic domains. Hence, we describe some recent proposed related works.

With aim to control a home remotely using an interface that can be accessed from any browser and anywhere, Albuquerque et al. (2019) have developed an embedded web server application named 'MyHOME'. The developed system is based on Arduino board and allows to users to control devices, monitor home stat and personalize the features. Due to the significant problem that caused by air quality on all being, Senthilkumar et al. (2020) designed a new smart embedded system for enabled air pollution monitoring. This system is built based on Internet of Things technology. Particularly, it is microprocessor based hardware that takes the advantages of IoT techniques. The designed system is prepared to gather multiples gases values and other physical parameters such as humidity and temperature. In the agricultural sector Snoussi et al. (2017) have conceived in 2017 an embedded web server for real-time greenhouse monitoring. Authors have designed a quite basic prototype of greenhouse surveillance and control system which is based on the Internet of Things solution. In addition, they have made use of some newly developed web technologies like JavaScript frameworks to further develop the website application. The designed web server provides an opportunity for farmers to capture some environmental data about the greenhouse and then customize the climatic requirements according to the needs of corps. Moreover, Almeida et al. (2020) developed an embedded server to automatically control corps irrigation based on the Internet of Things. The development of such solution allow to farmers to monitor crops. The installed sensors and actuators in the field are capable to exchange data with an embedded server. This system is based on Intel Edison device as hardware and MQTT as networking protocol. Besides, for interacting with the whole system, the embedded server has web interface that can be accessed via a web browser.

Within the industrial area, the development of contemporary manufacturing industry necessitates an independent industrial control system. Accordingly, Telagam et al. (2017) have proposed a smart sensor networking for real-time measurement of both temperature and humidity in industry. The offered system is based on IoT and employs the so-called Virtual Instrumentation Server. Once the actual values are measured, the outputs are visualized on a specific web page which can be accessed by the administrator after inputting his login and password.

24.3 Material and Methods

24.3.1 System Architecture

In order to design a new embedded system for water quality, we have integrated various materials and software. Besides, we have implemented various program using different programming languages. The global architecture of our considered system is illustrated in Fig. 24.1. As we can notice, this architecture consists of various parties including sensor module, actuator module, Wireless module, server applications, and clients. The functionality and operation of server is based on two main applications that are Web application and Database.

Server

In our proposed model the server plays an important role, without them the goal of our work will not be obtained. Hence, the server is able to read fresh data from sensors as it can send commands to actuators. It can read and stores data in local or remote data bases. It can receive user request analyses it contain then generate an adequate response. Furthermore, other roles can be added to the server by adding other programming lines.

Web Application

A web application is a computing program that runs on a web server. Hence, it is programmed using a client-server patterned structure. The user can access this application via Internet network and using a browser. Our designed web application has two fundamental roles:

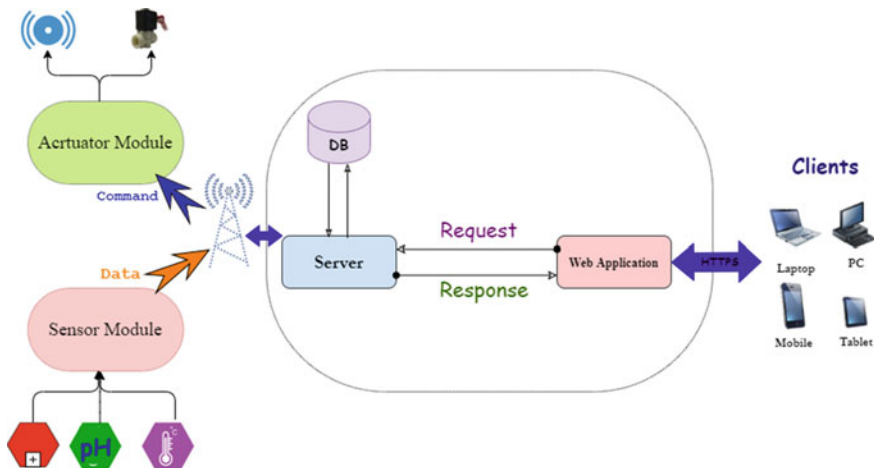


Fig. 24.1 Architecture of designed system

- Drawing graphs
- Giving statistical analysis.

Database

The task of most information systems is to translate data into information in order to produce knowledge that can be used for decision making. To do this, the system should be able to process data, contextualize it and provide synthesis and analysis techniques. For this purpose, database is specifically designed. In addition, databases can be structured in various ways and can accordingly take many forms. Nevertheless, the most common form is the relational database. For this reasons, in our architecture we have used MYSQL database in which data are organized into three tables. The first one is named measurement; it is planned for receiving measured values. The second one is called user; it contains user's information such as login and password. Besides, the third table is entitled location. It is designated for saving locations information where system is installed.

Sensor Module

The sensor module contains hardware components that allow collecting data about the physical environment where the device is placed. Generally, sensors are able to interact with a specific physical and chemical stimulus such as light, sound, pressure, temperature, movement, pH value, gazes, and conductivity. As depicted in Fig. 24.2, the sensor module of our designed system contains four sensors including temperature sensor, pH sensor, conductivity sensor and turbidity sensor. Therefore, they allow to our system to measure four values and send them to the server via WiFi module in real-time. In the other hand, if a user wants to measure other values he can connect other to our system.

Clients-terminals

In order to display the measured water parameters, the end user can log in to the created web application. For this reason, the user can use any mobile computing device, including a laptop, tablet, smartphone... In fact, the end user can use a smartphone or tablet to view the web page he/she wishes to see. Because, smartphones and tablets have both computational and communicational capabilities as well as they can be either hand-held or tucked safely into a personal pocket, allowing convenient use and access at the site.

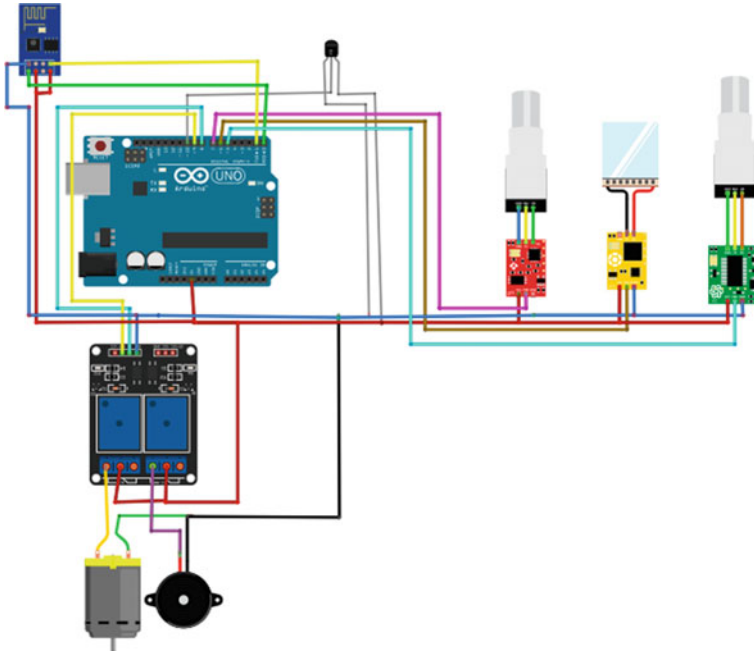


Fig. 24.2 Sensing and actuator modules

24.3.2 Used Materiel

In our proposed design, two different low cost processing card are used namely Raspberrie Pi and Arduino Uno. Furthermore, we have used four sensors, two actuators and a wireless module. These various materials are described in the following.

Raspberrie Pi

The Raspberrie Pi that we have chosen in our project is Raspberrie Pi 4B. In fact, we use this board because Raspberrie Pi is distinguished from other lightweight devices such as the Arduino. The Raspberrie Pi (Kumar and Jasuja 2017) has significant embedded memory resources (4Go) and computing capabilities (BCM2711, Cortex-A72 Quad core (ARM v8) SoC 64 bits 1.5 GHz) to provide both sensing function and webservice functionality. Furthermore, it can act as a data server that process simple and complicated data for providing service to the client requests in real-time.

Arduino

Arduino is a programmable electronic board that is equipped with a processor and a memory. On this board, we can connect various sensors such as temperature, humidity, vibration or light sensors. In addition, actuators can often be connected. In our designed system, we have used Arduino UNO for connecting both sensors and

actuator to the system. The Wi-Fi module is also linked to Arduino for connecting the sensor and actuator modules to the server.

Sensors and Actuators

A sensor is an object that aims to detect and collect physical, chemical or any other changes in its existence area. Then, it transforms them to data which can be easily and quickly comprehended by person or computer. With aims to detect water quality, we have connected to Arduino board four principal sensors to capture temperature, turbidity, pH value, and conductivity. However, we can add other ones if we want measure other water parameters.

In contrast, an actuator refers to device that enables to control its physical world. Principally, actuator is commanded by the devices to whom it was connected. So, its role is to convert commands into physical actions. Hence, our system comprises two actuators that are alarm and water pump. The role of the alarm is to product a sooner sound to prevent the manager located in the site and to inform them that something was wrong. However, water pump has as role pumping the water or stop the water stream.

Wireless Module

In our case the sensor and actuator modules cannot connect directly to the remote server. For this reason, we use the Wi-Fi module as a wireless gateway that provides the necessary technical and transmission mechanisms between different system components.

24.4 Results and Discussion

Once the implementation of our new introduced system was done and when all programing functionality was accomplished, the experimental validation tests were executed. As we have detailed before, the main goal of our system is to give to the end-user the ability to monitor and display the real time water measured values. In addition, the system allows controlling distantly and immediately installed actuators.

Before accessing to the web application, user must to prove his authenticity. Generally, user has to enter his login and password in the login page. This authentication procedure enables us to distinguish legitimate users from unauthorized ones. This distinction is a key to the trust and confidentiality of both users and their personal information, since only the owner of a profile is supposed to have the correct login information.

In fact, the performance of the communications between the various user requests and the actuator module has been tested under real conditions of use. For this reason, the user can connect to the web application via a browser. He can obtain access using different systems, including a laptop, a personal computer, a tablet or a smartphone.

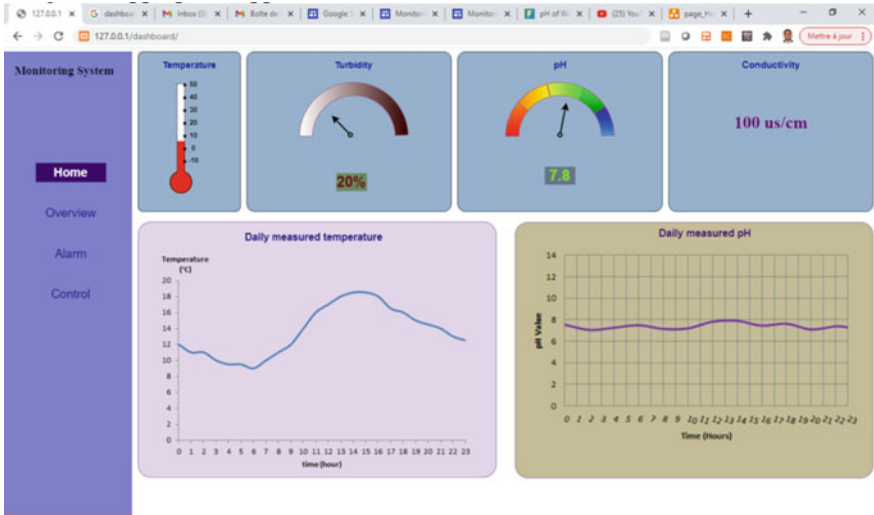


Fig. 24.3 Dashboard for real-time water monitoring

In the home page of web application (Fig. 24.3), a dashboard of water measured parameters of real-time are displayed. Hence, user can show four measured parameters in real-time. Those four parameters are temperature, turgidity, alkalinity (pH) and conductivity. We have here limited to those four parameters due to their importance to determine the quality of drinking water. However, our application is able to be extended for adding other parameters. The sophisticate graphics are used here to help users to visualize real-time captured values and for giving to our web application nice design and appropriate appearance.

On the other hand, according to the Fig. 24.4, user can visualize historical measurement. To do that, he has to activate overview page. Then, he can select which parameter he wants to illustrate. Next, he selects the date (day, month and year). Finally, he has to click on one of the three buttons ‘Daily’, ‘Monthly’ or ‘Yearly’. Each button allows visualizing historical data for a giving date. Firstly, the button ‘Daily’ allows visualizing the measured values in one day. Secondly, the button ‘Monthly’ displays historical measurement during one month. Finally, the ‘Yearly’ button lets to show the captured values along the year. Once one button is clicked, the measured values of selected parameter are displayed in form of graph. The graphs are drawing based on framework Angular.js. In the Fig. 24.5, user has selected temperature and the date 3/6/2021 then he has clicked on the button ‘Yearly’ as result he can see the graph of measured temperature during the year 2021.

As shown in Fig. 24.5, our developed web application has a page named ‘control’ that allow controlling water pump and alarm. It proposes two buttons (ON/OFF) for each actuator. If user clicks on the button ‘ON or OFF’ the web application sends request to the embedded server for activating the actuator (water pump or alarm). Once the user’s request reached the embedded server, this last one analyzes



Fig. 24.4 Visualization of historical data

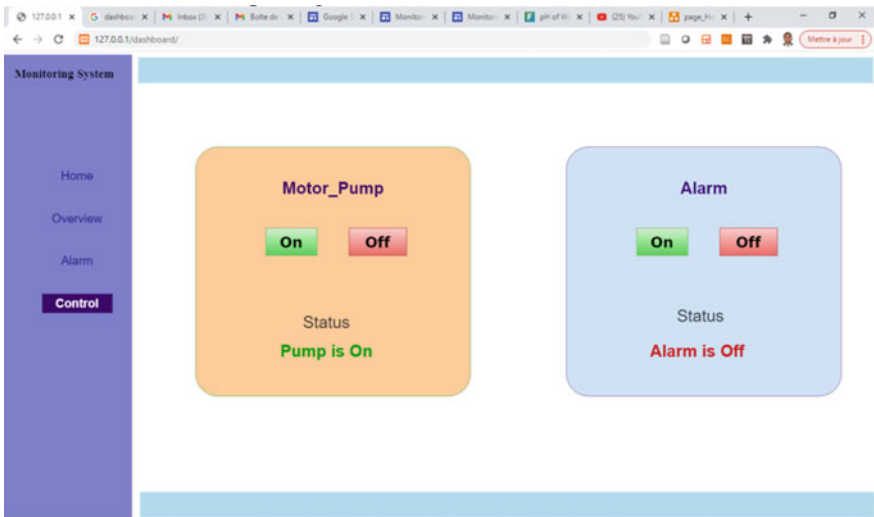


Fig. 24.5 Page for controlling actuator

its content. Based on the request type, the server sends the command (activation or deactivation) to the specific actuator (water pump or alarm). Hence, the server sends back the response to all connected users for updating the stat of actuators.

24.5 Conclusion

In this paper, an embedded web server system is effectively implemented and tested. The projected system is based on the IoT technology, it enables to monitor and control the water quality remotely and in real-time. Our system consists of sensor that can measure water parameters like temperature, turbidity, conductivity and pH. It also connected to the two actuators mainly water pump and alarm that can be controlled automatically or by user command. Furthermore, user can visualize captured data by accessing to web page in any browser. Hence, he can show data in form numerical values or in specific graphic. Our system is reachable from any PC, Laptop, Smartphone, or other.

References

- Alaoui SS, Aksasse B, Farhaoui Y (2019) Air pollution prediction through internet of things technology and big data analytics. *IJCISTUDIES* 8(3):177. <https://doi.org/10.1504/IJCISTUDIES.2019.102525>
- Azrou M, Farhaoui Y, Ouanan M et al (2019) SPIT detection in telephony over IP using K-means algorithm. *Procedia Comput Sci* 148:542–551
- Azrou M, Mabrouki J, Chaganti R (2021a) New efficient and secured authentication protocol for remote healthcare systems in cloud-IoT. *Secur Commun Netw* 2021:1–12. <https://doi.org/10.1155/2021/5546334>
- Azrou M, Mabrouki J, Guezzaz A et al (2021b) Internet of things security: challenges and key issues. *Secur Commun Netw* 2021:1–11
- Azrou M et al (2022) Machine-learning algorithms for efficient water quality prediction model. *Model Earth Syst Environ* 8(2):2793–2801. <https://doi.org/10.1007/s40808-021-01266-6>
- Boutahir MK, Farhaoui Y, Azrou M (2022) Machine learning and deep learning applications for solar radiation predictions review: Morocco as a Case of Study. In: Yaseen SG (ed) *Digital economy, business analytics, and big data analytics applications*, vol 1010. Springer International Publishing, pp 55–67
- Chaganti R et al (2022) A particle swarm optimization and deep learning approach for intrusion detection system in internet of medical things. *Sustainability* 14(19):12828
- Cirillo F et al (2020) Smart city IoT services creation through large-scale collaboration. *IEEE Internet Things J* 7(6):5267–5275
- de Albuquerque BHC et al (2019) Home automation using arduino platform on an embedded server. *IJAERS* 6(11):158–162. <https://doi.org/10.22161/ijaers.611.23>
- da Silva Almeida T, Roledo LB, de Carvalho RL, da Silva WG (2020) Embedded server to automatic control of wireless transducer network for irrigation based on Internet of things. *Revista Sítio Novo* 4(2):6–18
- Dimitrievski A et al (2021) Rural healthcare IoT architecture based on Low-energy LoRa. *Int J Environ Res Public Health* 18(14):7660
- Douiba M, Benkirane S, Guezzaz A. et al (2022a) An improved anomaly detection model for IoT security using decision tree and gradient boosting. *J Supercomput* 1–20
- Douiba M, Benkirane S, Guezzaz A et al (2022b) Anomaly detection model based on gradient boosting and decision tree for IoT environments security. *J Reliab Intell Environ* 1–12
- Ghizlane F, Mabrouki J, Ghrissi F, Azrou M (2022) Proposal for a high-resolution particulate matter (PM10 and PM2. 5) capture system, comparable with hybrid system-based internet of things: case of quarries in the Western Rif, Morocco, *Pollution*, vol 8, no 1, pp 169–180

- Guezzaz A, Asimi A, Mourade et al (2020) A multilayer perceptron classifier for monitoring network traffic. In: Farhaoui Y (ed) *Big data and networks technologies*, vol 81. Springer International Publishing, pp 262–270. https://doi.org/10.1007/978-3-030-23672-4_19
- Guezzaz A, Benkirane S, Azrou M et al (2021a) A reliable network intrusion detection approach using decision tree with enhanced data quality. *Secur Commun Netw* 2021:1–8
- Guezzaz A et al (2021b) A Mathematical validation of proposed machine learning classifier for heterogeneous traffic and anomaly detection. *Big Data Min Anal* 4:18–24
- Guezzaz A, Asimi A, Asimi et al (2021c) A distributed intrusion detection approach based on machine learning techniques for a cloud security. In: *Intelligent systems in big data, semantic web and machine learning*. Springer, pp 85–94
- Guezzaz A et al. (2022a) A lightweight hybrid intrusion detection framework using machine learning for edge-based IIoT security. *Int Arab J Inf Technol* 19
- Guezzaz A, Benkirane S, Azrou M (2022b) A novel anomaly network intrusion detection system for internet of things security. In *IoT and smart devices for sustainable environment* 129–138. Springer
- Karia DC, Adajania V, Agrawal M, Dandekar S (2021) Embedded web server application based automation and monitoring system. In: *2011 international conference on signal processing, communication, computing and networking technologies*, Thuckalay, Tamil Nadu, India, pp 634–637. <https://doi.org/10.1109/ICSCCN.2011.6024628>
- Khan F et al (2020) IoT based power monitoring system for smart grid applications. In: *2020 international conference on engineering and emerging technologies (ICEET)*, pp 1–5
- Kılıç Z (2020) The importance of water and conscious use of water. *Int J Hydrol* 4(5):239–241. <https://doi.org/10.15406/ijh.2020.04.00250>
- Kumar S, Jasuja A (2017) Air quality monitoring system based on IoT using Raspberry Pi. In: *2017 international conference on computing, communication and automation (ICCCA)*, pp 1341–1346
- Lv Z et al (2021) AI-empowered IoT security for smart cities. *ACM Trans Internet Technol* 21(4):1–21
- Mabrouki J, Azrou M, Farhaoui Y, El Hajjaji S (2020) Intelligent system for monitoring and detecting water quality, in big data and networks technologies, Farhaoui Y. Ed. Springer International Publishing, Cham 81:172–182. https://doi.org/10.1007/978-3-030-23672-4_13
- Mabrouki J, Azrou M, El Hajjaji S (2021) Use of internet of things for monitoring and evaluation water's quality: comparative study. *Int J Cloud Comput* 10(5–6):633–644
- Mabrouki J, Fattah G, Al-Jadabi N, Abrouki Y, Dhiba D, Azrou M, Hajjaji SE (2022) Study, simulation and modulation of solar thermal domestic hot water production systems. *Model Earth Syst Environ* 8(2):2853–2862
- Mabrouki J et al (2022) Smart system for monitoring and controlling of agricultural production by the IoT. In: *IoT and smart devices for sustainable environment*. Springer
- Mehmood MY et al (2021) Edge computing for IoT-enabled smart grid. *Secur Commun Netw*
- Senthilkumar R, Venkatakrishnan P, Balaji N (2020) Intelligent based novel embedded system based IoT enabled air pollution monitoring system. *Microprocess Microsyst* 77:103172. <https://doi.org/10.1016/j.micpro.2020.103172>
- Snoussi A et al (2017) Embedded web server implementation for real time greenhouse monitoring. In: *Proceeding of the international conference : ICOA'2017*, Editions Universitaires Européennes, pp 105–108
- Telagam N, Kandasamy N, Nanjundan M, Ts A (2017) Smart sensor network based industrial parameters monitoring in IOT environment using virtual instrumentation server. *Int J Onl Eng* 13(11):111. <https://doi.org/10.3991/ijoe.v13i11.7630>
- Wang EK et al (2021) Intelligent monitor for typhoon in IoT system of smart city. *J Supercomput* 77(3):3024–3043

Chapter 25

Crystal Structure and Impedance Spectroscopy Studies of New Orthophosphate $\text{Ba}_{2-x}\text{Pb}_x\text{Sr}(\text{PO}_4)_2$; ($0 \leq x \leq 2$)



M. Ben Baaziz, K. Azoulay, I. Bencheikh, R. Ghibate, M. Azdouz, L. Bih, and M. Azroul

Abstract In this work, we presented the results of the structural study of new solid solution orthophosphate materials of the type $\text{Ba}_{2-x}\text{Pb}_x\text{Sr}(\text{PO}_4)_2$; $0 \leq x \leq 2$ by applying the techniques of differential scanning calorimetry. We are also interested in the study of electrical properties by using the method of impedance spectrometry. Thermal analysis of orthophosphates shows that these materials can conserve their crystalline structure at high temperatures. The electrical properties of orthophosphates have been investigated. The results show that the temperature and the conductivity vary in the same direction for the different samples of the series.

Keywords Inorganic materials · $\text{Ba}_{2-x}\text{Pb}_x\text{Sr}(\text{PO}_4)_2$ · Impedance spectroscopy

M. B. Baaziz (✉) · M. Azdouz · M. Azroul

Laboratory of Materials Engineering for the Environment and Natural Resources, Department of Chemistry, Faculty of Science and Technology, Moulay Ismail University, 52000 Errachidia, Morocco

e-mail: m.benbaaziz@edu.umi.ac.ma

K. Azoulay · I. Bencheikh

Mohammed V University in Rabat, Rabat, Morocco

R. Ghibate

Laboratory of Biomolecular and Macromolecular Chemistry, Faculty of Sciences, Moulay Ismail University, 11201 Meknes, Morocco

L. Bih

Faculté des Sciences de Meknès, Equipe de Physico-Chimie de la Matière Condensée, PCMC, Meknes, Morocco

Département Matériaux et Procédés, ENSAM Meknès, Université Moulay Ismail, Meknes, Morocco

25.1 Introduction

Recently developed phosphate-based materials with promising electrochemical performance include NaMPO_4 , KMgPO_4 , $\text{Na}_{3.12}\text{M}_{2.44}(\text{P}_2\text{O}_7)_2$, $\text{Na}_2\text{FeP}_2\text{O}_7$, $\text{Na}_2\text{FePO}_4\text{F}$, and $\text{Na}_3\text{V}_2(\text{PO}_4)_3\text{F}_3$ (Miladi et al. 2016; Barker et al. 2003; Gover et al. 2006; Jian et al. 2012; Kim et al. 2012).

Due to their distinct properties, phosphates have been widely used in many applications arising from their Physico-chemical properties, specifically chemical stability and ecological characteristics (Salje and Devarajan 1981; Zachariassen 1948; Redden and Buerger 1969; Sugiyama and Tokonami 1990; Azdouz et al. 2018; Manoun et al. 2003; Popovic et al. 2002). Several instances of prospective uses for laser materials, luminescence, ceramics, fuel cells, optics, catalysts, magnetic materials, ion conductors, sensors, bone surgery, etc. (He et al. 2013; Huang et al. 2015; Qin et al. 2009; Yi et al. 2010; Tong et al. 2015; Tāle et al. 1979; Poort et al. 1996; Liang et al. 2003; Chen et al. 2011).

Therefore, it is necessary to develop scientific research on other types of synthetic orthophosphates to contribute to the valorization of these materials. To this end, we performed electrical measurements on orthophosphates $\text{Ba}_{2-x}\text{Pb}_x\text{Sr}(\text{PO}_4)_2$; $0 \leq x \leq 2$ using the impedance spectrometry method, to control the effect of voluminous cations on the variation of ionic conductivity. In addition, studies have already been conducted by researchers using the same technique on orthophosphate-based materials (Electrical conductivity in lithium orthophosphates 2003; Enneffati et al. 2018; Mielewczyk et al. 2010; Cho et al. 2016; Hassairi et al. 2017; Chtourou et al. 2017). The displacement of mobile species and the orientation of the dipoles formed are at the origin of the dielectric relaxation phenomena. Such a study permitted us to set up a correlation between the structural and electrical properties of the studied orthophosphates, as well as the conduction mechanism.

The principal objective of this study is the development of new materials with specific efficient properties, thermally stable and with good electrical properties, i.e. this work is principally related to the characterization of orthophosphates by differential scanning calorimetry. In addition, we have been interested the study of electrical properties by using the technique of impedance spectroscopy.

25.2 Experimental Procedure

25.2.1 Thermal Method

The thermal behavior of the orthophosphate samples was analyzed using Differential Scanning Calorimetry (LABSYS, Evo analyzer). The different compositions were heated between 30 and 640 °C in an alumina crucible under an inert atmosphere with a mass of 20 mg and a temperature rise rate of 10 °C/min.

25.2.2 Impedance Spectroscopy

The electric measurement of the orthophosphate materials is performed as a function of both temperature 563–663 K and frequency [10 Hz–1 MHz] using a Modulab MTS Solartron impedance analyzer driven by a microcomputer and connected to the Probostat cell holder system. The different compositions were ground into very fine powders and then transformed into pellets of 4 mm diameter and 2 mm thickness. These pellets are metallized by a silver paste on both sides and dried in an oven set at 120 °C for 12 h.

25.3 Results and Discussion

25.3.1 Thermal Behavior Analysis

The study of the thermal stability of the different samples of the series of solid solutions of the $\text{Ba}_{2-x}\text{Pb}_x\text{Sr}(\text{PO}_4)_2$; $0 \leq x \leq 2$ was carried out by the method of differential scanning calorimetry (DSC) to highlight any transformation which takes place during the heat treatment whether it concerns crystalline transformations or transfer of matter for a better understanding of these phenomena if they exist.

Figure 25.1 regroups the thermograms produced for the $\text{Ba}_{2-x}\text{Pb}_x\text{Sr}(\text{PO}_4)_2$; $0 \leq x \leq 2$ series. The thermal behavior of all the crystalline powders of orthophosphates is similar as illustrated by the succession of DSC thermal curves, no thermal accident has been recorded, and all the materials are very stable in the interval of temperature 30–640 °C. This signifies that orthophosphates of the type $\text{Ba}_{2-x}\text{Pb}_x\text{Sr}(\text{PO}_4)_2$; $0 \leq x \leq 2$ can retain their crystal structure and therefore resist high temperatures. These materials, despite being made up of many chemical elements, are thermally stable and these results obtained are encouraging for the possible use of this type of material for the containment of various chemical elements, especially those harmful (Ben Baaziz et al. 2018; 2019).

25.3.2 Analysis by Impedance Spectroscopy

Nyquist diagrams. The complex impedance of each orthophosphate is determined from Nyquist diagrams. Figure 25.2 illustrates the superposition of the Nyquist diagrams (or Cole–Cole diagrams) for the series of $\text{Ba}_{2-x}\text{Pb}_x\text{Sr}(\text{PO}_4)_2$; $0 \leq x \leq 2$, obtained at different temperatures. Analysis of the Cole–Cole diagrams (Fig. 25.2) shows that they consist of two distinct regions. One with high frequency and one with low frequency. The first corresponds to the volume properties of orthophosphate, while the second one evidenced the polarization phenomena at the electrode. This last region is characteristic of the development of diffusion furthermore because the

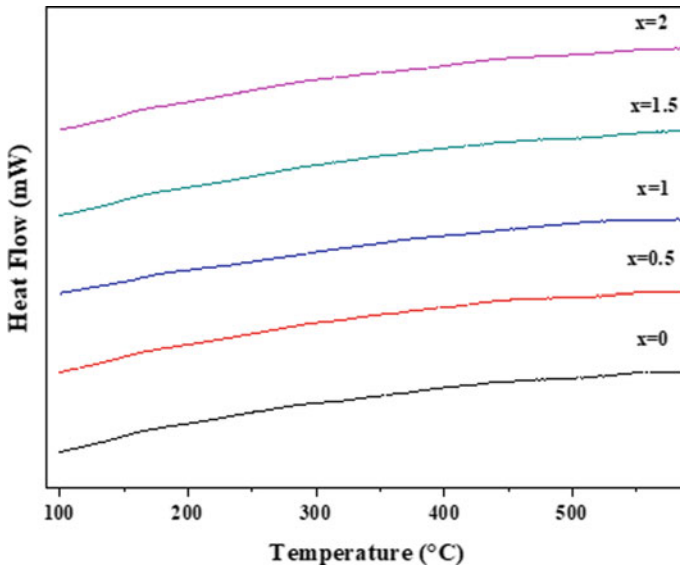


Fig. 25.1 Superposition of DSC thermograms of $\text{Ba}_{2-x}\text{Pb}_x\text{Sr}(\text{PO}_4)_2$; $0 \leq x \leq 2$

accumulation of ions at the electrolyte–electrode interface. Within the high-frequency domain, the ions don't have time to maneuver sufficiently and therefore the polarization isn't determined. A proportional increase in the impedance is then observed with the decrease in frequency.

Determination of electrical conductivity and activation energy. The resistance of the prepared orthophosphate was determined by extrapolation at the angle of zero phase shift and the intersection of the semicircle of the impedance spectrum with the Z' axis. The electrical conductivity of each orthophosphate sample is taken from the Nyquist diagram at a chosen temperature and estimated by applying the following Eq. (25.1).

$$\sigma = \frac{e}{s} \frac{1}{R} \quad (25.1)$$

where:

- e is the thickness of the sample;
- s is the area of the electrolyte–electrode contact;
- R is the sample resistance at zero frequency.

Figure 25.3 represents the variation of the conductivity (σ_{dc}) as a function of the inverse of the temperature ($1000/T$) for the orthophosphates of $\text{Ba}_{2-x}\text{Pb}_x\text{Sr}(\text{PO}_4)_2$; $0 \leq x \leq 2$. The variation of the conductivity σ_{dc} as a function of the temperature follows an Arrhenius-type law in the temperature interval 563 to 663 K. Indeed

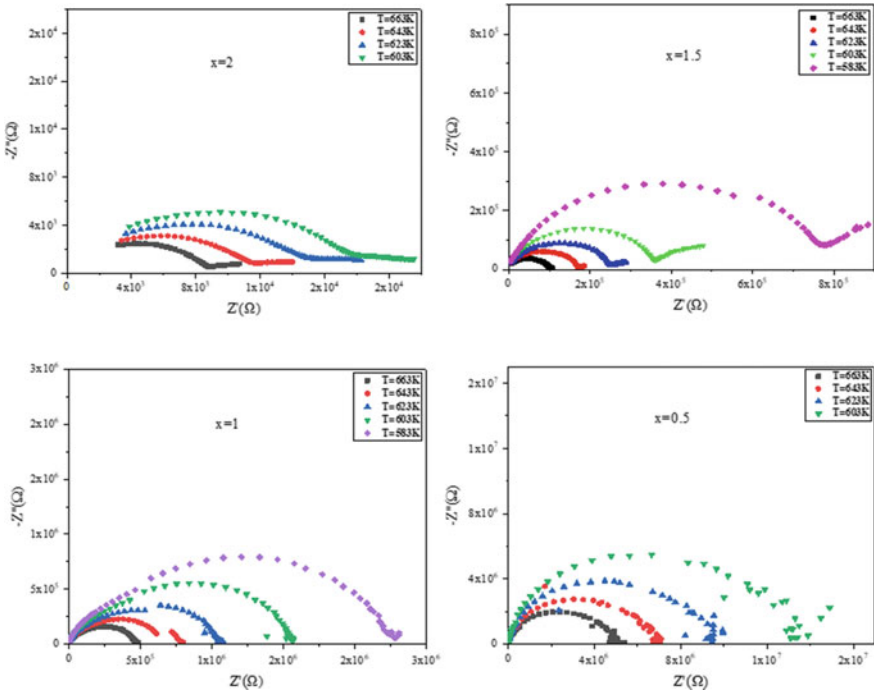


Fig. 25.2 Nyquist diagrams of orthophosphates $Ba_{2-x}Pb_xSr(PO_4)_2$; $0 \leq x \leq 2$ at different temperatures

for each composition we observe that the conductivity (σ) varies with temperature according to the following Eq. (25.2).

$$\sigma \cdot T = \sigma_0 \exp(-E_a / K_B T) \tag{25.2}$$

where:

- σ_0 is the pre-exponential factor;
- E_a is the activation energy;
- k_B is the Boltzmann constant;
- T is the absolute temperature.

Therefore, the conductivity is ionic in orthophosphates; it is related principally to the displacements of Ba^{2+} and Pb^{2+} ions in the different compositions. When the concentration of Pb increases in the $Ba_{2-x}Pb_xSr(PO_4)_2$; $0 \leq x \leq 2$ matrices, there is a monotonous increase in conductivity as a function of composition. This is mostly due to the size of the ions present in the lattice. On the other hand, the substitution of Ba^{2+} ions with a high radius (134 pm) by those of Pb^{2+} ions (120 pm) with a low radius induces an increase in the mobility of the ions (Shannon 1976).

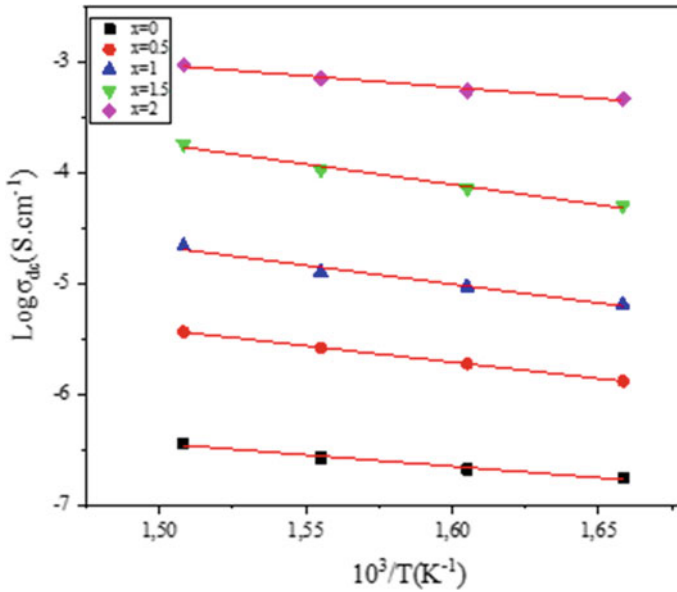


Fig. 25.3 $\text{Log}(\sigma_{\text{dc}})$ versus $1000/T$ plots of the orthophosphates $\text{Ba}_{2-x}\text{Pb}_x\text{Sr}(\text{PO}_4)_2$; $0 \leq x \leq 2$

We observe that the temperature and conductivity vary in the same direction for the different samples of the series. This indicates that the increase in temperature induces sufficient energy to have the mobility of the ions.

The dependence of the conductivity on temperature evolves according to an Arrhenius law (Fig. 25.3). This linear variation of the conductivity $\text{Log}(\sigma_{\text{dc}})$ as a function of the inverse of the temperature permits the determination of the conduction activation energy. The values of the electrical parameters of orthophosphates are given in Table 25.1.

Table 25.1 Electrical parameters of the orthophosphates $\text{Ba}_{2-x}\text{Pb}_x\text{Sr}(\text{PO}_4)_2$; $0 \leq x \leq 2$ at 663 K

x	Orthophosphates labels	Conductivity σ_{dc} (S/cm)	$\log(\sigma_{\text{dc}})$	Activation energy E_a (eV)
x = 0	$\text{Ba}_2\text{Sr}(\text{PO}_4)_2$	3.573×10^{-7}	- 6.447	0.408
x = 0.5	$\text{Ba}_{1.5}\text{Pb}_{0.5}\text{Sr}(\text{PO}_4)_2$	3.659×10^{-6}	- 5.437	0.586
x = 1	$\text{BaPbSr}(\text{PO}_4)_2$	2.152×10^{-5}	- 4.667	0.673
x = 1.5	$\text{Ba}_{0.5}\text{Pb}_{1.5}\text{Sr}(\text{PO}_4)_2$	1.818×10^{-4}	- 3.740	0.727
x = 2	$\text{Pb}_2\text{Sr}(\text{PO}_4)_2$	9.418×10^{-4}	- 3.026	0.406

25.4 Conclusion

The study of the electrical properties of orthophosphates with compositions $\text{Ba}_{2-x}\text{Pb}_x\text{Sr}(\text{PO}_4)_2$; $0 \leq x \leq 2$ was performed by impedance spectroscopy. Their electrical conductivities as a function of temperature evolve according to the Arrhenius type law. The increasing evolution of the conductivity $\text{Log}(\sigma_{\text{dc}})$ as a function of that of the temperature was observed for the different samples of the series. This indicates that the increase in temperature induces sufficient energy to have the mobility of ions.

Using differential scanning calorimetry (DSC), the thermal behavior of the various orthophosphate compositions was examined in this work. This analysis shows the thermal stability of these samples in the studied temperature range 30–640 °C.

References

- Azdouz M, Baaziz MB, Batan A, Azrou M, Lazor P, Manoun B (2018) Synthesis and structural characterization of $\text{Ba}_2\text{Pb}(\text{PO}_4)_2$ and $\text{BaPb}_2(\text{PO}_4)_2$ and study of thermal behavior of $\text{BaPb}_2(\text{PO}_4)_2$ at high temperature. *Chemi Res J* 3(3):17–33
- Baaziz MB, Azdouz M, Azrou M, Batan A, Manoun B (2018) Elaboration, rietveld refinements and vibrational spectroscopic studies of a new lacunar apatite series: $\text{NaPb}_{3-x}\text{Ca}_x\text{Cd}(\text{PO}_4)_3$ ($0 \leq x \leq 1$). *J Chem Res* 42:564–571
- Baaziz MB, Azdouz M, Azrou M, Manoun B, El Amraoui M (2019) Elaboration, vibrational study and thermal behavior of lacunar apatites $\text{NaPb}_{3-x}\text{CdxCa}(\text{PO}_4)_3$ ($0 \leq x \leq 1$). *J Struct Chem* 60 1285–1298
- Barker J, Saidi MY, Swoyer JL (2003) A sodium-ion cell based on the fluorophosphate compound NaVPO_4F . *Electrochem Solid-State Lett* 6:A1–A4
- Chen F, Yuan X, Xiong X, Liu L, Chin J (2011) Composition and luminescence properties of $\text{Ba}_3(\text{PO}_4)_2$: $\text{Ce}^{3+}/\text{Dy}^{3+}$ phosphor. *Rare Earth Soc* 29:450–454
- Cho W, Kim SM, Lee KW, Song JH, Jo YN, Yim T ... Kim YJ (2016) Investigation of new manganese orthophosphate $\text{Mn}_3(\text{PO}_4)_2$ coating for nickel-rich $\text{LiNi}_0.6\text{Co}_0.2\text{Mn}_0.2\text{O}_2$ cathode and improvement of its thermal properties. *Electrochimica Acta* 198:77–83
- Chtourou R, Louati B, Guidara K (2017) AC and DC conductivity study of $\text{KPb}_4(\text{PO}_4)_3$ compound using impedance spectroscopy. *J Alloys Compd* 727:771–777
- Enneffati M, Louati B, Guidara K, Rasheed M, Barillé R (2018) Crystal structure characterization and AC electrical conduction behavior of sodium cadmium orthophosphate. *J Mater Sci: Mater Electron* 29:171–179
- Gover RKB, Bryan A, Burns P, Barker J (2006) The electrochemical insertion properties of sodium vanadium fluorophosphate, $\text{Na}_3\text{V}_2(\text{PO}_4)_2\text{F}_3$. *Solid State Ionics* 177:1495–1500
- Hassairi S, Louati B, Guidara K (2017) Synthesis and characterisation of orthophosphate KPbPO_4 compound. *J Alloys Compd* 715:397–403 (2017)
- He ZZ, Zhang WL, Xia TL, Yu WQ, Cheng WD (2013) Crystal structure and magnetic properties of $\text{Pb}_2\text{Ni}(\text{PO}_4)_2$. *Dalton Trans* 42:5480–5484
- Huang S, Jing Q, Han J, Pan S, Wu H, Yang Z (2015) Three Alkali metal lead orthophosphates—syntheses, crystal structures and properties of APbPO_4 ($A = \text{K}, \text{Rb}, \text{Cs}$). *Eur J Inorg Chem* 9:1490–1495
- Jian Z, Zhao L, Pan Huilin et al (2012) Carbon coated $\text{Na}_3\text{V}_2(\text{PO}_4)_3$ as novel electrode material for sodium ion batteries. *Electrochem Commun* 14(1):86–89 (2012)

- Kim H, Park I, Seo DH, Lee S, Kim SW, Kwon WJ, Park Y, Kim CS, Jeon S, Kang K (2012) New iron-based mixed-polyanion cathodes for lithium and sodium rechargeable batteries: combined first principles calculations and experimental study. *J Am Chem Soc* 134:10369–10372 (2012)
- Liang H, Tao Y, Zeng Q, He H, Wang S, Hou X, Wang W, Su Q (2003) The optical spectroscopic properties of rare earth-activated barium orthophosphate in VUV-Vis range. *Mater Res Bull* 38:797–805
- Manoun B, Popovic L, de Waal D (2003) Rietveld refinements of a new solid solution $Ba(3-x)Sr_x(PO_4)_2$ ($0 \leq x \leq 3$). *Powder Diffr* 18:122–127
- Miladi L, Oueslati A, Guidara K (2016) Phase transition, conduction mechanism and modulus study of $KMgPO_4$ compound. *RSC Advances*. 6(86), 83280–83287 (2016). Author F (2016) Article title. *J* 2(5):99–110
- Mielewicz A, Molin S, Gdula K, Jasinski G, Kusz B, Jasinski P, Gazda M (2010) Structure and electric properties of double magnesium zirconium orthophosphate. *Mater Ceram* 62:477–480
- Poort S, Reijnhoudt H, Van der Kuip H, Blasse G (1996) Luminescence of Eu silicate host lattices with alkaline earth ions in a row $Ba_3(PO_4)_2$. *J Alloy Compd* 241 75–81
- Popovic L, Manoun B, de Waal D (2002) Crystal chemistry, vibrational spectra and factor group analysis of $Ba(3-x)Sr_x(PO_4)_2$ ($0 \leq x \leq 3$) solid solution series. *J Alloys Compd* 343:82–89
- Qin C, Huang Y, Shi L, Chen G, Qiao X, Seo HJ (2009) Thermal stability of luminescence of $NaCaPO_4$: Eu^{2+} phosphor for white-light-emitting diodes. *J Phys D Appl Phys* 42:185105
- Redden MJ, Buerger MJ (1969) Note on the symmetry and cell of calcium orthovanadate. *Zeitschrift für Kristallographie* 129:459–460
- Rissouli K, Benkhouja K, Ramos-Barrado JR, Julien C (2003) Electrical conductivity in lithium orthophosphates. *Mater Sci Eng: B* 98:185–189
- Salje E, Devarajan V (1981) Potts model and phase transition in lead phosphate $Pb_3(PO_4)_2$. *J Phys C: Solid State Phys* 14:L1029 (1981)
- Shannon RD (1976) Revised effective ionic radii and systematic studies of interatomic distances in halides and chalcogenides. *Acta Crystallographica Section A: Crystal Physics, Diffraction, Theoretical and General Crystallography* 32:751–767
- Sugiyama K, Tokonami M (1990) The crystal structure refinements of the strontium and barium orthophosphates. *Mineral J* 15L141–146
- Täle I, Kūlis P, Kronghauz V (1979) Recombination luminescence mechanisms in $Ba_3(PO_4)_2$. *J Lumin* 20:343–347 (1979)
- Tong M, Liang Y, Yan P, Wang Q, Li G (2015) Synthesis and luminescence properties of a bluish-green emitting phosphor $Ba_3(PO_4)_2$: Ce^{3+} , Tb^{3+} . *Opt Laser Technol* 75:221–228
- Yi L, Zhou L, Gong F, Lan Y, Tong Z, Sun J (2010) Preparation of $SrZn_2(PO_4)_2$: Eu^{2+} , Mn^{2+} phosphor and its photoluminescent properties. *Mater Sci Eng B* 172 132–135 (2010)
- Zachariasen WH (1948) The crystal structure of the normal orthophosphates of barium and strontium. *Acta Crystallographica* 1:263–265

Correction to: Investigation of the Energy and Emission from the Combustion of Argain Cake in a CHP System



Ayoub Najah EL Idrissi, Mohammed Benbrahim, and Nadia Rassai

Correction to:
Chapter 3 in: J. Mabrouki et al. (eds.), *Advanced Technology for Smart Environment and Energy*, Environmental Science and Engineering,

https://doi.org/10.1007/978-3-031-25662-2_3

In the original version of this chapter, the name of corresponding author of chapter 3 was published with a typo. This has been corrected from Ayoub Najah ELIdrissi to Ayoub Najah EL Idrissi. The correction chapter and the book has been updated with the changes.

The updated version of this chapter can be found at
https://doi.org/10.1007/978-3-031-25662-2_3

© The Author(s), under exclusive license to Springer Nature Switzerland AG 2023
J. Mabrouki et al. (eds.), *Advanced Technology for Smart Environment and Energy*,
Environmental Science and Engineering,
https://doi.org/10.1007/978-3-031-25662-2_26

C1